Technical Report Documentation Page

1. Report No. FHWA/TX-07/0-5197-1	2. Government Accession No.	3. Recipient's Catalog No.	
4. Title and Subtitle Effects of Increasing the Allowable Compressive Stress at Release of Presstressed Concrete Girders		5. Report Date January 2007	
		6. Performing Organization Code	
7. Author(s) David Birrcher and Oguzhan Bayrak		8. Performing Organization Report No. 0-5197-1	
9. Performing Organization Name and Address Center for Transportation Research The University of Texas at Austin 3208 Red River, Suite 200 Austin, TX 78705-2650		10. Work Unit No. (TRAIS)	
		11. Contract or Grant No. 0-5197	
12. Sponsoring Agency Name and Address Texas Department of Transportation Research and Technology Implementation Office P.O. Box 5080 Austin, TX 78763-5080		13. Type of Report and Period Covered Technical Report 9/1/04 - 2/28/07	
		14. Sponsoring Agency Code	
15. Supplementary Notes Project performed in cooperation with the Texas Department of Transportation and the Federal Highway Administration.			
16. Abstract In this report, the feasibility of increasing the allowable compressive stress limit at prestress transfer of $0.60f'_{ci}$ is evaluated. For this purpose, the live-load performance and initial camber of pretensioned beams was investigated. Static-load tests were performed on 24 scaled and 12 full-scale specimens that were subjected to a maximum compressive stress at release ranging from $0.46f'_{ci}$ to $0.91f'_{ci}$. From the comparison of the measured and predicted cracking loads of these test specimens, an increase of the allowable compressive stress to $0.65f'_{ci}$ was justified. For the specimens subjected to release stresses exceeding $0.65f'_{ci}$, premature cracking in flexure was detected due to nonlinear deformation at release and associated microcracking. In addition, an initial camber database of information from 223 pretensioned girders was compiled. The data suggested that increasing $0.60f'_{ci}$ did not affect the ability to accurately estimate initial camber. However, for a given section, higher cambers were detected as the compressive stress at release increased. Lastly, a simple technique for improving the initial camber estimates of conventional girders was presented as a feasibility study for future work.			
17. Key Words Allowable release stress, compressive stress limit, prestress transfer, initial camber		18. Distribution Statement No restrictions. This document is available to the public through the National Technical Information Service, Springfield, Virginia 22161; www.ntis.gov.	
19. Security Classif. (of report) Unclassified	20. Security Classif. (of this page) Unclassified	21. No. of pages 226	22. Price

Form DOT F 1700.7 (8-72) Reproduction of completed page authorized

Effects of Increasing the Allowable Compressive Stress at Release of Prestressed Concrete Girders

David Birrcher
Oguzhan Bayrak

Disclaimers

Acknowledgments

Table of Contents

List of Tables

List of Figures

PREAMBLE

Two distinct topics were covered in TxDOT Project 0-5197. These topics are addressed in two separate reports. In this report (0-5197-1), the effects of increasing the allowable compressive stress at prestress transfer of prestressed concrete girders are evaluated. In Report 0-5197-2, the allowable tensile stress limit at prestress transfer is investigated.

CHAPTER 1
Introduction

1.1   ALLOWABLE COMPRESSIVE STRESS AT PRESTRESS TRANSFER

In 1961 and 1963, the first code provisions for prestressed concrete members were adopted by the American Association of State Highway and Transportation Officials (AASHTO) and the American Concrete Institute (ACI), respectively (AASHTO, 1961 and ACI, 1963). To date, the allowable compressive stress in the concrete at prestress transfer adopted by these institutions has not changed. This allowable stress limit as it appears in the AASHTO LRFD Bridge Design Specifications (Interim 2005) and the ACI 318-05 Building Code Requirements (2005) is as follows:

- *The compressive stress limit for pretensioned and post-tensioned concrete components, including segmentally constructed bridges, shall be $0.60f'_{ci}$* (AASHTO, 2005).
- *Stresses in concrete immediately after prestress transfer shall not exceed the following: (a) Extreme fiber stress in compression...$0.60f'_{ci}$* (ACI, 2005).

In these provisions, f'_{ci} is the compressive strength of the concrete at prestress transfer.

In the last decade, a rising amount of attention has been given to increasing $0.60f'_{ci}$ within the precast/prestressed concrete industry. The reasons behind the increased interest are the potential benefits of relaxing the allowable compressive stress limit at prestress release. Some of these benefits include:

- the reduction in cycle time of precast facilities
- the reduction of external curing costs
- the reduction of the overall cement content
- the reduction of the number of debonded or harped strands
- the negation of increased cycle time from using low-alkali cement or from replacing cement with other cementitious materials
- the increase in span capabilities due to an increase in the number of prestressing strands in a given section
- the removal of "unnecessary" conservatism in current practice

In light of these economic, safety, and efficiency benefits, a number of research studies have been conducted to assess the feasibility of increasing the allowable compressive stress at transfer. In these studies, several effects of increasing the allowable stress were identified and studied (Section 2.2.3). Some effects included the increase in creep, camber, and prestress loss of beams subjected to release stresses in excess of the allowable limit. For the most part, the impact of increasing $0.60f'_{ci}$ on these investigated factors was minimal, thereby supporting the potential increase of the allowable compressive stress at release. However, none of the previous research studies investigated the live-load performance of pretensioned girders subjected to compressive stresses at prestress transfer in excess of the current allowable limit.

1.2   OBJECTIVES OF RESEARCH

A research project, funded by the Texas Department of Transportation, was initiated at the Ferguson Structural Engineering Laboratory at the University of Texas at Austin. The two main objectives of the project were to evaluate the impact of increasing the allowable compressive stress at release of $0.60f'_{ci}$ on (i) the live-load performance and (ii) the initial camber of prestressed concrete girders. This project is described in this report.

1.3   SCOPE OF RESEARCH

Within the current project, an extensive literature review, experimental research on the live load performance of pretensioned beams, and the compilation of an initial camber database were performed. In the literature review, historical and recent studies related to the allowable compressive stress at transfer were discussed. In addition, the early-age mechanical properties of high-strength concrete and the behavior of concrete due to initial and sustained compressive loading were presented. In the experimental program, three phases of beam tests were conducted to evaluate the live-load performance of pretensioned girders. In the first two phases, thirty-six pretensioned beams were tested statically to experimentally evaluate their cracking load. Twenty-four of the specimens were scaled rectangular, tee, and inverted-tee beams (Phase I). The remaining twelve specimens were full-scale TxDOT Type-A beams (Phase II). In the third phase, four of the scaled specimens were tested under fatigue loads (Phase III). Lastly, an initial camber database was compiled of data from 223 pretensioned girders. Twenty-six of these specimens were subjected to compressive stresses at release in excess of $0.60f'_{ci}$; the remaining specimens were conventional, full-scale girders fabricated in the state of Texas.

1.4   CHAPTER OUTLINE

In Chapter 2, a comprehensive literature review is outlined. The history of the allowable compressive stress at release and recent research studies associated with its increase are presented. The early-age mechanical properties of high-strength concrete, such as the stress-strain relationship in compression and the concrete modulus of elasticity, are also discussed. In addition, the behavior of normal- and high-strength concrete in uniaxial compression, due to both initial and sustained loads, is reviewed. Lastly, the equations used in three analysis procedures for estimating prestress losses are provided and described. The three procedures included the PCI Design Handbook Loss of Prestress Estimate (PCI, 2004), the NCHRP Report 496 Detailed Prestress Loss Method (Tadros et al., 2003), and the AASHTO LRFD Refined Loss of Prestress Estimate (AASHTO, Interim 2005).

In Chapter 3, the thirty-six test specimens used in the live-load performance evaluation of the current study are described. Twenty-four specimens were scaled rectangular, tee, and inverted-tee beams fabricated in a previous study, TxDOT Project 4086, with a maximum compressive stress at release ranging from $0.46f'_{ci}$ to $0.91f'_{ci}$ (Castro et al., 2004). The remaining twelve specimens were full-scale TxDOT Type-A girders fabricated at the Heldenfels Enterprises Inc. Corpus Christi, TX precast plant. The maximum compressive stress at transfer ranged from $0.55f'_{ci}$ to $0.75f'_{ci}$ for the Type-A beams.

In Chapter 4, the three phases of the experimental program are described. In phase I, the twenty-four scaled specimens were statically tested in four-point loading to create a constant moment region within the middle third of the span. In phase II, the twelve full-scale girders

were statically tested with a constant moment region equivalent in length to the tests of the scaled beams (5-feet). For all static tests, the measured cracking load of the specimen was experimentally evaluated. In phase III, four scaled beams were subjected to 2-million load cycles. Two of the specimens were conventionally-stressed at release; two were overstressed at release.

In Chapter 5, the results of the live-load performance evaluation part of the current study are presented and analyzed. The measured cracking load of each test specimen was compared to three cracking loads predicted using typical design calculations ($P/A \pm Mc/I$) and the three aforementioned analysis procedures for estimating prestress losses. Recommendations for the feasibility of increasing the allowable compressive stress at release based on the test data are presented.

In Chapter 6, the initial camber investigation of the current study is described. An initial camber database of information from 223 pretensioned girders was assembled and analyzed. Camber measurements from girders subjected to stresses within the allowable limit and to stresses in excess of $0.60f'_{ci}$ at release were included. For all of the pretensioned beams, the measured initial camber was compared to predicted camber. The impact of increasing $0.60f'_{ci}$ on the magnitude of initial camber and on the ability to accurately estimate it was evaluated. In addition, recommendations for improving the accuracy of the camber prediction of conventional girders fabricated in Texas are presented.

Lastly, in Chapter 7, the conclusions and recommendations of the current study are summarized. The effects of increasing the allowable compressive stress at release of $0.60f'_{ci}$ on the live-load performance and the initial camber of pretensioned members are listed. In addition, recommendations for future work are provided.

CHAPTER 2
Literature Review

2.1 OVERVIEW

In this literature review, four main topics related to the effects of increasing the allowable compressive stress at prestress transfer are discussed. First, the background of $0.60f'_{ci}$ is provided followed by recent discussions and research studies that investigated the feasibility of relaxing this allowable stress limit (Section 2.2). Second, the mechanical properties of high-strength concrete at early ages, particularly the modulus of elasticity and the stress-strain curve in compression, are reviewed (Section 2.3). Next, the behavior of normal- and high-strength concrete loaded in compression to various percentages of its ultimate strength is evaluated and quantified (Section 2.4). For this purpose, the effect of both initial and sustained loading is addressed. Lastly, the three analysis methods used in the current study to estimate the prestress loss of the test specimens are described (Section 2.5).

All of the topics reviewed herein are related to the current study, TxDOT Project 5197. The context of the current project was established by reviewing the historical background of $0.60f'_{ci}$ and the recent studies investigating its potential increase. In addition, knowledge of the mechanical properties of high-strength concrete at early ages was necessary to evaluate a stress limit imposed at prestress transfer. In particular, the research on the concrete modulus of elasticity was vital to the initial camber investigation included in the current project. Similarly, examining the performance of concrete under various levels of uniaxial compression was essential to the live-load evaluation part of the current study. This performance provided insight into the behavior of the precompressed tensile zone of a pretensioned member, and thus, into the cracking load of the member. Lastly, the use of three methods for estimating prestress loss was important for the accurate and unbiased prediction of the cracking loads of the test specimens.

2.2 HISTORY OF THE ALLOWABLE STRESSES

Over the last century, the development of code provisions governing the allowable stresses in concrete members has been influenced by many entities. The following section outlines this development with emphasis on the allowable fiber stresses in compression. The origins of these limits are traced back to the earliest provisions for plain and reinforced concrete in which allowable stress design was used. With the introduction of prestressed concrete, compressive stress restrictions were established at prestress transfer and during service. The origin of the compressive stress limit at prestress transfer is a focus of this section. Lastly, recent research studies and published discussions concerning this stress limit and its proposed increase are detailed. The factors investigated in these studies to support the increase of the allowable limit are particularly emphasized.

2.2.1 Code Provisions for Plain and Reinforced Concrete (Kerekes, 1954)

In the early 1900s, as a need for design and construction provisions of structural concrete was becoming apparent, allowable stresses were established for various stress conditions.

Originally, these limits were set to fixed stress values. However, as concrete technology developed and higher strength mixes were created, these limits were defined as percentages of the 28-day compressive strength of concrete. In 1910, the first appearance of these stresses was provided in the "Standard Building Regulations for Reinforced Concrete" (Kerekes, 1954). In this document, the allowable fiber stress in compression was set as $0.325f'_c$. Ultimate concrete compressive strengths up to 2,000-psi were recognized at this time.

In 1916, this stress was updated when the Joint Committee on Concrete and Reinforced Concrete submitted the "First Joint Committee Report on Concrete and Reinforced Concrete." In this document, a distinction between the end conditions of a member was introduced. The allowable fiber stress in compression adjacent to the support of a continuous member was $0.475f'_c$. Everywhere else, the allowable stress was $0.375f'_c$.

In 1925, the allowable stresses changed again. At this time, a second joint committee report was released which changed the working fiber stress to $0.45f'_c$ adjacent to the supports of continuous beams and to $0.40f'_c$ everywhere else. However, at this time, the American Concrete Institute (ACI) did not adopt these values. In ACI, these values were $0.41f'_c$ and $0.375f'_c$, respectively. It was not until 1936, in an updated version of the ACI code, that the allowable fiber stresses were changed to $0.45f'_c$ and $0.40f'_c$ for these two end conditions. Typical concrete strengths reached 3,750-psi at this time.

In 1941, the allowable concrete fiber stress was increased from $0.40f'_c$ to $0.45f'_c$ anywhere along a member. There was no longer a distinction between simple or continuous supports.

Over the next thirty years, the allowable fiber stress in compression did not change. With the introduction and eventual acceptance of *Ultimate Strength Design* as the primary design method in ACI in 1971, the importance of this stress for conventional reinforced concrete diminished. However, with the introduction of prestressed concrete in the U.S. around 1950, allowable fiber stress limits in compression assumed a new responsibility.

2.2.2   Code Provisions for Prestressed Concrete

According to Hawkins, there are two basic forms of prestressing, "circular" and "linear" (Hawkins, 1981). The development of the former technique is credited to the Preload Company of New York. Between 1935 and 1953, this company developed special wire winding machines to stress circular storage tanks. "Linear" prestressing, on the other hand, did not first appear in the U.S. until 1949 with the completion of the Walnut Lane Bridge in Philadelphia. Since this time, "linear" prestressing has experienced a tremendous amount of growth throughout the United States.

In 1942, the first committee on prestressed concrete was organized by the American Concrete Institute. The main purpose of the committee was "to review present knowledge of prestressed concrete, to develop design procedures, and to recommend needed research" (Hawkins, 1981). The committee expanded in 1949 due to the success of the Walnut Lane Bridge and then again, in 1952 to become the joint ACI-ASCE Committee 323 (later Committee 423) on Prestressed Concrete. Over the next several years, the committee focused on developing tentative recommendations for prestressed concrete. During this time as well, the Bureau of Public Roads recognized the need for an American standard code on prestressed concrete. In 1952, they distributed a document of limited design criteria focusing primarily on prestressed concrete bridges. After helpful comments and suggestions from the field, the Bureau published

the "Criteria for Prestressed Concrete Bridges" in 1955 (Erickson, 1957). Shortly there after, in January of 1958, ACI-ASCE Committee 323 released the "Tentative Recommendations for Prestressed Concrete." In both of these documents, the allowable stresses in compression at prestress transfer were identical. For pretensioned members, the stress at release was $0.60f'_{ci}$; for post-tensioned members, it was $0.55f'_{ci}$.

No definitive basis for these values was provided. However, at least two references alluded to the development and to the justification of these limits. In a paper by E. L. Erickson (1957), he stated that several authorities on the subject disagreed in the amount of allowable stresses to be imposed temporarily. For instance, Siess disapproved of $0.60f'_{ci}$ based on variability in concrete strength, reduced capacity due to sustained versus instantaneous loads, and variation of the prestressing force eccentricity. Researchers Hajnal-Konyi and Dobell supported lower release stresses of $0.45f'_{ci}$ and $0.50f'_{ci}$, respectively. On the other hand, some engineers accepted $0.60f'_{ci}$ as long as it was indeed temporary and would be reduced, such as Holley and Simpson. One justification for the 60-percent stress limit was that the highest compressive stress only occurs at the ends of pretensioned members (Erickson, 1957). These recommendations as listed in Table 2-1 suggest that the origin of the allowable release stress in compression was influenced by experimental research. No references were provided by Erickson (1957).

Table 2-1: Recommended levels of initial stress in concrete (Erickson, 1957)

Suggested By	Initial Stress	Condition
Hajnal-Konyi (England)	$0.45f'_{ci}$	---
Dobell (Preload Co.)	$0.50f'_{ci}$	---
Holley (MIT)	$0.60f'_{ci} - 0.40f'_{ci}$	$0.60f'_{ci}$ only if reduced to $0.40f'_{ci}$
Simpson (MIT)	$0.60f'_{ci} - 0.50f'_{ci}$	$0.60f'_{ci}$ only if reduced to $0.50f'_{ci}$
Siess (U. of Illinois)	$< 0.60f'_{ci}$	---
Bureau of Public Roads Criteria	$0.60f'_{ci}$	pretensioning
	$0.55f'_{ci}$	post-tensioning

Another justification of $0.60f'_{ci}$ was found in closing remarks of ACI-ASCE Committee 323 (1958) in regards to published comments concerning the allowable release stress. The following excerpt justified $0.60f'_{ci}$ based on empirical practice:

> *Here, production had preceded design recommendations, and the stress of $0.60f'_{ci}$ had already been widely established in the pretensioning industry. No ill effect had been reported in regard to strength and performance. Only camber proved difficult to control for certain building members (Committee 323, 1958).*

T.Y. Lin (1958) confirmed this empirical relationship, to some degree, in his comment on the recommendations of Committee 323:

> *Most of these values were empirically employed by pioneers of prestressed concrete, who at the time did not have as much knowledge and data as we now have, or as we will have. We as engineers who endeavor to seek the truth and to apply the laws of nature should not blindly follow these empirical values (1958).*

7

Clearly, the origin of the allowable stresses was not the main focus of his comment. Lin disapproved of the inclusion of "definite allowable values for all the stresses under all conditions" (Lin, 1958). He believed that these fixed values would lead to uneconomical and misleading results. In the end, he favored design theories similar to the current *Ultimate Strength Design* method of today in which ultimate strength is satisfied and serviceability is checked separately.

In 1961, the AASHTO Standard Specifications for Highway Bridges accepted $0.60f'_{ci}$ and $0.55f'_{ci}$ for prestressed concrete and post-tensioned concrete members, respectively. Shortly there after, in 1963, ACI Committee 318 adopted $0.60f'_{ci}$ as the allowable compressive stress with no distinction for prestressed or post-tensioned construction. These values are the same today.

2.2.3 Recent Research and Discussion

Over the last decade, the allowable stress in compression at prestress transfer has received an increasing amount of attention. The most recurring reasons for this interest are the economic and performance benefits of relaxing the limit in compression. Several of these benefits include the reduction in production time of precast facilities, the removal of the need for debonded or harped strands, and the increase in the number of prestressing strands in a given section. The following discussions and research studies illustrate the desire to increase the allowable release stress. In addition, these research studies emphasize certain factors that support the increase of the allowable stress limit. These factors are highlighted in the following discussion.

2.2.3.1 PCI Standard Design Practice, 1996, 1997, and 2003

In this document, the PCI Technical Activities Council and the PCI Committee on Building Code discussed certain aspects of the ACI Code that were in conflict with current practice or research. In reference to the allowable compressive stress at release for prestressed concrete, the PCI Committee suggested that the current limit of $0.60f'_{ci}$ is too conservative. For instance, in the first draft of this document, published in the PCI Journal in July/August of 1996, the committee stated:

> *...initial compression is frequently permitted to go higher in order to avoid debonding or depressing strands. No problems have been reported allowing compression as high as $0.75f'_{ci}$ (PCI, 1996).*

However, it seems that several of the reviewers of this document were in opposition. In the March/April PCI Journal of 1997, a second version of the PCI Standard Design Practice was submitted along with several critiques of the original document in the Reader Comments section. In this section, the following comment by Aswad (1997) was found:

> *I am uncomfortable with $0.75f'_{ci}$ for a compression stress right now. This is due to unresolved concerns of excessive creep and micro-cracking that are now being investigated by Professor Bruce Russell. I strongly recommend changing $0.75f'_{ci}$ to read instead: '...$0.67f'_{ci}$ near midspan and $0.70f'_{ci}$ at the beam's ends' (Aswad - PCI, 1997).*

The research investigation by Russell is discussed in Section 2.2.3.2. In the Committees Closure section of the same journal, the committee confirmed that "Several other reviewers were not

comfortable with allowing $0.75f'_{ci}$ for release compression. The document has been changed as suggested, pending results of research" (PCI, 1997). The excerpt on allowable stresses in the revised document reads "No problems have been reported by allowing compression as high as $0.70f'_{ci}$" (PCI, 1997).

In 2003, the PCI Standard Design Practice document was revised again. The new edition was published in the January/February PCI Journal of 2003. In reference to the allowable compressive release stress, the following excerpt appeared:

> *Recent research has shown that the compression limitations at transfer are more conservative than necessary, and have an effect on economy and safety. It has been common practice to allow compression up to $0.70f'_{ci}$ (PCI, 2003).*

The research referred to in this passage is that of Noppakunwijai et al. and is reviewed in Section 2.2.3.4. This version of the PCI Standard Design Practice is current to date.

From this standard design practice document, it is clear that many individuals within the precast/prestressed concrete industry support an increase of the current allowable stress in compression. In fact, it is "common practice" to exceed the code limit (PCI, 2003).

2.2.3.2 Russell and Pang, 1997

Russell and Pang investigated the impact of sustained compressive load on the strength of concrete in compression. To accomplish this task, twelve batches of concrete with 36 cylinders in each batch were cast. Two different concrete mixes were used. Mixture "A' had a nominal 1-day strength of 5,000-psi; mixture "B" had a nominal 1-day strength of 7,000-psi. The other research variables were the age of loading, the stress-to-strength ratio, and the duration of the sustained loading. For each batch, six cylinders were loaded to each of the following stress-to-strength ratios: 0.60, 0.70, and 0.80. For all of the loaded cylinders, unloaded, companion cylinders were cast. After established load duration, three of the loaded cylinders and three of the unloaded cylinders were tested in uniaxial compression.

For cylinders loaded after 1-day of curing and at stress-to-strength ratios of 0.60 and 0.70, the test results did not indicate any reduction in compressive strength. In fact, at these load levels, the compressive strength of the "test" cylinders and the "control" cylinders were essentially equivalent regardless of the load duration and mix design. However, for cylinders loaded at 1 day and to 80 percent of f'_{ci}, the sustained stress prematurely crushed two specimens. Based on the appearance of the failed cylinders, it was determined that they failed under pure compression without any eccentric load. It is interesting to note, however, that for the other cylinders loaded to this 80-percent level that did not fail prematurely, a compressive strength reduction was not detected. In conclusion, Russell and Pang suggested that the data from this portion of the research project supported the possibility of an increase in the allowable compressive stress at release to $0.70f'_{ci}$.

For cylinders loaded after 28-days of curing, significant strength reductions were detected for all of the investigated stress-to-strength ratios. Also, out of the two casts devoted to this loading age, two cylinders at a sustained stress of 80-percent of f'_{ci} failed prematurely. From this data, increasing the allowable compressive stresses for sustained loads was not recommended.

In this study, Russell and Pang experimentally evaluated the effect of varying levels of compressive stress on the compressive strength of concrete. They claimed that their findings indicated that an increase in the allowable compressive stress at release to $0.70f'_{ci}$ was a

possibility. However, this conclusion was based on two out of several dozen cylinders loaded to 0.80f'_{ci} that failed prematurely. No systematic investigation of the probability of failure or the required safety factor to avoid failure was included in the study. Also, of the cylinders loaded to that level that did not fail, no reduction in compressive strength was detected. It seems, therefore, that the compressive strength of concrete is not an adequate material property that can be used to quantify internal damage. Several researchers (Delibes Liniers, 1987 and (Gettu, Aguado, Oliveira, 1996) (Section 2.4.3.1 and 2.4.3.2) suggest other methods to evaluate internal damage.

2.2.3.3 Huo and Tadros, 1997

In the "Open Forum" section of a 1997 issue of the PCI Journal, Huo and Tadros analytically illustrated the behavior of prestressed concrete members at stress levels in excess of 0.60f'_{ci}. To accomplish this task, they performed a linear and a nonlinear analysis of a concentrically prestressed member. The approach consisted of progressively increasing the number of strands until the analysis procedure indicated that the section had failed by the crushing of the concrete ($f_c = f'_{ci}$). As expected, the linear analysis produced different results than the nonlinear analysis. The results demonstrated the inaccuracy of using a linear analysis to predict the failure of concrete members. In addition, the "self-relieving" characteristic of prestressed concrete was introduced.

For the linear and nonlinear analytical procedures, an 18-inch by 18-inch, concentrically prestressed section with the material properties assumed in Table 2-2 was chosen. In each case, the number of strands required to fail the section was theoretically derived. Afterwards, the two solutions were compared.

Table 2-2: Material properties of the 18"x18" member

Normal Weight Concrete	
f'_{ci}	3500 psi
E_{ci}	3587 ksi
Ultimate Concrete Strain (ε_{cu})*	0.003
Strain at peak stress (ε_o)*	0.00225
Prestressing Strands	
Type of strand	½-in. low-relaxation 270 ksi strands
E_{ps}	28,500 ksi
f_{pi}	189 ksi
A_{ps}	Variable

* Used only in the nonlinear analysis

The linear analysis was based on the commonly used relationship of $f = \varepsilon E$, where f is stress, ε is strain, and E is the modulus of elasticity. This relationship was assumed to be valid until failure. Equations 2-1 through 2-3 were used to determine the stresses and strains in the section. As the number of strands increased, the stress in the concrete, f_c, increased. When this stress equaled the strength of concrete at the time of release, f'_{ci}, the section was assumed to fail. This failure condition occurred with 45 strands.

$$f_c = \frac{\left(f_{pi} \cdot A_{ps}\right)}{\left[A_g + (n-1) \cdot A_{ps}\right]} \qquad (2\text{-}1)$$

$$\varepsilon = \frac{f'_{ci}}{E_{ci}} \qquad (2\text{-}2)$$

$$f_{po} = f_{pi} - n \cdot f_c \qquad (2\text{-}3)$$

where, $A_g = 324 \text{ in}^2$
            $n = E_{ps}/E_{ci} = 7.945$

The nonlinear analysis utilized a concrete stress-strain relationship presented by Hognestad as given in Equation 2-4 (1955). From this relationship, concrete was assumed not to fail until the ultimate strain of the concrete was reached, not the ultimate stress. For this study, an ultimate strain of 0.003 was used. It was noted in the study that this condition was consistent with displacement-controlled cylinder tests in which the ultimate strain of the concrete governs the failure. Also, it was suggested that pretensioned beams fail under this same condition. In addition, compatibility and equilibrium requirements of the section were satisfied in the nonlinear analysis. These requirements are presented as Equations 2-5 and 2-6. To analyze the section, Equations 2-4 through 2-6 were solved iteratively. For this purpose, a spreadsheet program was developed. The result of the nonlinear analysis indicated that the section would theoretically fail with 62 strands. The findings of each procedure are compared in Figure 2-1.

$$f_c = f'_{ci} \cdot \left[2 \cdot \frac{\varepsilon}{\varepsilon_0} - \left(\frac{\varepsilon}{\varepsilon_0} \right)^2 \right] ; \; \varepsilon < \varepsilon_{cu} \qquad (2\text{-}4)$$

$$f_{po} = f_{pi} - \varepsilon \cdot E_{ps} \qquad (2\text{-}5)$$

$$f_{po} \cdot A_{ps} = f_c \cdot A_c \qquad (2\text{-}6)$$

Number of strands
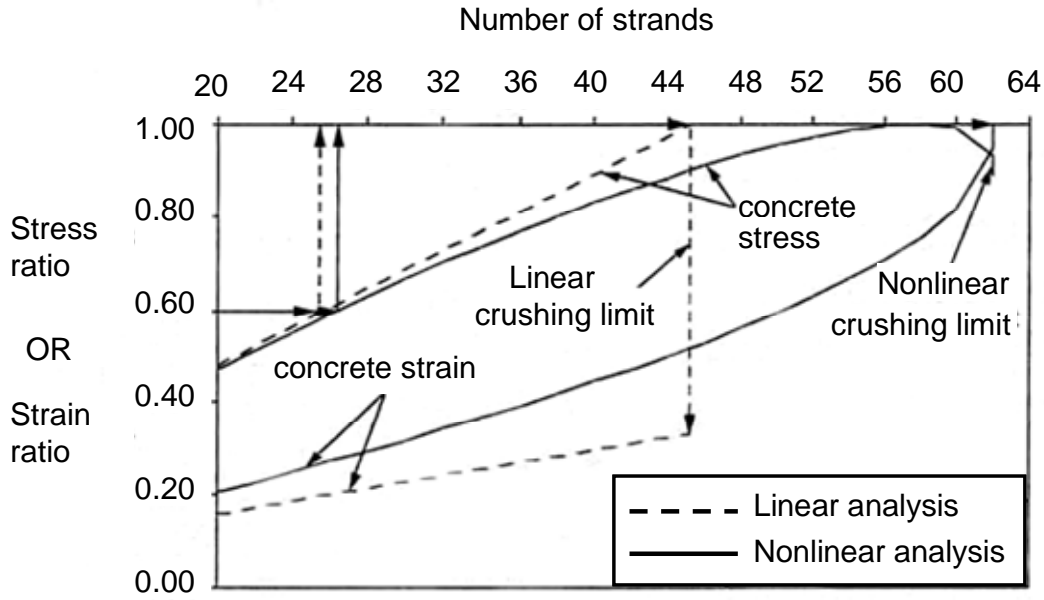
Figure 2-1: Results of linear and nonlinear analyses (Huo and Tadros, 1997)

Based on this analytical study, several observations were made. Huo and Tadros concluded that concrete fails when the ultimate strain is reached, not the ultimate stress. The linear approach indicated that 45 strands would crush the section, while the nonlinear approach indicated that 62 strands were required to crush the section. Also, Huo and Tadros addressed the compatibility of the two approaches up to the current code limit of $0.60f'_{ci}$. At this stress level, the nonlinear approach required 26 strands. The linear approach required 25 strands. As such, a linear analysis approach was accurate up until the current code limit. Lastly, Huo and Tadros addressed the behavior of prestressed concrete members. They noted that a pretensioned member behaves differently from a member subjected to externally applied forces because the pretensioning induces an internal set of stresses in the section. These stresses change as the prestressing force is transferred to the section and as the member undergoes long-term effects. This tendency was described as the "self-relieving" mechanism of pretensioned concrete. As a result, Huo and Tadros stated that stress in the strands before transfer of $0.70f_{pu}$ "can change to a value after release ranging from $0.65f_{pu}$ to $0.38f_{pu}$" (1997). The "self-relieving" mechanism of prestressed concrete is referred to again in Section 2.2.3.4.

In conclusion, Huo and Tadros did not make any definitive recommendations due to the influence of several contributing factors to the relaxation of the limit. They referred to the following factors: creep, shrinkage, concrete strength gain, bond capacity, confinement, and accidental eccentricity of the prestressing force. According to them, these factors had to be investigated before the limit is relaxed.

2.2.3.4 Noppakunwijai, Tadros, Ma, and Mast, 2001

In this research study, Noppakunwijai et al. developed a strength design approach to determine the compressive stress limit at prestress transfer. For a PCI standard, rectangular section, they compared the concrete release strength required by their proposed approach with

12

that provided by the allowable stress limit. Their proposed method produced a concrete release strength, f'_{ci}, that was considerably lower than that allowed in ACI and AASHTO. In addition, they proposed a simplified formula that computed an allowable release stress consistent with their strength design approach. The purpose of this formula was to facilitate the use of a higher maximum release stress with the current design approach until the strength design approach was accepted. Lastly, Noppakunwijai et al. fabricated two beams based on their proposed strength design method and monitored the camber growth and creep strains over time.

Noppakunwijai et al. stated that the purpose of stress limits due to unfactored loads, in general, was for serviceability requirements. Typical requirements include deflection, camber control, crack control, and fatigue. They claimed that the compressive stress limit at prestress transfer, however, "appears to be an indirect way of checking that concrete will not 'crush' due to prestress transfer" (Noppakunwijai et al., 2001). For this reason, they did not consider the compressive stress limit as a serviceability limit; and therefore, they suggested that it should be based on a strength design approach. Noppakunwijai et al. suggested that their approach was more consistent with current design practice for strength-related issues. Furthermore, they clarified that the tensile stress limit at release was a serviceability limit. The reason for this designation was that the tensile limit evaluates whether a section was cracked and therefore, met the necessary criterion.

Based on this justification, a strength design approach was developed to determine the allowable compressive stress at prestress transfer. The approach treated the prestressed beam as a reinforced concrete column subjected to an axial force and a corresponding moment consistent with the force in the prestressing strand at a given eccentricity. A load factor of 1.2 was applied to the initial prestressing force. Load factors of 0.8 or 1.2, based on the direction, were applied to the self-weight moment. A strength reduction factor, φ, of 0.70 was applied to the nominal axial and the bending moment capacities. The section was analyzed using typical flexural theory assumptions. The force diagram used in the sectional analysis is provided in Figure 2-2. Lastly, the strain compatibility and the equilibrium conditions of the section were met. These conditions are represented in Equations 2-7 through 2-10. From these relationships, the approach presented four equations with five unknowns: a, f'_{ci}, f'_s, f_s, and A'_s. Noppakunwijai et al. suggested choosing a certain concrete release strength or area of top tension steel and subsequently, solving for the other. These quantities directly depended on one another.
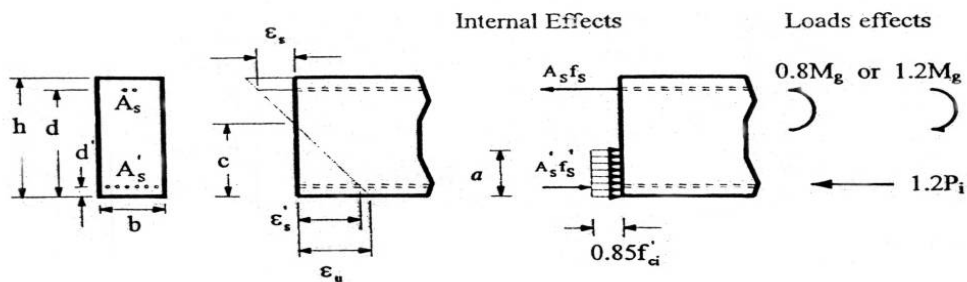
Figure 2-2: Force diagram for strength design method (Noppakunwijai et al., 2001)

$$\varepsilon'_s = \left(\frac{c-d'}{c}\right)0.003; \qquad f'_s = \varepsilon'_s E_{ps} \tag{2-7}$$

$$\varepsilon_s = \left(\frac{d-c}{c}\right)0.003; \qquad f_s = \varepsilon_s E_s \tag{2-8}$$

$$0.85 f'_{ci} ba + A'_s f'_s - A_s f_s = \frac{1.2 P_i}{\phi} \tag{2-9}$$

$$0.85 f'_{ci} ba\left(\frac{a}{2} - d'\right) - A_s f_s (d - d') = \frac{(0.8 \ \ or \ \ -1.2) M_g}{\phi} \tag{2-10}$$

With the proposed approach, the required compressive strength at release as a function of the area of top reinforcement for a PCI standard rectangular section, 16RB40, was computed. At the required amount of top reinforcement according to ACI and the PCI Design Handbook, the concrete release strengths obtained from each approach were compared. The release strength based on an allowable compressive stress at release of $0.60 f'_{ci}$ was 4,622-psi. The release strength obtained from the proposed strength design approach was 3,811-psi. This concrete strength corresponds to an equivalent compressive stress limit of $0.73 f'_{ci}$. The results of the comparison are illustrated in Figure 2-3.
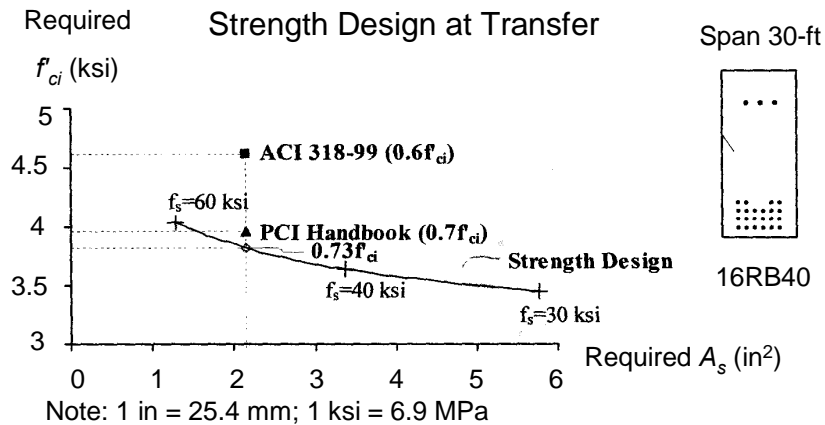
Figure 2-3: The results of the proposed strength design method (Noppakunwijai et al., 2001)

In addition, Noppakunwijai et al. emphasized that a major advantage of the proposed approach was the ability to rationally size top reinforcement. Currently, ACI specifies the area of top reinforcement to be based on an uncracked sectional analysis in which a steel stress of 30-ksi cannot be exceeded. The proposed strength design method allowed the amount of top reinforcement to vary based on the targeted concrete release strength.

Next, a formula was developed to replace the uniform value of $0.60 f'_{ci}$. Accordingly, designers could take advantage of higher release stresses as determined by the new strength design method without giving up the traditional stress approach. The formula was based on the cross-sectional geometry of a member and compared favorably with the results of their strength design approach. The formula is included as Equation 2-11.

14

$$K = \left(0.60 + \frac{y_b}{5 \cdot h}\right)f'_{ci} \le 0.75f'_{ci} \qquad (2\text{-}11)$$

Lastly, to examine the effects of allowable stresses in excess of $0.60f'_{ci}$ on the creep and camber performance of a prestressed member and to validate their proposed design method, two inverted-tee specimens were fabricated. The targeted compressive stresses at release for the two specimens were $0.85f'_{ci}$ at the end of the member and $0.71f'_{ci}$ at midspan. Type III cement was used with ready mixed concrete. One day after the beams were cast, detachable mechanical strain (DEMEC) gauges were attached to the concrete surface to measure the change in concrete strain over time. Then, the beams were released. The actual stresses at the end of the member were calculated as $0.79f'_{ci}$ for Specimen 1 and $0.84f'_{ci}$ for Specimen 2. For reference, the concrete strength for Specimens 1 and 2 were 5,900-psi and 5,600-psi, respectively. No visual indications of damage were observed for the specimens.

Over approximately 100-days, the creep, shrinkage, and camber performance of the beams were measured. The authors were able to predict the change in concrete strain over time due to creep and shrinkage with available methods. In addition, the initial and long-term camber at midspan were monitored and predicted well within reasonable margins of error. As a result, the authors detected no negative impact due to the increased levels of compressive stress at release. The authors justified these findings based on the nature of bonded pretensioned girders. They claimed that these girders are "an internal system of forces that has some degree of self-adjusting capability" (Noppakunwijai et al., 2001). As a result, increased stresses at release cause increased amounts of prestress loss which, in turn, reduces the stress on the section. In addition, the authors emphasized that a pretensioned girder is not as stressed as a conventional linear analysis would suggest. In fact, an inelastic analysis of the section at high levels of compressive stress reveals lower stresses on the section.

In conclusion, Noppakunwijai et al. suggested that the allowable compressive stress limit at prestress transfer be eliminated. The proposed strength design approach would be used in its place. However, before its official adoption, Equation 2-11, based on the cross-sectional geometry of the section, would replace the current uniform value of $0.60f'_{ci}$. They justified their findings by their ability to accurately estimate the creep, shrinkage, and camber performance of two overstressed beams.

The entire premise of the strength design approach was based on the claim that the compressive stress at release is not a serviceability limit. This claim is the only justification for creating a strength design approach to calculate the allowable compressive stress at release. Currently, in the ACI code, the stress limit of $0.60f'_{ci}$ is listed in Section 18.4 as a "serviceability requirement." In addition, several researchers have suggested that concrete loaded in excess of 60-percent of its strength experiences microcracking and unwanted creep effects (Section 2.4). From these studies and the findings of the current research project, $0.60f'_{ci}$ appears to be a serviceability limit.

2.2.3.5 Readers Comments in PCI Journal (Seguirant, 2002)

In the January/February 2002 edition of the PCI Journal, Steve Seguirant, the Director of Engineering at Concrete Technology Corporation, listed his comments and concerns with the strength design approach of Noppakunwijai et al. Initially, Seguirant commended the authors for

creating a rational approach to an important issue. In addition, he referred to the historical background of the allowable release stresses. He stated "the current code requirements are arbitrary at best, and are not based on science or research…these arbitrary provisions are limiting the span capabilities of pretensioned concrete flexural members" (Seguirant, 2002).

Throughout the discussion, Seguirant listed some concerns with the proposed design approach. The most relevant issue to this research study was his disapproval of the approximate formula, provided as Equation 2-11. In this equation, the allowable release stress is calculated as a function of the section geometry. As a result, there is no longer a correlation between the release strength of concrete and the area of top reinforcement, one of the advantages of the strength design approach. In conclusion, Seguirant stated:

> *In my opinion, there seem to be enough questions associated with the approximate formula that it should be abandoned. I was hoping that the research would indicate a simple single value of K, somewhat higher than 0.6, that would be applicable to all conditions. This does not appear to be the case. If the designer does not wish to use the strength design method, then the current rules should apply (Seguirant, 2002).*

In this quote, 'K' is the coefficient multiplying the strength of concrete at release. For the current allowable stress $0.60f'_{ci}$, 'K' equals 0.60.

2.2.3.6 Readers Comments in PCI Journal (Noppakunwijai et al., 2002)

In the same January/February 2002 edition of the PCI Journal, Noppakunwijai et al. responded to all of Seguirant's concerns. In regards to the historical background of the current provisions, they reinforced their position by stating that "It is time to remove some of the unnecessary conservatism created when this material was introduced" (Noppakunwijai et al., 2002). Later on in the discussion, Noppakunwijai et al. addressed the issue of the approximate formula. By and large, they agreed to the limitations of the approximate formula and in short, supported the use of the strength design approach as the primary design technique.

2.2.3.7 Castro, Kreger, Bayrak, Breen, and Wood, 2004

This research study, referred to as TxDOT Project 4086, was funded by the Texas Department of Transportation and conducted at the University of Texas at Austin from September 2001 to August 2003. The results of this study initiated the current research project described herein, TxDOT Project 5197. More specifically, the beams fabricated under Project 4086 were used in the live-load testing portion of Project 5197. The factors influencing the design and fabrication of these specimens are provided in sufficient detail in Section 3-2. In addition, the concrete mix properties used in this study and the inventory of all of the fabricated section types are provided in Tables 3-5 and 3-6, respectively.

In Project 4086, Castro et al. investigated the feasibility of increasing the allowable compressive stresses at prestress release. To accomplish this task, 30 scaled pretensioned beams were fabricated with varying levels of stress at prestress transfer. The compressive stresses at release ranged from $0.46f'_{ci}$ to $0.91f'_{ci}$. The variables investigated in the experimental program included: the maximum stress at prestress release, the cross-section geometry, the rate of strength gain, and the concrete mix design. Only the observations concerning the stresses at release are presented herein.

To assess the impact of increasing the allowable stress at prestress release, the behavior of each of the beams was monitored when the prestressing force was transferred to the beam and for 90-days afterwards. In particular, the initial and long-term camber was monitored. This experimental data were compared to predicted values of initial and long-term camber. Three techniques were employed to predict these values. In two techniques, camber was calculated by numerical integration of the curvature distribution determined by either strain-compatibility or a layered, non-linear analysis. For the long-term camber calculations within these two procedures, prestress losses due to creep, shrinkage, and relaxation were accounted for. The last camber prediction technique included the use of the initial and long-term PCI camber equations. The initial camber equation corresponds to the linear-elastic procedure relating curvatures to moments in which the dead load deflection is subtracted from the upward deflection due to the eccentric prestressing force. To calculate long-term camber, PCI suggests multiplying the deflection due to dead weight and due to the eccentric prestressing force by constants. The results presented by Castro et al. were the camber values predicted with the elastic, strain-compatibility approach.

After the beams were fabricated and monitored for 90-days, the impact of varying levels of stress at release on camber growth was evaluated. The 10-day and 90-day measured camber for all of the specimens were compared to estimated values. From the results, several observations were made. Camber increased in all cases with increasing levels of stress at prestress transfer. In general, the 10-day camber was more accurately predicted for beams subjected to release stresses within the allowable limit than for beams subjected to higher release stresses. This observation illustrated the negative effect of the stresses at release on initial camber. The 90-day camber, on the other hand, was generally more accurately predicted than the short-term camber even though it was not always conservatively predicted. From these observations, Castro et al. concluded that pretensioned concrete beams could be subjected to stresses exceeding the allowable limit "as long as long-term camber response is adequately predicted and values are acceptable to the engineer of record" (2004).

At the conclusion of the research project, it became clear that a recommendation to relax the maximum allowable compressive stress at prestress transfer could not be made without a better understanding of the impact of increasing this limit. In essence, Castro et al. (2004) recommended that the impact of elevated compressive stresses on the live load performance of the girder must be evaluated before the allowable stress is changed. These additional conclusions are reported in TxDOT Report 0-4086-S (Kreger and Bayrak, 2005). As a result, TxDOT Project 5197, the project that is described in this report, was initiated.

2.2.3.8   Chairman's Message in PCI Journal (D'Arcy, 2005)

In the July/August 2005 edition of the PCI Journal, D'Arcy outlined the indications of good prestressed concrete design with his message entitled "Good Performance – The Engineer's Quest." Within this article, he stated:

> *...the essence of a sound design is twofold: (1) good performance under service loads, overload conditions, and environmental conditions, and (2) integrity of the structure at the end of its intended service life. Too many engineers focus only on stresses and ultimate capacity, ignoring such effects as camber and deflection (D'Arcy, 2005).*

17

In essence, D'Arcy supported a performance-based design approach in which "artificial stress limits" are not always satisfied but "the members absolutely perform better" (D'Arcy, 2005). Controlling the deflection and the camber are the primary design concerns. In addition, he included additional design guidelines that mirrored the findings of the PCI Standard Design Practice to support his concepts. In these guidelines, D'Arcy referenced the allowable release stress in compression. He stated:

> *Research has shown that pretensioned members can perform well even with release stresses up to 0.90f'$_{ci}$. Therefore, a nominal increase to 0.75f'$_{ci}$ would appear appropriate. This adjustment would provide more efficiency in production and better camber control (D'Arcy, 2005).*

A reference for the research referred to in this quote was not provided. In the subsequent edition of the PCI Journal, two engineers submitted comments referring to the allowable stress at prestress transfer. A summary of their comments are listed herein.

In the September-October 2005 issue of the PCI Journal, Professor Maher K. Tadros replied to the Chairman's Message by D'Arcy. Tadros congratulated the proposal of the chairman to search for innovation in the engineering field and to question assumptions and design procedures of the past. In particular, Tadros showed his support for the removal of the "artificial compressive stress limits" in reference to the allowable compressive stress at release of a pretensioned girder. While illustrating the benefits of the removal of this limit on the precast/prestressed industry, he also pointed out that the "structure must perform well during its service life" (Tadros, 2005). The primary concerns he referred to are deflection and camber.

Also, Stephen J. Seguirant responded to the Chairman's Message by Chairman Tom D'Arcy. In his reply, Seguirant agreed with the chairman's appraisal that camber and deflection are more important to the performance of a pretensioned girder than any arbitrary stress. Later in his reply, Seguirant addressed the allowable compressive stress at release. He noted that "several years ago" ACI 318 did not increase the release stress from 0.60f'_{ci} to 0.70f'_{ci} by only a few votes (Seguirant, 2005). The primary concerns were microcracking and increased creep. Furthermore, he stated that an increase in stress at the member ends to 0.75f'_{ci} would be appropriate based on research in which release stresses as high as 0.84f'_{ci} at member ends did not cause problems. This research was reviewed in Section 2.2.3.4. Lastly, he encouraged the funding of further research to investigate allowable stresses at release. He emphasized flexural members with harped strands in which high release stresses are near midspan.

2.2.3.9 Hale and Russell, 2006

In this investigation, Hale and Russell fabricated four pretensioned girders and monitored their prestress loss for one year. At release, these girders were subjected to varying levels of compressive stress. The stress ranged from 0.57f'_{ci} to 0.82f'_{ci}. The purpose of the study was twofold. The first objective was to compare the measured prestress losses with three prestress loss prediction methods used in design practice. The three prediction methods included the AASHTO LRFD Bridge Design Specifications method (2004), the PCI Design Handbook method, and the NCHRP Report 496 method. Additionally, the prestress losses of pretensioned beams subjected to elevated compressive release stresses were documented in this study. In this task, Hale and Russell addressed "whether the losses indicate that a damaged condition exists in the concrete due to excessive compressive stress at release" (2006).

Four I-shaped girders were fabricated with an overall depth of 24-inches and a length of 24-feet. The concrete used in this study was composed of Type III cement, crushed limestone from Davis, Oklahoma, washed river sand from Dover, Oklahoma, and water-reducing admixtures. Two different mixture designs were used. The differences between the mixture designs were the amount of entrained air and the amount of river sand. The components of the two designs and the designation of the girder to mixture design are provided in Table 2-3. As seen in this table, two beams were cast from each mix. However, the targeted release stresses for the girders with the same concrete were $0.60f'_{ci}$ and $0.75f'_{ci}$. Since the girders with the same concrete were cast on the same line, the amount of debonding in each beam varied to obtain different release stresses. Prior to the release of the specimens but after the forms were removed, detachable mechanical strain (DEMEC) gauge targets were attached to the concrete surface. These instruments were applied in several locations to measure the loss of the prestressing force.

Table 2-3: Mixture proportions for girders 1 to 4 (Hale and Russell, 2006)

	Girders 1 and 4	Girders 2 and 3
Cement (lb/yd^3)	900	900
Coarse aggregate (lb/yd^3)	1790	1790
Fine aggregate (lb/yd^3)	1217	1040
Water (lb/yd^3)	234	234
Water-cementitious ratio	0.26	0.26
Targeted total air content (%)	2	6
Calculated unit weight (lb/ft^3)	153.4	146.8

At release, the concrete strength of the beams was not as expected and therefore, the targeted stresses at release of $0.60f'_{ci}$ and $0.75f'_{ci}$ were not met. Instead, the maximum compressive stress at release of girders 1 through 4 was $0.65f'_{ci}$, $0.82f'_{ci}$, $0.69f'_{ci}$, and $0.57f'_{ci}$, respectively. These stresses were calculated using the transformed section properties, the initial prestressing force, and the allowable stress design equation ($P/A \pm Mc/I$). In the three cases in which the stress exceeded 60% of the release strength of the concrete, an effective modulus was used in the computation of the transformed properties and the elastic shortening losses. This effective modulus was represented as the slope of a secant line through the origin and the point on Hognestad's parabola that corresponded to the concrete stress required to provide equilibrium.

The prestress loss in each of the beams was monitored for one year. These measured losses were compared to the predicted losses calculated using the AASHTO LRFD Bridge Design Specifications method (2004), the PCI Design Handbook method, and the NCHRP Report 496 method. In general, the NCHRP Report 496 method predicted the losses more accurately than the other two procedures. However, this method slightly underestimated the losses, producing an estimate on the unsafe side. The AASHTO method and the PCI Design Handbook method both overestimated the total losses, providing a conservative estimate. The ratio of the measured to the predicted losses of the four girders is given in Table 2-4. The compressive stress at release is included for reference.

19

Table 2-4: Ratio of Predicted to Measured Prestress Losses (Hale and Russell, 2006)

Girders	Release Stress (% of f'_{ci})	Location	Ratio of Measured to Predicted Losses		
			AASHTO 2004	Zia et al. (PCI)	NCHRP Report 496
1	64.9	Ends	0.72	0.81	1.07
		Center	0.68	0.77	1.01
2	82.1	Ends	0.92	0.89	1.04
		Center	0.95	0.92	1.08
3	69.3	Ends	0.93	0.94	1.05
		Center	0.92	0.94	1.05
4	56.9	Ends	0.73	0.84	1.08
		Center	0.74	0.84	1.09
Average			0.82	0.87	1.06

The total amount of prestress losses increased with increasing compressive release stress. In fact, Hale and Russell noted that the measured prestress loss as a percentage of the initial jacking stress was proportional to the compressive stress at release. This ratio was essentially the same for all four beams. Furthermore, this relationship was used to claim that a damaged condition does not exist in the overstressed girders. In the words of the authors:

> ...the ratio of losses to release stresses is approximately the same for all four beams regardless of the amount of compressive release stresses...It is the authors' view that these data provide strong evidence that the allowable release strength of 0.60f'_{ci} can be relaxed to allow higher compressive stresses to be imposed on the concrete immediately after release (Hale and Russell, 2006).

The ratios described herein are listed in Table 2-5. At the conclusion of the study, Hale and Russell recommended the increase of the current allowable stress limit of 0.60f'_{ci} to 0.70f'_{ci} based on the results of this research.

Table 2-5: Prestress Loss Effects of Large Compressive Stresses at Release (Hale and Russell, 2006)

Girders	1	2	3	4	5
	Release Stress (%)	Measured Pre-stress Loss (ksi)	Jacking Stress (ksi)	(2)/(3) (%)	(4)/(1)
1	64.9	56.8	204.25	27.8	0.43
2	82.1	72.0	202.20	35.6	0.43
3	69.3	59.2	200.76	29.5	0.43
4	56.9	51.6	204.47	25.2	0.44

In this study, the loss of prestressing force was evaluated for beams subjected to elevated release stresses. The proportional increase in losses with release stress was perceived as a positive indication for an increase in the allowable compressive stress at release. However, it is

unclear how the results of the study supported an increase to $0.70f'_{ci}$ when all four beams behaved similarly according to their criteria. By their standards, an increase to $0.82f'_{ci}$ was justified. In addition, to accurately estimate the inelastic deformation at prestress transfer of the overstressed girders, the nonlinear behavior of the concrete was taken into account. This practice is not typical in current prestressed concrete design.

2.2.3.10 Summary of recent research

In the research studies summarized in the preceding sections, several effects of increasing the allowable stress in compression at prestress transfer were investigated. The effects studied in each research project are summarized in Table 2-6. For the most part, the evaluation of these effects positively supported the increase of the compressive stress at release.

Table 2-6: Effects of increasing the release stress: summary

Researchers	Studied Effects of Increasing Release Stress	Scope of Experimental Work
Russell and Pang (1997)	Compressive strength	432 – cylinders
Huo and Tadros (1997)	Nonlinear behavior	None
Noppakunwijai et al. (2001)	Creep, shrinkage, camber, and transverse strain	2 – IT girders
Castro et al. (2004)	Camber	30 – Rect., IT, T girders
Hale and Russell (2006)	Effective prestressing force	4 – I girders

2.3   PROPERTIES OF HIGH-STRENGTH CONCRETE AT EARLY AGES

Throughout the precast/prestressed concrete industry, high-strength concrete (HSC), $f'_{ci} >$ 7,000-psi, is extensively used to maintain an efficient production schedule. The mechanical properties of HSC are significantly different from conventional, normal-strength concrete (NSC). As a result, over the last few decades, extensive research has been conducted to evaluate the performance of high-strength concrete at mature ages. However, only a few research investigations have focused on the properties of high-strength concrete at early ages. In these studies, early age properties are considered those properties measured within the first 24-hours of initial casting. The following review focuses on the stress-strain curve in compression, the modulus of elasticity, and the tensile strength of concrete particularly within the first 24-hours of casting. The two objectives of this section are (i) to highlight the mechanical properties of high-strength concrete at typical release times and (ii) to research the main contributors to an effective estimation of the modulus of elasticity at early ages.

2.3.1   Khan, Cook, and Mitchell, 1995

In this study, Khan, Cook, and Mitchell investigated stress-strain characteristics of low-, medium-, and high-strength concrete subjected to compression at early ages. In addition, they addressed the effects of different curing conditions on the mechanical properties of concrete, the effects of different strength mixtures on the temperature rise in large masses of concrete, and the

adequacy of empirical modulus of elasticity equations at various strength levels. This review focuses on the compressive strength gain and the modulus of elasticity of the different mixtures over time.

The three mixes corresponding to low-, medium-, and high-strength concrete had approximate 28-day strengths of 4,000-psi (30-MPa), 10,000-psi (70-MPa), and 14,500-psi (100-MPa). In all of the mixes, limestone was used as the coarse aggregate; one type of river sand was used as the fine aggregate. To facilitate demolding at early ages, special plastic molds were used. Sulfur capping was performed on all of the cylinders tested at an age of less than 24-hours. At ages greater than 24-hours and for only the medium- and high-strength mixes, the end surfaces were ground. For the compression tests, the cylinders were loaded in increments of strain to acquire the post-peak response.

For a given curing condition, cylinders were tested in compression at frequent intervals particularly within the first 24-hours. After which, the time between each test varied based on the curing condition. In each case, however, a response consistent with that of mature concrete was obtained. Khan et al. discovered that during the first few hours of hydration, all of the mixes exhibited "extremely low moduli, low compressive strength, and very high strains corresponding to the peak compressive stress" (Khan, Cook, and Mitchell, 1995). In fact, it was not until approximately 24-hours of curing that the stress-strain behavior resembled that of a 28-day-old specimen. The stress-strain response for a temperature-controlled, 10,000-psi mix at several ages is illustrated in Figure 2-4. According to this plot, at 16½-hours, a relatively high-strength concrete mix deformed considerably more nonlinearly than at 3-days.
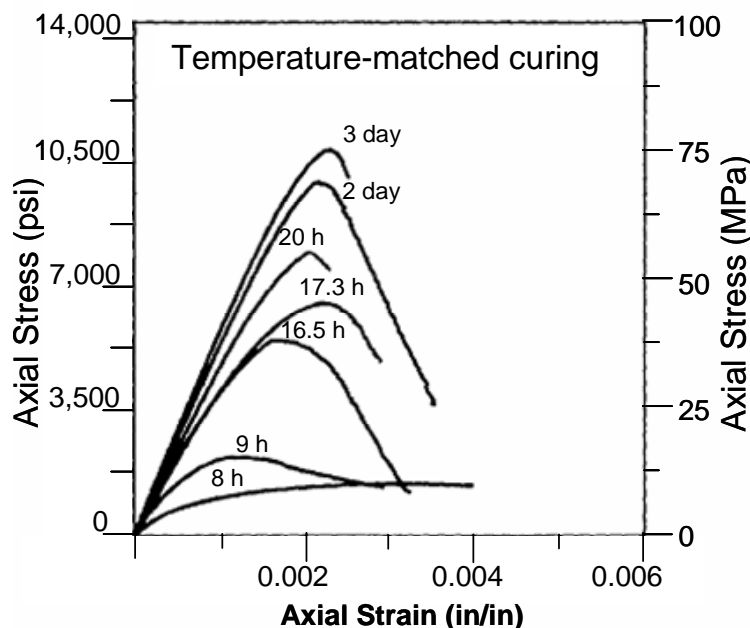
Figure 2-4: Stress vs. strain plots of a 10,000-psi concrete mix at various ages (Khan, Cook, and Mitchell, 1995)

In addition, Khan et al. compared the measured modulus of elasticity according to ASTM C469-94 with two commonly used empirical relationships. The first expression was adopted by

22

ACI-318 and was originally derived in 1960 by Pauw for normal-strength, normal-weight and lightweight concrete (Pauw, 1960). In response to the development of high-strength concrete, Carrasquillo, Nilson, and Slate derived another expression in 1981 (Carrasquillo et al., 1981). This expression was adopted by ACI-363 and applies to normal weight concrete with strengths between 3,000- and 12,000-psi. These relationships are included as Equations 2-12 and 2-13, respectively.

$$E_c = w_c^{1.5} \cdot 33 \cdot \sqrt{f'_c}\, psi \tag{2-12}$$

where, w_c = unit weight of concrete (pcf)
f'_c = compressive strength of the concrete (psi)

$$E_c = 40,000\sqrt{f'_c} + 1.0x10^6\, psi \tag{2-13}$$

where, f'_c = compressive strength of the concrete (psi)

Khan et al. evaluated the adequacy of these expressions from very early ages to 91 days for all of the mixes. Based on their results, they concluded that both of these expressions were not appropriate at early ages. In both cases, the expressions overestimated the modulus for concrete at very low strengths and at early ages. However, it is important to note that at a typical prestress release strength of approximately 4,000-psi, the modulus was well predicted by both expressions. For concrete strengths exceeding 7,000-psi, the ACI-363 expression was considerably more accurate. These findings are demonstrated in Figure 2-5.
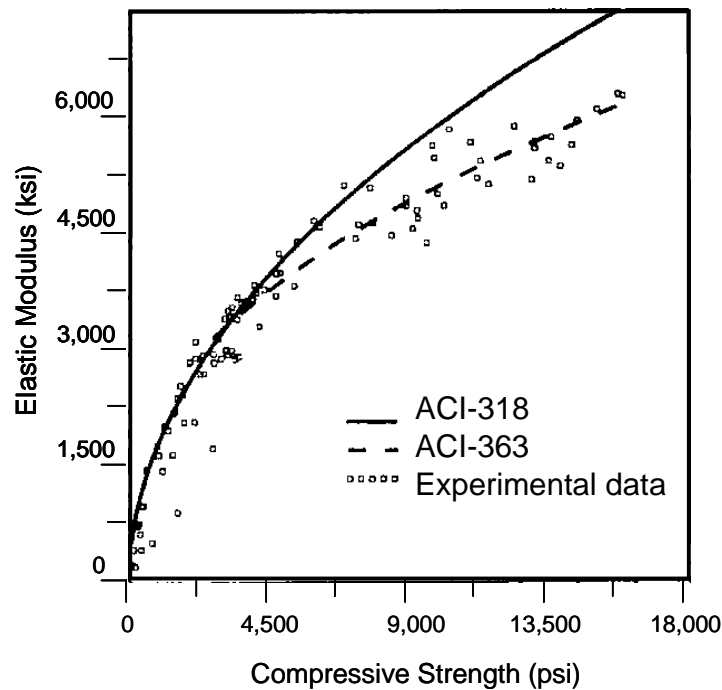
Figure 2-5: Average elastic modulus values versus the average compressive strength of concrete at various ages (Khan, Cook, and Mitchell, 1995)

23

2.3.2   Cetin and Carrasquillo, 1998 and Myers and Carrasquillo, 1998

In this research project, high performance concrete typically used in Texas bridges was evaluated. In one portion of the project, the effects of the coarse aggregate type on the static modulus of elasticity were investigated. Four different rock types consisting of trap rock, dolomitic limestone, calcitic limestone, and crushed river gravel were used. Also, the amount of coarse aggregate in each mixture design varied as 36-, 40-, or 44-percent of the total weight of the mixture. The standard cylinder compression test ASTM C39-93 and the standard cylinder modulus of elasticity test ASTM C469-94 were performed at 1-, 7-, 28-, and 56-days.

The measured modulus of elasticity data revealed a relationship between the modulus and both the aggregate type and the rock content. Regardless of the percentage of coarse aggregate, the concretes with trap rock, dolomitic limestone, and crushed river gravel exhibited modulus values higher than the ACI-318 and ACI-363 empirical expressions for a wide range of compressive strengths. On the other hand, the modulus of elasticity of the calcitic limestone concrete was accurately estimated by the ACI-363 expression for the most part. In regards to the influence of the rock content on the modulus of elasticity, the elastic modulus slightly increased as the coarse aggregate content increased. All of these results are depicted in Figure 2-6 to 2-8.

1 ksi = 6.895 MPa
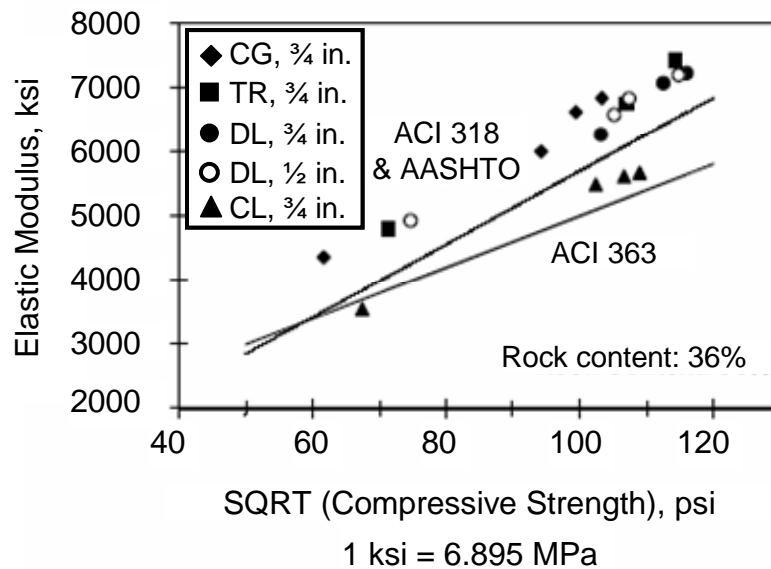
Figure 2-6: Elastic modulus development for concretes with 36% aggregate content (Myers and Carrasquillo, 1998)

24
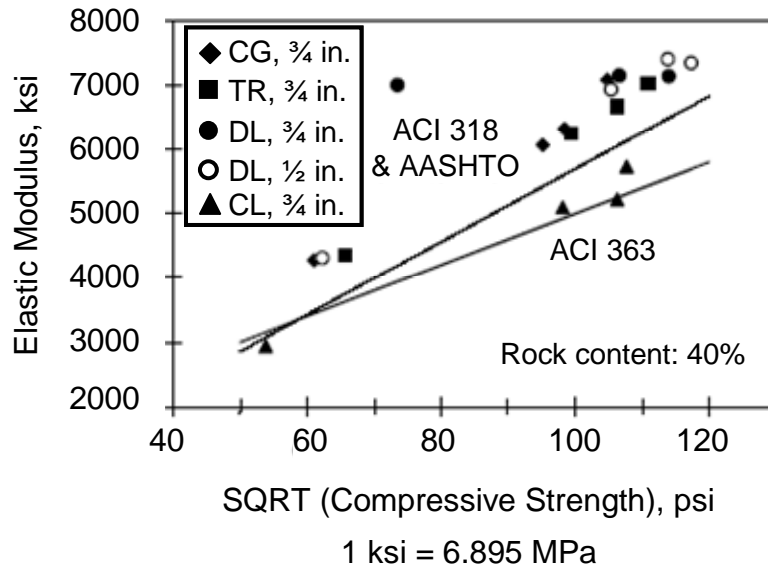
Figure 2-7: Elastic modulus development for concretes with 40% aggregate content (Myers and Carrasquillo, 1998)
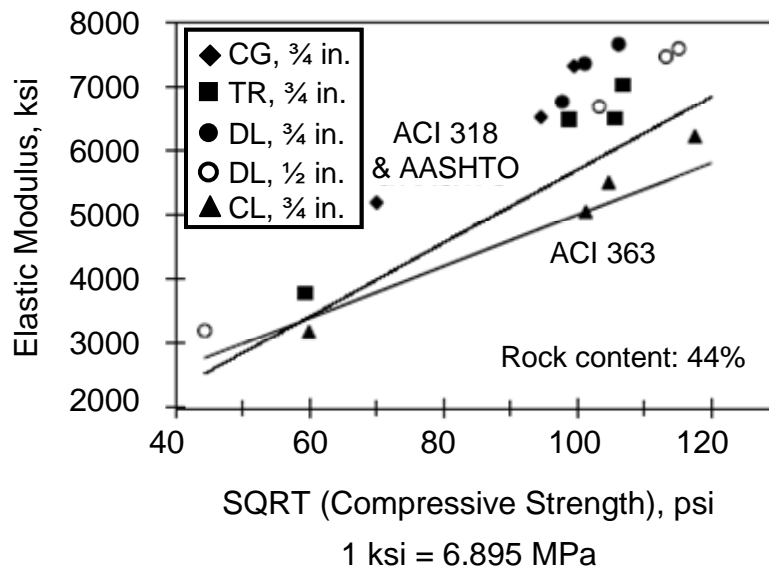
Figure 2-8: Elastic modulus development for concretes with 44% aggregate content (Myers and Carrasquillo, 1998)

In conclusion, Cetin and Carrasquillo noted that a "single empirical equation to estimate the elastic modulus with reasonable accuracy" does not exist for high-performance concrete (1998). They attribute this fact to the maturity of the cement paste and the increased importance of coarse aggregate type in high-performance concrete. For these concrete mixes, it is important to note that the modulus of 1-day concrete ranged from approximately 60- to 75-percent of the modulus of mature concrete.

25

2.3.3 Mokhtarzadeh and French, 2000

In this comprehensive research investigation, over 6,000 tests were performed to evaluate the compressive strength, modulus of elasticity, and tensile strength of high-strength concrete. Several mix designs were incorporated into this study with 28-day compressive strengths ranging from 8,000 to 18,600-psi. Some variables of the mix designs included the use of Type I and Type III cement, various percentages of silica fume and fly ash, five types of superplasticizer, and several different coarse aggregates, namely limestone, granite, and river gravel. For the purposes of this discussion, only the results of the modulus of elasticity portion of the testing program are reported.

In the modulus of elasticity investigation within this research project, the following variables were evaluated: specimen size, specimen age, and aggregate type. In regards to specimen size, 202 companion pairs of cylinders were tested according to the standard modulus of elasticity test, ASTM C469. Each pair consisted of a 4x8-inch cylinder and a companion 6x12-inch cylinder and was cast at the same time and with the same concrete mix. This data, presented in Figure 2-9, suggested that the measured modulus from 4x8-inch cylinders is on average 620-ksi higher than that from 6x12-inch cylinders.
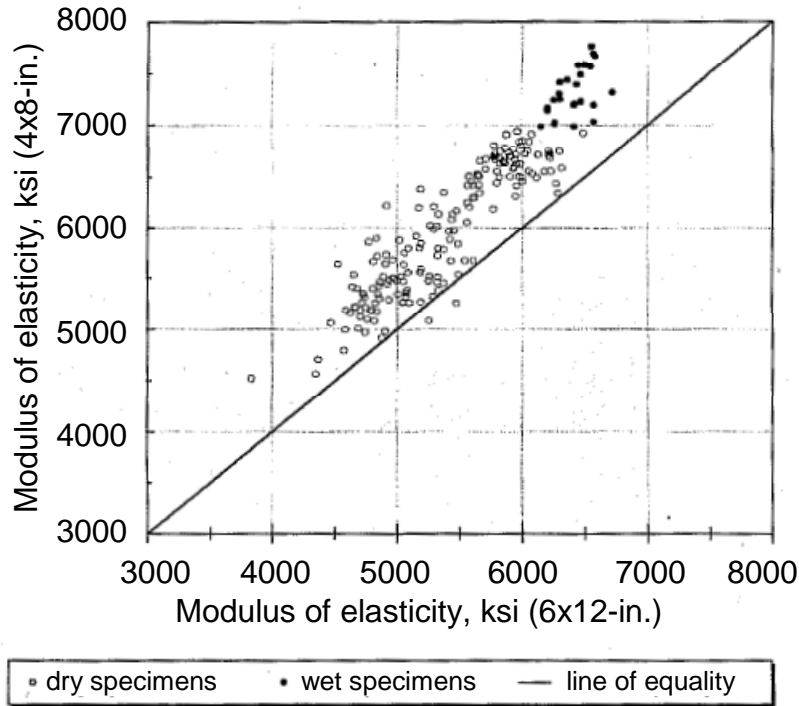
Figure 2-9: Effect of cylinder size on static elastic modulus of elasticity tests (Mokhtarzadeh and French, 2000)

The early-age growth of the static modulus of elasticity was also investigated. According to 314 sets of heat-cured specimens, the 1-day modulus was approximately 98-percent of its 28-day value. In the compressive strength portion of this study, Mokhtarzadeh and French reported the 1-day strength of heat-cured concrete as a percentage of the 28-day strength. For high-

26

strength concrete, this ratio ranged from 0.79 to 0.93. As such, it is probable that the early-age modulus was considerably higher than expected.

In regards to the coarse aggregate type, a significant amount of scatter was present. In general, the stiffness of concretes with river gravel was higher than that with limestone. However, Mokhtarzadeh and French (2000) indicated that it was "difficult to generalize a coefficient for a certain aggregate type because the relative aggregate properties may vary from one source to another." As seen in Figure 2-10, these data were plotted along with the ACI-318 and ACI-363 expressions. In general, the modulus of elasticity of the mixtures that contained round gravel exceeded both the ACI-318 and the ACI-363 empirical expressions for a wide range of compressive strengths. The elastic modulus of the concrete with limestone as the coarse aggregate, on the other hand, primarily fell between the two expressions. For the limited data with compressive strength values less than 8,000-psi, the ACI 318 expression considerably underestimated the modulus of elasticity of the concrete with the round gravel and accurately estimated that of the concrete with the limestone aggregate.
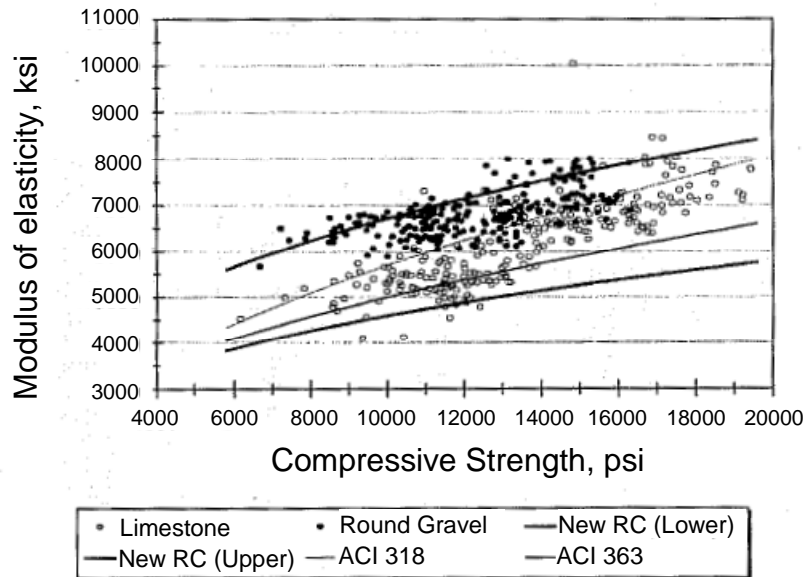
Figure 2-10: Effect of aggregate type on static modulus of elasticity tests (Mokhtarzadeh and French, 2000)

2.4 BEHAVIOR OF CONCRETE IN UNIAXIAL COMPRESSION

The magnitude of the prestressing force does not remain constant over the life of a pretensioned beam. At prestress transfer, the force in the prestressing strand is transmitted to the entire member. This force causes the beam to shorten in length which, in turn, reduces the amount of force in the strand, a phenomenon commonly referred to as elastic shortening. At this stage, immediately after prestress transfer, the allowable release stresses must be satisfied according to the AASHTO Bridge Design Specifications and the ACI-318 Building Code

Requirements. Over time, long-term effects such as creep and shrinkage of the concrete and relaxation of the strand further reduce the prestressing force.

Based on the location and magnitude of the prestressing force, prestressed concrete beams are typically subjected to compressive stresses at the bottom fiber and tensile stresses at the top fiber of the section. At release, the bottom portion of the section is subjected to some initial level of compressive stress. Due to the loss of prestressing force and the gain of concrete strength over time, the compressive stress level at release is typically at a maximum. Over time, the loss of prestressing force and the gain of concrete strength level off, and a certain sustained compressive stress exists in the bottom fibers of the section. The behavior of normal- and high-strength concrete in compression due to both of these loading conditions (initial and sustained loads) is investigated in this section. Also, a technique to quantify the amount of internal damage due to these loading conditions is presented. It is important to note that in all of the subsequent research studies, the concrete specimens were tested at mature ages. As a result, at the conclusion of this section, an attempt to correlate the findings of these research studies to the case in which concrete is loaded at early ages, as in prestressed concrete, is presented.

2.4.1 Concrete Subjected to Initial Loading

The primary components of concrete are the aggregates and the cement paste. By themselves, these materials behave elastically under uniaxial compression until failure. It is when they are combined, that an inelastic stress-strain relationship exists (Shah and Winter, 1966). As a result, the response of a concrete specimen is governed by the interaction between the paste and the aggregates. Several researchers throughout the development of concrete as a structural material have investigated its behavior at all levels of load and at failure. In these studies, damage to the internal microstructure is evaluated throughout the response in compression. The results of two such studies are discussed in this section.

2.4.1.1 Richart, Brandtzaeg, and Brown, 1929

In this research study, both plain and spirally reinforced columns of mature age were tested in uniaxial compression. Only the plain concrete tests are reported in this review. The concrete was composed of standard Portland Cement, sand, and gravel obtained from the Wabash River at Attica, Indiana. For the plain concrete investigation, five circular columns measuring 10-inches in diameter and 40-inches in length were loaded to failure. The failure stress on the specimens ranged from 1,940-psi to 2,290-psi. The results of these tests are discussed herein.

Based on these tests, detailed observations on the behavior of plain concrete at several load levels and as it approached failure were made. The behavior of the specimens was separated into three distinct stages. The first stage of the stress-strain curve featured an essentially linear relationship between the stress and the longitudinal strain. This behavior was maintained for at least 25-percent of the ultimate load. The second stage was triggered by a deviation from this linear-elastic portion. Brandtzaeg theorized that this departure was due to "*plastic sliding on elementary planes at scattering points and in every direction within the specimen*" (Richart et al., 1929). As this plastic deformation increased, lateral pressure was placed on the surrounding intact elements. The tensile failure of these confining elements marked the beginning of the third stage. In this stage, the internal microstructure broke down,

eventually leading to failure. Richart et al. noted that the third stage typically began around 75- to 85-percent of the maximum load. The findings of this research study are visually depicted in Figure 2-11.
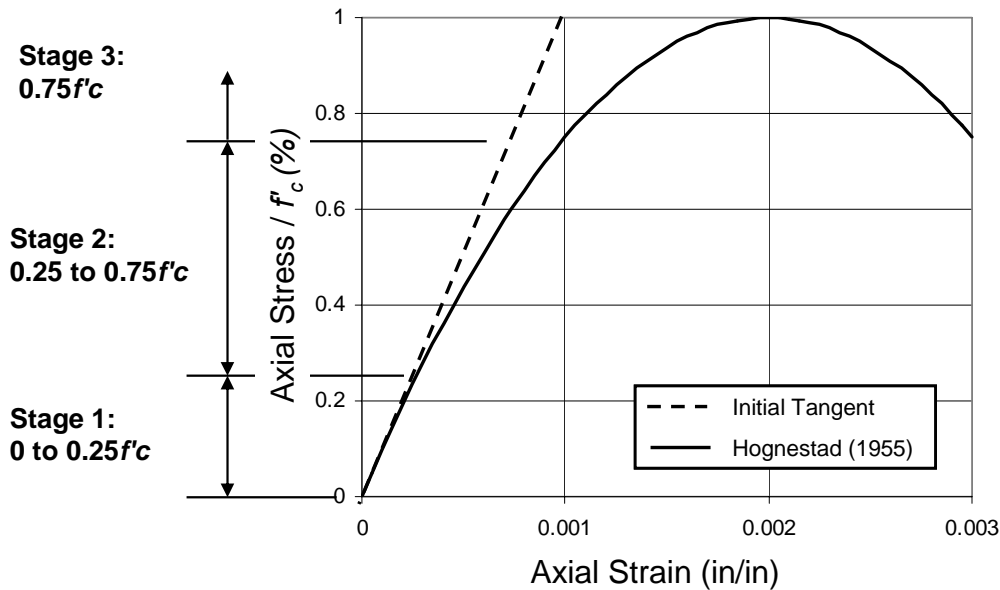
Figure 2-11: Visual depiction of three stages discussed by Richart et al. (1929) using Hognestad's parabola for concrete (1955)

2.4.1.2   **Hsu, Slate, Sturman, and Winter, 1963**

Hsu, Slate, Sturman, and Winter studied the correlation between microcracking and the inelastic behavior of concrete under uniaxial compression until failure. The results from ten 4x8-inch cylinder tests were reported. Each of the specimens was loaded to various levels of strain, unloaded, sliced, and then examined using microscopy or x-ray photography. The concrete was comprised of Portland Type I cement and coarse aggregates from local glacial deposits near Ithaca, New York. The specimens were cured for 197 days under controlled conditions until the day before the test. The average compressive strength of the concrete was 3,150-psi.

As a result of the investigation, Hsu et al. identified three types of internal microcracks: bond cracks, mortar cracks, and aggregate cracks. Before load is applied to a concrete cylinder, bond cracks exist at the interface between the aggregate and the mortar. MacGregor suggested these "no-load bond cracks" are the result of the aggregate restraining the shrinkage of the paste during hydration (MacGregor, 1997). According to Hsu et al., these cracks do not significantly increase in size or number until 30-percent of the ultimate load is reached. As the load is increased above this approximate level, the propagation of bond cracks forces the stress to redistribute to other uncracked portions of the aggregate-paste interface. This effect causes the slope of the stress-strain curve to slightly decrease. As the load increases further, cracks entirely within the mortar begin to develop. These mortar cracks attempt to bridge adjacent bond cracks. At 70- to 90-percent of the ultimate load, a continuous pattern of microcracking exists due to an increase in size and number of the mortar cracks. More nonlinearity in the stress-strain response

accompanies this further breakdown of the microstructure. This level of load is considered the "critical" load. Hsu et al. included a table in their report that refers to critical loads and initial cracking loads from various other researchers. For the reader's convenience, this table is included herein as Table 2-7.

Table 2-7: Crack and critical load observations by various researchers

(Hsu, Slate, Sturman, and Winter, 1963)

Researcher	Loads where microcracks start	Critical load
Brandtzaeg (1929)		0.75-0.85 P_{ult}
Berg (1950)	First observed cracks on the surface of specimens 0.55-0.6 P_{ult}	
Jones (sonic) (1952)	0.25-0.3 P_{ult}	
L'Hermite (sonic) (1954)	"Crackling noise" 0.5-0.75 P_{ult}	
Hognestad (1951)		0.71-0.96 P_{ult}
Rüsch (1959)	Noise begins 0.5 P_{ult}	Noise increases rapidly 0.75 P_{ult}

Essentially, the work of Hsu, Slate, Sturman, and Winter in 1963 is in direct agreement with the findings of Richart, Brandtzaeg, and Brown in 1929. Both groups of researchers associated the departure of the stress-strain curve from the linear region as an indication of damage to the internal microstructure. Also, both groups identified a critical load (0.70P_{ult} and 0.75P_{ult}, respectively) that signified the start of the internal breakdown of the structure. Even though the compressive strengths of the specimens presented here were substantially low, the same inelastic behavior exists for normal-strength concrete of today (MacGregor, 1997).

2.4.2 Concrete Subjected to Sustained Loading

Microcracking can also result from the effects of sustained loads. As early as 1907, the negative implications of sustained load on concrete were realized (Davis and Davis, 1931). Around this time, theories associated the "flow of concrete" with the presence of sustained stress, the present-day phenomenon known as creep.

Concrete creep is defined as the continual deformation of a specimen under sustained compressive stress. This continual deformation is the result of the compression of unhydrated pockets of water within the microstructure of the concrete. Therefore, the amount of creep strain is proportional to the amount of unhydrated water in the specimen. As such, creep deformation is more critical for concrete at early ages as opposed to mature concrete. Over time, a bond forms between these pockets of water and the surrounding paste. This bond prevents the full recovery of creep strains upon the removal of the sustained load (MacGregor, 1997).

Several research studies have focused on the behavior of concrete under sustained loads. Two such studies are discussed in the following section with an emphasis on the sustained-load strength and the creep proportionality limit of normal- and high-strength concrete.

2.4.2.1   *Ngab, Slate, and Nilson, 1981*

In 1981, Ngab, Slate and Nilson experimentally investigated the internal microcracking and the creep of high- and normal-strength concrete subjected to short- and long-term loads. Ngab et al. defined normal-strength concrete in the range of 3,000- to 5,000-psi, and high-strength concrete in the range of 9,000- to 12,000-psi. For their research study, 84 specimens measuring 3.5 x 3.5 x 10.5-inches were tested. The concrete was comprised of Portland Type I cement and local aggregates from near Ithaca, New York.

In the microcracking evaluation part of the study, concrete specimens were loaded to a specified stress-to-strength ratio ranging from 0.30 to 0.85. In all cases, the specimens were moist-cured for 28-days prior to loading. Before and after loading, designated specimens were cut using a diamond-blade masonry saw with a careful procedure to prevent any additional microcracking. The observed cracks were mapped onto full-size photographs of the concrete slices and measured with a digitizer. The results of this portion of the study indicated that high-strength concrete was superior to normal-strength concrete in regards to microcracking.   In general, the total length of bond cracks was much greater for normal-strength concrete than for high-strength concrete subjected to the same load levels and for the same duration. Evidence of this performance due to short-term loading is illustrated in Figure 2-12 and due to sustained-loading in Figure 2-13. In both figures, the specimens were loaded to 65-percent of f'_c, but for the specimens in Figure 2-13, the load was sustained for 60-days. It is important to note that the cracks illustrated in these four cracking maps run perpendicular to the direction of the applied compressive load.
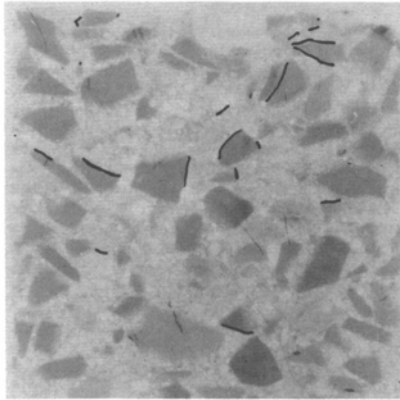
High-Strength Concrete
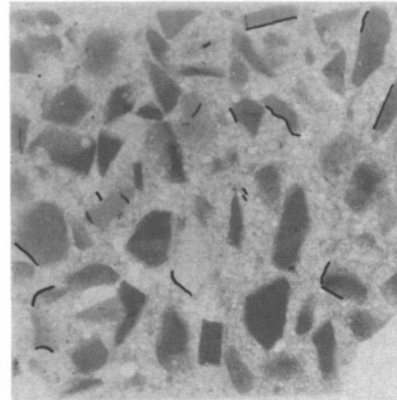
High-Strength Concrete
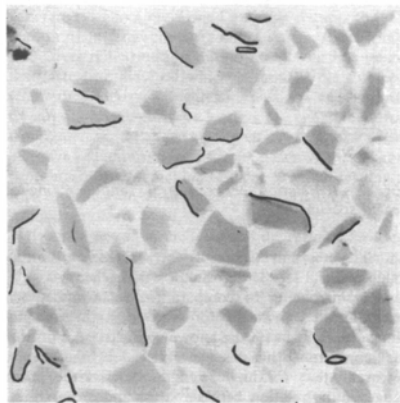
Normal-Strength Concrete
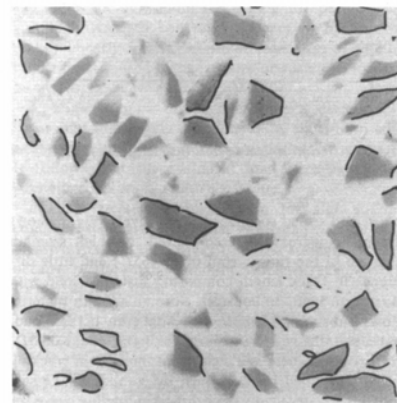
Normal-Strength Concrete

Figure 2-12: Typical cracking maps for specimens loaded to 0.65f'c and unloaded

(Ngab, Slate, and Nilson, 1981)

Figure 2-13: Cracking maps for unsealed creep specimens loaded to 0.65f'c for 60-days

(Ngab, Slate, and Nilson, 1981)

In the creep evaluation part of the research study, the relationship between applied stress and creep strain was investigated. For this purpose, the concrete specimens were loaded in special creep racks that used a spring loading system with a level arm. The creep specimens were subjected to a specified stress-to-strength ratio for 60-days after moist-curing for at least 28-days. The results of the testing indicated that creep of high-strength concrete increased linearly with the applied stress-to-strength ratio until approximately 70-percent of f'_c (Figure 2-14). From research conducted by others, it was known that the creep of normal-strength concrete increased linearly until only 30- to 50-percent of f'_c. Ngab et al. associated the difference in creep behavior for normal- and high-strength concrete with the superior resistance to microcracking of the latter with respect to the former.
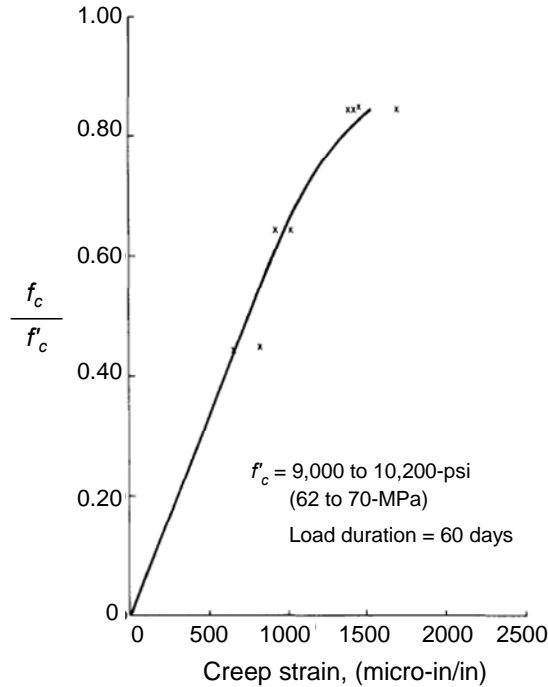
Figure 2-14: The stress-to-strength ratio and creep strain relationship

(Ngab, Slate, and Nilson, 1981)

2.4.2.2   *Smadi, Slate, and Nilson, 1985 and 1987*

In a research study by Smadi, Slate, and Nilson, the sustained load strength and the creep response of low-, medium-, and high-strength concretes were evaluated and compared. For the purposes of this study, low-strength concrete (LSC) was defined as 3,000 to 3,500-psi. Medium-strength concrete (MSC) was defined as 5,000 to 6,000-psi, and high-strength concrete (HSC) was defined as 8,500 to 10,000-psi. The concrete was made of Portland Type I cement, sand, and coarse aggregate from a local deposit near Ithaca, New York. All of the specimens used in this study were 4x8-inches cylinders. They were cured in a moist room for approximately 28-days before testing. The main variables of the study were the applied stress-to-strength ratios and the effects of different concrete strength.

In this study, HSC, MSC, and LSC specimens were loaded to stress-to-strength ratios ranging from 0.40 to 0.95. To apply the load, either a 400-kip hydraulic testing machine or a standard creep frame with a lever arm was used. For the sustained-load tests, the applied load was maintained within 300-pounds of the target load for a set period of time or until failure occurred. The specimens that failed under sustained load are summarized in Table 2-8. The specimens that did not fail were monitored and analyzed for creep. Based on the data presented in Table 2-8, Smadi et al. concluded that the long-term sustained strength of high-strength concrete is approximately 80- to 85-percent of f'_c. That of low- and medium-strength concrete is approximately 75- to 80-percent of f'_c.

33

Table 2-8: Results of premature failures due to sustained-load testing

(Smadi, Slate, and Nilson, 1985 and 1987)

Concrete Type	f_c / f'_c	Total # of cylinders	# of cylinders that failed due to sustained load	Time of failure after loading (range)
HSC	0.95	2	2	45 sec.
	0.90	8	8	7.6 to 46.5 min.
	0.85	6	4	61 to 240 min.
	0.80	6	2	14 days
MSC	0.95	6	6	0.33 to 3.5 min.
	0.90	6	6	1.8 to 8.5 min.
	0.85	6	6	12 to 62 min.
	0.75	6	2	49 days
LSC	0.95	2	2	23 sec.
	0.90	2	2	2.3 min.
	0.85	2	2	35 min.
LMSC	0.80	4	3	52 to 151 min.

The creep deformations of the LSC, MSC, and HSC specimens that did not fail under sustained load were evaluated and compared for up to 60-days. In general, the findings coincided with that of Ngab et al. (1981). Smaller magnitudes of creep strain, creep coefficient, and specific creep were obtained for HSC as compared to MSC and LSC. In addition, the proportionality limit between creep and the applied stress-to-strength ratio was evaluated as 65-percent of ultimate. The authors stated that:

> ...the stresses in HSC can be increased safely up to the creep proportionality limit, or up to about 65-percent of ultimate, without causing significant crack formation…the deviation of creep from linearity with increasing stress is believed to be due to a significant increase in bond cracks along the mortar-aggregate interface. Such cracks increase in number and in length under increasing monotonic loads as well as under sustained loads (Smadi et al., 1987).

For reference, the proportionality limit for HSC evaluated by Ngab et al. (1981) was 70-percent of ultimate.

Lastly, Smadi et al. discussed a theory of A.M. Neville. Neville suggested that failure occurs under sustained loads below the short-term loading strength because a critical strain limit is reached (Neville, 1959). Smadi et al. (1985) claimed that their findings reasonably agreed with this theory. They proposed that concrete under sustained load fails when the total strain of the specimen, due to initial loading, creep, shrinkage, etc., slightly exceeds the strain at maximum stress due to short-term loading. For this study, they estimated the critical strain limits to slightly exceed the following values: 3,000, 2,400, and 2,200-microstrain for HSC, MSC, and LSC, respectively. A similar finding was reported by Ngab et al. in 1981. In the conclusions of their study, they stated:

The amount of microcracking for both normal and high strength concretes appears to be approximately linearly related to strain, regardless of whether strain is caused by short-term or sustained loading, or by shrinkage (Ngab et al., 1981).

These findings seem to suggest that the strain in the member is a more appropriate measure of damage than stress. As a result, for prestressed concrete, the concept of a "self-relieving mechanism" as suggested by Huo and Tadros (1997) and Noppakunwijai et al. (2001) is an indicator of damage more so than a beneficial characteristic. The higher initial strain imposed on a member subjected to elevated levels of stress at release induces more damage than the initial strain associated with the current stress limit.

2.4.3   Quantifying Internal Damage

In the previously-reviewed research studies on the behavior of concrete under initial and sustained loading, microcracking was an indicator of damage. The two research studies discussed in this section quantify this internal damage by measuring the transverse tensile strength of concrete previously loaded in compression. The effects of initial and sustained compressive loading are addressed in these studies.

2.4.3.1   Delibes Liniers, 1987

The primary objective of this study was to examine the loss of tensile strength of concrete when it is loaded in uniaxial compression. To accomplish this task, concrete cylinders were cast, loaded in compression to a specified percentage of their strength, maintained for a specified period of time, and then split according to ASTM C496-71. Ultrasonic measurements were included to corroborate the findings of the split-cylinder tests. The following variables were investigated: magnitude of compressive stresses, duration of the loading, aggregate type, curing process, and the direction of the applied compressive load relative to the final tensile load. In this investigation, damage to the internal microstructure of the concrete was associated with the loss of tensile strength.

The results of the study indicated that the tensile capacity of the specimens decreased as the applied compressive stress-to-strength ratio increased and as the duration of load increased. For specimens loaded in compression for only 1-minute, several general observations were made. At approximately 90-percent of the compressive strength of the specimen, the tensile capacity reduced by up to 30-percent. At 65-percent of the compressive strength, the reduction in tensile strength stabilized. Lastly, small losses in tensile capacity of less than 10-percent were detected even at a stress-to-strength ratio of 0.50. In addition, some observations were made concerning specimens under sustained compressive loads. At a stress-to-strength ratio of 0.75 and above, "*instability and compressive rupture*" occurred in some cases (Delibes Liniers, 1987).

The test results for specimens stored under general curing conditions and loaded for 1-minute and 15-minutes are illustrated in Figure 2-15 and 2-16, respectively. The reduction in tensile strength as the stress-to-strength ratio increases is established in the plots. Also, from the comparison of these two plots, the additional damage initiated by a moderate period of sustained load of only 15-minutes is illustrated. The summary of the test results, included as Figure 2-17, applied to conventional concrete under general curing conditions.
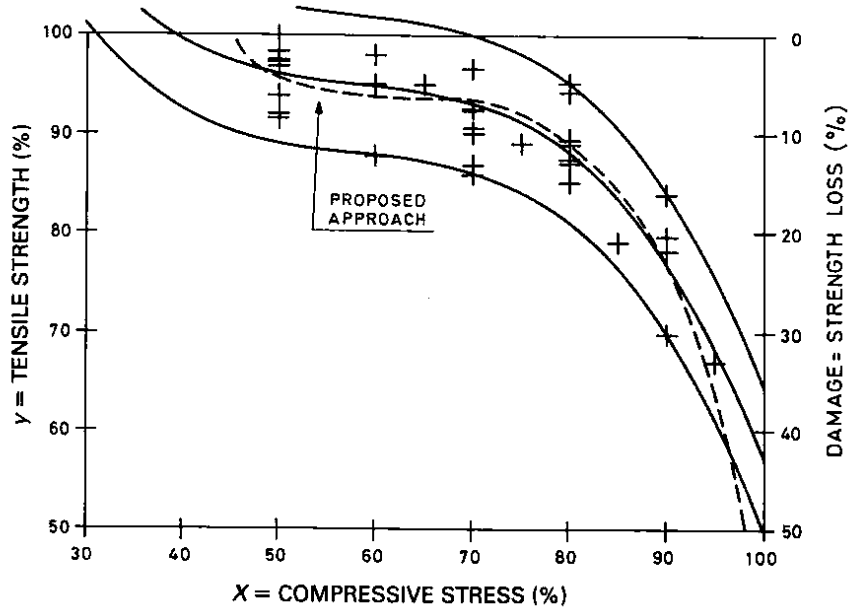
Figure 2-15: Test results for cylinders loaded for 1-minute under general curing conditions (Delibes Liniers, 1987)
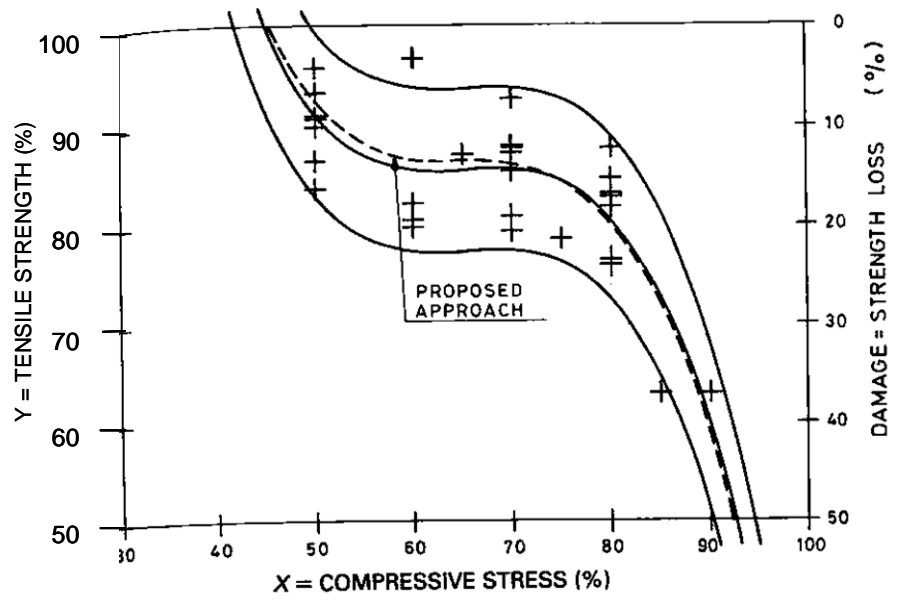
Figure 2-16: Test results for cylinders loaded for 15-minutes under general curing conditions (Delibes Liniers, 1987)

36
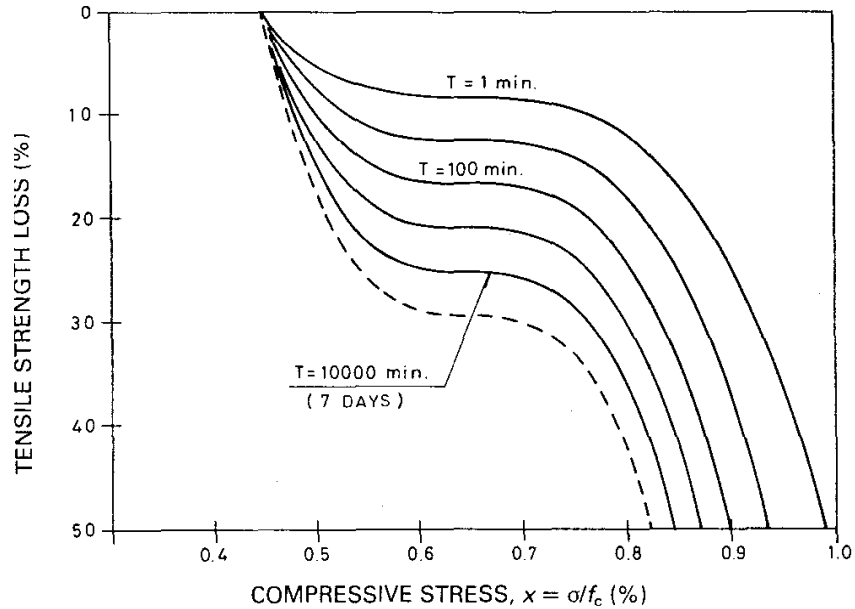
Figure 2-17: Summary of tensile strength loss for conventional concrete and curing techniques (Delibes Liniers, 1987)

Also, the direction of the compressive load with respect to the tensile failure plane was studied in this project. According to the Delibes Liniers, microcracks typically formed in the direction of the applied load. As such, tensile failure planes that were parallel to the direction of the applied compressive stress were investigated in this study. However, one series of specimens were used to test the reduction in tensile capacity where the failure plane was perpendicular to the direction of the applied compressive stress. It was stated that the results "*were quite clear, leading to the conclusion that 'damage' in a direction perpendicular to the compression was almost negligible*" (Delibes Liniers, 1987). However, no data for this series was provided. This finding was interesting in regards to the cracking maps reported by Ngab et al. (1981) (Figure 2-12 and 2-13). In those specimens, significant microcracks were detected in the perpendicular direction with respect to the compressive loading.

At the end of the study, it was stated that "*the necessity of limiting compressive stress under 60% of the strength is confirmed*" (Delibes Liniers, 1987). He also indicated that in situations where corrosion protection is essential, additional limitations on compressive stress should be placed because reduction in tensile capacity was present for compressive loads below 60-percent. In short, the negative effects of compressive stress on the tensile strength of concrete were illustrated in this study. Furthermore, the tensile strength of concrete was proven to be a suitable indicator of internal damage to the microstructure of concrete.

2.4.3.2 Gettu, Aguado, and Oliveira, 1996

In 1996, the splitting tensile strength of concrete was again used to quantify internal microcracking. In this study, Gettu, Aguado, and Oliveira evaluated the splitting strength of high-strength concrete cubes after the cubes were subjected to "*monotonic and cyclic compressive loadings*" (Gettu, Aguado, Oliveira, 1996). Each side of the cube measured 3.94-inches (100-mm). The concrete used in this research project was comprised of Type I cement,

river sand, crushed granite, water, silica fume, and superplasticizers. At 28-days, the cylinder and cube compressive strengths were 10,900-psi (75.4-MPa) and 11,400-psi (78.4-MPa), respectively. The results of the static load cube tests and the cyclic load cube tests are summarized herein.

At an approximate age of 28-days, cubes were loaded in uniaxial compression to the following applied stress-to-strength ratios: 0.25, 0.35, 0.4, 0.45, 0.5, 0.55, 0.6, 0.7, 0.8, and 0.85. After 15-minutes of sustained load, the cube was unloaded and split. The orientation of the splitting test was such that the failure plane was in the direction of the applied compressive stresses as in the tests by Delibes Liniers (1987). The damage or loss of tensile strength was plotted versus the stress-to-strength ratio and was calculated with Equation 2-14. From these results, it was concluded that the internal damage of the high-strength concrete was *"negligible until about 60-percent of the peak load"* was reached (Gettu et al., 1996). The findings of the statically loaded cubes are provided in Figure 2-18.

$$d_m = 1 - \frac{\sigma_t}{f_t} \qquad (2\text{-}14)$$

where, σ_t = measured splitting tensile strength

f_t = "virgin" splitting tensile strength as previously determined from tests on control specimens
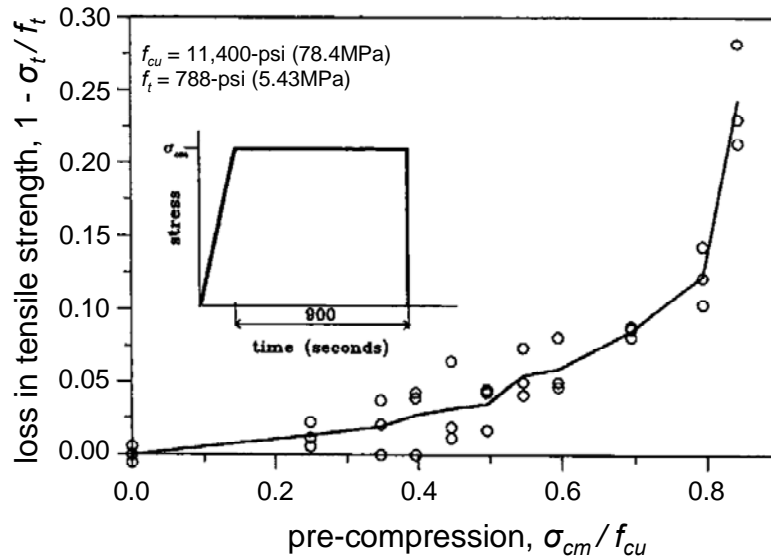
Figure 2-18: Loss of tensile strength of cubes subjected to sustained compressive stresses (Gettu, Aguado, Oliveira, 1996)

In addition, some of the concrete cubes were subjected to cyclic loads for 900-seconds at a frequency of 1-Hertz. The load range was between $0.05\sigma_{cc}$ and σ_{cc}, where σ_{cc} varied from $0.25f_{cu}$ to $0.85f_{cu}$. After the loading program, the cubes were split such that the failure plane was in the direction of the cyclic compressive stresses, as in static test procedure. The damage was also calculated as before (Equation 2-14) and was plotted against the mean applied stress, σ_{ccm}. The results indicated that damage was detected at lower load levels under cyclic loading than under static loading. The findings of this portion of the project are presented in Figure 2-19.

38
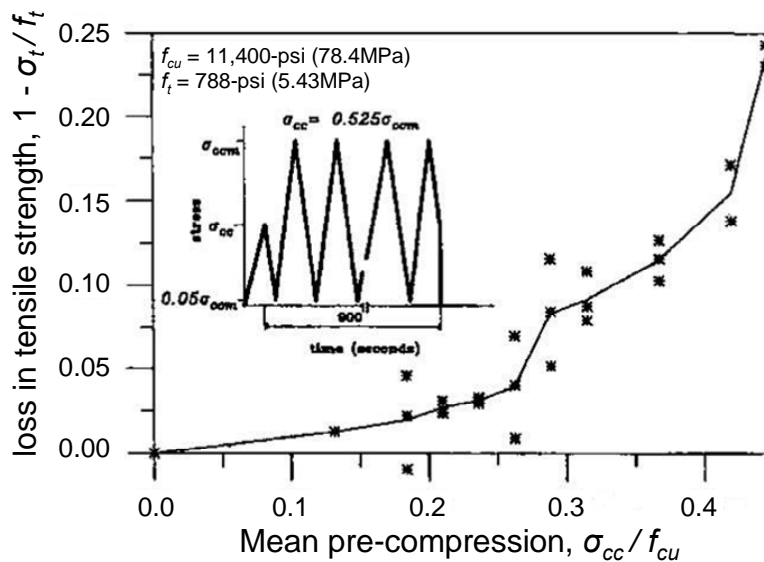
Figure 2-19: Loss of tensile strength of cubes subjected to cyclic loading (Gettu, Aguado, Oliveira, 1996)

In short, the findings of Gettu et al. (1996) were in agreement with that of Delibes Liniers (1987). Both research studies quantified the effect of high levels of compressive stress on the microstructure of the concrete. Gettu et al. determined that the internal damage due to the compressive stress was negligible until a stress-to-strength ratio of 0.60 was reached. Delibes Liniers (1987) observed stability in the loss of tensile strength at a stress-to-strength ratio of 0.65.

2.4.4   Correlation to Behavior of Prestressed Concrete Girders

In the previous three sections, several research investigations were reviewed in which the behavior of concrete in uniaxial compression was investigated. In general, these research studies were fundamental to understanding the behavior of normal- and high-strength concrete subjected to initial and sustained loading. Unfortunately, the materials and the loading conditions in these studies were not exactly consistent with that of prestressed concrete girders, the focus of the current project. As such, the differences between the conditions of these research investigations and that of prestressed concrete was addressed so that the findings of these studies can be applied to the current project with the proper perspective. The most evident differences included:

- Normal strength concrete at mature ages vs. high-strength concrete at early ages
- Uniformly distributed compressive stresses in the cylinder and cube tests vs. strain gradient stress distribution in prestressed concrete beams

In regards to the first inconsistency, high-strength concrete (HSC) is used in prestressed concrete girders, not normal-strength concrete (NSC). Also, the bottom fibers of the pretensioned girder are typically loaded in compression at early ages, well within the first 24-hours of casting. While it was evident that HSC at mature ages performed considerably better in regards to microcracking and creep than NSC (Section 2.4.2), the stress-strain relationship of HSC at typical release times is not as linear as at mature ages. This finding was presented by

39

Khan, Cook, and Mitchell in Figure 2-4. In this plot, the nonlinear response of HSC in compression at 16.5-hours was illustrated. Since nonlinear deformation is directly linked to internal microcracking (Section 2.4.1), the results of the microcracking investigations discussed herein seem applicable to a certain degree to HSC at early ages as is the case in prestressed concrete applications.

In regards to the second inconsistency, there is some difficulty correlating the results of concrete cylinder tests and concrete cube tests with prestressed concrete members. One main discrepancy is that the distribution of compressive stress in the cylinders and the cubes is uniform, while the compressive stress in a prestressed concrete beam gradually decreases over the section height. In a research investigation by Karsan and Jirsa, the difference between the stress-strain response in compression of a member with a uniform stress distribution and with a stress gradient was evaluated (1970). Nineteen specimens were loaded with a strain gradient in compression in which the strain at one face of the specimen was varied while at the other face, the strain was kept at zero. The test data confirmed that "*the stress-strain curve for concrete under a strain gradient was essentially the same as for concentric compression*" (Karsan and Jirsa, 1970). As a result, the behavior of cylinders and cubes under uniform compression seem applicable to the bottom-fibers of a prestressed concrete member. It should be noted that the presence of a stress gradient in a prestressed concrete member restricts the critical region to the bottom-fibers of the section.

2.5 ANALYSIS METHODS FOR PRESTRESS LOSS

In the current research project, the pretensioned beams described in Sections 3.2 and 3.3 were analyzed with typical design procedures to determine the required moment to crack the specimen. An estimate of the effective prestressing force after short- and long-term losses was required. The total prestress loss and prestress gain over the life of a pretensioned member is depicted in Figure 2-20 (Tadros et al., 2003). The losses applicable to the current study included the elastic shortening loss due to member shortening, the long-term losses due to creep and shrinkage of the concrete, and the long-term relaxation of the prestressing strand. The three methods utilized to estimate these effects were as follows:

- PCI Design Handbook Loss of Prestress Estimate (PCI, 2004)
- NCHRP Report 496 Detailed Prestress Loss Method (Tadros et al., 2003)
- AASHTO LRFD Refined Loss of Prestress Estimate - Interim 2005 Edition (AASHTO, 2005)

For the purposes of this report, these methods are referred to as the PCI, NCHRP, and AASHTO procedures, respectively.
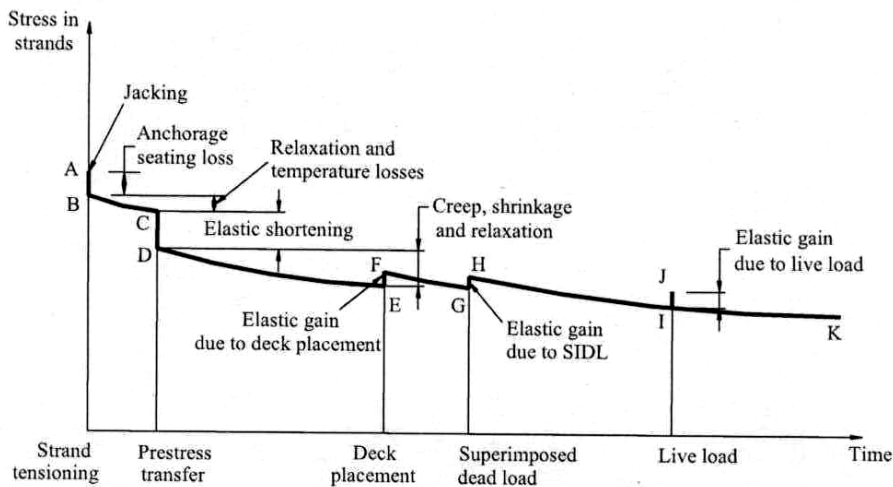
Figure 2-20: Stress versus time in strands of a pretensioned concrete girder (Tadros et al., 2003)

The aforementioned procedures were chosen to address the common practice followed by prestressed concrete designers and the current "state-of-the-art" in the industry. The PCI method, as developed by Zia et al. in 1979, is the oldest and simplest of the three procedures. This method is referenced in Chapter 18 of ACI 318-05. The NCHRP Report 496 method was developed in a study funded by the Transportation Research Board of the National Academies. The purpose of the study was "to help designers obtain realistic estimates of prestress losses in high-strength pretensioned concrete bridge girders and thus achieve economical designs" (Tadros et al., 2003). This procedure represented the current "state-of-the-art." In Section 5.9.5.4 of the AASHTO LRFD Bridge Design Specifications Interim 2005 edition, the refined estimates of time-dependent losses were updated based on the recommendations of the NCHRP Report 496. Previously in the 2004 AASHTO LFRD Specifications, the refined prestress loss estimates did not incorporate the creep and shrinkage formulas of Section 5.4.2.3. After the NCHRP Report 496 was released, updated high-strength concrete versions of these formulas were incorporated into a more rigorous prestress loss estimation procedure. While there are many similarities between the NCHRP Report 496 and the procedure in the AASHTO Interim 2005 Specifications, conservative simplifications are present in the AASHTO procedure to aid design engineers. For this reason, both of the procedures were included in the current research study. Some general characteristics of the three procedures are provided in Figure 2-21. Each of the procedures is discussed in greater detail in the following sections.

41
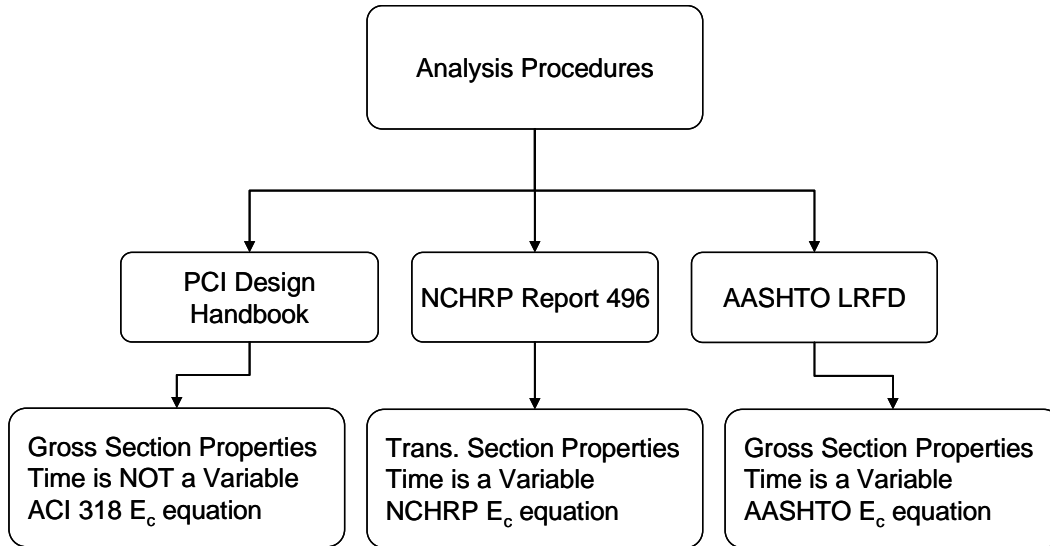
Figure 2-21: General characteristics of three analysis procedures

2.5.1   PCI Design Handbook Estimate of Prestress Loss

This procedure was developed by members of ACI-ASCE Committee 423 as a means for "*obtaining reasonably accurate values for the various code-defined sources of loss*" (Zia et al., 1979). The total losses are divided into four components: elastic shortening (ES), creep of concrete (CR), shrinkage of concrete (SH), and relaxation of the prestressing strands (RE). It is important to note that the gross section properties and an estimation of the prestressing force immediately after transfer are to be used for the elastic shortening calculation. Also, the initial modulus of the concrete is used for the elastic shortening losses while the 28-day concrete modulus is used for creep losses. Lastly, these calculations are not based on a variable timeframe. Rather, they represent the total losses that a given member will experience at the end of its design life. The other three procedures utilize time-dependent stress loss expressions. The loss estimates used in this procedure for each component are provided in Table 2-9.

Table 2-9: PCI equations for estimating loss of prestress (PCI, 2004)

COMPONENT	EQUATIONS
Elastic Shortening	$ES = K_{es} E_{ps} f_{cir} / E_{ci}$ where K_{es} = 1.0 for pretensioned members E_{ps} = modulus of prestressing tendons (ksi) $E_{ci} = w_c^{1.5} \cdot 33 \sqrt{f'_{ci}}$ psi w_c = unit weight of the concrete (pcf) f'_{ci} = compressive strength at release (psi) $f_{cir} = K_{cir} \left(\dfrac{P_i}{A_g} + \dfrac{P_i e^2}{I_g} \right) - \dfrac{M_g e}{I_g}$ K_{cir} = 0.9 for pretensioned members P_i = initial p/s force directly before transfer (kips) A_g = area of gross section (in.²) I_g = moment of inertia of gross section (in.⁴) e = eccentricity of prestressing tendons (in) M_g = dead load moment (in-kips)
Creep	$CR = K_{cr} \left(E_{ps} / E_c \right) \left(f_{cir} - f_{cds} \right)$ where K_{cr} = 2.0 for normal weight concrete E_c = 28-day modulus of concrete (ksi) $f_{cds} = \dfrac{M_{sd} e}{I_g}$ M_{sd} = superimposed dead load moment (in-kips)
Shrinkage	$SH = \left(8.2 x 10^{-6} \right) K_{sh} E_{ps} \left(1 - 0.06 V/S \right) \left(100 - R.H. \right)$ where K_{sh} = 1.0 for pretensioned members V/S = volume to surface area ratio (inches) R.H. = average relative humidity (%)
Relaxation	$RE = \left[K_{re} - J \left(SH + CR + ES \right) \right] C$ where K_{re} = 5-ksi for 270-ksi low-relaxation strands J = 0.040 for 270-ksi low-relaxation strands C = coefficient determined in Table 4.7.3.2 in PCI Design Handbook

2.5.2 NCHRP Report 496 Detailed Prestress Loss Method

In this research study sponsored by the Transportation Research Board, Tadros et al. reviewed current prediction methods in the literature, developed a refined procedure to estimate prestress losses, and conducted an experimental study to test the proposed guidelines. The final proposed procedure was more applicable to high-strength concrete products than previous methods. In this study, new equations estimating the following material properties were developed: modulus of elasticity, creep of concrete, and shrinkage of concrete. For the most part, these formulas were similar to other material property equations found in (i) Section 5.4.2 of the AASHTO LRFD Design Specifications, (ii) ACI 209R-92, and (iii) Chapter 3 of "Prestressed Concrete Structures" by Collins and Mitchell to name a few (AASHTO, 2004, ACI 209, 1992, and Collins and Mitchell, 1997). Slight changes to these formulas were made based

on experimental data obtained from the literature and the experimental testing conducted within the project.

In addition, two 'K' factors were included into each of the material property equations. The first factor, K_1, accounted for the difference between local materials and the national average. The second factor, K_2, altered the equation so that the result would represent the upper bound, lower bound, or average value. Only the 'K' factors for the modulus of elasticity equation were derived in the NCHRP study. These factors were derived for four states corresponding to the locations of experimental research conducted within the project. The chosen states included Nebraska, New Hampshire, Texas, and Washington. For Texas, a K_1 factor of 1.321 was suggested. A value in excess of one reflected the presence of significantly stiffer aggregates in Texas as opposed to the rest of the nation. All of the material property equations recommended by NCHRP Report 496 are provided in Table 2-10.

Table 2-10: NCHRP equations for material properties (Tadros et al., 2003)

PROPERTY	EQUATIONS
Modulus of Elasticity	$E_c = 33,000 K_1 K_2 \left(0.140 + \dfrac{f_c'}{1000}\right)^{1.5} \sqrt{f_c'}$ where K_1 = factor representing difference between local and national average K_2 = factor representing the upper or lower bound limits f_c' = strength of concrete at time in question (ksi)
Shrinkage Strain	$\varepsilon_{sh} = 480 * 10^{-6} \gamma_{sh} K_1 K_2$ where K_1 & K_2 = same as above $\gamma_{sh} = k_{td} k_s k_{hs} k_f$ $k_{td} = \dfrac{t}{61 - 4f_{ci}' + t}$, $k_{hs} = 2.00 - 0.0143H$, $k_s = \dfrac{1064 - 94V/S}{735}$, $k_f = \dfrac{5}{1 + f_{ci}'}$ t = age of concrete after loading (days) H = relative humidity (%) V/S = volume to surface ratio (in)
Creep Coefficient	$\psi(t, t_i) = 1.90 \gamma_{cr} K_1 K_2$ where K_1 & K_2 = same as above $\gamma_{cr} = k_{td} k_{la} k_s k_{hc} k_f$ $k_{la} = t_i^{-0.118}$, $k_{hc} = 1.56 - 0.008H$, k_{td}, k_s, k_f = same as above t_i = age of concrete when load is applied (days)

With these refined material property formulas, Tadros et al. (2003) developed a procedure to estimate the total loss of the prestressing force. The method consisted of computing the total loss as the summation of several components corresponding to various stages in the life of a girder. In the computation of the long-term components, provisions were made to account

for the continual reduction in the level of sustained stress over time due to these long-term losses. This reduction allowed for some creep and relaxation recovery and yielded a slightly larger effective modulus of concrete. The components of the total prestress loss derived in this procedure that are relevant to the current research study included the elastic shortening of the girder, the creep and shrinkage of the girder concrete, and the relaxation of the prestressing strands.

There are several unique aspects of the NCHRP prestress loss procedure. First, the elastic shortening loss is automatically accounted for by using the transformed properties of the section and the initial prestressing force before release. In other words, a separate estimate for the elastic shortening loss is not needed in calculating the bottom fiber stress at prestress transfer if the transformed section properties and the initial prestressing force are used. This feature is illustrated in the cracking load calculation performed using the loss estimates of this procedure (Section 5.2.2.2). In the computation of the loss due to creep, the initial modulus of concrete was used. It is interesting to note that the 28-day modulus was recommended in the PCI Procedure. Another interesting quality of this refined procedure was the age-adjusted modulus of elasticity factor, K_{it}. This factor was included in the calculation of the stress loss due to creep, shrinkage, and relaxation to adjust the effective modulus of elasticity of the concrete based on the slightly decreasing level of sustained load over time. In the computation of K_{it} an ultimate creep coefficient, $\psi(t_f,t_i)$ is used. In calculating the loss of prestressing force due to creep, the creep coefficient that corresponds to the amount of time under sustained load, $\psi(t_t,t_i)$, is used. This distinction is minimal for the current study. In addition to the K_{it} factor, a reduction factor φ_i was used to estimate the losses due to the relaxation of the prestressing strand. This reduction factor reduced the intrinsic relaxation loss formula developed by Magura et al. in 1964 to account for the "*steady decrease in strand prestressing due to creep and shrinkage of the concrete*" (Tadros et al., 2003). All of the equations used in this prestress loss procedure are provided in Table 2-11.

Table 2-11: NCHRP equations for estimating prestress loss (Tadros et al., 2003)

COMPONENT	EQUATIONS
Elastic Shortening	$\Delta f_{pES} = \dfrac{E_p}{E_{ci}} f_{cgp}$ where E_{ps} = modulus of prestressing tendons (ksi) $\quad\quad E_{ci}$ = initial modulus of concrete (ksi) $f_{cgp} = P_i \left(\dfrac{1}{A_{ti}} + \dfrac{e_{pti}^2}{I_{ti}} \right) - \dfrac{M_g e_{pti}}{I_{ti}}$ P_i = initial prestressing force directly before transfer (kips) A_{ti} = area of transformed section at transfer (in.^{2}) I_{ti} = moment of inertia of transformed section at transfer (in.^{4}) e_{pti} = eccentricity of strands of transformed section at transfer (in.) M_g = dead load moment (in.-kips)
Shrinkage	$\Delta f_{pSR} = \varepsilon_{sh} E_p K_{it}$ where $K_{it} = \dfrac{1}{1 + n_i \rho_n \alpha_n \left(1 + \chi \psi(t_f, t_i) \right)}$ $n_i = \dfrac{E_p}{E_{ci}}$, $\quad p_n = \dfrac{A_{ps}}{A_n}$, $\quad \alpha_n = \left(1 + \dfrac{A_n e_{pn}^2}{I_n} \right)$, $\quad \chi \approx 0.70$ A_{ps} = area of prestressing strands (in.^{2}) A_n = area of net section (in.^{2}) e_{pn} = eccentricity of prestressing strands of net section (in.) I_n = moment of inertia of net section (in.^{4})
Creep	$\Delta f_{pCR} = n_i f_{cgp} \psi(t_f, t_i) K_{it}$
Relaxation	$\Delta f_{pR} = \phi_i L_r K_{it}$ where $L_r = \dfrac{f_{pi}}{45} \left(\dfrac{f_{pi}}{f_{py}} - 0.55 \right) \log\left(\dfrac{24t_2 + 1}{24t_1 + 1} \right)$ f_{pi} = initial stress in strands (ksi) f_{py} = yield strength of strands (ksi) t_1 = initial age of concrete (days) t_2 = final age of concrete (days) $\phi_i = 1 - \dfrac{3\left(\Delta f_{pSR} + \Delta f_{pCR} \right)}{f_{po}}$

2.5.3 AASHTO LRFD Refined Loss of Prestress Estimate – Interim 2005

In the interim 2005 version of the AASHTO LRFD Design Specifications, a refined prestress loss procedure was updated based on the recommendations of the NCHRP Report 496. For the most part, the long-term material property equations developed in the NCHRP Report 496 were adopted into the AASHTO Specifications. The most substantial difference between the two procedures was the absence of 'K' factors in the creep and shrinkage property equations present in the AASHTO version. Both 'K' factors were removed from the creep coefficient and

the shrinkage strain equations. In regards to the modulus of elasticity equation, however, the NCHRP equation was not adopted in full. Instead of the empirical relationship for the unit weight of concrete, w_c, endorsed by NCHRP, the actual unit weight was preserved in the AASHTO equation. In addition, the K_2 factor was not adopted while the K_1 factor was. A value of 1.0 for K_1 was recommended unless physical tests are performed and acceptable to the authority of jurisdiction. In short, the differences in the material property equations between the two procedures were minimal. The equations as presented in Section 5.4.2 of AASHTO are included in Table 2-12.

Table 2-12: AASHTO equations for estimating material properties (AASHTO, 2005)

PROPERTY	EQUATIONS
Modulus of Elasticity	$E_c = 33,000 K_1 w_c^{1.5} \sqrt{f_c'}$ ksi where K_1 = factor representing difference between local and national average, taken as 1.0 unless determined by physical test and properly approved w_c = unit weight of concrete, not more 0.155-kcf (kcf) f_c' = strength of concrete at time in question (ksi)
Shrinkage Strain	$\varepsilon_{sh} = -k_{vs} k_{hs} k_f k_{td} 0.48 x 10^{-3}$ where $k_{vs} = 1.45 - 0.13(V/S)$, $k_{hs} = 2.00 - 0.014 H$ $k_f = \dfrac{5}{1 + f_{ci}'}$, $k_{td} = \dfrac{t}{61 - 4 f_{ci}' + t}$, t = age of concrete after loading (days) H = relative humidity (%) V/S = volume to surface ratio (in)
Creep Coefficient	$\psi(t, t_i) = 1.90 k_{vs} k_{hc} k_f k_{td} t_i^{-0.118}$ where $k_{hc} = 1.56 - 0.008 H$, k_{vs}, k_f, k_{td} = same as above t_i = age of concrete when load is applied (days)

In Section 5.9.5 of the AASHTO LRFD Design Specifications Interim 2005 edition, the procedure for estimating the total loss of prestressing force is presented in the main body of the code. As in the other two procedures, the total prestress loss is calculated as the summation of several short- and long-term components. The loss components relevant to this study include those due to elastic shortening, creep and shrinkage of the concrete, and the relaxation of the prestressing strand. In calculating the elastic shortening losses, the AASHTO procedure utilizes the same equations as in the PCI Method. The gross section properties and 90-percent of the initial prestressing force are recommended for this calculation. This approach differs from the NCHRP method and results in two inconsistent calculations between the two approaches. They include the losses associated with elastic shortening and the amount of sustained concrete stress at the location of the prestressing strand used in the creep calculation. As a result, the loss due to creep is different in each method even though the creep equations are identical. In computing the stress loss due to shrinkage of the concrete, the AASHTO procedure is essentially equivalent to the NCHRP Report 496 method. The only exception is in the computation of the K_{it} factor.

In the AASHTO procedure, gross section properties are used. In the NCHRP procedure, net section properties are used. This difference only slightly affects the loss due to shrinkage. Lastly, the NCHRP equation for the loss due to the relaxation of the prestressing strand was simplified before it was adopted into the main body of the AASHTO Specifications. The equation was simplified to provide a more user-friendly expression. The stress loss equations as listed in the AASHTO LRFD Bridge Design Specifications are presented in Table 2-13.

Table 2-13: AASHTO LRFD Bridge Design Specifications equations for estimating loss of prestress (AASHTO, 2005)

COMPONENT	EQUATIONS
Elastic Shortening	$\Delta f_{pES} = \dfrac{E_p}{E_{ci}} f_{cgp}$ where E_{ps} = modulus of elasticity of prestressing tendons (ksi) $\quad\quad E_{ci}$ = initial modulus of elasticity of concrete (ksi) $f_{cgp} = 0.9 P_i \left(\dfrac{1}{A_g} + \dfrac{e_{pg}^2}{I_g} \right) - \dfrac{M_g e_p}{I_g}$ P_i = initial prestressing force immediately before transfer (kips) A_g, e_{pg}, and I_g are gross section properties as in PCI method M_g = dead load moment (in-kips)
Shrinkage	$\Delta f_{pSR} = \varepsilon_{sh} E_p K_{it}$ where $K_{it} = \dfrac{1}{1 + \dfrac{E_p}{E_{ci}} \dfrac{A_{ps}}{A_g} \left(1 + \dfrac{A_g e_{pg}^2}{I_g} \right) \left[1 + 0.7 \psi(t_f, t_i) \right]}$ A_{ps} = area of prestressing strand (in^2)
Creep	$\Delta f_{pCR} = \dfrac{E_p}{E_{ci}} f_{cgp} \psi(t_t, t_i) K_{it}$
Relaxation	$\Delta f_{pR} = \dfrac{f_{pt}}{K_L} \left(\dfrac{f_{pt}}{f_{py}} - 0.55 \right)$ where f_{pt} = stress in strands immediately after transfer (ksi) $\quad\quad f_{py}$ = yield strength of strands (ksi) $\quad\quad K_L$ = 30 for low relaxation strands

2.6 SUMMARY

In this extensive literature survey, four topics related to the effects of increasing the allowable compressive stress at release were covered. First, the origin of the $0.60f'_{ci}$ stress limit was presented. Primarily, it was based on successful practice in the field; however, the opinions of several researchers in regards to the appropriate value of the allowable compressive stress were discussed in a paper by Erickson (1957). From this paper, it seems likely that the selection of $0.60f'_{ci}$ was influenced by research as well. Over the last decade, several research studies investigated the feasibility of increasing the allowable compressive stress at release. The effects

of increasing the allowable compressive stress studied in these investigations were summarized in Table 2-6. Some effects included the increase in creep, camber, and prestress loss. In general, the impact of increasing $0.60f'_{ci}$ on any of the studied effects was minimal; and an increase of the allowable stress (to at least $0.70f'_{ci}$) was supported. However, at the conclusion of the study by Castro et al., it was recommended that the live-load performance of overstressed girders be investigated (2004). Hence, the current project, TxDOT Project 5197 was initiated.

Second, the mechanical properties of high-strength concrete, particularly the concrete modulus of elasticity, were reviewed. Several researchers demonstrated the influence of the coarse aggregate type on the magnitude of the elastic modulus (Sections 2.3.2 and 2.3.3).

Third, the behavior of normal- and high-strength concrete due to initial and sustained loading in compression was discussed. In several investigations, the nonlinear deformation of concrete loaded in compression was linked to microcracking, or internal damage, in the concrete (Richart et al., 1929; Hsu et al., 1963; Ngab et al., 1981; and Smadi et al., 1985 and 1987). Two other studies quantified this internal damage with a reduction in the tensile strength of concrete previously-loaded in compression (Delibes Liniers, 1987 and Gettu et al., 1996). Even though the concrete specimens in these studies were tested at mature ages, the findings were applied to prestressed concrete and to the current research project with the proper perspective (Section 2.4.4). It was shown that when high-strength concrete is loaded to high-levels of compressive stress at typical prestress release times of approximately 16.5-hours, it undergoes nonlinear deformations (Khan et al., 1995). As such, the general findings of the microcracking investigations seemed applicable to the current study.

Fourth, the three analysis methods used in the current study to estimate the short- and long-term prestress losses of the test specimens were described. They included the PCI Design Handbook Loss of Prestress Estimate (PCI, 2004), the NCHRP Report 496 Detailed Prestress Loss Method (Tadros et al., 2003), and the AASHTO LRFD Refined Loss of Prestress Estimate (AASHTO, Interim 2005). In this report, these methods are referred to as the PCI, NCHRP, and AASHTO procedures, respectively.

CHAPTER 3
Test Specimens

3.1   OVERVIEW

In the live-load behavior evaluation part of the current research study, twenty-four scaled beams and twelve full-scale girders were tested in flexure. The scaled specimens were designed and constructed in TxDOT Project 4086 with a maximum compressive stress at release ranging from $0.46f'_{ci}$ to $0.91f'_{ci}$. In Project 4086, the rectangular, inverted-tee, and tee sections were designed to represent TxDOT standard I-, U-, and double-tee girders, respectively (Castro et al., 2004). The design and fabrication of these specimens are discussed in Section 3.2. In addition, twelve full-scale TxDOT Type-A beams were produced at a local precast pretensioned beam fabrication plant with a maximum stress at release ranging from $0.55f'_{ci}$ to $0.75f'_{ci}$. The production of the full-scale beams is described in Section 3.3.

3.2   DESIGN AND FABRICATION OF TXDOT PROJECT 4086 BEAMS

In TxDOT Project 4086 (9/2001 to 8/2003), the behavior at prestress transfer and the camber growth of 30 small-scale specimens was evaluated to assess the feasibility of increasing the allowable release stress in compression. In the design of the beams, the research team considered several parameters that might contribute to the behavior of the specimens at prestress transfer. These factors included: the level of compressive stress at release, the shape of the cross-section, the stress gradient due to the prestressing force, the type of coarse aggregate, and the rate of strength gain of the concrete mix. The contributions of each variable in the design of the 4086 beams are explained in this section. In addition, details of the fabrication of the beams are provided. Match-curing technology was utilized to correlate the strength gain of the specimen with that of the release cylinders. Also, strain gauges were applied to all of the prestressing strands to accurately infer the prestressing force before and after transfer. An inventory of the scaled beams tested under the current project is listed in Section 3.2.2.

3.2.1   Design of the Project 4086 Beams

One of the key parameters that was used in the design of the 4086 specimens was the maximum compressive stress in the concrete at prestress transfer. As such, the beams were designed and fabricated to cover a wide range of maximum compressive stresses at release, from $0.46f'_{ci}$ to $0.91f'_{ci}$. These values were calculated as the nominal stress at the end of the member with Equation 3-1, the allowable stress design equation typically utilized in prestressed concrete design (Castro et al., 2004).

$$f_{bot} = \frac{P_o}{A_g} + \frac{P_o e_p y_b}{I_g}$$
(3-1)

where, P_o = prestressing force immediately after transfer (kips)
                  e_p = eccentricity of prestressing strands of gross section (in.)
                  y_b = distance from geometric centroid to bottom fiber (in.)

51

A_g = area of gross section (in.^{2})

I_g = moment of inertia of gross section (in.^{4})

It is important to note that linear-elastic material behavior is assumed in Equation 3-1. This assumption is not entirely valid at the high levels of stress in many of the small-scale beams. Therefore, the compressive stress at release was also calculated using an inelastic procedure in which the nonlinear behavior of the concrete was taken into account. A software package called RESPONSE was utilized by Castro to perform the inelastic analysis (Castro et al., 2004). A nonlinear stress-strain curve for high-strength concrete developed by Thorenfeldt, Tomaszewicz, and Jensen was incorporated into the layered-section analysis program RESPONSE (Collins and Mitchell, 1997). The maximum compressive stress at release calculated according to this procedure ranged from $0.47f'_{ci}$ to $0.84f'_{ci}$. As expected, lower levels of stress were computed with the nonlinear approach for the overstressed beams. The release stresses according to this nonlinear analysis are presented in the TxDOT Project 4086 report (Castro et al., 2004). Sample calculations for the nominal release stresses at the ends of the member are provided in Appendix A for the Project 4086 beams. The release stresses calculated at the location of prestress transfer were included in Appendix A for reference.

In addition, three different section types were designed and fabricated to evaluate the effect of the cross-sectional shape on the release behavior of the beam. Previous researchers have identified the shape of the cross-section as an important parameter in the behavior of pretensioned girders (Lin, 1958 and Noppakunwijai et al., 2001). As such, three TxDOT standard sections, the I-, U-, and double-tee girder, were chosen for Project 4086. To simplify their fabrication, the standard shapes were represented as rectangular, inverted-tee, and tee girders, respectively. The ratio of the geometric centroid position to the height of the section was used to correlate the standard TxDOT shape to the laboratory specimen. This ratio was computed as y_b divided by h, where y_b is the distance to the geometric centroid from the bottom fiber of the section; and h is the section height. The average y_b/h ratio for each standard shape was approximately matched in the design of the scaled specimens. This ratio for the TxDOT standard I-, U-, and double-tee girders was 0.46, 0.41, and 0.68, respectively. The y_b/h ratio for the rectangular, inverted-tee, and tee beams was 0.50, 0.41, and 0.66, respectively. In addition, the specimens were designed at an approximate scale of 3:1 to ease their handling, testing, and fabrication. The reduction in size reduced the moments due to the dead load of the member at prestress transfer. As a result, the maximum concrete stress at release near the ends of the beam was only slightly larger than the stress near midspan. All of the beams were 15-feet in length.

The TxDOT standard shapes are illustrated in Figure 3-1 – 3-3. The dimensions and geometric properties of the three standard sections are provided in Table 3-1 – 3-3. All of the small-scale section types fabricated under Project 4086 are included in Figure 3-4.

52
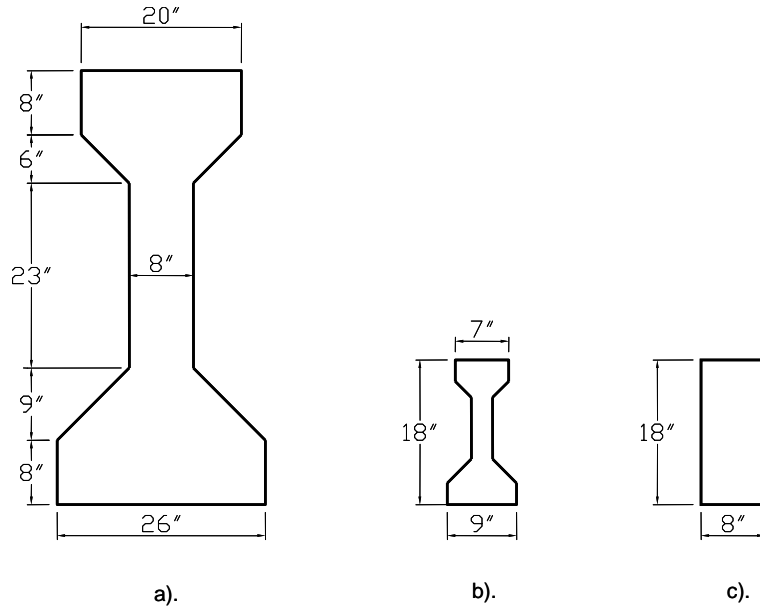
Figure 3-1: a) Cross-section of AASHTO Type IV I-girder; b) 1:3 Scaled Type IV girder; c) 8-in by 18-in test specimen

Table 3-1: Properties of AASHTO Type IV I-girder (TxDOT, 2005)

Beam Type	Width (in)	Depth (in)	y_t (in)	y_b (in)	A (in^2)	I (in^4)	y_b/h
AASHTO TYPE IV	26	54	29.25	24.75	788.4	260,403	0.46
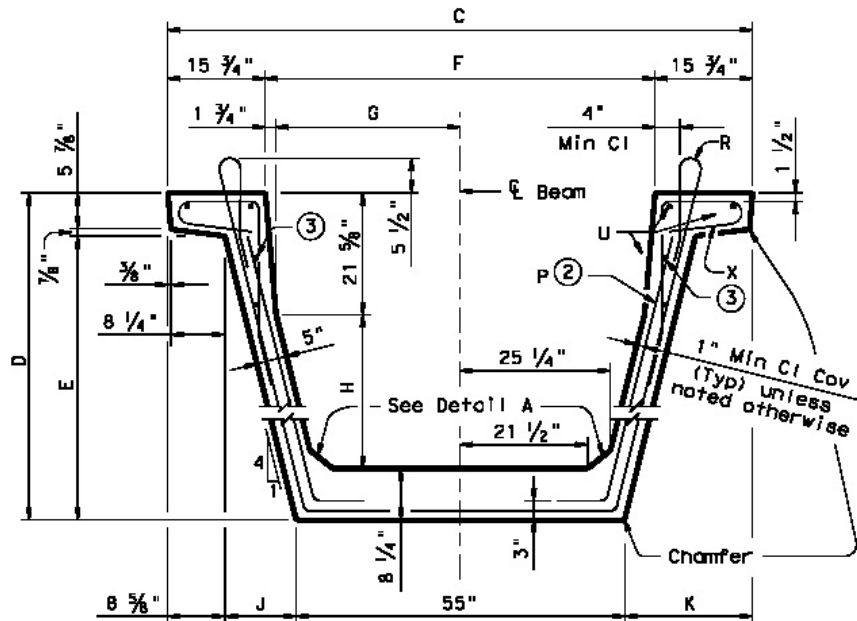
Figure 3-2: Cross section of TxDOT U-girders (TxDOT, 2005)

53

Table 3-2: Properties of standard TxDOT U-girders (TxDOT, 2005)

Beam Type	C (in)	D (in)	y_t (in)	y_b (in)	A (in^2)	I (in^4)	y_b/h
U40	89	40	23.66	16.30	979.9	183,108	0.41
U54	96	54	31.58	22.36	1120.0	403,020	0.41
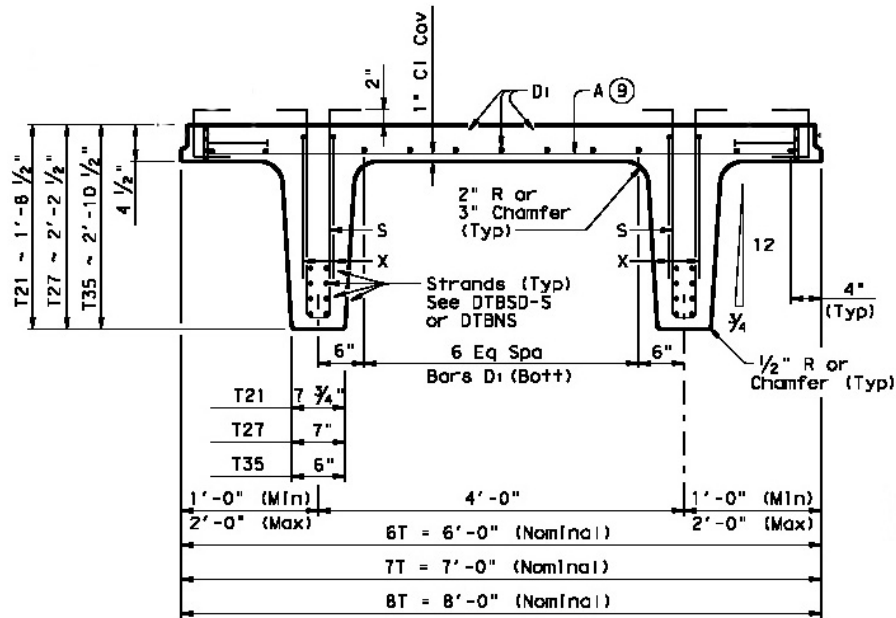
Figure 3-3: Cross section of TxDOT double-tee girders (TxDOT, 2005)

Table 3-3: Properties of standard TxDOT double-tee girders (TxDOT, 2005)

Beam Type	Width (ft)	Depth (in)	y_t (in)	y_b (in)	A (in^2)	I (in^4)	y_b/h
6T21	6.00	20.50	6.88	13.62	603	21,140	0.66
7T21	7.00	20.50	6.50	14.00	657	22,292	0.68
8T21	8.00	20.50	6.17	14.33	711	23,283	0.70
6T27	6.00	26.50	8.99	17.51	691	42,511	0.66
7T27	7.00	26.50	8.51	17.99	745	44,881	0.68
8T27	8.00	26.50	8.08	18.42	799	46,942	0.70
6T35	6.00	34.50	11.79	22.71	795	84,325	0.66
7T35	7.00	34.50	11.18	23.32	849	89,017	0.68
8T35	8.00	34.50	10.65	23.85	903	93,159	0.69
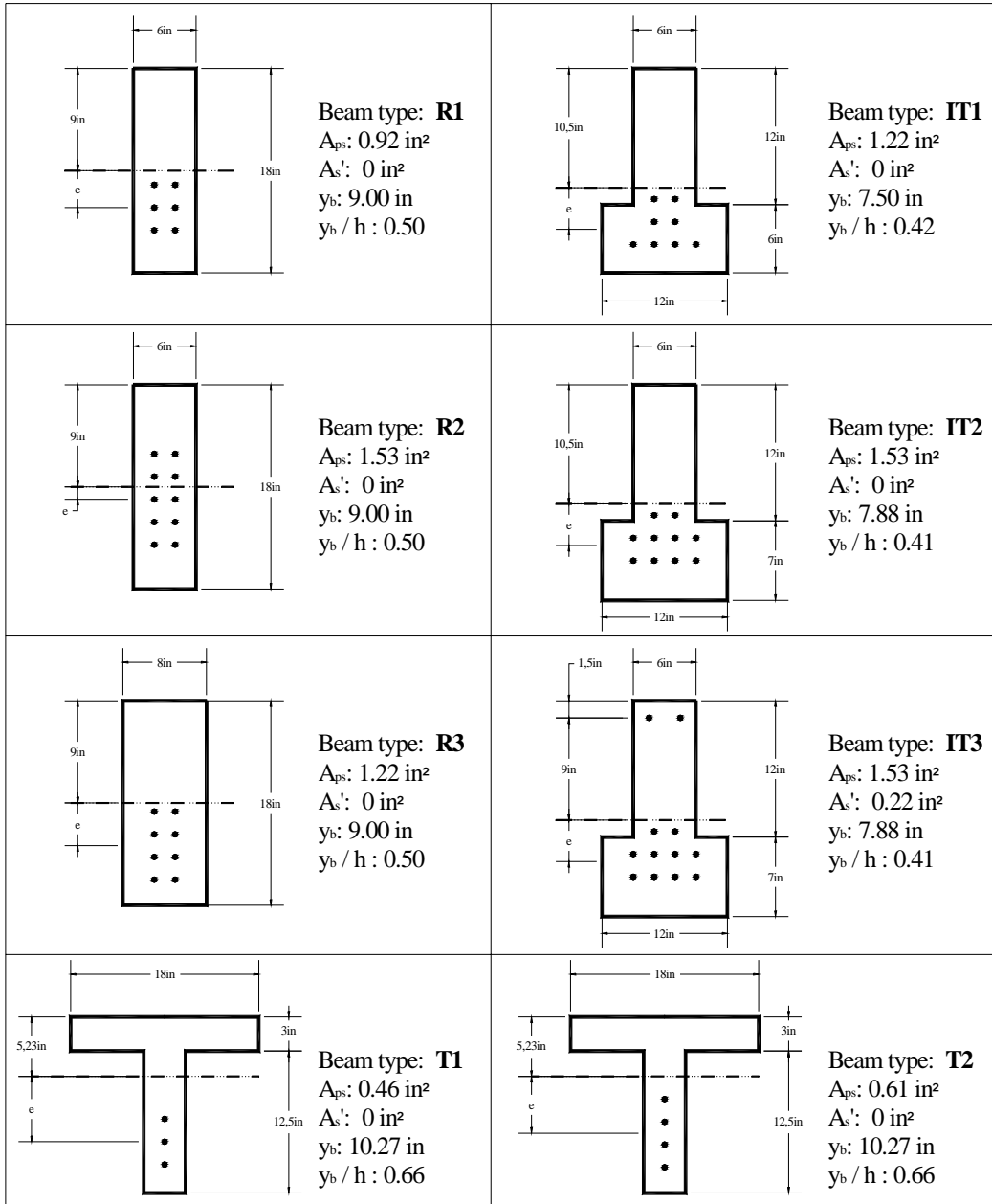
Figure 3-4: Small-scale test specimen cross sections (Castro et al., 2004)

The stress gradient at release was also investigated in Project 4086. It was considered especially important for pretensioned members subjected to high levels of compressive stress at release due to the risk of excessive creep (Castro et al., 2004). For a given section, the stress gradient is a function of the location of the prestressing force with respect to the geometric centroid. For instance, in flexural members, the center of gravity of the prestressing strands is typically located near the bottom of the section. With an appropriate magnitude of force, the bottom fibers of the section are subjected to compressive stresses while the top fibers of the section are subjected to tensile stresses. As a result, a relatively high stress gradient exists as the

stress changes fairly rapidly over the height of the section. In other cases in which the center of gravity of the prestressing strands is located near the geometric centroid, a more uniform distribution of compressive stress exists. The latter arrangement produces a low stress gradient because the values do not change rapidly over the section height. To evaluate the effect of the stress gradient on the release behavior and the camber growth of a prestressed girder, two beams with relatively low gradients were designed. These beams are designated as beam type R2 in Figure 3-4.

In addition to the straight prestressing strands, the only other steel reinforcement was two longitudinal bars placed in the IT3 section types and confinement steel at the ends of each beam. The confinement reinforcement consisted of #3 longitudinal bars supporting #3 stirrups. It was located within the first 27-inches at the ends of each test specimen to resist the bursting stresses at prestress transfer. Since the Project 4086 beams were only fabricated for camber evaluation, no additional reinforcement, such as shear reinforcement, was included in the members.

3.2.1.1 Concrete Mix Design

Lastly, three different concrete mixture designs were used in the specimens fabricated under Project 4086. They were based on typical high-strength concrete mixes used by a regional precast manufacturing plant. The first two mixes were identical with the exception of the coarse aggregate type. The first mix used round river gravel; the second mix used crushed limestone. In the previously-reviewed research studies of Cetin and Carrasquillo (1998), Myers and Carrasquillo (1998), and Mokhtarzadeh and French (2000), it was demonstrated that concrete with river gravel was stiffer than that with crushed limestone in general. Comparing the response of similar beams with each of the first two mixes evaluated the effect of the aggregate on the camber and creep performance of the member. In the third mixture design, the same materials of mix 2 were used with the exception of the cementitious materials. A portion of the Type III cement was replaced with Class C fly ash. This replacement technique is used in Texas to decrease the amount of alkalis in the mix, thus decreasing the development of alkali-silica reaction. However, the replacement of Type III cement also decreases the rate of strength gain. Since pretensioned members are subjected to compressive and tensile stresses at early ages, the rate of strength gain is very influential to the camber growth. As a result, with the inclusion of the third mixture design, the performance of pretensioned beams fabricated with concrete mixture designs containing Class C fly ash was evaluated. More specifically, the effects of a reduced rate of strength gain on the camber growth were observed. The properties of the aggregates and the proportions of the three mixture designs are illustrated in Table 3-4 and 3-5, respectively.

Table 3-4: Aggregate properties (Castro et al., 2004)

Property	River Rock	Crushed Limestone	River Sand
Gradation	ASTM C33 Grade 56	ASTM C33 Grade 56	ASTM C33
Max. Aggregate Size	1 inch	1 inch	-
Fineness Modulus	-	-	2.74
Specific Gravity	2.62	2.52	2.62
Particle Shape	Rounded	Angular	-

Table 3-5: Project 4086 concrete composition (per cu. yd.) and characteristics

(Castro et al., 2004)

Components / Property	Mix 1	Mix 2	Mix 3
Water / Cementitious Materials Ratio	0.33	0.33	0.34
Water (lbs)	204	203	182
Alamo Type III Cement (lbs)	608	608	373
W.A. Parish Class C Fly Ash (lbs)	-	-	170
Natural River Sand (lbs)	1183	1177	1322
1-inch River Rock (lbs)	2044	-	-
1-inch Crushed Limestone (lbs)	-	2042	2006
High-range water-reducing admixture (oz) -Rheobuild 1000 by Master Builders-	158	158	109
Retarding admixture (oz) -Pozzolith 300R by Master Builders-	21	21	16
Unit weight (lbs/ft^3)	154	155	150
7-day Compressive Strength (psi)	8330	8670	6375
28-day Compressive Strength (psi)	10030	10000	7390
28-day Modulus of elasticity (ksi)	5900	4850	5010
Slump (in)	7	8.5	9

3.2.2 Fabrication of the Project 4086 Beams

The scaled specimens were fabricated at the Ferguson Structural Engineering Laboratory (FSEL) at the University of Texas at Austin in a pretensioning bed modified and constructed under TxDOT Project 4086. The prestressing bed (Figure 3-5) contained three pretensioning lines, 40-feet in length. Six beams were fabricated in each cast with two beams in each line. Thirty beams were produced in five separate casts.

Figure 3-5: Prestressing bed with rectangular, tee, and inverted-tee beams (photograph courtesy of Alfredo Castro)

The section type, mix design, casting date, and maximum calculated compressive and tensile stresses at release of the Project 4086 beams are listed in Table 3-6. It is important to note that the naming system for each beam was changed during the course of the current research project (TxDOT Project 5197). The maximum stress at release calculated at the end of the member and the order in which the beams were statically tested are reflected in the new naming system. The designation for each beam as determined in both projects, 4086 and 5197, is listed in Table 3-6 for reference. Six beams fabricated within TxDOT Project 4086 were damaged over the course of Projects 4086 or 5197. As such, they were not included in Table 3-6. In the following sections, the stressing, concrete casting, and prestress transfer operations used in the fabrication of the Project 4086 beams are described. Additional information on these beams such as release stress calculations, section properties, and shop drawings is provided in Appendix A.

Table 3-6: Details of small-scale beam specimens

Mix Type	Cast Date	Proj. 4086 Designation	Proj. 5197 Designation	Maximum Stress (P/A ± Mc/I)*		f'_{ci} (psi)	Age (hrs)
				σ_{BOTTOM}	σ_{TOP}		
Mix # 1	6/26/2002	R1-60-1 (a)	R1-52-1-T8	$-0.52f'_{ci}$	$1.6\sqrt{f'_{ci}}$	5735	12
		R1-60-1 (b)	R1-52-1-T7	$-0.52f'_{ci}$	$1.6\sqrt{f'_{ci}}$	5735	12
		R1-70-1 (a)	R1-50-1-T1	$-0.50f'_{ci}$	$1.6\sqrt{f'_{ci}}$	6025	13
		R1-70-1 (b)	R1-49-1-T2	$-0.49f'_{ci}$	$1.5\sqrt{f'_{ci}}$	6025	13
		R1-75-1 (a)	R1-46-1-T5	$-0.46f'_{ci}$	$1.5\sqrt{f'_{ci}}$	6275	14
		R1-75-1 (b)	R1-48-1-T6	$-0.48f'_{ci}$	$1.5\sqrt{f'_{ci}}$	6275	14
	8/13/2002	T1-74-2	T1-68-2-T17	$-0.68f'_{ci}$	$3.9\sqrt{f'_{ci}}$	4220	7
		T1-82-2	T1-62-2-T18	$-0.62f'_{ci}$	$5.2\sqrt{f'_{ci}}$	4220	7
		IT1-76-2	IT1-68-2-T20	$-0.68f'_{ci}$	$4.1\sqrt{f'_{ci}}$	3815	7
		IT1-84-2	IT1-73-2-T19	$-0.73f'_{ci}$	$9.8\sqrt{f'_{ci}}$	3815	7
	9/24/2002	R3-76-3	R3-75-3-T9	$-0.75f'_{ci}$	$3.7\sqrt{f'_{ci}}$	4065	10
		R3-82-3	R3-78-3-T3	$-0.78f'_{ci}$	$7.1\sqrt{f'_{ci}}$	4065	10
		T2-76-3	T2-79-3-T16	$-0.79f'_{ci}$	$1.5\sqrt{f'_{ci}}$	3950	10
		T2-85-3	T2-86-3-T15	$-0.86f'_{ci}$	$4.2\sqrt{f'_{ci}}$	3950	10
		IT3-85-3	IT3-79-3-T21	$-0.79f'_{ci}$	$9.0\sqrt{f'_{ci}}$	4065	10
		IT2-85-3	IT2-76-3-T22	$-0.76f'_{ci}$	$8.8\sqrt{f'_{ci}}$	4320	10
Mix # 2	12/5/2002	R3-76-4	R3-78-4-T11	$-0.78f'_{ci}$	$3.7\sqrt{f'_{ci}}$	3800	14
		R3-82-4	R3-83-4-T12	$-0.83f'_{ci}$	$7.3\sqrt{f'_{ci}}$	3800	14
		IT3-85-4	IT3-83-4-T24	$-0.83f'_{ci}$	$9.1\sqrt{f'_{ci}}$	3800	14
Mix # 3	3/4/2003	R3-76-5	R3-75-5-T10	$-0.75f'_{ci}$	$3.5\sqrt{f'_{ci}}$	4045	15
		R3-82-5	R3-80-5-T4	$-0.80f'_{ci}$	$7.1\sqrt{f'_{ci}}$	4045	15
		T2-76-5	T2-91-5-T14	$-0.91f'_{ci}$	$1.9\sqrt{f'_{ci}}$	3465	15
		IT3-85-5	IT3-79-5-T23	$-0.79f'_{ci}$	$9.3\sqrt{f'_{ci}}$	4045	15
		IT2-85-5	IT2-80-5-T13	$-0.80f'_{ci}$	$9.0\sqrt{f'_{ci}}$	4045	15

* At end of the member

3.2.2.1   *Stressing and casting operation*

The first step in the fabrication of the Project 4086 beams was the instrumentation and stressing of the prestressing strands. Each strand was instrumented with at least two electrical strain gauges to accurately estimate the force in the strand. The orientation of the gauge on the prestressing strand is illustrated in Figure 3-6. Due to the angle of the gauge with respect to the longitudinal axis of the prestressing strand, a calibration curve was developed by Rogers and Castro (Castro et al., 2004). With the curve, the measured strain from the gauges was correlated with the stress in the strand. After the gauges were in place, the non-prestressed reinforcement was tied; and the formwork was secured. Lastly, the prestressing strands were stressed to the

required level with a single-strand stressing jack and hydraulic pump. The jacking force exceeded the required initial force to account for the relatively large seating losses consistent with a short prestressing bed.
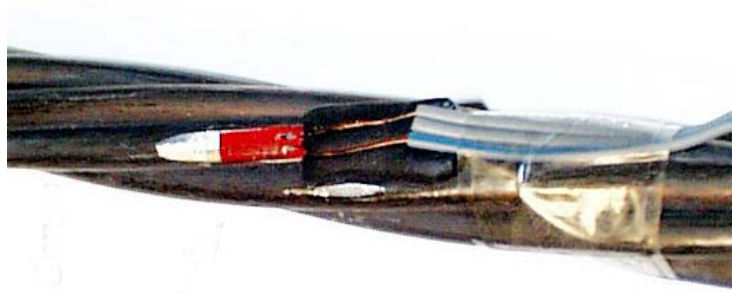
Figure 3-6: Strain gauge mounted along individual wire (Castro et al., 2004)

The next step in the fabrication process was the concrete casting. Before the concrete was placed, thermocouples were positioned at the approximate location of maximum temperature within each section. These locations are depicted in Figure 3-7. In each case, the thermocouple arrangement provided a worse-case scenario in terms of releasing the beams as early as possible. The concrete was batched and mixed at the laboratory in a concrete mixing truck. With the help of an overhead hopper, the concrete was placed in the formwork with care to prevent the damage of the strain gauges and the thermocouples. Immediately after casting, each beam was covered with wet burlap.
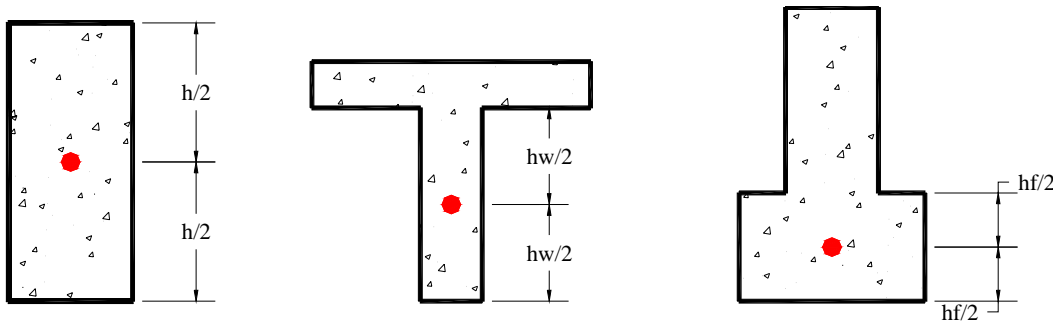
Figure 3-7: Position of the thermocouples in 4086 beams (Castro et al., 2004)

3.2.2.2   *Prestress transfer operation*

As the beams cured, a temperature match-curing system (Sure Cure) matched the temperature of the beams fabricated in each of the three lines with four temperature-controlled cylinders (4x8-inch). These four cylinders were used to determine the concrete release strength of each line (2 beams). Conventional cylinders placed next to the beam were also used to estimate the early-age compressive strength gain and to provide the 28-day strength.

Shortly before release, the wet burlap was removed and linear potentiometers were installed on the pretensioned beams to measure the initial camber. The initial camber measurements are discussed in greater detail in Section 6.3. The prestressing force was released

by flame-cutting the prestressing strands, one wire at a time. Care was taken to heat the strands as slowly as possible and to subject the section to the prestressing force symmetrically. A more detailed account of the casting operation and the Sure Cure system is provided in the TxDOT Project 4086 report (Castro et al., 2004).

3.3   DESIGN AND FABRICATION OF TxDOT TYPE-A BEAMS

In addition to the scaled specimens, twelve full-scale I-girders were fabricated and tested in the current study. These beams were tested for two reasons. First, there was a gap in the range of maximum compressive release stress provided by the Project 4086 beams. Data from the full-scale girders filled this gap. Second, the chosen beam type is used in practice and therefore, validates the laboratory testing program. Forty-feet long TxDOT Type-A beams were selected. Slight modifications to the standard design were made to target specific levels of maximum compressive stress at release. All twelve girders were fabricated by Heldenfels Enterprises, Inc. at their Corpus Christi precast prestressed beam fabrication plant. The modification of the standard design, the concrete mixture design, the fabrication procedure, and the inventory of the Type-A beams are explained in this section.

3.3.1   Design of TxDOT Type-A Beams

The standard TxDOT design for Type-A beams was modified for the full-scale specimens in this study. A specific, non-standard strand pattern was developed for all of the specimens. Fourteen ½-inch diameter 270-ksi low-relaxation strands were utilized in the section. Of the fourteen strands, four were deflected to minimize compressive and tensile stresses in the end regions. The deflected strands were pulled down at two locations, five-feet on either side of the midspan of the girder. The resulting compressive stresses at release were at a maximum at the hold-down locations but were only slightly lower at midspan. In general, the compressive bottom-fiber stress at midspan was approximately 0.5-percent of f'_{ci} lower than the stress at the hold-down point. The number of strands and their pattern were the same for all of the full-scale specimens. The only variable controlling the maximum compressive stress at prestress transfer was the release strength of the concrete, f'_{ci}. For the twelve girders, the targeted concrete strength at release ranged from 3,900-psi to 5,400-psi.   The corresponding maximum compressive stress at release ranged from $0.75f'_{ci}$ to $0.55f'_{ci}$, respectively.

The section dimensions and the strand pattern are illustrated in Figure 3-8. The section properties are provided in Table 3-7. The targeted release strength and maximum release stress of each of the twelve specimens are listed in Table 3-8.
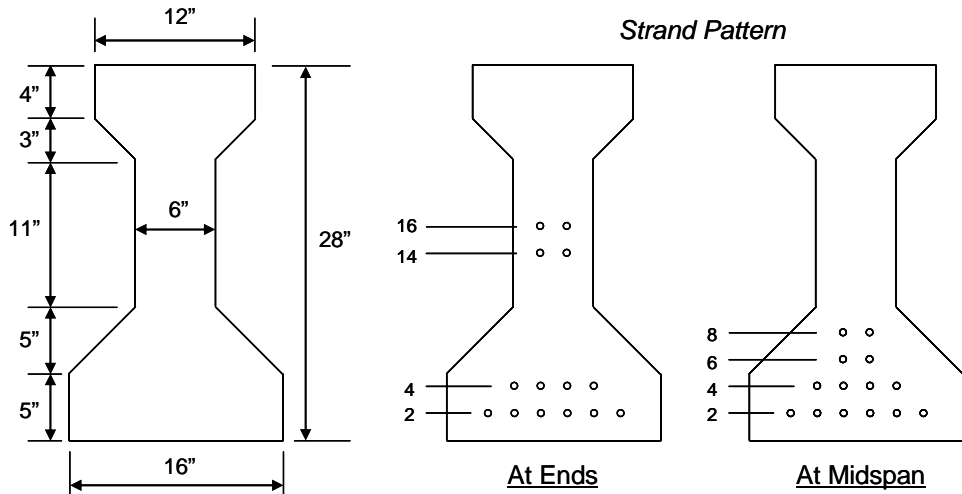
Figure 3-8: TxDOT Type-A beam dimensions and altered strand pattern

Table 3-7: Section properties of TxDOT Type-A beam

Beam Type	y_t (in)	y_b (in)	A (in^2)	I (in^4)	w (p/ft)
A	15.39	12.61	275.4	22,658	287

Table 3-8: Targeted maximum release stress and strength of the Type-A beams

Beam Mark	Targeted σ_{BOTTOM}	Targeted Range of f'_{ci} (psi)	Number of Beams
A55	-0.55f'_{ci}	5300 – 5500	1
A60	-0.60f'_{ci}	4800 – 5000	2
A65	-0.65f'_{ci}	4400 – 4600	3
A67	-0.67f'_{ci}	4300 – 4500	3
A70	-0.70f'_{ci}	4000 – 4200	2
A75	-0.75f'_{ci}	3800 – 4000	1

The rest of the beam design was in accordance with the AASHTO LRFD Bridge Design Specifications as depicted in the TxDOT standard design. Double-legged stirrups were included throughout the girder with a maximum spacing in the midspan region of 12-inches. Standard confinement steel enclosing the strands was adequate for the prestressing force in the modified section. Also, enough vertical steel was in place to satisfy bursting stress requirements. Lastly, the tensile stress limit at release of $7.5\sqrt{f'_{ci}}$ (with f'_{ci} in psi) was satisfied everywhere along the member. Two #5-bars were oriented longitudinally in the top flange to resist the tensile forces and control the crack widths if the beam cracked at release. A shop drawing and sample release stress calculation for one of the fabricated full-scale girders is included in Appendix B.

3.3.1.1   Concrete Mix Design

Two concrete mixture designs, named mix 4 and mix 5 herein, were used for the twelve full-scale girders (Table 3-9). Both class-H concrete mixes were designed by the precast manufacturing facility and were consistent with mixes used in standard pretensioned beams. Due to the stringent requirements on release strength and on speed of construction for the full-scale beams, it was vital for the concrete to gain strength at a consistent and rapid rate each time the mix was batched. Mix 4 was used for the first fabricated Type-A beam. Mix 5 was used for the other eleven girders. After the first beam was cast with mix 4, the concrete did not gain strength as fast as the precasters had hoped. To keep with their schedule, they released the first beam when the concrete reached 5,000-psi instead of the targeted release strength of 5,400-psi. As a result, the first fabricated beam was a type A60 beam as opposed to a type A55. For the next eleven casts, mix 5 was used without any problems. For reference, the date of each cast and the age of each beam at prestress transfer are provided in Section 3.3.2.

The components of both mixture designs are listed in Table 3-9. Type III cement and round, river gravel were used in both mixes. Mix 5 had a smaller water-to-cement ratio than mix 4. To offset this reduction, a larger quantity of superplasticizer was used with an overall finer gradation of aggregates in mix 5.

Table 3-9: Concrete mix designs used in Type-A beams, per cy. (HEI, 2006)

Components	Mix 4	Mix 5
Water / Cement Ratio	0.33	0.31
Water (lbs)	231	201
Alamo Type III Cement (lbs)	696	658
Fine Aggregate (lbs)	1133	1278
Coarse Aggregate: Round, River Gravel (lbs)	1994	1885
High-range water-reducing admixture (oz)	50[1]	126[2]
Retarding admixture (oz) **-Sika Plastiment-**	7	10
Theoretical Unit weight (lbs/ft^3)	150	149

[1]**Sika Viscocrete 2100**
[2]**Sikament N**

3.3.2   Fabrication of Full-scale TxDOT Type-A Beams

The twelve full-scale girders were fabricated by Heldenfels Enterprises, Inc. at their Corpus Christi, Texas precast pretensioned beam manufacturing plant.   The beams were constructed individually in the prestressing bed shown in Figure 3-9. Each beam was released close to the specified range of compressive strength. It is important to note that since each beam was constructed individually, twelve unique girders were produced with different concrete strengths at prestress transfer. The inventory of the twelve beams, the release strength of each girder, and the corresponding stress at release is provided in Table 3-10. The stressing, concrete casting, prestress transfer, and transportation procedures for the full-scale girders are discussed in the following sections.

Figure 3-9: Prestressing bed at HEI Corpus Christi Plant (photograph courtesy of Chris Leonard)

Table 3-10: Details of full-scale beam specimens

Concrete Mix #	Test Specimen Designation	Maximum Release Stresses*		f'_{ci} (psi)	Age (hrs)	Date of Cast
		σ_{BOTTOM}	σ_{TOP}			
Mix 5	A55-T25	$-0.55f'_{ci}$	$6.1\sqrt{f'_{ci}}$	5500	11	7/13/2006
Mix 4	A60-T26	$-0.60f'_{ci}$	$6.3\sqrt{f'_{ci}}$	5010	16	7/12/2006
Mix 5	A63-T27	$-0.63f'_{ci}$	$6.4\sqrt{f'_{ci}}$	4790	11	7/14/2006
	A66-T28	$-0.66f'_{ci}$	$6.6\sqrt{f'_{ci}}$	4550	7	7/17/2006
	A67-T29	$-0.67f'_{ci}$	$6.6\sqrt{f'_{ci}}$	4450	14	7/18/2006
	A66-T30	$-0.66f'_{ci}$	$6.6\sqrt{f'_{ci}}$	4500	9	7/19/2006
	A69-T31	$-0.69f'_{ci}$	$6.7\sqrt{f'_{ci}}$	4330	8	7/20/2006
	A68-T32	$-0.68f'_{ci}$	$6.7\sqrt{f'_{ci}}$	4390	9	7/21/2006
	A67-T33	$-0.67f'_{ci}$	$6.6\sqrt{f'_{ci}}$	4480	7	7/24/2006
	A73-T34	$-0.73f'_{ci}$	$6.9\sqrt{f'_{ci}}$	4080	10	7/25/2006
	A71-T35	$-0.71f'_{ci}$	$6.8\sqrt{f'_{ci}}$	4180	7	7/26/2006
	A75-T36	$-0.75f'_{ci}$	$7.0\sqrt{f'_{ci}}$	3960	7	7/27/2006

*At hold-down point (A-A)
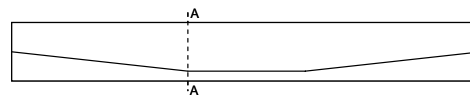
3.3.2.1 Stressing and casting operation

The fabrication sequence of the full-scale beams consisted of several steps. First, the prestressing strands were stressed to the appropriate jacking stress according to pressure gauges at the live end of the bed. The elongation of the strand at each end was checked to confirm the pressure reading. These measurements were used to ensure that the actual prestressing force was within 5-percent of the required force. After the strands were fully-stressed, the non-prestressed reinforcement was tied in place; and the steel formwork was secured. The concrete was mixed at a batching plant on site and transferred to the beam with motorized hoppers. Each beam was cast in approximately two lifts. Afterwards, the top surface was covered with wet burlap and tarps.

3.3.2.2 Prestress transfer operation

Approximately twenty-four 4x8-inch concrete cylinders were tested periodically to map the strength gain of each girder. All of the compression tests conformed to ASTM C39-04. It is important to note that the cylinders cured next to the beam beneath a heavy tarp until the compression tests were performed. Temperature match-curing technology was not used for the fabrication of the full-scale beams. Once the concrete was within 1,000-psi of the targeted release strength, two cylinders were tested every 20-minutes or as needed to document the strength growth. When the average strength of the two cylinders reached within ±100-psi of the targeted strength, the beam was released. With this procedure, the girders were released at the appropriate times.

After the required compressive strength was reached, the formwork was removed; and the strand attached to each hold-down mechanism was flame-cut with an oxy-acetylene torch. Then, the torch was used to cut the prestressing strands at the end of the girder one wire at a time. The strands were cut as slowly as possible and in a symmetric pattern. After the entire prestressing force was transferred to the member, the initial camber was measured at the midspan of the beam. Following the approval of the quality-control inspector, the beam was lifted from the bed and placed in the storage yard.

3.3.2.3 Shipment and storage

Four beams were shipped at a time on a flatbed truck from Corpus Christi to the Ferguson Structural Engineering Laboratory in Austin, Texas. Each beam was at least 7-days old at the time of shipment. In the laboratory, a 25-ton crane with a 40-feet steel spreader beam was used to lift each beam from the truck. The lifting points of each girder were approximately 1-foot from the ends of the beam. Each beam was stored in the laboratory until the time of the test. The crane hook and the transfer beam lifting one of the fabricated specimens is depicted in Figure 3-10.

Figure 3-10: Lifting a Type-A girder from a flatbed truck in FSEL

3.4   SUMMARY

Twenty-four scaled beam specimens and twelve full-scale girders were tested in this research study. The small-scale specimens were fabricated under a previous research project, TxDOT Project 4086, with the maximum compressive stress at release ranging from $0.46f'_{ci}$ to $0.91f'_{ci}$. These rectangular, inverted-tee, and tee sections were designed at a scale of 3:1 to represent standard TxDOT I-, U-, and double-tee girders, respectively. The twelve full-scale girders were TxDOT Type-A beams in which a non-standard strand pattern was developed to obtain a specific range of the maximum release stresses for given release strengths. As a result, the strand pattern and beam dimensions were the same for all twelve girders; the only variable was the release strength of the concrete. For these girders, the actual release strengths ranged from 5,500-psi to 3,960-psi producing maximum release stresses ranging from $0.55f'_{ci}$ to $0.75f'_{ci}$. The experimental program that utilized the test specimens described in this chapter is summarized in Chapter 4.

CHAPTER 4
Experimental Program

4.1 OVERVIEW

The experimental program for the current research project consisted of three phases:
- Phase I: Static testing of scaled (Project 4086) beams (24 tests)
- Phase II: Static testing of full-scale Type-A girders (12 tests)
- Phase III: Fatigue testing of scaled (Project 4086) beams (4 tests)

The first phase consisted of the static testing of the twenty-four scaled specimens described in Section 3.2. For these tests, the beams were loaded up to approximately 30-percent above their measured cracking load or until failure. The load was applied to produce a constant moment region over the middle third of the beam. During the test, different instruments such as string potentiometers, DCDTs, and foil gauges were used to monitor the midspan deflection, the support deflections, and the concrete and strand strains in the test region.

The second phase consisted of the static testing of the twelve full-scale girders described in Section 3.3. The test setup and procedure were very similar to that used in the testing of the scaled beams. The maximum applied load was approximately 30-percent above the measured cracking load. Also, the load was applied to produce a constant moment region in the middle of the span of approximately the same length as the constant moment region used in the testing of the scaled beams, 5-feet. The midspan deflection, support deflections, and the applied load were monitored throughout the tests of the full-scale girders.

The third phase consisted of the fatigue testing of four scaled specimens that were previously cracked during the first phase of the experimental program. Two of the fatigue specimens were subjected to conventional stresses at release; two were subjected to elevated stresses at release. In all four cases, a load range corresponding to 25-percent above and 65-percent below the measured cracking load was applied to the specimens for two million cycles. These three phases of the experimental program are described in this chapter.

4.2 PHASE I: STATIC TESTING OF SCALED BEAMS

Static testing was performed on the twenty-four scaled pretensioned beams fabricated in TxDOT Project 4086 to experimentally evaluate the cracking load. The loading protocol, test setup, and instrumentation and data acquisition for the testing of the scaled beams are discussed in the following sections.

4.2.1 Load Protocol

The beams were loaded at a constant rate of approximately 100-pounds per second. In the linear-elastic range, the applied load was increased in 5-kip increments. In the nonlinear range, the applied load was increased in smaller increments to detail the inelastic portion of the load-deflection response. The amount of load in the later increments depended on the additional capacity of the section being tested. At the anticipated cracking load and at each load step afterwards, the load was maintained, the beam was inspected, the crack propagation was mapped on the beam, and the widths of selected cracks were measured with a crack comparator card. In

addition, pictures were taken at a fixed location to illustrate the crack growth and beam deflection as the load increased. During the first phase of the experimental program, it was not clear which beams would be tested in fatigue. As such, the beams were not loaded to failure. The maximum load applied to the scaled specimens was approximately 30-percent higher than the measured cracking load. A visual depiction of the loading protocol for the type R1 beam is provided in Figure 4-1.
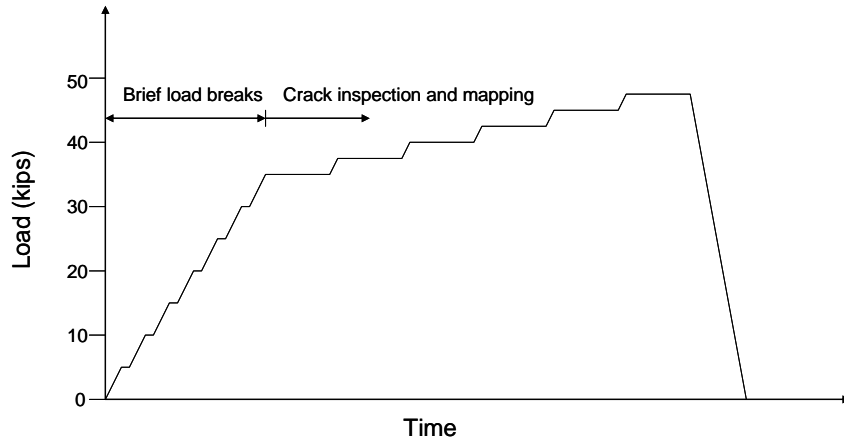
Figure 4-1: Depiction of load program for type R1 beam

4.2.2   Test Setup

The twenty-four small-scale beams were subjected to four-point loading. A reaction frame consisting of two back-to-back channels that spanned two columns was bolted to the strong floor of the laboratory at the midspan of the beam (Figure 4-2 and 4-3). A double-acting hydraulic ram integral with a load cell was fastened to the bottom of the back-to-back channels. The ram and load cell assembly included a clevis at the top where it connected to the back-to-back channels and a clevis at the bottom where it connected to a stiff, spreader beam. Via the spreader beam, the load was applied to the third points of the girder. This arrangement created a constant moment region within the middle third of the beam (4-feet 10-inches). Two steel plates (2x6-inches and ½-inch thick) were used as the load bearings beneath the spreader beam. Due to imperfections along the concrete surface, a thin layer of hydrostone was applied between the steel plates and the top of the beam. Once it hardened, the hydrostone fixed the location of the steel plates over the course of the test. For safety concerns, a lateral brace was attached to each column to stabilize the specimen in case a test specimen laterally buckled or rotated (Figure 4-3). One-inch of clearance was maintained between the braces and the sides of the beam to ensure that the beam resisted the entire applied load. It should be noted that none of the test specimens experienced lateral buckling or came into contact with the lateral braces during the static tests.

The beam was simply supported. At each end, the beam reacted against concrete blocks. To achieve simply-supported end conditions, two steel plates sandwiching a round bar were arranged between the end of the beam and the concrete block. For the pinned end condition, the bar was welded to the bottom steel plate. For the roller end condition, the bar was allowed to roll

68

freely. The span between the centerlines of the two bars was 14 ½-feet. The "pinned" support condition is illustrated in Figure 4-4.
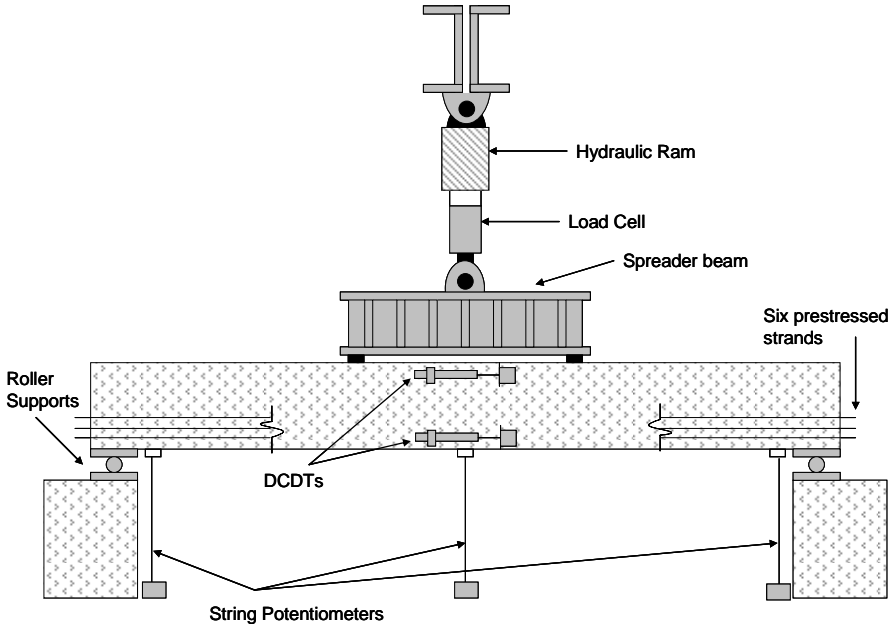
Figure 4-2: Test setup for static testing of small-scale girders (Type R1)

Figure 4-3: Picture of test setup for static testing of small-scale girders

Figure 4-4: "Pinned" support condition with bar welded to the bottom plate

4.2.3   Instrumentation and Data Acquisition

All of the instrumentation measured changes in voltage. The voltage readings were scanned into a computer where they were converted to the proper engineering quantities by specific calibration equations. For the small-scale tests, the applied load, the midspan deflection, the support deflections, the incremental strain in the prestressing strands, and the top and bottom strain in the section were recorded. The following devices were used to obtain this information:

- 100-kip capacity load cell
- 3 – 5-inch string potentiometers
- electrical strain gauges afixed to the prestressing strands
- ¾-inch direct current displacement transducers (DCDTs) mounted to the exterior of the beam

The external instrumentation for the static tests of the scaled beams is depicted in Figure 4-2 and 4-3.

The load was measured using a 100-kip capacity load cell. The load cell was calibrated prior to the static testing of the scaled beams to ensure its accuracy. Over the course of a test, the load cell readings were confirmed with a pressure gauge attached to the hydraulic line. Multiplying the reading on the pressure gauge by the internal area of the ram gave a consistent and reasonable estimation for the applied load. As such, the load cell measurements were verified. The same load cell was used in every static test of every scaled beam.

String potentiometers were used at the ends and at the midspan of the beam to measure vertical deflections. In the first four tests, the ends of the beam were supported by neoprene pads. String potentiometers were placed next to the bearing locations to measure the compression of the pads so that it could be subtracted from the midspan deflection. However, after the first four tests, it was apparent that using a steel bar with two steel plates would produce more consistent results. This end condition created a more defined span length and increased the

accuracy of the midspan deflection measurement. Nevertheless, the string potentiometers at the ends of the beam were kept in place and were monitored for all of the subsequent tests. At midspan, the string potentiometer was located along the longitudinal axis of the beam and directly beneath the center of the hydraulic ram. For all of the string potentiometers, the base was bolted to a wooden board and weighted down to fix its position. The coiled wire from the string potentiometer was hooked to a small piece of plywood that was epoxied to the bottom surface of the beam.

The strain in the prestressing steel was monitored throughout each test by strain gauges on the prestressing strands. The gauges were attached to an individual wire of the prestressing strand during the fabrication of the TxDOT Project 4086 beams. A calibration curve was developed to correlate the measured strains with the stress in the strand (Castro et al., 2004 and Rogers, 2002). Primarily, the gauges were in place to accurately measure the force in the prestressing strands immediately before and after prestress transfer. It is important to note that they did not measure the long-term losses in the prestressing force. Even though the gauges were approximately 3-years old at the time of the static test, a number of them were still functional. They were zeroed before the load was applied and therefore, only measured the strain in the section due to the applied load. Assuming a complete bond between the strand and the concrete, the gauges monitored the incremental strain in both the concrete and the steel. The number of gauges in each beam varied depending on the section type. For the conventionally-stressed, rectangular beams, there were two gauges per strand; and they were positioned as in Figure 4-5. In all cases, the gauges were located near midspan, well within the region of constant moment.

Elevation
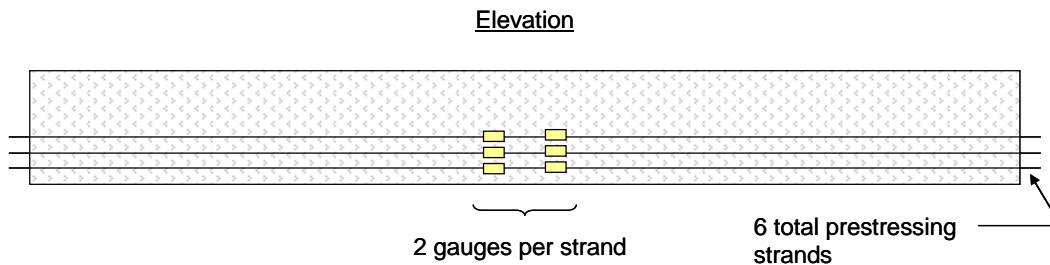
Figure 4-5: Location of strain gauges for type R1 beams

Lastly, the strain near the top and the bottom of the section was monitored with direct current displacement transducers or DCDTs. They were chosen for this task due to their high degree of accuracy. The DCDTs were mounted to both sides of the beam one-inch from the extreme fibers of the section, at the top and the bottom. To attach each device, two ¼-inch diameter holes were drilled in the side of the beam, 5 ½-inches apart. Steel anchors were secured in the holes and tightened into place. An aluminum clamp that gripped the DCDT was attached to one anchor. An aluminum angle that provided the reaction for the piston of the DCDT was secured to the other anchor. Both the clamp and the angle were tightened into place to fix their position during the test. Also, each DCDT was positioned at the middle of its total deflection capacity to ensure the most accurate deflection readings. The steel anchors provided a fixed gauge length that the measured deflection of the DCDT was divided by to obtain the top and

bottom strain. The aluminum hardware and a DCDT are illustrated in Figure 4-6 and Figure 4-7, respectively.

Figure 4-6: Aluminum clamp and angle before DCDT installation

Figure 4-7: DCDT used to measure bottom strain during the static test

4.3 PHASE II: STATIC TESTING OF FULL-SCALE BEAMS

Static testing was also performed on the twelve full-scale girders described in Section 3.3 to experimentally evaluate their cracking load. The loading protocol, test setup, and instrumentation and data acquisition of the static testing of the full-scale Type-A girders are discussed in the following sections.

72

4.3.1 Load Protocol

The full-scale beams were loaded at an approximate rate of 100-pounds per second. The load was increased steadily with brief pauses until it reached 55-kips. At 55-kips and for every additional 5-kip increment, the load was maintained; and the beam was visually inspected for cracks. All of the cracks were mapped on the beam and measured with a crack comparator card. Pictures were taken throughout the test to detail the crack propagation. After the applied load reached 80-kips (approximately 30-percent above the measured cracking load), the beam was slowly unloaded. To capture the post-cracking load-deflection response, the beam was reloaded at an approximate rate of 300-pounds per second. The second loading procedure provided a smooth curve that was used to supplement the original test. A sketch visually depicting the load program for the full-scale tests is provided in Figure 4-8.
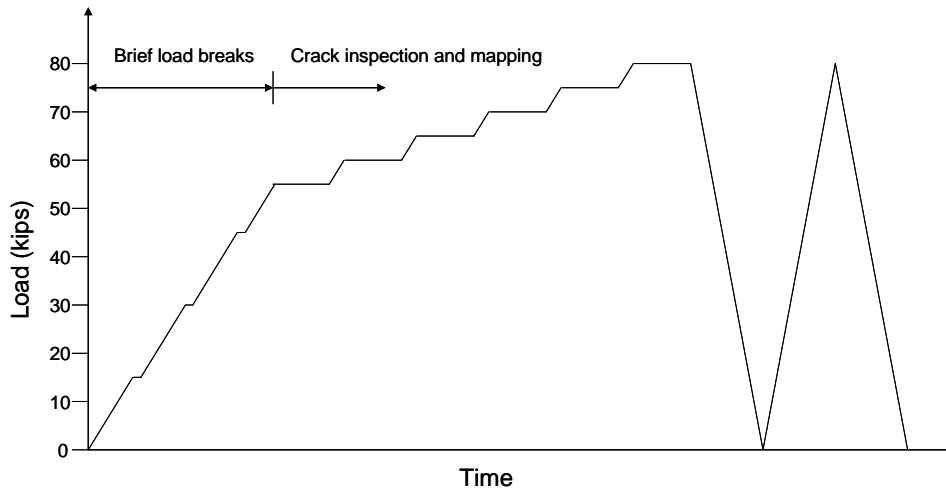
Figure 4-8: Depiction of loading protocol for tests of full-scale girders

4.3.2 Test Setup

As in the tests of scaled beams, the full-scale girders were subjected to four-point loading. The reaction frame consisted of two columns bolted to the strong floor with back-to-back channels spanning between them. A single-acting hydraulic ram attached to a steel plate was bolted to the bottom of the back-to-back channels. Beneath the ram, the following items were stacked on top of one another: a 100-kip capacity load cell, a spherical head, and a 64-inch long spreader beam. On top of the load cell, a machined steel cap was fitted to the load-bearing surface. The other end of this cap was machined as a sleeve that accepted the piston head of the ram as it extended. There was additional clearance in the sleeve of the cap to permit minor adjustments in alignment. To account for slight eccentricities or unparallel surfaces, a spherical head was placed between the load cell and the spreader beam. The diameters of the load cell and the spherical head and the width of the spreader beam were all approximately 8-inches. The spreader beam rested atop two small steel plates (2x8-inches and ½-inch thick) that were positioned 2 ½-feet on either side of the midspan of the pretensioned girder. A thin layer of hydrostone was placed beneath the steel plates to account for the uneven top surface of the girder concrete. Each one of the aforementioned items was carefully aligned with an accuracy of an 1/8

73

of an inch to ensure the symmetric loading of the specimen. As hydraulic fluid was transferred into the ram by a pneumatic pump, the piston extended and began loading the specimen once it contacted the top of the machined cap. The midspan portion of the test setup is depicted in Figure 4-9.

Figure 4-9: Midspan region of test-setup for full-scale beams

At the ends of the full-scale girder, the same support conditions were utilized as in the tests of the small-scale beams. Two steel plates sandwiching a round steel bar were placed between the ends of the girder and concrete support blocks. Simply supported boundary conditions were achieved by welding the bar to the bottom steel plate at one end of the girder. This end condition represented a pinned support. At the other end, the bar was permitted to roll freely, representing a roller support. The roller support condition for one of the tests of the full-scale girders is illustrated in Figure 4-10. Notice the longitudinal placement of the beam in regards to the location of the plate-and-roller support. The length of this particular beam exceeded the 40-foot design length by approximately 1-inch. As a result, each end of the beam slightly hung over the edge of the support. For an ideal 40-foot beam, the edge of the 6-inch wide plate was flush with the bottom edge of the 1-inch chamfer. In all cases, a centerline-to-centerline span of 39 1/3-feet was maintained. A sketch and picture illustrating the static test setup for the full-scale Type-A girders is provided in Figure 4-11 and 4-12, respectively.

Figure 4-10: Roller support condition at one end of full-scale girder
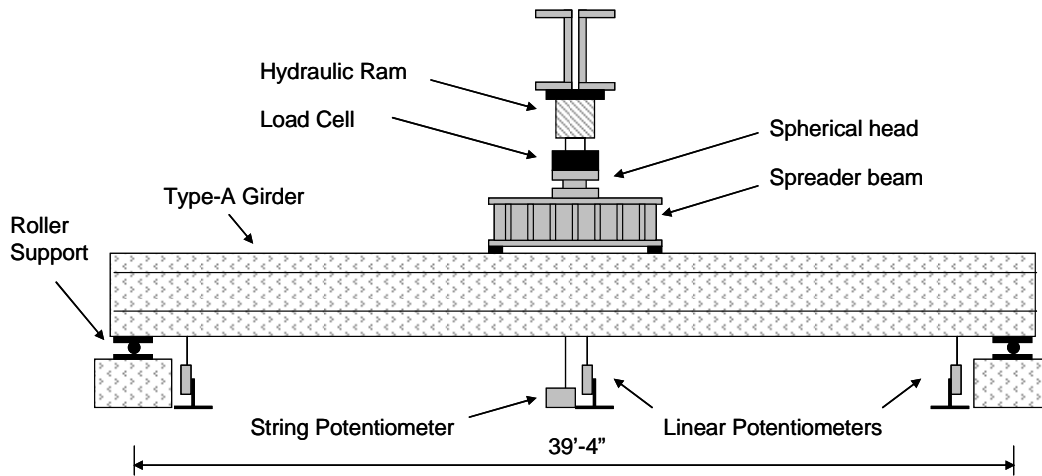
Figure 4-11: Test setup for static testing of full-scale girders (not to scale)

Figure 4-12: Picture of test setup for static testing of full-scale girders

4.3.3 Instrumentation and Data Acquisition

The instrumentation used in the full-scale tests measured changes in voltage that were converted to engineering quantities using individual, calibration equations. The midspan deflection, the support deflections, and the applied load were acquired in this manner with the following devices:

- 100-kip capacity load cell
- 10,000-psi pressure transducer
- 5-inch string potentiometer
- 3 – 6-inch linear potentiometers

The applied load was measured directly with a load cell and indirectly with a pressure transducer. Prior to the static testing of the full-scale girders, both of these devices were calibrated to ensure their accuracy. The load cell was positioned as seen in Figure 4-9 and as described in Section 4.3.2. The pressure transducer was attached to the hydraulic line supplying the fluid to the ram. Measured pressure readings from the transducer were converted to applied load estimates with the internal area of the ram. In this manner, the load cell readings were confirmed. It is important to note that the applied load measurements reported in this report were the load cell readings.

The midpsan deflection was measured with a string potentiometer and confirmed with a linear potentiometer. The base of the string potentiometer was bolted to a steel plate to fix its position. The end of the coiled wire was attached to a hook embedded in a small plywood block. The block was epoxied to the bottom surface of the girder. In addition, a linear potentiometer was clamped to a metal stand and reacted against the bottom of the beam. As the beam deflected, the coiled wire of the string potentiometer and the piston of the linear potentiometer

retracted. These devices were placed side-by-side transversely at the midspan of the girder. They are depicted in Figure 4-13.

Figure 4-13: Midspan deflection instruments used in static testing of full-scale beams

For precautionary reasons, the deflections at the supports were also measured with linear potentiometers. Primarily, these devices were in place to detect the movements of the supports. No problems of this nature were detected.

4.4   PHASE III: FATIGUE TESTING OF SCALED BEAMS

As the main supporting elements in bridges, pretensioned girders are subjected to repetitive loads imposed by cars and trucks over their service life. Fatigue tests attempt to simulate the effects of this loading history in a relatively short period of time. For prestressed concrete members, fatigue strength is typically governed by the fatigue of the prestressing strands (Reese, 1983). For the purposes of Project 5197, the fatigue life of the prestressing strands was outside the scope of the current study. Instead, the fatigue performance of the bottom-fiber concrete was the main focus. As a result, the load range used for the fatigue tests was selected to effectively open and close previously-formed flexural cracks. The fatigue performance of the precompressed concrete around the flexural cracks was evaluated.

Four scaled beams were tested under fatigue loads in this phase of the experimental program. The test specimens, loading protocol, test setup, and instrumentation and data acquisition for the fatigue tests are detailed in the following sections.

4.4.1 Fatigue Test Specimens

Four of the TxDOT Project 4086 scaled specimens described in Section 3.2 were used in this portion of the experimental program. Two beams were subjected to allowable stresses at release; two beams were subjected to elevated stresses at release. The two conventionally-stressed specimens were selected based on the number of functioning internal strain gauges and the unharmed surface condition of the concrete. Additional considerations were made for the overstressed beams. One beam was selected with the same mixture design (mix 1) as the two conventionally-stressed beams. The other beam, fabricated with mix 3, was chosen based on its performance in the static test. The static test results are discussed in detail in Section 5.2. Both of the overstressed beams had several functioning internal strain gauges and had adequate concrete surface conditions. The four specimens tested in phase III of the experimental program are listed in Table 4-1. The maximum compressive stress in the concrete at prestress transfer for these specimens ranged from $0.48f'_{ci}$ to $0.80f'_{ci}$.

Table 4-1: Specimens tested under fatigue loads

Test Specimen Designation	Maximum compressive stress at release ($P/A \pm Mc/I$)
R1-48-1-T6	$-0.48f'_{ci}$
R1-52-1-T7	$-0.52f'_{ci}$
R3-78-3-T3	$-0.78f'_{ci}$
R3-80-5-T4	$-0.80f'_{ci}$

4.4.2 Load Protocol

The load range used in the fatigue tests was based on the experimentally measured cracking loads obtained in Phase I of the experimental program. The maximum load was set at 25-percent above the measured cracking load. This level was chosen as a reasonable overload for pretensioned members. The minimum load, on the other hand, was established to subject the bottom fibers of the section to compressive stresses (due to the effective prestressing force). In practice, the minimum load is representative of a superimposed dead load. The minimum load was approximately 35-percent of the measured cracking load. It is important to note that the fatigue strength of the prestressing strands was not the objective of this part of the project. Rather, the performance of the bottom-fiber concrete was the main concern. Since the stress range of the strands typically governs the fatigue behavior of cracked pretensioned beams, it was kept low enough so that strand fatigue was not critical. Each beam was exposed to a total of 2,000,000 cycles at a constant frequency of 1.7-Hz.

Before the fatigue test was initiated, each cracked specimen was loaded statically. The same instrumentation used in the initial static test of the uncracked beam was monitored. The purpose of the initial test was to determine the response of the cracked girder within the new test setup before it was exposed to fatigue loading. At several 'stages' within the total duration of the fatigue test, additional static tests were performed. For these tests, the fatigue loading was stopped, the same static-test instrumentation was installed, and the static load performance was monitored. Also, the propagation and width of the flexural cracks were noted. The measured

data and the visual observations from each stage were compared to that of the previous stage to determine the impact of the preceding number of fatigue cycles. The loading protocol for each fatigue specimen is illustrated in Figure 4-14. In this figure, the static tests are depicted by a solid line with an arrow at the end. The static loading stages established for the four specimens were as follows:

- 0 cycles
- 100,000 cycles
- 300,000 cycles
- 1,000,000 cycles
- 2,000,000 cycles
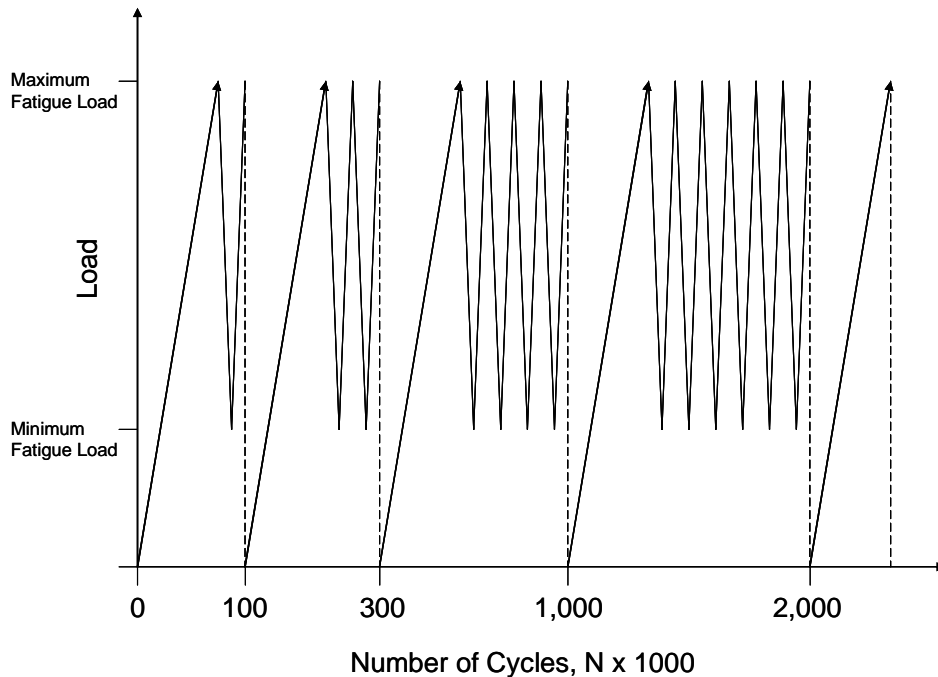
Figure 4-14: Loading protocol for fatigue tests

4.4.3   Test Setup

The entire fatigue test setup was comprised of equipment manufactured by the MTS Corporation. The components included: a 55-kip capacity hydraulic actuator, a 407 model servocontroller, a 290 model hydraulic service manifold, and a 20-gpm hydraulic pump. Together, these components effectively maintained the user-controlled program in a safe and efficient manner. The fatigue loading protocol was created and stored in the servocontroller. When the fatigue loading was initiated, the controller directed the opening and closing of the servovalve in the hydraulic actuator. Additional information was sent back and forth from the valve and the controller to monitor how efficiently the system was matching the desired program. The oil was transferred through the hydraulic lines by the pump. Before it reached the servovalve, the oil passed through the service manifold. In the service manifold, the desired hydraulic pressures were obtained and regulated through the use of hydraulic accumulators.

79

Also, the valve in the service manifold, as controlled by the servocontroller, was used as an on-off switch for the system. If an undesired limit was reached during the test, the controller shut off this valve. An illustration of the closed-loop fatigue testing equipment is provided in Figure 4-15.
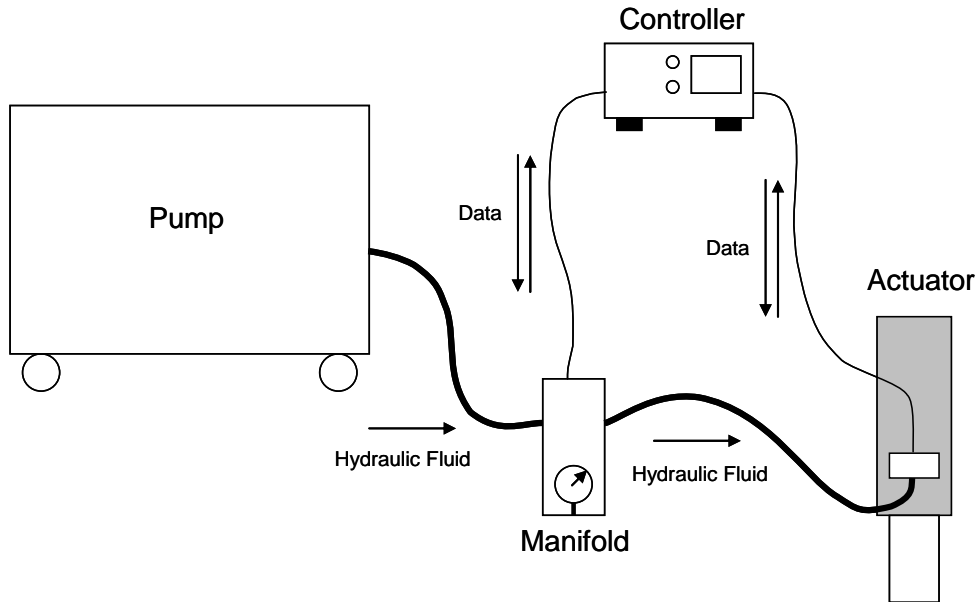
Figure 4-15: Schematic of the fatigue testing equipment

As compared with the static tests, the fatigue tests required the use of a more sophisticated hydraulic actuator. The actuator was equipped with an internal load cell and a linear variable displacement transducer (LVDT). The actuator could be controlled though either load or displacements. Since the fatigue range for the pretensioned specimens was based on their measured cracking load, the load-controlled option was chosen. Before the fatigue testing was initiated, the ram and load cell were calibrated to ensure the appropriate measurement of the applied load. As in the static tests, the load was applied at the midspan of the specimen and was transferred to the third points by a spreader beam.

The other differences between the fatigue test setup and the static test setup were the supporting elements. Due to the application of cyclic load in the fatigue tests, several aspects of the test setup had to be conducive to repetitive loading, for strength and stability purposes. For instance, neoprene pads were positioned between the spreader beam and the top surface of the girder to transfer the applied load. The pads were approximately ¾-inches thick with thin steel plates between three layers of neoprene. In addition, neoprene pads replaced the plate-and-bar end conditions at the ends of the fatigue specimens. The increased friction between the pads and the underside of the beam limited the gradual movement of the specimen. One disadvantage of the flexible end conditions was the inability to precisely pinpoint the location of the end reaction. It was estimated that the resultant of the reaction force was located at the centroid of the bearing area. To maintain the same span length of 14 ½-feet as in the static tests, the pads were positioned so that the last 6-inches of each end of the beam were in contact with the pad. Therefore, the clear span between the pads was 14-feet while the centerline to centerline distance

was 14 ½-feet. The compression of the neoprene pads were accounted for in calculating the net midspan deflection. The final difference between the static test setup and the fatigue test setup was the inclusion of lateral braces from one column to the spreader beam. The purpose of the braces was to prevent the spreader beam from moving out-of-plane due to the presence of potential eccentric loads during the dynamic test. The braces were pinned at both ends so that the applied load was not resisted by the braces. The test setup for the fatigue testing is illustrated in Figure 4-16 and 4-17.
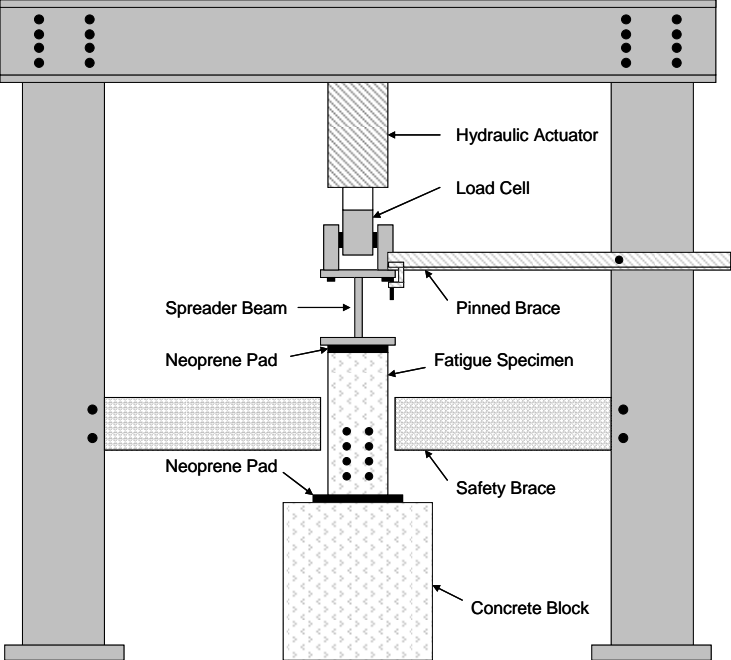
Figure 4-16: Test setup for fatigue testing

Figure 4-17: Picture of test setup for fatigue testing

4.4.4   Data Acquisition and Instrumentation

During the fatigue tests, the controller monitored the load range, the number of cycles, the displacement of the actuator, and the error in the program. Restrictive limits were established for all of these measurements to ensure the proper correlation between the actual response of the system and the input program. If one of the limits was exceeded, the controller stopped the test. As a result, the proper response of the fatigue system was ensured for all 2,000,000-cycles. The frequency was inputted by the user and remained constant throughout the test. The number of cycles updated continuously with the controller displaying the maximum number reached.

For the static tests performed at the end of each fatigue stage, the same data acquisition system and instrumentation used in Phase I of the experimental program were utilized. The deflection at the supports was measured with string potentiometers to account for the compression of the neoprene pads. In addition, the same internal strain gauges and DCDTs were employed to measure the load-incremental-strain response.

4.5   SUMMARY

The three phases of the experimental program included the static testing of 24 scaled specimens, the static testing of 12 full-scale girders, and the fatigue testing of 4 scaled specimens. In the static tests of the small-scale beams, the specimens were loaded to produce a constant moment across the middle third of the span. The maximum load was approximately 30-percent higher than the measured cracking load. During the test, the load, the midspan deflection, the support deflections, the strain in the prestressing strands, and the bottom and top

strain in the section were monitored. In the static tests performed on the full-scale beams, the specimens were also loaded so that a constant moment region was created. The length of the constant moment region was the same as that used in testing the scaled beams (approximately 5-feet). The maximum load applied to the full-scale specimens was also approximately 30-percent above the measured cracking load. During these static tests, only the midspan deflection, the support deflections, and the load applied on the specimen were monitored. Lastly, four of the rectangular, scaled specimens were tested under fatigue loads for 2 million cycles. Two of these specimens were conventionally-stressed, and two of them were subjected to elevated compressive stresses at release. The load range was 25-percent above and 65-percent below the measured cracking load. At several stages throughout the test, the fatigue loading was stopped, and a static test was performed. The results of the tests performed in all three phases of the experimental program are summarized in Chapter 5.

CHAPTER 5
Analysis of Test Results

5.1 OVERVIEW

In this chapter, the results of 36 static-load tests and 4 fatigue tests are presented and analyzed. For the static tests, the measured cracking loads are compared to estimated cracking loads. In order to estimate the cracking loads, prestress losses were calculated with the following prestress loss methods: PCI Design Handbook Loss of Prestress Estimate (PCI, 2004), the NCHRP Report 496 Detailed Prestress Loss Method (Tadros et al., 2003), and the AASHTO LRFD Refined Loss of Prestress Estimate (AASHTO, Interim 2005). For the purposes of this report, these methods are referred to as the PCI, NCHRP, and AASHTO procedures, respectively. The individual loss components calculated according to each procedure are included for reference. For the fatigue tests, the impact of cyclic loading on two conventionally-stressed beams and two overstressed beams was evaluated.

5.2 RESULTS OF STATIC TESTS

Flexural cracks form in prestressed concrete members when the tensile stress in the concrete exceeds its tensile strength. The load at which the first flexural crack forms is the cracking load. In the current project, the methods used to measure and estimate the cracking load for the scaled and full-scale specimens are presented herein. In addition, the predicted cracking loads are compared to the measured cracking loads to evaluate the impact of increasing the allowable release stress in compression on the live-load performance of the pretensioned member.

5.2.1 Measured Cracking Loads

An uncracked, prestressed concrete member behaves elastically in flexure until the cracking load is reached (Lin and Burns, 1963; Nilson, 1987; and Collins and Mitchell, 1997). As seen in Figure 5-1, the member remains uncracked for a significant portion of the flexural response due to the precompression in the bottom fibers of the section. Two variables that are linearly proportional to the applied load within the elastic range of the flexural response include the midspan deflection and the strain in the section. One simple indication of the cracking load is the load at which these relationships cease to be linear. In addition, the visual appearance of cracks is an obvious means to assess the cracking load. A combination of these data sets as listed in Table 5-1 was used to determine and verify the measured cracking loads of the test specimens.
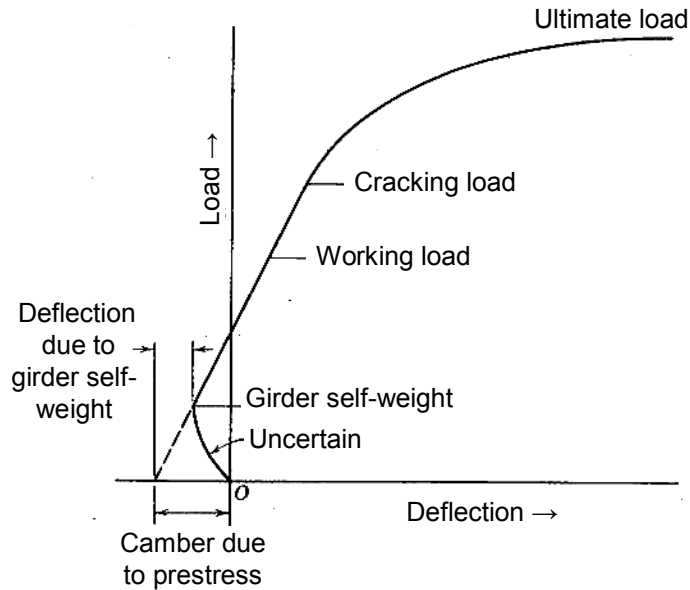
Figure 5-1: Load-deflection response for a typical prestressed concrete beam (Lin and Burns, 1963)

Table 5-1: Sets of data used to measure cracking loads of test specimens

Girder Type	Sets of Data
Scaled Beams (Rect., Tee, and Inverted-tee)	Load vs. midspan deflection (string potentiometer)
	Load vs. bottom strain in section (DCDT)
	Load vs. strain in prestressing strands (strain gauges)
	Visual observations
Full-scale Beams (TxDOT Type-A)	Load vs. midspan deflection (linear potentiometer)
	Load vs. midspan deflection (string potentiometer)
	Visual observations

In regards to the load-deflection responses and the load-strain responses, the same simple technique was applied to experimentally evaluate the cracking load (See Figure 5-2 for an example). A straight line was traced along the initial, predominantly linear portion of the curve. Then, a second straight line was traced along the portion of the curve that first illustrated a decrease in the stiffness of the girder. The load at which the two lines intersected was termed the measured cracking load. For all practical purposes, the point at which the load-deformation response deviated from the initial tangent was identified. In using this technique, it was important to distinguish between a change in stiffness and a drop in the applied load at each load interval.

5.2.1.1   Small-scale Test Specimens

For the scaled beams, the first data set used to determine the measured cracking load was the load versus midspan deflection plot. The aforementioned technique is illustrated in Figure 5-2 for the rectangular section R1-52-1-T7 and in Figure 5-3 for the tee-section T2-91-5-T14.

86
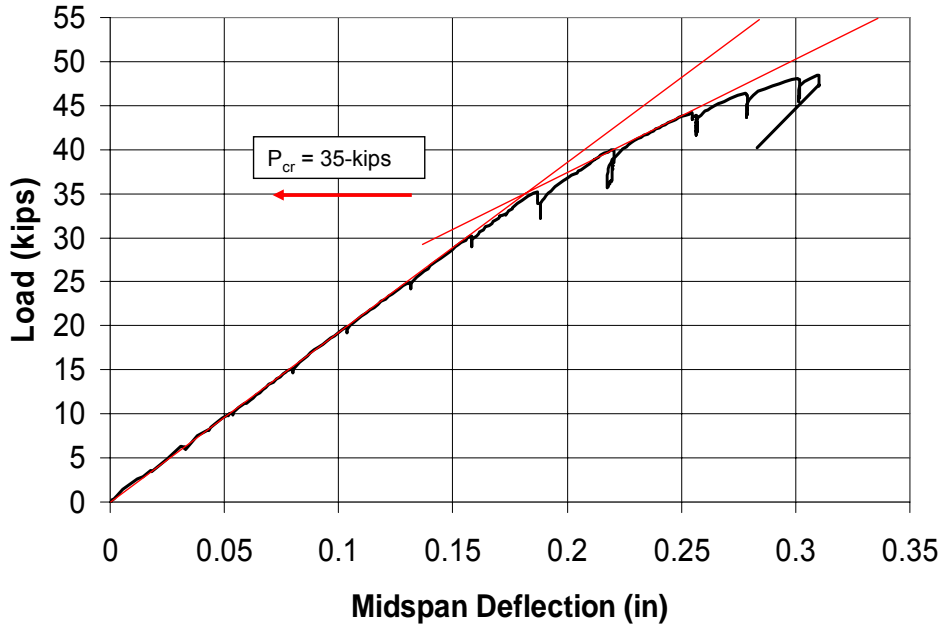
Figure 5-2: Load versus midspan deflection for R1-52-1-T7
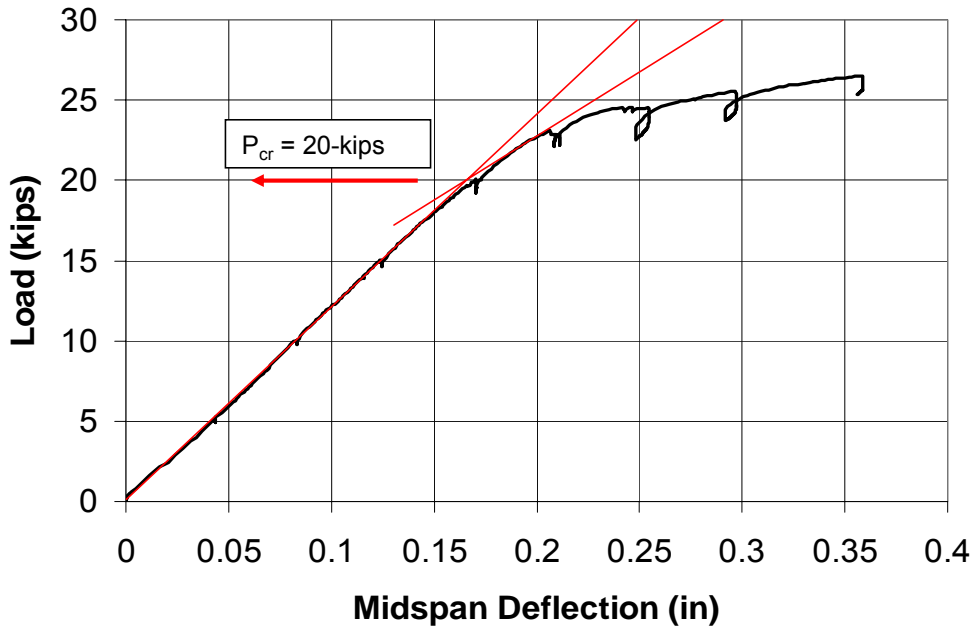
Figure 5-3: Load versus midspan deflection for T2-91-5-T14

The load-versus-bottom-strain plots were also used to confirm the cracking load. With the DCDTs described in Section 4.2.3, the strain 1-inch from the top and the bottom of the extreme fiber of the section was monitored. Like the midspan deflection, the strain in the section increased linearly before the beam was cracked and nonlinearly afterwards. The load-versus-bottom-strain plots measured the opening of the flexural cracks in addition to the strain in the

section and therefore, were used more often than the top-strain plots. Two sample graphs illustrating this data set are provided in Figure 5-4 and in Figure 5-5 for the tee-section T2-79-3-T16 and the rectangular section R3-83-4-T12, respectively.
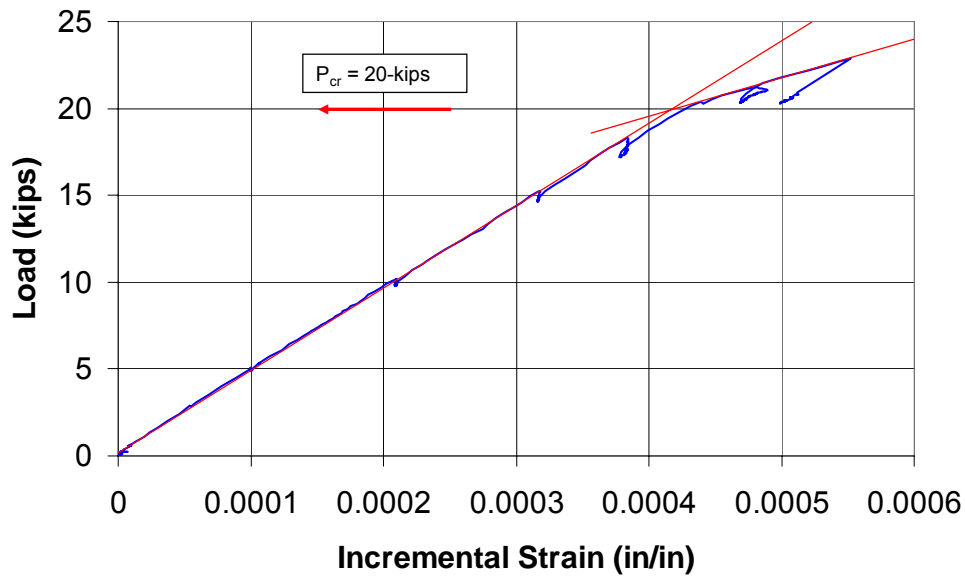
Figure 5-4: Load versus strain 1-inch from bottom fiber for T2-79-3-T16
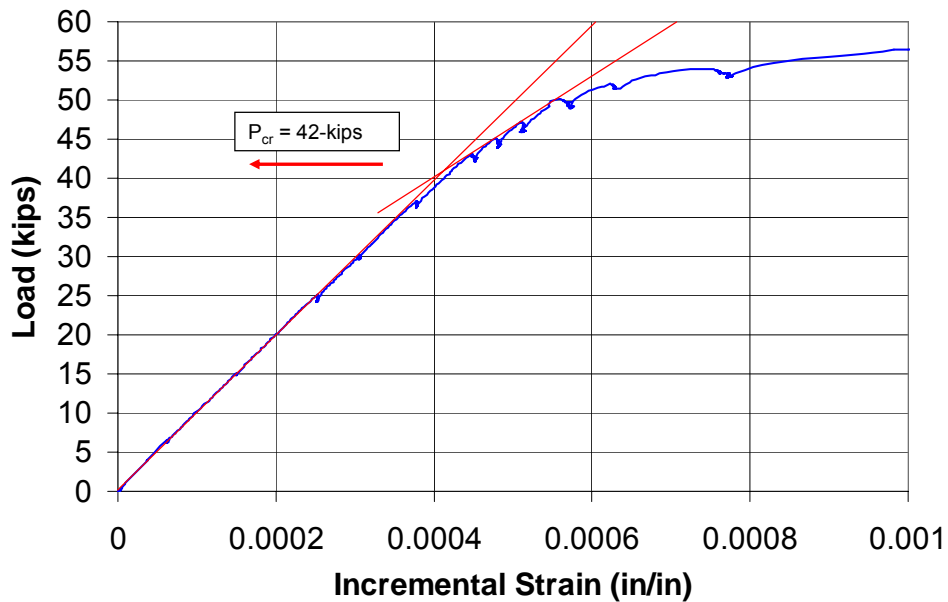
Figure 5-5: Load versus strain 1-inch from bottom fiber for R3-83-4-T12

The incremental strain in the prestressing strands was monitored during the test with electrical strain gauges. These measurements also represented the strain in the section at the location of the strands due to the applied load assuming that the strands and the surrounding concrete formed a complete bond. As such, the cracking load was confirmed with this data set as

well. A sample load-versus-incremental-strain plot for the rectangular section R3-78-3-T3 is provided in Figure 5-6.
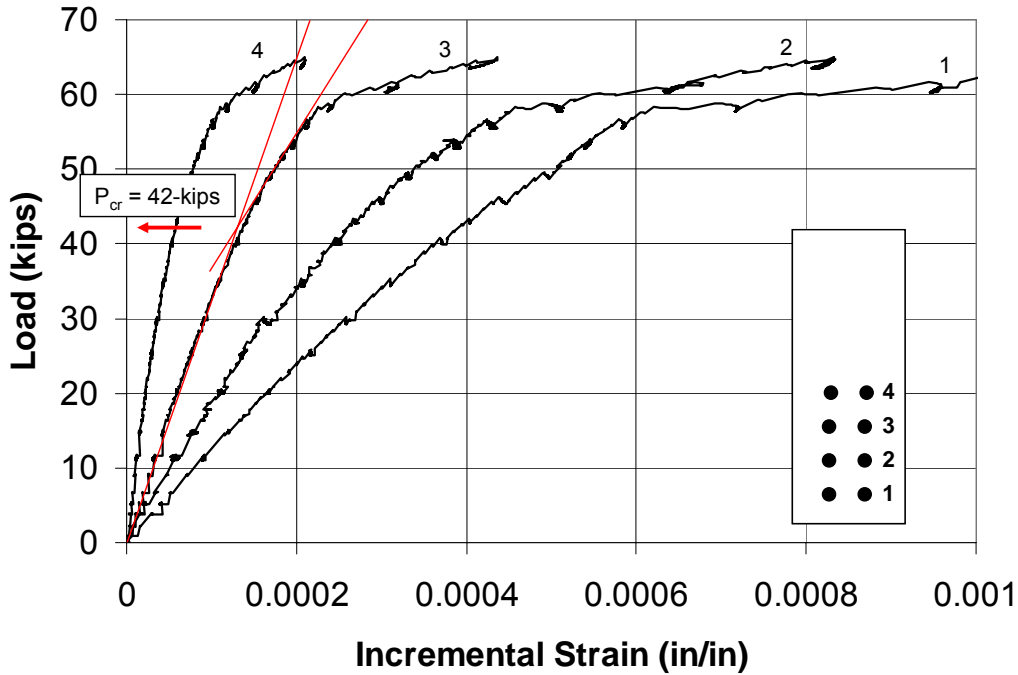
Figure 5-6: Load versus strain from internal strain gauges for R3-78-3-T3

Lastly, for the small-scale specimens, the cracking load was verified with visual inspections of the beam at and near the expected cracking load. The entire constant moment region was examined at each relevant load increment. Pictures illustrating when the first cracks were observed are provided for IT1-73-2-T19 and R1-52-1-T7 in Figure 5-7 and 5-8, respectively. The typical crack pattern at the maximum applied load (approximately 30-percent above the cracking load) for a small-scale beam is provided in Figure 5-9.
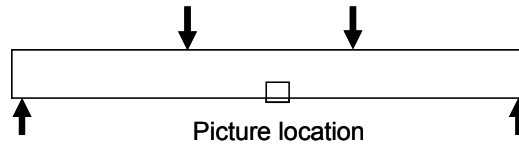
Figure 5-7: Documentation of first crack for IT1-73-2-T19 (picture was taken at P$_{app}$ = 75-kips)
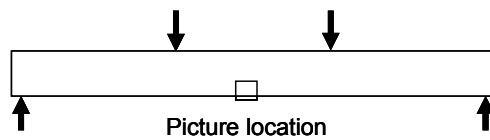
Figure 5-8: Documentation of first crack for R1-52-1-T7 (picture was taken at P$_{app}$ = 35-kips)

Maximum crack width = 0.007-inches
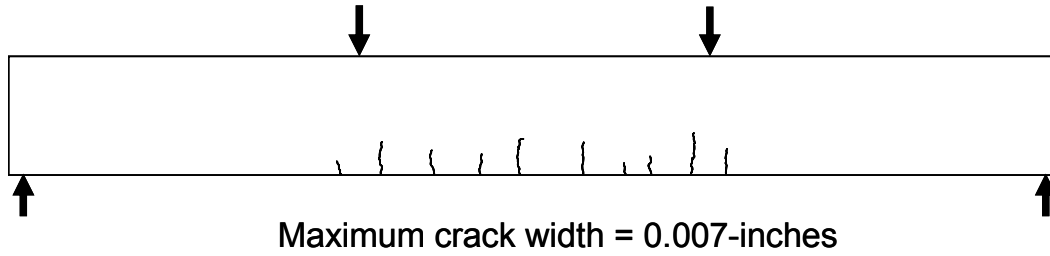
Figure 5-9: Typical crack map at maximum applied load for small-scale beam

5.2.1.2 Full-scale Test Specimens

The data sets used to measure the cracking loads of the full-scale TxDOT Type-A beam specimens are outlined in Table 5-1. The load-versus-midspan-deflection responses were the primary means of evaluating the cracking loads. Sample load-deflection plots as obtained by the load cell and the linear potentiometer readings at midspan are provided in Figure 5-10 and 5-11 for the full-scale girders A66-T28 and A75-T36, respectively.
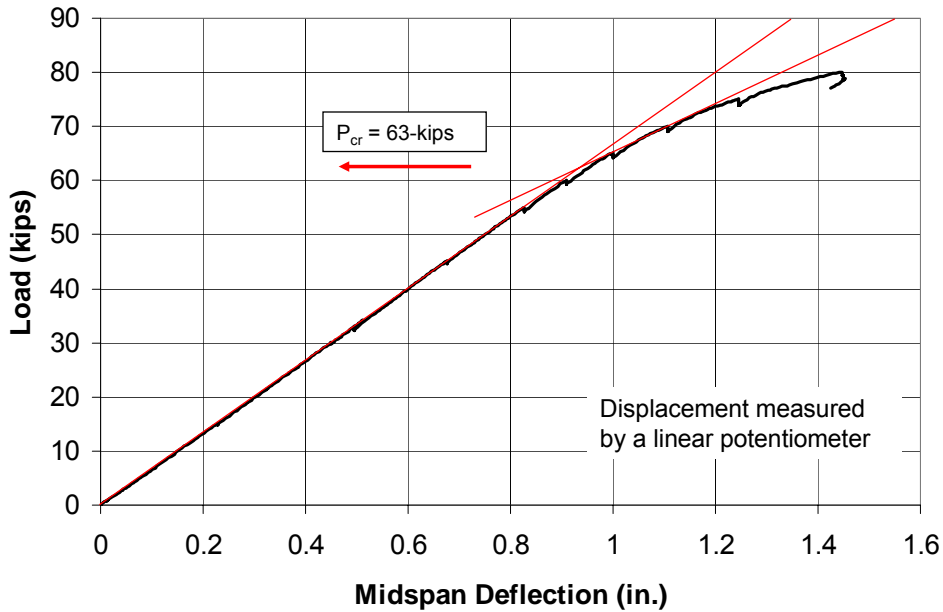
Figure 5-10: Load versus midspan deflection for A66-T28

91
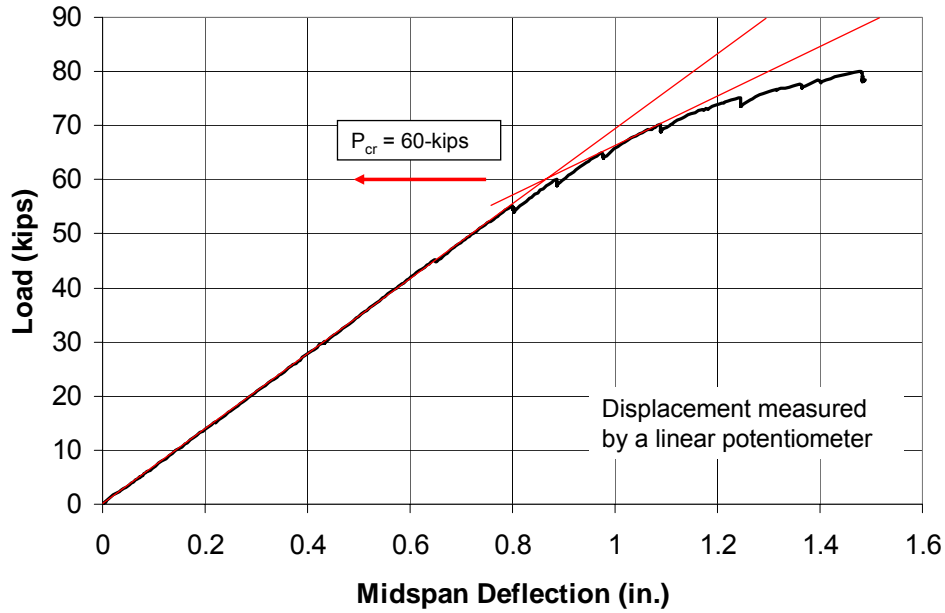
Figure 5-11: Load versus midspan deflection for A75-T36

Sample load-deflection plots as obtained by the load cell and the string potentiometer readings at midspan are included as Figure 5-12 and 5-13 for the Type-A beams A63-T27 and A66-T30, respectively.
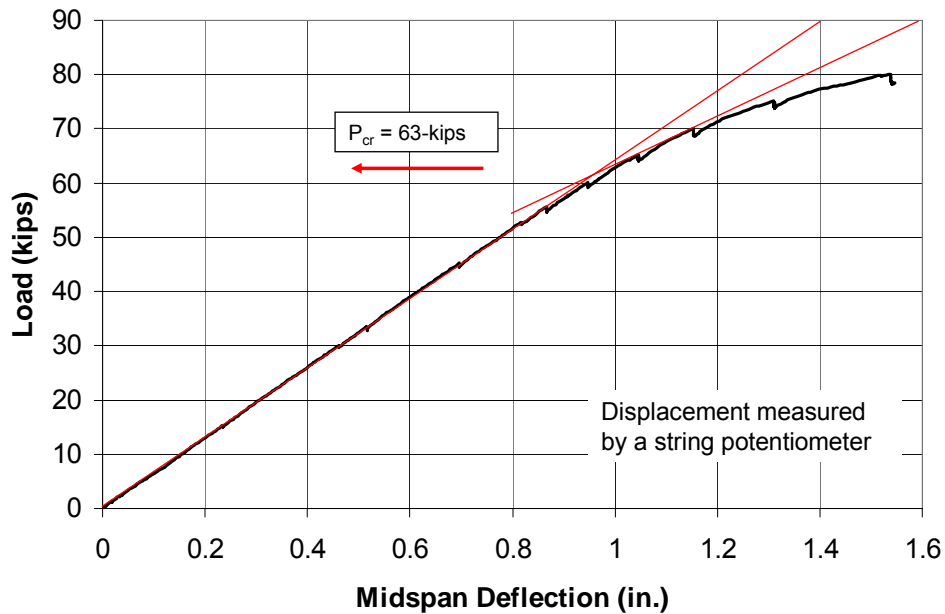
Figure 5-12: Load versus midspan deflection for A63-T27
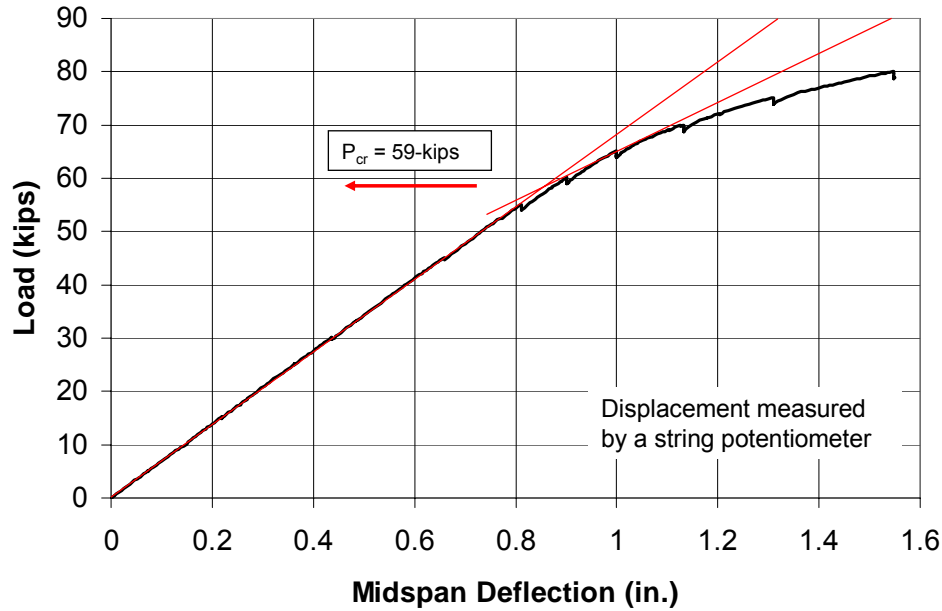
Figure 5-13: Load versus midspan deflection for A66-T30

Lastly, for the full-scale girders, the measured cracking loads were verified with the visual detection of the first flexural crack. There was not one consistent location within the constant moment region where the first crack appeared. In many cases, two or three first cracks appeared simultaneously at midspan, beneath either load point, or somewhere in between. It is important to note that the flexural cracks were of hairline width when they first developed. However, for all of the documented first cracks, the cracks extended and widened with additional load confirming that they were indeed flexural cracks.

Pictures illustrating the visual observation of the first crack for the girders A67-T29 and A73-T34 are provided in Figure 5-14 and 5-15, respectively. The measured cracking load for each full-scale beam is depicted in Table 5-2. Also, the typical crack pattern at the ultimate applied load for one of the Type-A girders is illustrated in Figure 5-16.

93

P_app = 60-kips P_app = 75-kips

Picture location
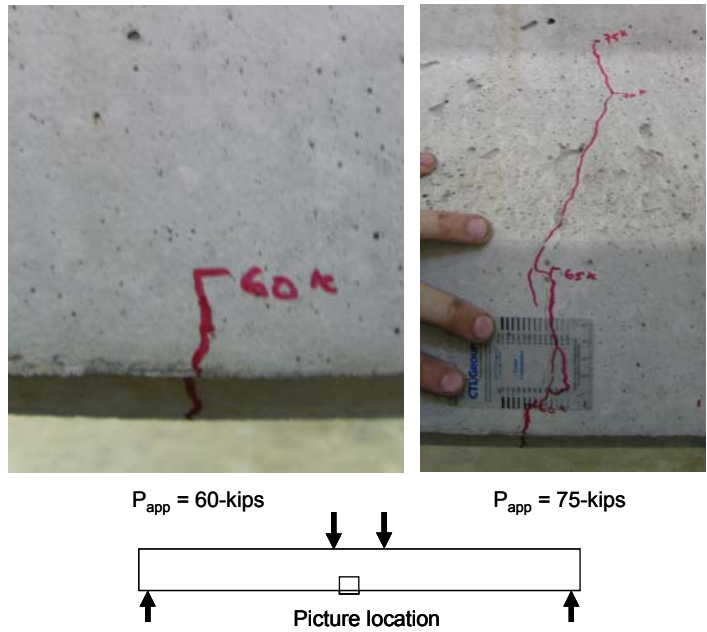
Figure 5-14: Documentation of first flexural crack for A67-T29

P_app = 55-kips P_app = 80-kips

Picture location
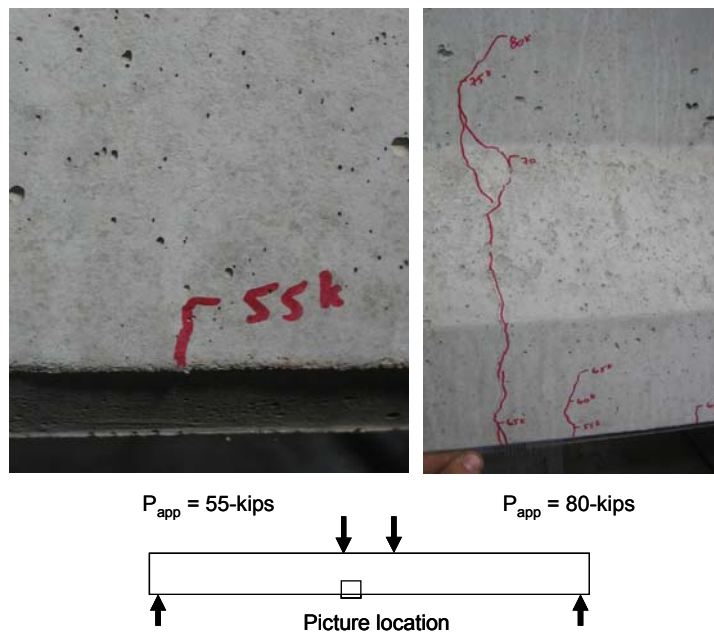
Figure 5-15: Documentation of first flexural crack for A73-T34

Table 5-2: Measured and observed cracking loads for full-scale beams

Test Specimens Designation	Measured Cracking Load (kips)	Maximum Crack Width at Maximum Applied Load (80-kips) (in.)	Date of the Test
A55-T25	62	0.010	8/10/2006
A60-T26	63	0.010	8/10/2006
A63-T27	63	0.010	8/11/2006
A66-T28	63	0.013	8/14/2006
A67-T29	60	0.013	8/15/2006
A66-T30	59	0.016	8/16/2006
A69-T31	60	0.010	8/17/2006
A68-T32	58	0.013	8/18/2006
A67-T33	63	0.013	8/22/2006
A73-T34	57	0.016	8/23/2006
A71-T35	63	0.013	8/23/2006
A75-T36	60	0.013	8/24/2006

Maximum crack width = ~0.016-inches
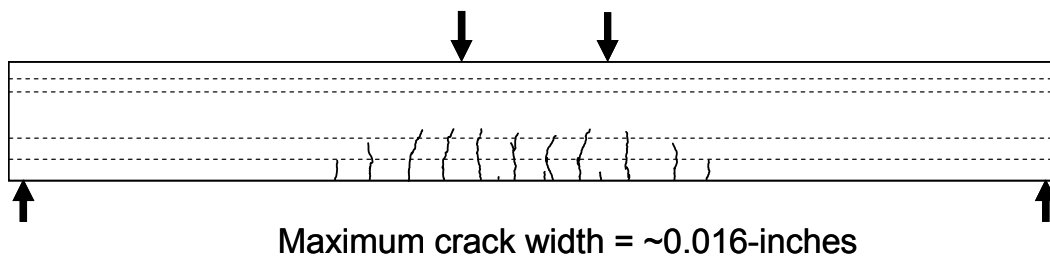
Figure 5-16: Typical crack map at maximum applied load for full-scale beam

In Table 5-2, the measured cracking load, the maximum crack width at the maximum applied load, and the test date for each full-scale beam are provided. The cracking loads listed in Table 5-2 were those obtained from the load-deflection plots. For consistency with the scaled beams, these cracking loads were used in the evaluation of the live-load performance of the full-scale girders. It should be noted that the load at which the first crack was observed for each beam was restricted to five-kip increments as determined by the loading protocol. In most cases, the first flexural crack was visually observed at the next possible load break following the cracking load obtained from the load-deflection plots. In a couple of cases, as with the Type-A beam A73-T34 depicted in Figure 5-15, the observed cracking load was slightly less than the cracking load obtained from the load-deflection plots. For these cases, it was consistent and

conservative to use the loads obtained from the load-deflection plots. Another observation from Table 5-2 was in regards to the maximum crack width measured in each test. On average, as the compressive stress at release increased, the maximum crack width at 80-kips slightly increased.

The extensive instrumentation utilized throughout the testing of the small-scale beams and the agreement of the measured and observed cracking loads for the full-scale specimens ensured that the appropriate cracking load was measured. Furthermore, the use of the same techniques (inspection of load-deformation plots and visual observation) for the test specimens guaranteed the consistency of the results. It is important to realize that the techniques used to measure the cracking load were only accurate within approximately 1-kip. However, shifting the measured cracking loads by 1-kip in either direction will not affect the general trend of the results. The measured cracking loads for the scaled and full-scale beams are provided with the predicted cracking loads in Section 5.2.3.

5.2.2 Predicted Cracking Loads

The scaled beams were tested approximately 3-years after they were cast. The full-scale beams were tested approximately 28-days after they were cast. In both cases, it was necessary to estimate the effective prestressing force at the time of the test. To accomplish this task, the following prestress loss procedures as described in Section 2.5 were utilized:

- PCI Design Handbook method (2004)
- NCHRP Report 496 procedure (2003)
- AASHTO LRFD Specifications procedure (Interim 2005)

For the purposes of this report, these methods are referred to as the PCI, NCHRP, and AASHTO procedures, respectively. The PCI procedure was not used for the full-scale girders because it is intended for an estimate of the total loss of the prestressing force, not the losses at an intermediate stage before all volume changes have occurred. All three prestress loss procedures were used for the small-scale specimens.

The estimated losses included those due to elastic shortening of the member, due to creep and shrinkage of the concrete, and due to relaxation of the prestressing steel. With these losses taken into account, the moment required to crack the girder was calculated. For each procedure, the equations used to calculate the cracking moment are provided in the following sections. The midspan load required to produce the cracking moment was calculated with Equations 5-1 and 5-2 for the small- and full-scale beams, respectively. Sample calculations illustrating the prestress losses and cracking load calculations are provided in Appendix A for the small-scale specimens and in Appendix B for the full-scale specimens.

$$P_{predicted\_s} = \left(\frac{6}{L_s}\right)\left(M_{cr\_s}\right)$$
(5-1)

where, L_s = centerline to centerline span, 14.5-ft

$$P_{predicted\_f} = \left(\frac{4}{L_f - 5'}\right)\left(M_{cr\_f}\right)$$
(5-2)

where, L_f = centerline to centerline span, 39 1/3-ft

For all of the test specimens, the estimated cracking loads using each loss procedure were compared to the measured cracking loads using Equation 5-3. The accuracy of the cracking load estimate using the measured cracking load as the baseline number was calculated with this percent difference formula.

$$Accuracy_{CL} = \left(\frac{P_{measured} - P_{predicted}}{P_{measured}} \right) \times 100 \qquad (5\text{-}3)$$

Where, $P_{measured}$ = cracking load measured during static test (kips)
          $P_{predicted}$ = cracking load estimated with analysis procedure (kips)

For each analytical procedure, the cracking load prediction accuracy was calculated for the test specimens. The accuracy values were plotted versus the compressive release stress at the critical section. The critical section is defined as the section subjected to the maximum applied moment that was exposed to the highest compressive stress at release. For all of the test specimens, the critical section was directly beneath either load point. At these locations, the applied moment was at a maximum and the compressive release stress was slightly higher than the stress at midspan. For the small-scale beams, the stress at the critical section was a few percent of f'_{ci} smaller than the maximum release stress calculated at the end of the member. For the full-scale girders, the stress at the critical section was very similar to the maximum release stress at the hold-down points, five-feet from the midspan of the beam.

5.2.2.1 PCI Design Handbook Method

To estimate the cracking moment, the total losses calculated from the PCI procedure were subtracted from the initial prestressing force before transfer to obtain the effective prestressing force at the time of the test. In accordance with the assumptions of the procedure, the gross section properties were used in the calculation. The cracking moment equation used in the PCI procedure is included as Equation 5-4.

$$M_{cr} = \left(\frac{I_g}{c_b} \right) \left(\frac{P_{eff}}{A_g} + \frac{P_{eff} e c_b}{I_g} - \frac{M_g c_b}{I_g} + f_r \right) \qquad (5\text{-}4)$$

where, I_g = gross moment of inertia (in^4)
          c_b = distance from geometric centroid to extreme bottom fiber (in)
          P_{eff} = prestressing force after all losses (kips)
          A_g = gross area (in^2)
          e = eccentricity of prestressing strands (in)
          M_g = moment due to dead load (in-kips)
          f_r = tensile strength of concrete taken as $\dfrac{7.5}{1000} \sqrt{f'_c}$ (ksi)
          f'_c = compressive strength of concrete (psi)

The accuracy of the cracking load calculation for the small-scale specimens using the PCI Design Handbook procedure for estimating prestress losses is depicted in Figure 5-17. As the compressive stress at release increased for all three section types (rectangular, tee, and inverted-

97

tee), the ability to accurately predict the cracking load decreased. In fact, for a few specimens that were subjected to a release stress of approximately $0.80f'_{ci}$ and above, the cracking loads were overestimated by 20-percent. On the contrary, for all girders subjected to release stresses within the allowable limits, the cracking load was predicted within 5-percent accuracy. The variables affecting the distinct downward trend depicted in Figure 5-17 will be discussed in greater detail when all three analysis procedures are compared in Section 5.3.
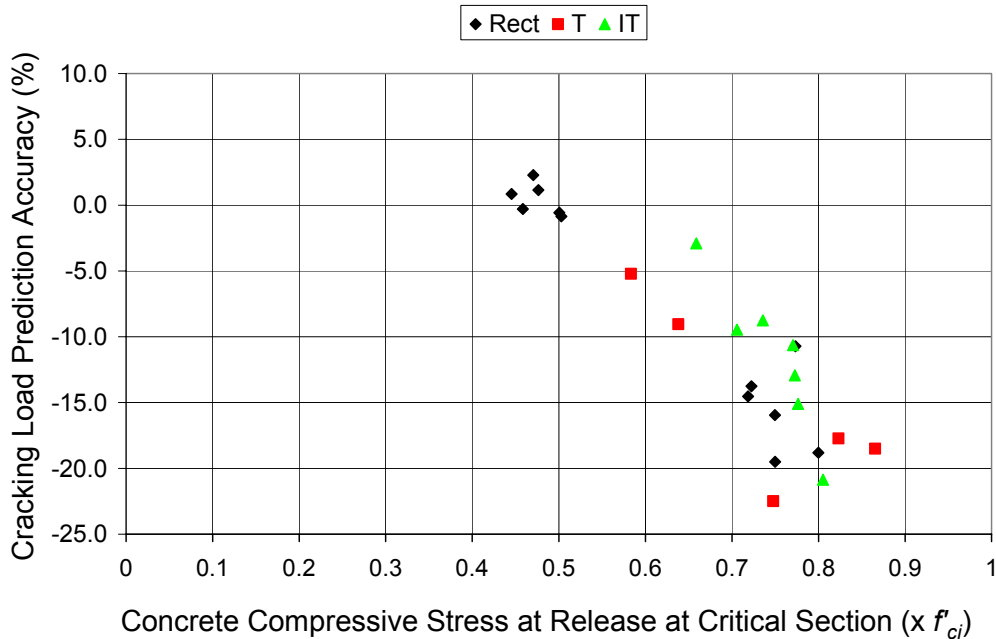
Figure 5-17: Accuracy of cracking load prediction using PCI Method

5.2.2.2   NCHRP Report 496 Method

In the NCHRP method, the cracking moment was calculated according to the guidelines of the procedure. First, the bottom-fiber, release stress was computed at the midspan of the beam with the initial prestressing force and transformed section properties. After that, the reduction in the initial stress was calculated using $\Delta f_{pT\text{-}ES}$, the summation of the long-term loss components Δf_{pCR}, Δf_{pSR}, and Δf_{pR}. The loss due to elastic shortening was automatically accounted for during the calculation of the initial release stress. The initial, bottom-fiber stress minus the long-term stress reduction equaled the effective bottom-fiber stress. The cracking moment was computed as the moment required to overcome this effective bottom-fiber stress and the tensile strength of the concrete. Transformed section properties were used throughout the cracking load calculation. The aforementioned calculations are displayed as Equations 5-5 – 5-7.

Bottom-fiber stress after transfer:

$$f_{cbi} = P_i \left(\frac{1}{A_{ti}} + \frac{e_{pti} y_{bti}}{I_{ti}} \right) - \frac{M_g y_{bti}}{I_{ti}} \tag{5-5}$$

98

where,
P$_i$ = initial prestressing force immediately before transfer (kips)
A$_{ti}$ = area of transformed section at transfer (in.^{2})
e$_{pti}$ = eccentricity of strands of transformed section at transfer (in.)
y$_{bti}$ = distance to the geometric centroid from the bottom fiber of the transformed section at transfer (in.)
M$_g$ = dead load moment (in.-kips)

Change in stress due to long term losses:

$$\Delta f_{cb} = -\frac{\Delta P}{A_{tt}} - \frac{\Delta P e_{ptt} y_{btt}}{I_{tt}}$$

(5-6)

where,
$$\Delta P = \Delta f_{pT-ES} A_{ps}$$

A$_{tt}$, e$_{ptt}$, y$_{btt}$, and I$_{tt}$ are the geometric properties of the transformed section at the time of test

$$\Delta f_{pT-ES} = \Delta f_{pSR} + \Delta f_{pCR} + \Delta f_{pR}$$

Predicted Cracking Load:

$$M_{cr} = \frac{I_{tt}}{y_{btt}} \left(f_{cbi} - \Delta f_{cb} + f_r \right)$$

(5-7)

where,
$$f_r = \frac{7.5}{1000} \sqrt{f_c'}$$

It is important to note that the above cracking load calculation is essentially equivalent to Equation 5-8. Using the effective prestressing force with the net section properties is equivalent to using the initial prestressing force with the transformed section properties (Huang, 1972).

$$M_{cr} = \frac{I_{tt}}{y_{btt}} \left(\frac{P_{eff}}{A_{nt}} + \frac{P_{eff} e_{pnt} y_{bnt}}{I_{nt}} - \frac{M_g y_{bti}}{I_{ti}} + f_r \right)$$

(5-8)

where,
$$P_{eff} = P_i - \left(\Delta f_{pES} + \Delta f_{pSR} + \Delta f_{pCR} + \Delta f_{pR} \right) A_{ps}$$

I$_{tt}$, y$_{btt}$, M$_g$, y$_{bti}$, I$_{ti}$, f$_r$, and P$_i$ were defined above.
Δf_{pES}, Δf_{pSR}, Δf_{pCR}, Δf_{pR}, and A$_{ps}$ were defined in Table 2-11.
A$_{nt}$, e$_{pnt}$, y$_{bnt}$, and I$_{nt}$ are the properties of the net section at the time of test

Also, in the NCHRP procedure, an equation for the modulus of elasticity of concrete was recommended. It is included as Equation 5-9.

$$E_c = 33,000 K_1 K_2 \left(0.140 + \frac{f_c'}{1000} \right)^{1.5} \sqrt{f_c'}$$

(5-9)

In Equation 5-9, two 'K' factors (K$_1$ and K$_2$) were included. K$_2$ was selected based on the need for an average, upper-bound, or lower-bound estimate. For the current project, a value of 1.0 for K$_2$ was appropriate because the accuracy of the cracking load estimate was the focus of the study. K$_1$ represented the difference between local materials and the national average. As noted in Section 2.5.2, the suggested K$_1$ factor for Texas concretes was 1.321 (Tadros et al., 2003). This factor in excess of unity reflected the relatively stiffer coarse aggregates present in

Texas as compared to the rest of the nation. For all of the concrete mix designs used in the test specimens, a K_1 factor of 1.321 was not justified. For the small-scale beams, a K_1 factor of 1.0 for mix 1 and mix 3 and a K_1 factor of 0.8 for mix 2 agreed favorably with measured modulus of elasticity values. The presence of crushed limestone without any fly ash and significant scatter in modulus data justified the lower stiffness of mix 2. The agreement between the NCHRP E_c equation with these factors and the measured values is illustrated in Table 5-3. The adequacy of the K factors for the small-scale beams is discussed in greater detail in Section 5.3.1.

Table 5-3: Comparison of measured modulus of elasticity to NCHRP equation

Mix Design	Measured – Project 4086		NCHRP and AASHTO Procedure		
	f'_c (psi)	E_c (ksi)	E_c (ksi)	K_1	K_2
1	10,030	5900	6080	1.0	1.0
2	10,000	4850	4850	0.8	1.0
3	7,390	5010	5076	1.0	1.0

For the full-scale beams, a K_1 factor of 1.1 was appropriate. This factor was obtained by comparing the average modulus of elasticity values according to the NCHRP equation with measured modulus data back-calculated from the initial-slope of the twelve load-deflection plots. For each load-deflection plot, a value of E_c was selected such that the initial-slope was matched with the approximation provided by Equation 5-10. The average for the modulus of elasticity values obtained in this manner was approximately 6,200-psi. The average empirical modulus based on the 28-day strengths of cylinders tested with each beam was approximately 5,500-ksi. As a result, a K_1 factor of 1.1 (6,200/5,500) was recommended. The same K_1 factor for all of the beams was justified because the range of measured and empirical modulus values was reasonably low. A sample load-deflection plot with an estimate for the initial linear portion is depicted in Figure 5-18 for A55-T25.

$$\Delta_{mid} = \left(\frac{Pa}{24E_c I} \right) \left(3L^2 - 4a^2 \right) \tag{5-10}$$

where, P = concentrated load applied 2 ½-feet each side of midspan (kips)
L = span of the specimen, (472-inches)
a = distance from support to concentrated load, (203-inches)
E_c = modulus of elasticity of concrete (ksi)
I = moment of inertia of section (in^4)
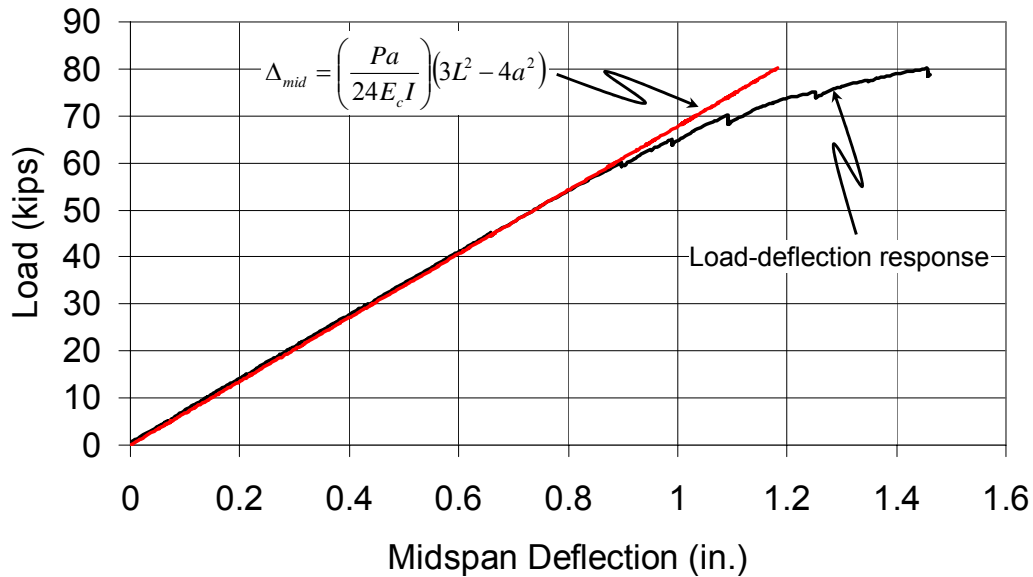
Figure 5-18: Estimated initial slope of load-deflection plot to obtain modulus for A55-T25

The accuracy of the cracking load estimate using the prestress loss equations of NCHRP Report 496 is depicted in Figure 5-19. In this plot, the full-scale data points are included with the small-scale specimens. It is clear that the full-scale beams and the small-scale beams provide consistent results. This consistency was the direct result of the use of transformed section properties as per NCHRP Report 496. For all beam types, the accuracy of the cracking load estimate decreased as the compressive stress at release increased. For the beams subjected to a compressive release stress at the critical section approaching $0.80f'_{ci}$, the cracking loads were overestimated by up to 15-percent. For the beams stressed to $0.60f'_{ci}$ or less, the cracking loads were fairly well-estimated with the lower-bound at approximately -4-percent.
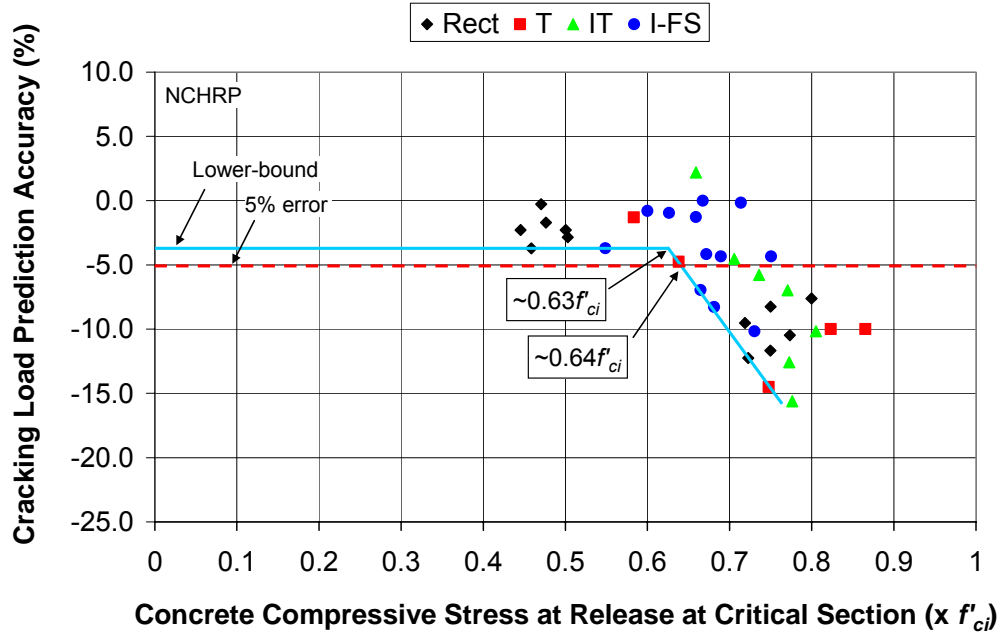
Figure 5-19: Accuracy of cracking load prediction using NCHRP Method

The data in Figure 5-19 was analyzed in two ways. First, the lower-bound to the data was traced for the beams subjected to release stresses within and exceeding the allowable limit. The accuracy of the cracking load estimate for the beams stressed to $0.60f'_{ci}$ or less was considered acceptable (-4-percent) and was used as the baseline for the comparison of the beams stressed to higher levels than the allowable limit. From this approach, the data suggested that release stresses in excess of $0.63f'_{ci}$ negatively affected the ability to predict the cracking load. Second, a horizontal line at -5-percent accuracy of the cracking load estimate was superimposed on the plot. In this case, an error in the cracking load prediction of -5-percent was considered acceptable and was used as the acceptance criterion to evaluate the cracking load prediction of the beams subjected to release stresses higher than $0.60f'_{ci}$. From this approach, the data suggested that the release stress in compression at the critical section in excess of $0.64f'_{ci}$ negatively affected the ability to predict the cracking load. In both cases (lower-bound and -5-percent criteria), premature cracking initiated at a similar compressive stress at release. Due to the approximations consistent with measuring and estimating the cracking loads of pretensioned beams, the significance of $0.63f'_{ci}$ or $0.64f'_{ci}$ as a definitive and final value is limited. Rather, the general trend of the data should be emphasized. In Figure 5-19, the trend of the data indicated that beams subjected to release stresses between $0.60f'_{ci}$ and $0.70f'_{ci}$ cracked sooner than beams subjected to lower release stresses. Factors influencing the premature cracking of the highly-stressed beams are discussed in Section 5.2.3.

It is important to note that all of the section types are represented on the diagonal portion of the lower bound to the data. This finding suggested that the effect of increased compressive stresses at release was not limited to one beam type.

5.2.2.3 AASHTO LRFD Method

For the AASHTO procedure, the cracking moment was calculated with the gross section properties and the effective prestressing force. The effective prestressing force was computed as the initial force minus all short- and long-term losses. The equation is depicted in Equation 5-11.

$$M_{cr} = \left(\frac{I_g}{c_b}\right)\left(\frac{P_{eff}}{A_g} + \frac{P_{eff}e_pc_b}{I_g} - \frac{M_gc_b}{I_g} + f_r\right) \qquad (5\text{-}11)$$

where,
I_g = moment of inertia of gross section (in.^{4})
c_b = distance from geometric centroid to extreme bottom fiber (in.)
P_{eff} = prestressing force after all losses (kips)
A_g = area of gross section (in.^{2})
e_p = eccentricity of prestressing strands (in.)
M_g = moment due to dead load (in.-kips)
f_r = tensile strength of concrete taken as $\dfrac{7.5}{1000}\sqrt{f_c'}$ (ksi)
f_c' = compressive strength of concrete (psi)

The same K_1 factor used in the NCHRP procedure was used in the AASHTO procedure. In the commentary of the AASHTO LRFD Interim 2005 Specifications, the use of a K_1 factor as "determined by physical test, and as approved by the authority of jurisdiction" is permitted (AASHTO LRFD, 2005).

The accuracy of the cracking load prediction according to the prestress loss equations of the AASHTO procedure is depicted in Figure 5-20. The results were very similar to that of the NCHRP Report 496 method. The primary difference between the two plots was the upward shift of all data points in the AASHTO plot with respect to the NCHRP plot due to the use of gross-section properties and a slightly different equation for the modulus of elasticity. This upward shift was more significant for the full-scale girders than for the small-scale beams due to the heightened impact on the moment of inertia of the transformed section in the case of the former.
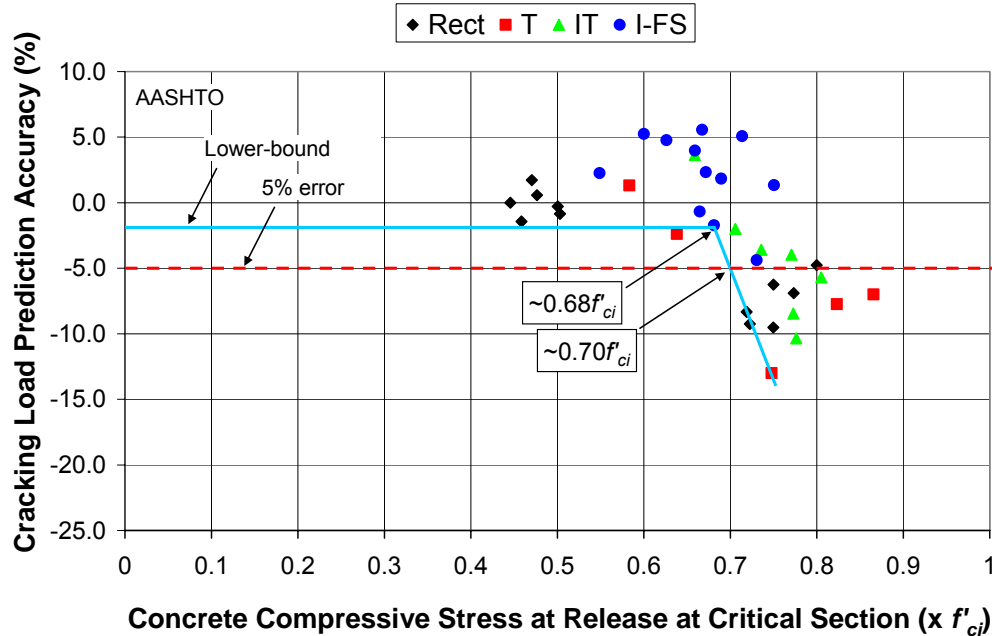
Figure 5-20: Accuracy of cracking load prediction using AASHTO Method

As with the NCHRP plot (Figure 5-19), the data in Figure 5-20 was analyzed in two ways. From the lower bound of the data, it was suggested that the compressive stress at release at which premature cracking initiated was approximately $0.68f'_{ci}$. From the -5-percent acceptance criterion, the initiation of premature cracking appeared to occur at approximately $0.70f'_{ci}$. Comparing these values to those obtained through the use of the NCHRP prestress loss procedure, it is clear that a higher allowable release stress is implicitly suggested through the use of the AASHTO procedure (i.e. $0.68f'_{ci}$ vs. $0.63f'_{ci}$ or $0.70f'_{ci}$ vs. $0.64f'_{ci}$). However, due to the size variation between the scaled and full-scale girders, the use of the geometric properties of the transformed section as suggested in the NCHRP procedure seems more appropriate for comparison purposes. The full-scale specimens are affected more by the selection of the appropriate geometric properties than the scaled specimens.

It should be emphasized that the definitive stress values at which premature cracking occurred according to each prestress loss method (NCHRP and AASHTO) should not be blindly accepted. Due to the limitations inherent in the accuracy of estimating and measuring the cracking load of pretensioned members, engineering judgment should be used in the analysis of the results. According to both prestress loss procedures (Figure 5-19 and Figure 5-20), the general trend of the cracking load data suggested that premature cracking initiates at a compressive release stress at the critical section between $0.63f'_{ci}$ and $0.70f'_{ci}$. In addition, looking at the data from a lower-bound perspective or a fixed -5-percent acceptance criteria did not greatly affect the results. A recommendation for increasing the allowable compressive stress at release is provided in the next section after the explanation is given for the premature cracking of the test specimens subjected to release stresses in excess of the range of $0.63f'_{ci}$ to $0.70f'_{ci}$.

104

5.2.3 Summary of Static Test Results

The measured cracking loads, the predicted cracking loads, and the accuracy of each estimate according to Equation 5-3 are provided in Table 5-4 for the small-scale specimens and in Table 5-5 for the full-scale specimens.

Table 5-4: Measured and predicted cracking loads and prediction accuracy for the scaled beams

Test Specimen Designation	σ_{BOTTOM} at Critical Section (x f'_{ci})	Measured Cracking Load (kips)	Predicted Cracking Loads and Accuracy					
			PCI Design Handbook		NCHRP Report 496		AASHTO LRFD 2005	
			Kips	%	Kips	%	Kips	%
R1-52-1-T8	0.50	35	35.2	-0.6	35.8	-2.3	35.1	-0.3
R1-52-1-T7	0.50	35	35.3	-0.9	36.0	-2.9	35.3	-0.9
R1-50-1-T1	0.48	35	34.6	1.1	35.6	-1.7	34.8	0.6
R1-49-1-T2	0.47	35	34.2	2.3	35.1	-0.3	34.4	1.7
R1-46-1-T5	0.45	35	34.7	0.9	35.8	-2.3	35.0	0.0
R1-48-1-T6	0.46	35	35.1	-0.3	36.3	-3.7	35.5	-1.4
T1-68-2-T17	0.64	21	22.9	-9.0	22.0	-4.8	21.5	-2.4
T1-62-2-T18	0.58	23	24.2	-5.2	23.3	-1.3	22.7	1.3
IT1-68-2-T20	0.66	55	56.6	-2.9	53.8	2.2	53.0	3.6
IT1-73-2-T19	0.71	55	60.2	-9.5	57.5	-4.5	56.1	-2.0
R3-75-3-T9	0.72	42	48.1	-14.5	46.0	-9.5	45.5	-8.3
R3-78-3-T3	0.75	42	48.7	-16.0	46.9	-11.7	46.0	-9.5
T2-79-3-T16	0.75	20	24.5	-22.5	22.9	-14.5	22.6	-13.0
T2-86-3-T15	0.82	22	25.9	-17.7	24.2	-10.0	23.7	-7.7
IT3-79-3-T21	0.77	63	69.7	-10.6	67.4	-7.0	65.5	-4.0
IT2-76-3-T22	0.74	64	69.6	-8.7	67.7	-5.8	66.3	-3.6
R3-78-4-T11	0.75	40	47.8	-19.5	43.3	-8.2	42.5	-6.3
R3-83-4-T12	0.80	42	49.9	-18.8	45.2	-7.6	44.0	-4.8
IT3-83-4-T24	0.81	58	70.1	-20.9	63.9	-10.2	61.3	-5.7
R3-75-5-T10	0.72	40	45.5	-13.8	44.9	-12.3	43.7	-9.3
R3-80-5-T4	0.77	42	46.5	-10.7	46.4	-10.5	44.9	-6.9
T2-91-5-T14	0.87	20	23.7	-18.5	22.0	-10.0	21.4	-7.0
IT3-79-5-T23	0.78	57	65.6	-15.1	65.9	-15.6	62.9	-10.4
IT2-80-5-T13	0.77	58	65.5	-12.9	65.3	-12.6	62.9	-8.4
Average				-10.2		-7.0		-4.4

Table 5-5: Measured and predicted cracking loads and prediction accuracy for the full-scale beams

Test Specimen Designation	σ_{BOTTOM} at Critical Section $(x\,f'_{ci})$	Measured Cracking Load (kips)	Predicted Cracking Loads and Accuracy			
			NCHRP Report 496 2003		AASHTO LRFD 2005	
			Kips	%	Kips	%
A55-T25	$-0.55f'_{ci}$	62	64.3	-3.7	60.6	2.3
A60-T26	$-0.60f'_{ci}$	63	63.5	-0.8	59.7	5.2
A63-T27	$-0.63f'_{ci}$	63	63.6	-1.0	60.0	4.8
A66-T28	$-0.66f'_{ci}$	63	63.8	-1.3	60.5	4.0
A67-T29	$-0.67f'_{ci}$	60	62.5	-4.2	58.6	2.3
A66-T30	$-0.66f'_{ci}$	59	63.1	-6.9	59.4	-0.7
A69-T31	$-0.69f'_{ci}$	60	62.6	-4.3	58.9	1.8
A68-T32	$-0.68f'_{ci}$	58	62.8	-8.3	59.0	-1.7
A67-T33	$-0.67f'_{ci}$	63	63.0	0.0	59.5	5.6
A73-T34	$-0.73f'_{ci}$	57	62.8	-10.2	59.5	-4.4
A71-T35	$-0.71f'_{ci}$	63	63.1	-0.2	59.8	5.1
A75-T36	$-0.75f'_{ci}$	60	62.6	-4.3	59.2	1.3
Average				-3.8		2.1

In the aforementioned plots (Figure 5-17 to 5-20) and tables (5-4 and 5-5), a similar trend existed. The cracking loads of the beams subjected to compressive stresses at release less than the range of $0.63f'_{ci}$ to $0.70f'_{ci}$ were estimated consistently and accurately in general. However, as the compressive stress at release increased in excess of this stress range, the accuracy of the cracking load estimate decreased. The beams subjected to high stresses at release cracked sooner than predicted. The primary explanation for the premature cracking of the beams subjected to these high stress levels is linked to the nonlinear behavior of the highly-stressed beams at prestress transfer. The nonlinear behavior is the result of internal damage in the bottom fibers of the section and is not conservatively estimated with typical design calculations in regards to the cracking load estimate. These two effects of the inelastic behavior of overstressed members are discussed in the next two sections.

5.2.3.1 Internal Damage

In the literature review chapter, several research studies were discussed that associated the inelastic response of concrete loaded in compression with microcracking, or internal damage. In particular, two investigations quantified this internal damage with measurements of the tensile strength of concrete previously loaded in compression (Delibes Liniers, 1987 and Gettu et al., 1996). The results of these studies indicated that as concrete is subjected to initial compressive stresses in the inelastic range, reductions in tensile strength are present. These reductions

increase significantly under sustained loads. In fact, Gettu et al. (1996) discovered that concrete loaded in compression to 80-percent of its strength and maintained at this level for 15-minutes exhibited tensile strength reductions of approximately 12-percent (Figure 2-18). For the same stress level and load duration, Delibes Liniers (1987) reported a tensile strength loss of approximately 17-percent (Figure 2-16). For the beans tested in the current study, a 17-percent decrease in tensile strength is consistent with approximately a 4-percent decrease in the cracking load estimate.

In general, these studies seem applicable to the behavior of prestressed concrete beams. Karsan and Jirsa concluded that the extreme fibers of concrete loaded with a strain gradient deformed in the same manner as concrete subjected to a uniform strain (1970). Also, even though the level of stress in the bottom fiber of a pretensioned beam reduces over time, an assumption of 15-minutes of sustained stress is reasonable and likely conservative in regards to the conditions at prestress transfer. Lastly, it was illustrated that at conventional release times (~16 ½-hours) the stress-strain response of typical high-strength concrete is still considerably nonlinear (Khan, Cook, and Mitchell, 1995). For these reasons, the highly-stressed beams in the current study likely underwent inelastic deformations at transfer. Since nonlinear deformation is concurrent with internal damage, it seems plausible that internal damage contributed to the premature cracking of the highly-stressed beams.

5.2.3.2 *Nonlinear vs. Linear-Elastic Stress Calculations*

The second explanation for the premature cracking of the beams subjected to stresses in excess of the allowable limit was the reliance on linear-elastic principles in the prestress loss and cracking load calculations. In their theoretical evaluation of overstressed pretensioned members, Huo and Tadros discovered that linear elastic assumptions were essentially valid up to the current allowable limit of $0.60f'_{ci}$ (Huo and Tadros, 1997). Above this limit, the nonlinear response of the pretensioned member departed from the assumed linear response, thereby violating the elastic assumption (Figure 2-1). Some potential differences between the assumed linear response and the actual nonlinear response at prestress transfer of the test specimens with compressive release stresses higher than the allowable limit include:

      (i)   Larger strains at extreme fibers due to nonlinear response
      (ii) Nonlinear creep deformations if stress exceeds linear proportionality limit
      (iii) Less stress for a given strain if material deforms nonlinearly

In regards to overestimating the cracking loads of the highly-stressed beams in the current study, the discrepancy highlighted in item (iii) above was the most significant. At prestress transfer, the beams subjected to high levels of compressive stress deformed nonlinearly. As such, a lower level of stress existed in the bottom-fibers than that computed with the elastic, working stress equation. To accurately estimate the cracking load, this smaller stress should be incorporated into the cracking load calculation as the initial precompression stress that must be overcome to crack the section. Consider the inelastic, high-strength concrete model and the linear-elastic approximation displayed in Figure 5-21 (Thorenfeldt, Tomaszewicz, and Jensen, 1987). The nonlinear model matches the concrete stress-strain curve measured at 16 ½-hours by Khan, Cook, and Mitchell (Figure 2-6). The linear model utilizes the ACI 318 modulus of elasticity expression (Equation 2-12). As a result, it passes through the origin and $0.40f'_c$ (Collins and Mitchell, 1997). For a given strain of 0.0009, the stress according to the linear

model is $0.80f'_c$. For the same strain, the stress according to the nonlinear model is $0.74f'_c$. For a concrete compressive strength of 4,000-psi, the difference between these two stress values is 240-psi. Applying this reduction to either the AASHTO or NCHRP cracking load estimates reduced the cracking load by approximately 8-percent.
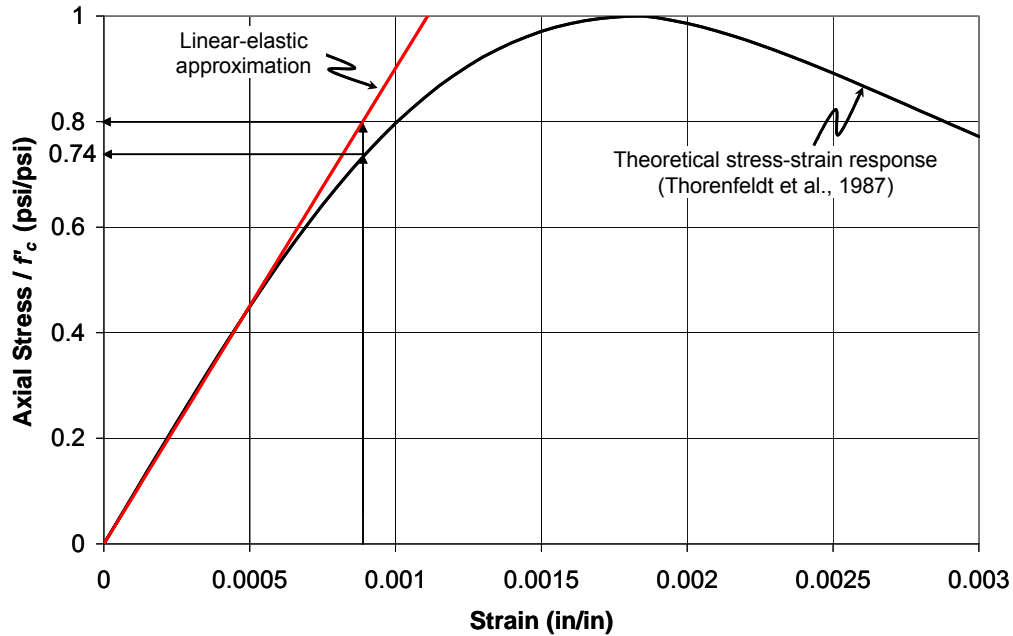
Figure 5-21: Linear and nonlinear concrete loaded in compression models (Thorenfeldt et al., 1987)

It is clear that if the nonlinear performance of the overstressed beams was accounted for then the cracking loads would be better estimated. However, accounting for this behavior does not mitigate the presence of internal damage that is concurrent with nonlinear deformation. It accounts for the internal damage. Internal damage or microcracking affects the durability of the member and reduces the tensile capacity of the concrete as previously noted. In addition, it seems impractical to adjust current design principles (P/A ± Mc/I) to account for inelastic deformations (nonlinear formulations).

In conclusion, the allowable release stress in compression is a serviceability limit. It is used to ensure the satisfactory condition of the precompressed tensile zone of a pretensioned beam. Likewise, it is used to ensure that an accurate cracking load estimate is obtained as illustrated with the aforementioned test results. As a result, the benefits from potential modifications to the current limit should be carefully evaluated against potential losses in the quality of the prestressed concrete product. As a conservative interpretation, a higher allowable compressive release stress ($> 0.60f'_{ci}$) should ensure the same initial cracking performance as the current allowable release stress. With this methodology, the test results presented herein were analyzed. The data according to the NCHRP method (Figure 5-19) and AASHTO method (Figure 5-20) suggested a potential increase of the allowable release stress to a value within the range of $0.63f'_{ci}$ to $0.70f'_{ci}$. It should be noted, however, that in regards to the actual behavior of the specimens, the use of transformed section properties as in the NCHRP method is more

appropriate. An increase in the allowable release stress to $0.63f'_{ci}$ or $0.64f'_{ci}$ was indicated according to the NCHRP method. In addition, for the purposes of a national design code limit, an increase in the allowable compressive stress at release should be limited to sensible increments. For these reasons, an increase of the allowable compressive stress at release to $0.65f'_{ci}$ seems appropriate for the specimens tested within the current study. One concern with this recommendation is the limited variables considered within this test program. In regards to relaxing a national code limit, it seems prudent and comprehensive to explore additional mix designs (especially with differing coarse aggregate types) and section types that might be more critical than those considered herein.

5.3 COMPARISON OF THREE ANALYSIS PROCEDURES

In the three analytical procedures, the total loss of the prestressing force was divided into four components: elastic shortening, creep and shrinkage of the concrete, and relaxation of the prestressing strands. These individual components are discussed in the following sections to illustrate the effect on the cracking load performance of the test specimens and to explain the difference between the PCI procedure and NCHRP and AASHTO procedures.

5.3.1 Elastic Shortening Losses

The elastic shortening losses obtained in Project 4086 were inferred from measured strains. These "measured" elastic shortening losses were compared to the losses predicted in the three analysis procedures. The accuracy of the different elastic shortening calculations was evaluated with these comparisons. In addition, the impact of the inelastic behavior of the overstressed beams at transfer was assessed.

5.3.1.1 *Measured and Predicted Elastic Shortening Losses*

For the scaled specimens fabricated under Project 4086, electrical strain gauges were affixed to each prestressing strand near the midspan of the beam. A calibration curve was developed to associate the measured strains with the stresses in the strand (Castro et al., 2004 and Rogers, 2002). For each beam, all of the "inferred" stresses were averaged to obtain the stress in the strands before and after prestress transfer. In addition, since the strands were stressed a couple of days before each beam was cast, an estimate of the relaxation loss during this time was subtracted from the measured values. An estimate was required because the stress loss due to relaxation is not accompanied with a measurable change in strain. For this purpose, an approximate value of $0.01f_{pi}$ was subtracted from the stress immediately before transfer. The "measured" elastic shortening losses for each beam were calculated simply as the difference between the stress before (f_{pi}) and the stress after (f_{po}) prestress release. The average stress in the strands for each beam immediately before and after prestress transfer is provided in Appendix A.

In each analytical procedure, the loss due to the elastic shortening of the member was estimated. The two variables that affected the accuracy of the elastic shortening loss included the equation for the modulus of elasticity and the combination of section properties and prestressing force used in each procedure. These variables are summarized in Table 5-6.

Table 5-6: Variables of elastic shortening loss estimate for three procedures

Procedure	Modulus of Elasticity, E_c[*]	Force and Properties
PCI	$E_{ci} = w_c^{1.5} \cdot 33\sqrt{f'_{ci}}$	0.9P_i and Gross Section Properties
AASHTO	$E_c = 33,000 K_1 w_c^{1.5} \sqrt{f'_c}$	0.9P_i and Gross Section Properties
NCHRP	$E_c = 33,000 K_1 K_2 \left(0.140 + \dfrac{f'_c}{1000}\right)^{1.5} \sqrt{f'_c}$	P_i and Transformed Section Properties

*Descriptions of the modulus equations are provided in Section 2.5

The elastic shortening calculation in the AASHTO and PCI procedures were almost identical. In both procedures, the gross section properties and an estimate for the prestressing force immediately after release of 0.9P_i were used. Even though the stress in the strands after transfer was "measured" with strain gauges, the approximate value of 0.9P_i was utilized for consistency with typical design procedures. The only difference between the loss calculations was the incorporation of a K_1 factor in the AASHTO procedure as recommended by the NCHRP report 496 (Table 5-3). This discrepancy affected those beams comprised of concrete mixture 2 for which K_1 equaled 0.8. For the other specimens, a K_1 factor of 1.0 was used.

The elastic shortening calculation in the NCHRP 496 procedure was significantly different. Several researchers have emphasized that the approach in PCI and AASHTO does not accurately predict the elastic shortening losses (Huang, 1972, Noppakunwijai et al., 2001, and Hennessey, 2002). Instead, the initial prestressing force with the transformed section properties or the force after transfer with the net section properties should be used to calculate the elastic loss. The initial prestressing force with the transformed section properties was used in the NCHRP 496 procedure. In addition, a different modulus of elasticity equation was recommended in the NCHRP 496 procedure. This equation was similar to the AASHTO equation with the exception of an empirical relationship for the unit weight of concrete instead of the actual unit weight.

The elastic shortening losses calculated for all of the small-scale beams by each procedure are included with the measured losses in Table 5-7.

Table 5-7: Estimated and "measured" elastic shortening losses of scaled beams

Mix Design	Test Specimen Designation	Measured Elastic Shortening Loss (ksi)	Predicted Elastic Shortening Losses (ksi)		
			PCI Design Handbook	NCHRP 496	AASHTO LRFD 2005
Mix # 1	R1-52-1-T8	13.5	11.9	13.0	11.9
	R1-52-1-T7	13.4	12.0	13.1	12.0
	R1-50-1-T1	13.5	11.6	12.7	11.6
	R1-49-1-T2	12.2	11.4	12.5	11.4
	R1-46-1-T5	12.7	11.1	12.1	11.1
	R1-48-1-T6	12.1	11.3	12.3	11.3
	T1-68-2-T17	10.6	12.7	14.0	12.7
	T1-62-2-T18	17.0	12.8	14.1	12.8
	IT1-68-2-T20	16.4	14.2	15.6	14.2
	IT1-73-2-T19	20.8	16.0	17.4	16.0
	R3-75-3-T9	16.7	14.2	16.1	14.2
	R3-78-3-T3	18.7	15.3	17.2	15.3
	T2-79-3-T16	14.1	13.2	15.1	13.2
	T2-86-3-T15	15.9	15.4	17.4	15.4
	IT3-79-3-T21	21.4	17.1	19.1	17.1
	IT2-76-3-T22	17.5	16.5	18.5	16.5
Mix # 2	R3-78-4-T11	19.9	14.5	20.2	18.1
	R3-83-4-T12	21.7	15.8	21.9	19.8
	IT3-83-4-T24	26.6	17.7	24.3	22.1
Mix # 3	R3-75-5-T10	17.5	14.9	16.2	14.9
	R3-80-5-T4	18.7	16.2	17.5	16.2
	T2-91-5-T14	17.7	15.3	16.7	15.3
	IT3-79-5-T23	22.0	17.9	19.3	17.9
	IT2-80-5-T13	22.5	17.8	19.2	17.8
Average		17.2	14.4	16.5	14.9

5.3.1.2 *Accuracy of Elastic Shortening Loss Estimates*

For the small-scale beams, the elastic shortening losses estimated in the PCI, AASHTO, and NCHRP 496 procedures were plotted with the corresponding measured losses. The accuracy of each procedure was assessed by the position of the data points with respect to the line of equality. Data points falling below the line of equality denoted an underestimation of the elastic shortening loss. The plots for the PCI, AASHTO, and NCHRP 496 procedures are provided in Figure 5-22, 5-23, and 5-24, respectively.
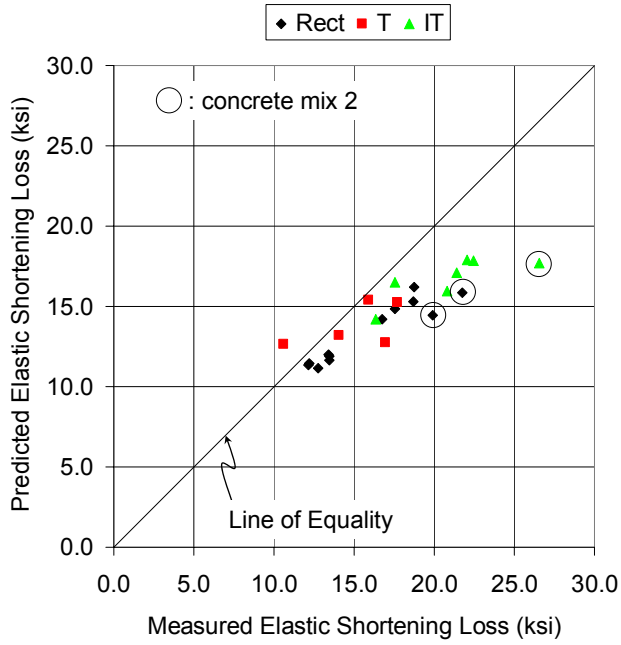
Figure 5-22: Accuracy of elastic shortening losses according to PCI
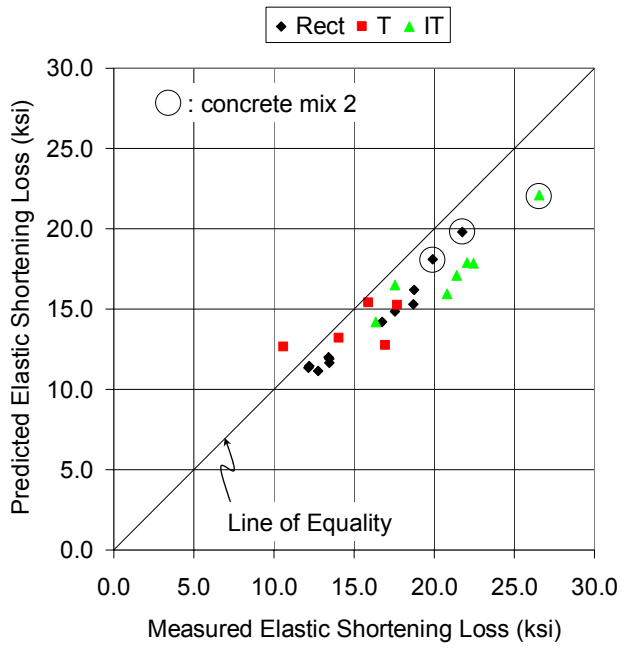
Figure 5-23: Accuracy of elastic shortening losses according to AASHTO

112
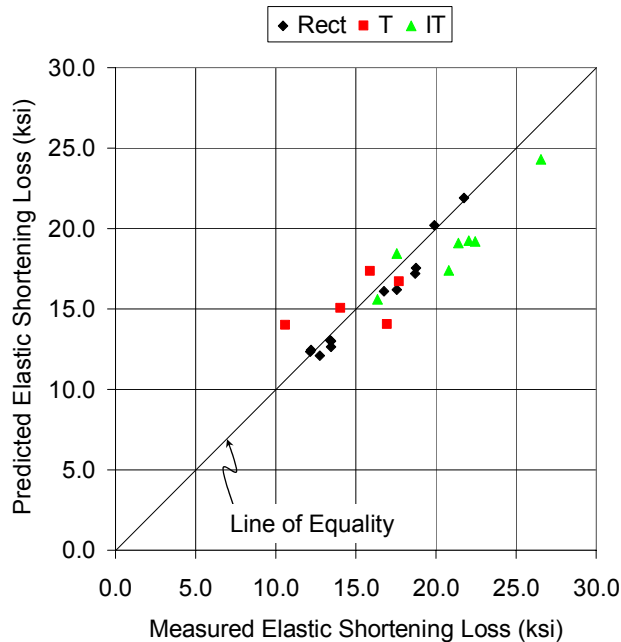
Figure 5-24: Accuracy of elastic shortening losses according to NCHRP 496

The accuracy of the elastic shortening loss estimates according to the PCI procedure (Figure 5-22) was nearly equivalent to that according to the AASHTO procedure (Figure 5-23). The only exceptions were the three data points corresponding to the beams with concrete mixture design 2. Using a K_1 factor of 0.8 for these three specimens in the AASHTO procedure improved the elastic shortening loss estimate considerably. As a result, the use of the K_1 factor was further justified.

On average, the elastic shortening losses were better estimated when the NCHRP 496 procedure (Figure 5-24) was used than when the AASHTO procedure (Figure 5-23) was used. Primarily, the increased accuracy was the result of a better estimated modulus of elasticity in the NCHRP 496 procedure. The empirical formula for the unit weight of concrete present in the NCHRP E_c equation calculated weights ranging from approximately 144- to 146-pcf. The measured unit weights used in the AASTHO procedure ranged from 150- to 155-pcf. As a result, the modulus of elasticity estimated with the NCHRP procedure was smaller than that calculated with the AASHTO procedure. This smaller elastic modulus corresponded to a larger and more accurate elastic shortening loss. Using the initial prestressing force with the transformed section properties in the NCHRP procedure, as opposed to 90-percent of the initial force with the gross section properties, slightly improved the elastic shortening loss estimates. However, due to the small-scale of these specimens, this difference was not as significant as the difference in concrete modulus.

5.3.1.3 *Impact of Inelastic Behavior at Release on Elastic Shortening Loss*

The measured elastic shortening losses were also compared to the predicted losses to address if the inelastic behavior of the overstressed beams at release impacted the accuracy of the calculations. For this comparison, only the NCHRP elastic shortening loss estimates were used.

113

The elastic shortening losses are plotted versus the maximum compressive stress at release for the rectangular sections and for the tee and inverted-tee sections in Figure 5-25 and 5-26, respectively.
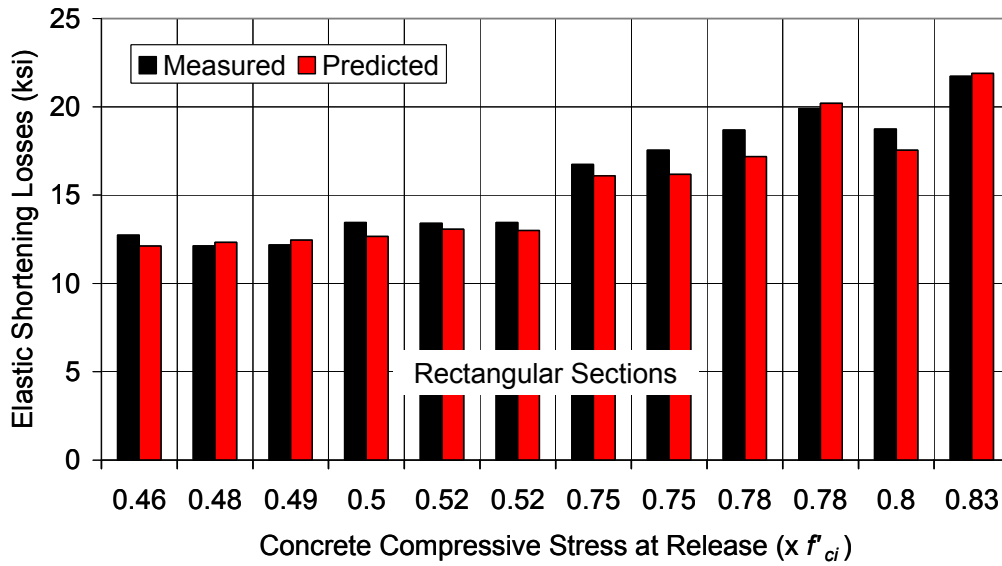
Figure 5-25: NCHRP elastic shortening losses for the rectangular beams
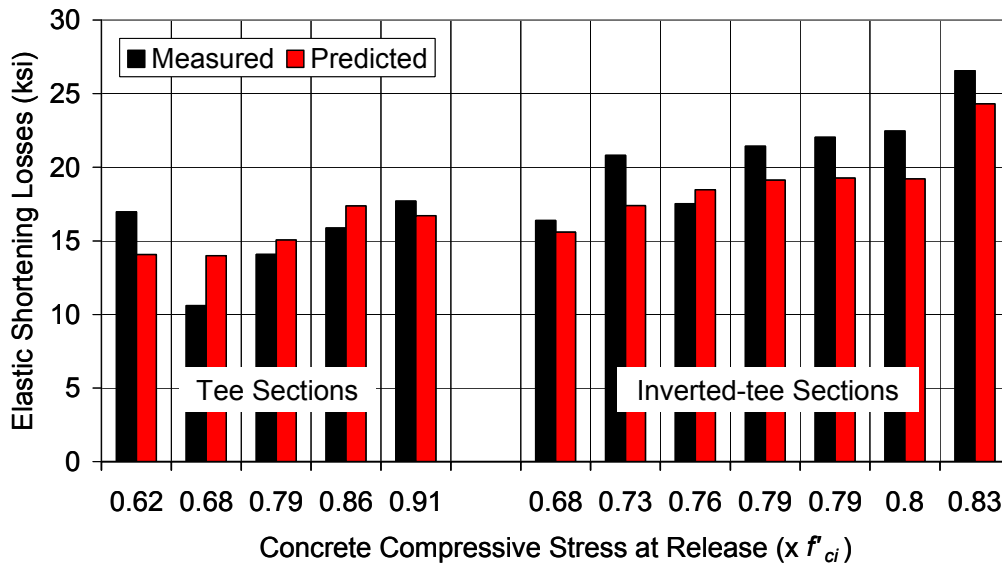
Figure 5-26: NCHRP elastic shortening losses for tee and inverted-tee beams

From the comparison of the measured to predicted elastic shortening losses in Figure 5-25 and 5-26, a couple of observations are made. First, for all three section types (rectangular, tee, and inverted-tee), the "measured" elastic shortening losses increased with increasing compressive stress at release. While this finding is expected, it should be noted in regards to increasing the allowable stress. Second, regardless of the compressive stress at release, the

114

elastic shortening loss estimates for the rectangular and tee sections are fairly accurate. For the highly-stressed inverted tee specimens, however, the elastic shortening losses were slightly under-predicted. It is possible that the nonlinear deformations at transfer of the inverted-tee beams contributed to the higher-than-predicted elastic shortening losses. Regardless, it is important to note that this slight difference between the estimated and "measured" elastic shortening losses did not greatly contribute to the discrepancy in the cracking load predictions. For instance, a 15-percent difference in the elastic shortening loss calculation is approximately a 1 ½-percent difference in the cracking load calculation.

5.3.2 Long-term Prestress Losses

The long-term prestress loss components of the PCI, NCHRP, and AASHTO procedures include the prestress loss due to creep and shrinkage of the concrete and the relaxation of the prestressing steel. The PCI equations for these components were originally derived for final service-load checks and therefore, represent total loss values. On the other hand, time-dependent expressions are utilized in the NCHRP 496 and AASHTO procedures that permit the calculation of various loss components at any time throughout the life of a pretensioned member. Since the scaled beam-specimens were tested approximately 3-years after they were cast, most of the total loss in prestressing force should have occurred. As such, it seems acceptable to compare the time-dependent loss components with the total prestress loss components for the scaled specimens. It is important to note that none of the long-term prestress loss components were measured. Instead, the components estimated by using each procedure are compared to explain the discrepancy between the cracking load prediction plots of the small-scale beams (Figure 5-17 – 5-20). The equations used in each procedure for the three prestress loss components were listed in Section 2.5.

The long-term prestress loss component that varied the most between the PCI method and the NCHRP-496 and AASHTO methods was the loss due to creep of the concrete. The estimated creep losses for the small-scale beams from all three procedures are provided in Table 5-8 and displayed in Figure 5-27. In Figure 5-27, the values are plotted versus an ascending maximum compressive stress at release for each cross-section.

Table 5-8: Estimated prestress loss due to concrete creep of small-scale beams

Mix Design	Test Specimen Designation	Creep Losses (ksi)		
		PCI	NCHRP	AASHTO
Mix # 1	R1-52-1-T8	18.4	17.7	16.3
	R1-52-1-T7	18.5	17.8	16.4
	R1-50-1-T1	18.4	16.5	15.2
	R1-49-1-T2	18.1	16.3	15.0
	R1-46-1-T5	18.0	15.5	14.3
	R1-48-1-T6	18.3	15.8	14.5
	T1-68-2-T17	16.4	25.2	23.0
	T1-62-2-T18	16.6	24.9	22.8
	IT1-68-2-T20	17.5	27.2	25.0
	IT1-73-2-T19	19.7	29.7	27.6
	R3-75-3-T9	18.1	25.7	23.1
	R3-78-3-T3	19.4	26.8	24.3
	T2-79-3-T16	16.5	27.8	24.8
	T2-86-3-T15	19.3	30.9	28.1
	IT3-79-3-T21	21.7	30.5	27.8
	IT2-76-3-T22	21.6	28.4	25.9
Mix # 2	R3-78-4-T11	17.8	31.8	29.2
	R3-83-4-T12	19.5	33.6	31.3
	IT3-83-4-T24	21.8	38.0	35.6
Mix # 3	R3-75-5-T10	22.0	25.7	23.9
	R3-80-5-T4	24.0	27.2	25.5
	T2-91-5-T14	20.9	32.7	30.4
	IT3-79-5-T23	26.5	30.6	28.8
	IT2-80-5-T13	26.4	30.4	28.6
Average		19.8	26.1	24.1
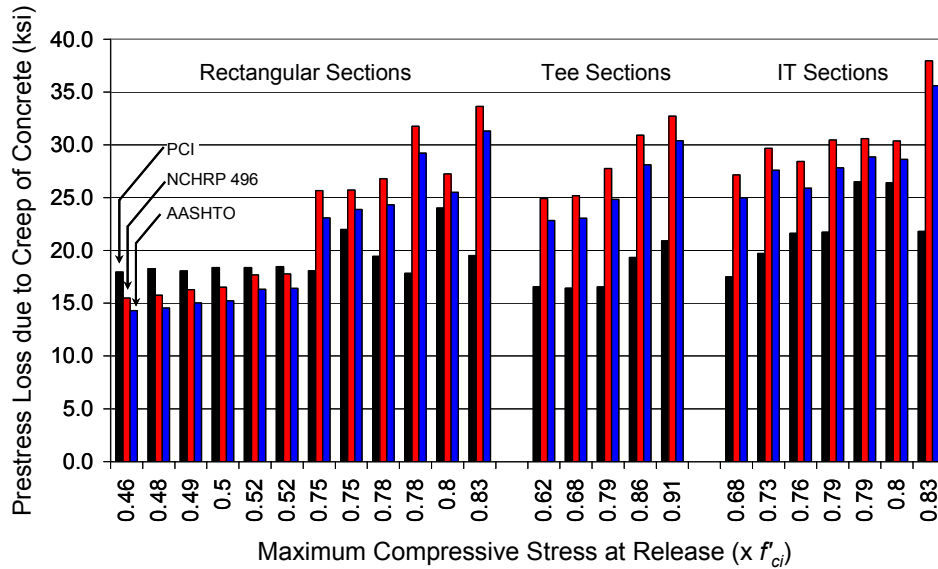
Figure 5-27: Estimated prestress loss due to creep of small-scale beams

In Figure 5-27, the difference in the estimated creep loss between the PCI procedure and the NCHRP 496 and AASHTO procedures is illustrated. This difference is the result of the creep coefficient and modulus of elasticity utilized in each calculation. In the PCI procedure, a constant creep coefficient equal to 2.0 for normal-weight concrete was assumed in all cases. In the NCHRP and AASHTO procedures, the creep coefficient was estimated based on several characteristics, most notably the concrete strength factor (k_f) and the size factor (k_s). Since these factors varied considerably for the beams of different cross-sections and mix designs, the calculated creep coefficient varied. For reference, the average calculated creep coefficient in the AASHTO procedure for the R1, R3, T, and IT sections were approximately 1.6, 2.1, 2.4, and 2.2, respectively. The most significant difference between the PCI creep equation and the NCHRP 496 and AASHTO creep equations was the use of the elastic modulus of concrete. In PCI, the ACI 318 equation for the concrete modulus was used with the 28-day compressive strength of the concrete, f'_c. In the NCHRP 496 and AASHTO creep equations, the compressive strength of the concrete at release, f'_{ci}, was used in the modulus of elasticity calculation. This difference was substantial for the overstressed members because, in general, the release strengths were much lower than the 28-day strengths. For the six conventional beams, the release strengths were closer to the 28-day compressive strengths. In addition, a K_1 factor of 0.8 was utilized for concrete mix 2 in both the NCHRP and AASHTO procedures. These differences explain the discrepancy between the estimated creep losses in the three procedures.

In addition, the estimated prestress losses due to shrinkage of the concrete and due to relaxation of the prestressing strands were compared for the three analysis methods. The shrinkage and relaxation induced prestress losses for all of the scaled beams are depicted in Figure 5-28 and 5-29, respectively. The losses due to shrinkage and relaxation are listed in tabular format for the small-scale specimens in Appendix A. The losses due to elastic shortening, shrinkage and creep of the concrete, and relaxation of the strands are listed in tabular format for the full-scale beams in Appendix B.

117
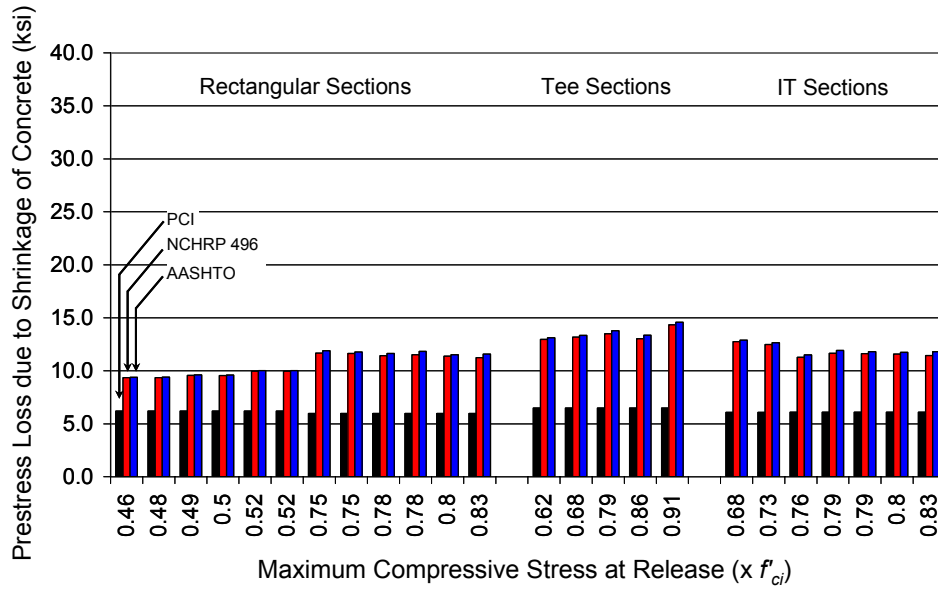
Figure 5-28: Estimated prestress loss due to shrinkage of small-scale beams
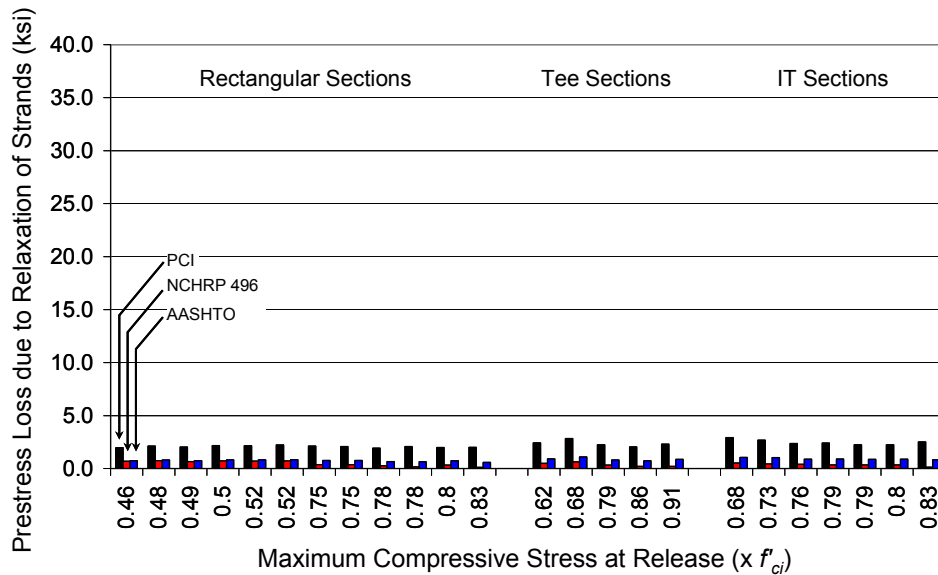
Figure 5-29: Estimated prestress loss due to relaxation of prestressing strands

For all of the small-scale beams, a lower prestress loss due to shrinkage was estimated in the PCI procedure as compared to the NCHRP 496 and AASHTO procedures. The most apparent difference was a lower relative humidity factor utilized in the PCI procedure compared to those used in the NCHRP and AASHTO procedures.

On the other hand, the relaxation losses estimated in the PCI procedure were higher than those estimated using the NCHRP 496 or AASHTO methods. The magnitudes of the relaxation

loss component were considerably less than the creep and shrinkage components and therefore, did not contribute greatly to the total loss of the prestressing force.

5.3.3 Total Prestress Losses

For the small-scale beams, the total loss of the prestressing force estimated with the PCI, NCHRP 496, and AASHTO analytical procedures is provided in Table 5-9 and in Figure 5-30. In each case, the total loss was the summation of the losses due to elastic shortening, creep and shrinkage of the girder concrete, and relaxation of the prestressing strands.

Table 5-9: Estimated total prestress loss of the small-scale beams

Mix Design	Test Specimen Designation	Total Losses (ksi)		
		PCI	NCHRP	AASHTO
Mix # 1	R1-52-1-T8	38.6	41.3	39.1
	R1-52-1-T7	38.9	41.5	39.2
	R1-50-1-T1	38.4	39.4	37.3
	R1-49-1-T2	37.7	38.9	36.8
	R1-46-1-T5	37.3	37.6	35.5
	R1-48-1-T6	37.9	38.2	36.1
	T1-68-2-T17	38.4	53.0	50.1
	T1-62-2-T18	38.2	52.4	49.6
	IT1-68-2-T20	40.7	56.0	53.1
	IT1-73-2-T19	44.4	60.0	57.2
	R3-75-3-T9	40.4	53.8	49.9
	R3-78-3-T3	42.6	55.6	51.9
	T2-79-3-T16	38.5	56.6	52.6
	T2-86-3-T15	43.3	61.5	57.6
	IT3-79-3-T21	47.3	61.6	57.7
	IT2-76-3-T22	46.5	58.5	54.8
Mix # 2	R3-78-4-T11	40.3	63.6	59.7
	R3-83-4-T12	43.3	66.9	63.2
	IT3-83-4-T24	48.1	73.8	70.3
Mix # 3	R3-75-5-T10	44.9	53.9	51.3
	R3-80-5-T4	48.2	56.5	54.0
	T2-91-5-T14	44.9	63.9	61.1
	IT3-79-5-T23	52.7	61.8	59.4
	IT2-80-5-T13	52.6	61.5	59.1
Average		42.7	54.5	51.5
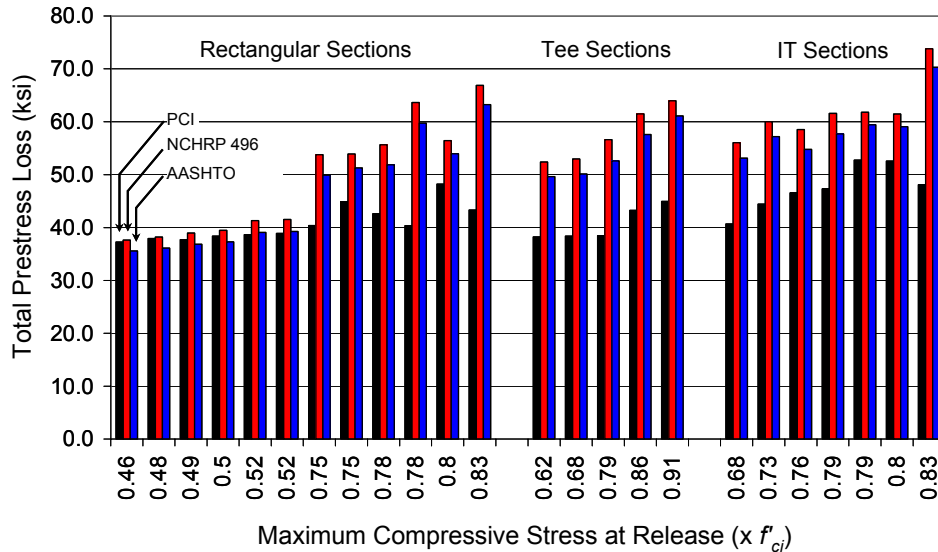
Figure 5-30: Estimated total loss of prestressing force of small-scale beams

As seen in Figure 5-30, the total estimated loss of the prestressing force was different in each procedure. It is clear that for the highly stressed members more prestressing loss was calculated in the NCHRP 496 and AASHTO procedures than in the PCI procedure. However, this discrepancy is not a direct result of the compressive stress levels at release but rather the inherent differences between the loss calculations of each procedure. The smaller total losses estimated in the PCI procedure contributed significantly to the steep downward trend in the cracking load prediction plot according to PCI (Figure 5-17). In regards to the NCHRP and AASHTO procedures, the total estimated prestress loss was similar. This conclusion was expected since essentially the same equations were used in each procedure. The two major discrepancies were (i) the use of gross section properties in the AASHTO procedure and transformed section properties in NCHRP 496 procedure and (ii) the slightly different modulus of elasticity of concrete equations used in each.

5.4   RESULTS OF FATIGUE TESTS OF SCALED BEAMS

In the fatigue testing phase of the experimental program, the behavior of two conventionally-stressed, scaled beams (R1-48-1-T6 and R1-52-1-T7) was compared to that of two scaled beams (R3-80-5-T4 and R3-78-3-T3) subjected to higher stresses at release. To facilitate the comparison, the static load response of each beam was monitored at various stages of the fatigue loading, after a predetermined number of cycles were completed. The data obtained from the tests at each stage and the visual observations made throughout the fatigue program are presented and analyzed in this section.

5.4.1   Measured Data

The static load-midspan deflection response was obtained after 0; 100,000; 300,000; 1,000,000; and 2,000,000 cycles of fatigue loading. The load-deflection plot at each stage was used to calculate the stiffness, K, of the initial portion of the curve. The stiffness at each stage

was normalized with the stiffness obtained before the specimen was subjected to any fatigue cycles, at stage 0. For all four fatigue specimens, the normalized stiffness was plotted versus the number of load-cycles completed to assess how the fatigue loading affected the stiffness of the member. The reduction in stiffness of the four beams was compared to evaluate the effect, if any, of the compressive release stress levels on the fatigue performance of the specimens. At each stage, the stiffness, K, was computed with Equation 5-12 as the slope of the initial portion of the curve.

$$K_N = \frac{P_{cr}}{\Delta_N} \tag{5-12}$$

where, P_{cr} = original measured cracking load (kips)
Δ_N = net midspan deflection at P_{cr} (in.)
N = denotes number of fatigue cycles

It is important to note that the compression of the neoprene pads at the end supports of the fatigue specimens was subtracted from the total midspan deflection measurement to obtain the net midspan deflection. The load-deflection plot for fatigue specimen R1-48-1-T6 is presented in Figure 5-31. The reduction in stiffness of all four fatigue specimens are depicted in Figure 5-32.
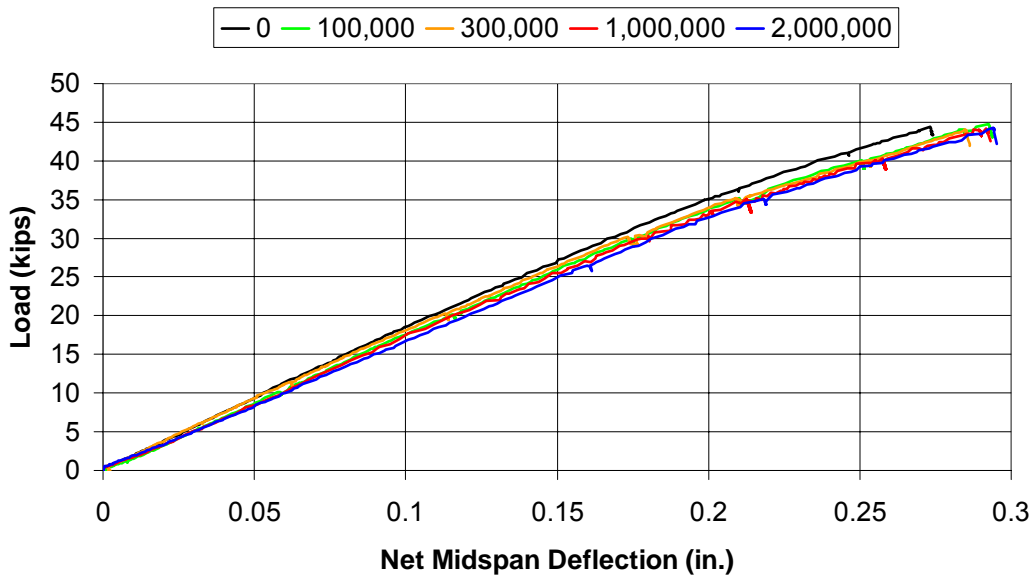
Figure 5-31: Load vs. midspan deflection at each fatigue stage for R1-48-1-T6
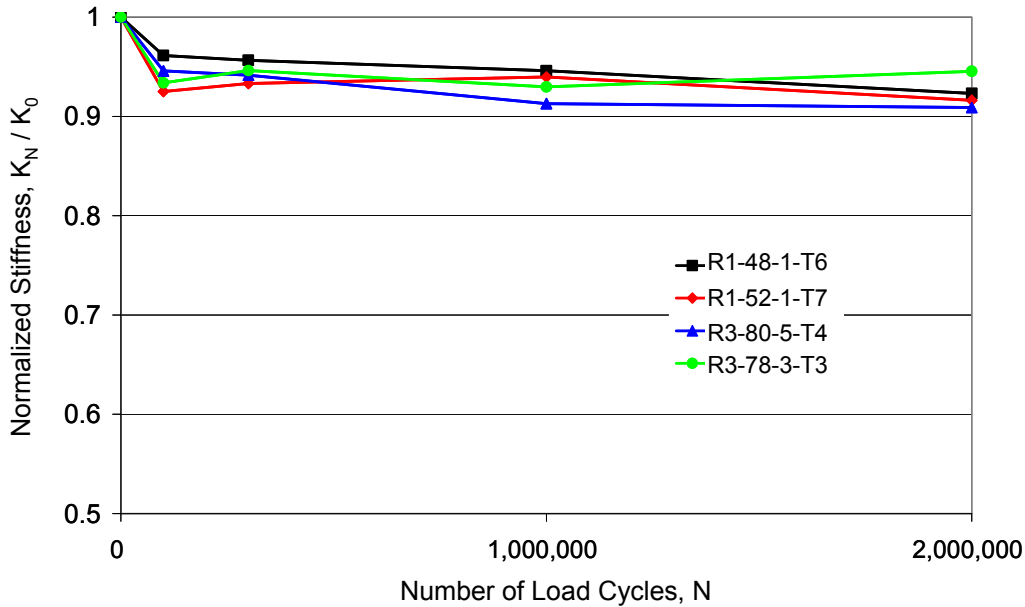
Figure 5-32: Reduction in stiffness of specimens subjected to fatigue loading

In Figure 5-31, it is clear that the stiffness of specimen R1-48-1-T6 did not significantly reduce as a result of the fatigue program. The load-deflection plots from each stage are tightly grouped. The same finding is confirmed in Figure 5-32. For R1-48-1-T6, the stiffness of the initial portion of the response decreased to 96-percent of the pre-fatigue stiffness after 100,000 cycles. After 2,000,000 cycles, the stiffness reduced to 92-percent of the original value. Similar conclusions can be drawn from Figure 5-32 for the other three specimens. For the most part, the largest, but overall minor, reduction in stiffness occurred after the first 100,000 cycles were applied. At the conclusion of the fatigue loading program, the stiffness of each member ranged from 94- to 91-percent of the pre-fatigue stiffness. Similar conclusions were drawn from the comparisons of the load-strain relationships monitored during each fatigue stage.

5.4.2 Visual Observations

The increase in length of several flexural cracks within the constant moment region was monitored for all four test specimens. At each fatigue stage, the length of one typical flexural crack at midspan, L_N, was recorded. It was normalized with the original length of the crack before the fatigue program was initiated, L_0. The normalized length (L_N/L_0) of a typical flexural crack for each fatigue specimen is illustrated in Figure 5-33. From Figure 5-33, it is clear that the crack length increased only slightly over the course of the fatigue loading program. For specimen R1-48-1-T6, the length of a typical crack increased by approximately 20-percent after 2,000,000 cycles of fatigue loading. For all of the specimens, the length of the main flexural cracks did not increase after 1,000,000 cycles of fatigue loading.

123
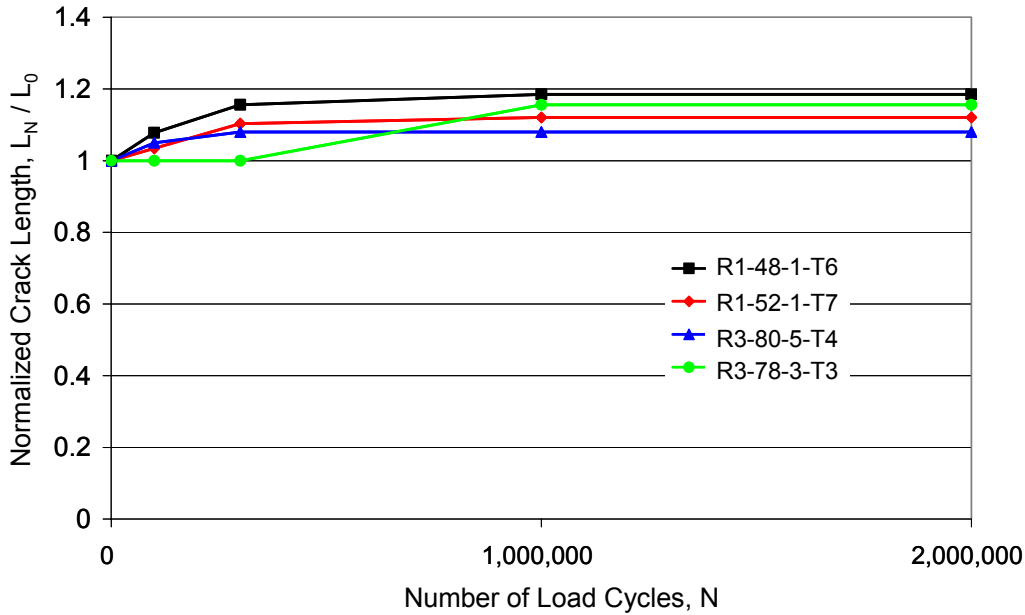
Figure 5-33: Increase in crack length of specimens subjected to fatigue loading

In addition, the width of several flexural cracks was recorded throughout the fatigue program for the four specimens. With increasing number of fatigue cycles, the width of a typical flexural crack for conventional and overstressed beams was slightly larger than in previous cycles at the same load level. However, the difference was small; and in general, the width at the maximum applied load was consistent throughout the fatigue program. As a result, the effect of additional fatigue cycles was minimal in regards to increasing crack widths.

5.4.3 Summary of Fatigue Results

Two conventional and two initially higher-stressed girders were subjected to cyclic loading to evaluate the effect of high levels of compressive stress at prestress transfer on their fatigue performance. In particular, the opening and closing of flexural cracks in the bottom fibers of the pretensioned beams was emphasized. The stress range in the prestressing strands imposed by the fatigue program was limited to avoid reaching the fatigue strength of the tendons. From the aforementioned test results, no appreciable difference in the performance between the conventional and initially higher-stressed beams was detected. For all of the specimens, the reduction in stiffness and the increase in crack length as a result of the fatigue loading were minimal.

However, it was evident from the results of the static load tests of all 36 test specimens (Section 5.2) that as the compressive stress at transfer increased, the initially higher-stressed beams cracked sooner than predicted. If a beam cracks prematurely, strand fatigue problems due to an increase in the stress range of the strands may appear that would not have existed otherwise. The conservative prediction of the cracking load to avoid fatigue problems under service loads was emphasized in a research study by Reese (1983). In addition, if a beam cracks prematurely, the slight reduction in stiffness induced by the cyclic loading may arise that would

124

not have existed if the cracking load was accurately predicted. This serviceability concern may affect some members.

5.5   SUMMARY

In the live-load performance evaluation of the current research project, 36 static-load tests and 4 cyclic-load tests were performed. The purpose of these tests was to evaluate the impact of increasing the allowable value of compressive stress at transfer from the current value of $0.60f'_{ci}$ on the live-load performance of the member. The results of the static-load tests are summarized in Figure 5-34.
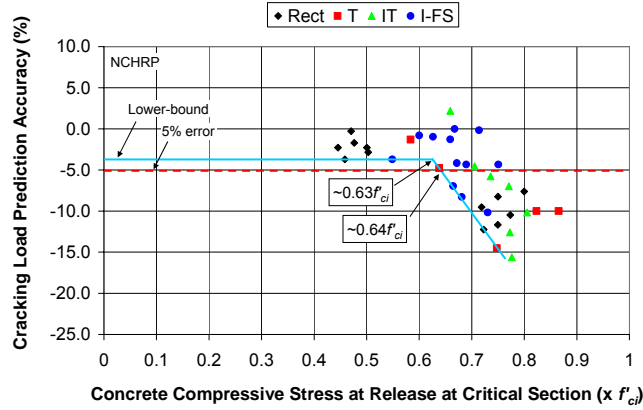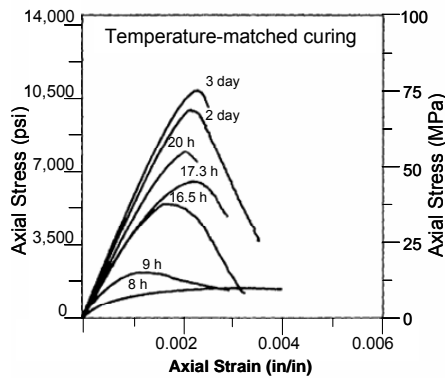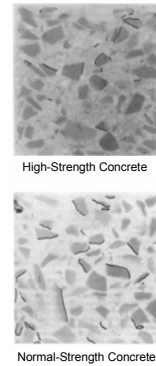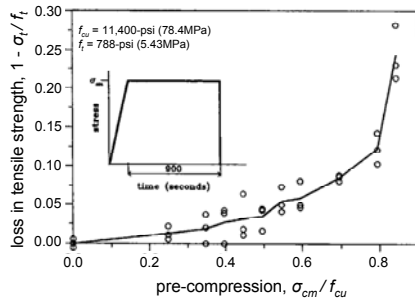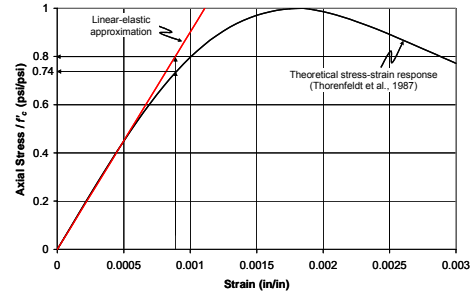
Figure 5-34: (a): Accuracy of cracking load prediction using NCHRP procedure; (b): Stress-strain curves of HSC at various ages (Khan et al., 1995); (c): Microcracking in concrete due to short-term loading (Ngab et al., 1981); (d): Loss of tensile strength of concrete under 15-min. of compressive stress (Gettu et al., 1996); (e): Linear vs. nonlinear stress calculations (Thorenfeldt et al., 1987)

For the beams tested in the current study, an increase in the allowable compressive stress at release to $0.65f'_{ci}$ seems justified. The test specimens subjected to compressive release stresses at the midspan of the beam up to $0.65f'_{ci}$ performed comparably to those subjected to compressive stresses at release within the current allowable limit ($\leq 0.60f'_{ci}$) (Figure 5-34: (a)).

126

However, in regards to the multitude of beam types and mixture designs used in Texas, the current study was limited in scope. For the test specimens subjected to compressive stresses at release significantly in excess of $0.65f'_{ci}$, premature, flexural cracking under static loads was detected (Figure 5-34: (a)). The premature cracking of the overstressed beams was linked to the nonlinear deformation of the bottom fibers of the section at prestress transfer in two ways.

First, when high-strength concrete is loaded to high-levels of compressive stress at typical prestress release times (approximately 16 ½-hours), it undergoes nonlinear deformations (Figure 5-34: (b)). For this reason, several research studies that correlated nonlinear deformations of normal-strength, mature concrete with microcracking were applicable to the current study (Richart et al., 1929; Hsu et al., 1963; Ngab et al., 1981; and Smadi et al., 1985 and 1987). For instance, while the cracking maps depicted in Figure 5-34: (c) illustrated the superior performance of high-strength concrete as compared to normal-strength concrete, the loading was applied at mature ages. Since high-strength concrete is considerably nonlinear at early ages, it seems plausible that microcracking in the bottom-fibers of a pretensioned beam approached that of the normal-strength specimen illustrated in Figure 5-34: (c). In addition, the internal damage present in concrete loaded to high compressive stress levels was quantified with reductions in tensile strength (Delibes Liniers, 1987; and Gettu et al., 1996) (Figure 5-34: (d)). As such, one potential reason for the premature cracking of the overstressed beams was due to a reduction in tensile strength of the bottom-fiber concrete due to the internal microcracking induced by nonlinear deformations at prestress transfer.

Second, the nonlinear deformation at prestress transfer is not conservatively estimated in regards to the cracking load prediction. In a study by Huo and Tadros (1997), for a given strain in the inelastic range of the concrete, it was shown that a lower stress is calculated with a nonlinear analysis than with a linear analysis (Figure 5-34: (e)). Since typical prestressed concrete design calculations (P/A ± Mc/I) are based on linear-elastic behavior and it was determined that the overstressed beams are deforming nonlinearly at release, an inconsistency exists. In the cracking load predictions of the overstressed beams, it seems that the bottom-fiber, compressive stress at release is overestimated. As such, the moment required to overcome the bottom-fiber stress and crack the section is overestimated. Therefore, the second potential reason for the premature cracking of the overstressed girders was the overestimation of the bottom-fiber compressive stress at release. It is evident that if the nonlinear behavior of the overstressed beams was accounted for, the cracking loads could be better estimated. However, accounting for this behavior does not mitigate the presence of the internal damage concurrent with nonlinear deformation. It accounts for the internal damage.

In regards to the cyclic-load performance of the four scaled beams, the conventional beams performed comparably to the initially higher-stressed beams. That is the performance of the bottom-fibers of the section due to repeated opening and closing of flexural cracks were not affected by the different levels of compressive stress at release. However, it should be noted that the premature cracking of initially higher-stressed girders due to static loads can expose the specimen to fatigue-related problems, such as an increase in the stress range of the prestressing strands and a slightly reduced stiffness of the member.

127

CHAPTER 6
Initial Camber

6.1 OVERVIEW

The purpose of the initial camber study was twofold. First, with camber data from 197 standard, full-scale girders, the current state of camber prediction for beams fabricated in Texas was evaluated. In this context, a simple technique for improving the accuracy of initial camber estimates was presented. Second, with camber data from 26 girders subjected to a range of compressive stresses at release, the impact of increasing $0.60f'_{ci}$ (permissible compressive stress at release) on the initial camber of a member was assessed. In order to accomplish these goals, the initial camber measurements of all 223 pretensioned members were compiled into a database. In this chapter, the specimens in the database are introduced, the methods of measuring and estimating the initial camber of the beams are provided, and the measured initial camber is compared to predicted camber. The complete initial camber database in tabular format is provided in Appendix C.

Due to concrete creep, concrete shrinkage, and steel relaxation, the camber of a pretensioned member changes over time, particularly at early ages. However, accurately estimating it at the initial stage before these effects contribute to the magnitude of the camber is valuable. For instance, the initial camber is the starting point for estimating the final camber or the camber at erection. If the initial camber estimate is inaccurate, these long-term estimates will also be inaccurate. In addition, in regards to increasing the allowable compressive stress of $0.60f'_{ci}$, it was determined by Castro et al. (2004) that the accuracy of the initial camber estimations were more critical and more variable than the long-term component of the camber. For these reasons, the initial camber was focused on in the current study.

6.2 SPECIMENS IN DATABASE

Initial camber data was compiled for 223 prestressed concrete girders. Of the 223 specimens, 197 were standard, full-scale bridge girders subjected to compressive stresses at release within the current code limit. They were fabricated at two of the many precast pretensioned beam production plants in the state of Texas. The section types included:

- 132 – AASHTO Type-IV girders
- 65 – TxDOT Type-C girders

Details of these standard bridge girders are provided in this section.

The remaining 26 pretensioned girders were from the live-load behavior evaluation part of the current research project. Most of these specimens were subjected to compressive stresses at release in excess of the current allowable limit of $0.60f'_{ci}$. The section types included:

- 6 – scaled rectangular girders (Section 3.2)
- 3 – scaled tee girders (Section 3.2)
- 5 – scaled inverted-tee girders (Section 3.2)
- 12 – full-scale TxDOT Type-A girders (Section 3.3)

The scaled specimens were fabricated at the Ferguson Structural Engineering Laboratory at the University of Texas at Austin (Castro et al., 2003). The Type-A beams were fabricated at a precast pretensioned beam production facility. The inventory of the non-standard girders used in the camber study is included in this section.

6.2.1 Standard, Full-Scale Girders

A variety of standard section types are used by the Texas Department of Transportation (TxDOT) for typical bridge projects throughout the state. Two of these section types, the AASHTO Type-IV and the TxDOT Type-C, were included in the initial camber database compiled in this project. The dimensions for these beams types are provided in Figure 6-1 and Table 6-1. The section properties are provided in Table 6-2.
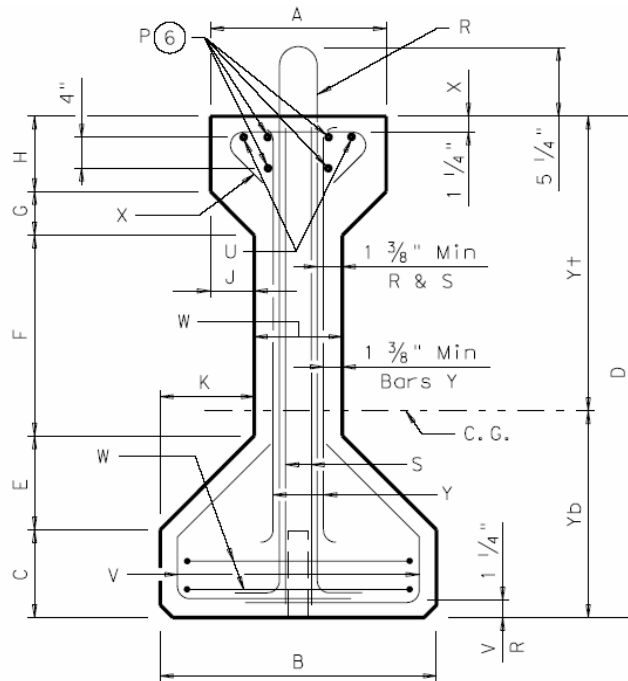
Figure 6-1: Standard TxDOT I-girder section (TxDOT, 2005)

Table 6-1: Beam Dimensions of Standard TxDOT I-girders (TxDOT, 2005)

Beam Type	A (in.)	B (in.)	C (in.)	D (in.)	E (in.)	F (in.)	G (in.)	H (in.)	J (in.)	K (in.)	W (in.)
C	14	22	7	40	7.5	16	3.5	6	3.5	7.5	7
IV	20	26	8	54	9	23	6	8	6	9	8

130

Table 6-2: Section Properties of Standard TxDOT I-girders (TxDOT, 2005)

Beam Type	y_t (in.)	y_b (in.)	A (in.^{2})	I (in.^{4})	Weight (plf)
C	22.91	17.09	494.9	82,602	516
IV	29.25	24.75	788.4	260,403	821

The 65 Type-C girders and 112 of the 132 Type-IV girders were produced at the Heldenfels Enterprises, Inc. (HEI) San Marcos, TX plant. The beams were cast between July 2003 and July 2006. The transportation of one Type-IV girder from the prestressing bed to the storage yard at the HEI San Marcos plant is shown in Figure 6-2.

Figure 6-2: Transportation of a Type-IV girder at HEI San Marcos plant

The remaining 20 Type-IV girders were produced at the Texas Concrete Company, Inc. (TCC) Victoria, TX plant. All of these beams were cast on the 1st or 2nd of August, 2006. The removal of forms for a line of Type-IV girders prior to prestress release is depicted in Figure 6-3.

Figure 6-3: Form removal for a line of Type-IV girders at TCC Victoria plant

A fairly wide range of variables that influence the initial camber of pretensioned girders were present in the beams fabricated at these two facilities. The range of some of these parameters is listed in Table 6-3. The four coarse aggregates used in the concrete mixture designs of the conventional, full-scale girders are identified in Table 6-4.

Table 6-3: Range of parameters for conventional girders in database

Parameter	Type-IV	Type-C
Length (ft.)	70 to 120	60 to 90
f'_{ci} (psi)	4,800 to 8,400	5,800 to 7,600
Comp. Stress at Release (x f'_{ci})	0.19 to 0.60	0.30 to 0.60
Coarse Aggregate Type	2 – Round river gravel 1 – Crushed limestone 1 – Crushed river gravel	1 – Round river gravel 1 – Crushed limestone
Age at Release (hrs.)	11 to 71	17 to 43

Table 6-4: Identification of the coarse aggregates used in the database

Coarse Aggregate		Pretensioned Beam	
Type	Provider	Fabricator	Type
Round River Gravel	TXI-Owens Pit	HEI San Marcos	IV and C
Crushed Limestone	Hansen-Ogden Quarry	HEI San Marcos	IV and C
Crushed River Gravel	Yarrington Road Pit	HEI San Marcos	IV
Round River Gravel	Fordyce Murphy Quarry	TCC Victoria	IV

6.2.2 Non-standard, Scaled and Full-Scale Girders

The non-standard, pretensioned girders that were included in the initial camber database are listed in Table 6-5. All of these specimens were tested in the live-load behavior evaluation part of the current research project discussed in previous chapters. Of the scaled specimens described in Section 3.2, 14 were included in the camber database because their initial camber was measured accurately (Castro et al., 2004). The 14 scaled beams were fabricated at the Ferguson Structural Engineering Laboratory at the University of Texas at Austin. All 12 full-scale TxDOT Type-A beams described in Section 3.3 were included in the initial camber database. The twelve girders were produced at the Heldenfels Enterprises, Inc. Corpus Christi, TX plant. Some parameters that influence the initial camber for these unconventional girders are provided in Table 6-6. Additional information on these specimens such as section dimensions, section properties, and concrete mixture details can be found in their respective sections of Chapter 3.

Table 6-5: Details of the non-standard specimens in the camber database

Concrete Mix #	Project 5197 Designation	Maximum Release Stresses		f'_{ci} (psi)	Age (hrs)	Date of Cast
		σ_{BOTTOM}	σ_{TOP}			
Mix 1	R3-75-3-T9	$-0.75f'_{ci}$	$3.7\sqrt{f'_{ci}}$	4065	10	9/24/2002
	R3-78-3-T3	$-0.78f'_{ci}$	$7.1\sqrt{f'_{ci}}$	4065	10	
	T2-79-3-T16	$-0.79f'_{ci}$	$1.5\sqrt{f'_{ci}}$	3950	10	
	T2-86-3-T15	$-0.86f'_{ci}$	$4.2\sqrt{f'_{ci}}$	3950	10	
	IT3-79-3-T21	$-0.79f'_{ci}$	$9.0\sqrt{f'_{ci}}$	4065	10	
	IT2-76-3-T22	$-0.76f'_{ci}$	$8.8\sqrt{f'_{ci}}$	4320	10	
Mix 2	R3-78-4-T11	$-0.78f'_{ci}$	$3.7\sqrt{f'_{ci}}$	3800	14	12/5/2002
	R3-83-4-T12	$-0.83f'_{ci}$	$7.3\sqrt{f'_{ci}}$	3800	14	
	IT3-83-4-T24	$-0.83f'_{ci}$	$9.1\sqrt{f'_{ci}}$	3800	14	
Mix 3	R3-75-5-T10	$-0.75f'_{ci}$	$3.5\sqrt{f'_{ci}}$	4045	15	3/4/2003
	R3-80-5-T4	$-0.80f'_{ci}$	$7.1\sqrt{f'_{ci}}$	4045	15	
	T2-91-5-T14	$-0.91f'_{ci}$	$1.9\sqrt{f'_{ci}}$	3465	15	
	IT3-79-5-T23	$-0.79f'_{ci}$	$9.3\sqrt{f'_{ci}}$	4045	15	
	IT2-80-5-T13	$-0.80f'_{ci}$	$9.0\sqrt{f'_{ci}}$	4045	15	
Mix 5	A55-T25	$-0.55f'_{ci}$	$6.1\sqrt{f'_{ci}}$	5500	11	7/13/2006
Mix 4	A60-T26	$-0.60f'_{ci}$	$6.3\sqrt{f'_{ci}}$	5010	16	7/12/2006
Mix 5	A63-T27	$-0.63f'_{ci}$	$6.4\sqrt{f'_{ci}}$	4790	11	7/14/2006
	A66-T28	$-0.66f'_{ci}$	$6.6\sqrt{f'_{ci}}$	4550	7	7/17/2006
	A67-T29	$-0.67f'_{ci}$	$6.6\sqrt{f'_{ci}}$	4450	14	7/18/2006
	A66-T30	$-0.66f'_{ci}$	$6.6\sqrt{f'_{ci}}$	4500	9	7/19/2006
	A69-T31	$-0.69f'_{ci}$	$6.7\sqrt{f'_{ci}}$	4330	8	7/20/2006
	A68-T32	$-0.68f'_{ci}$	$6.7\sqrt{f'_{ci}}$	4390	9	7/21/2006
	A67-T33	$-0.67f'_{ci}$	$6.6\sqrt{f'_{ci}}$	4480	7	7/24/2006
	A73-T34	$-0.73f'_{ci}$	$6.9\sqrt{f'_{ci}}$	4080	10	7/25/2006
	A71-T35	$-0.71f'_{ci}$	$6.8\sqrt{f'_{ci}}$	4180	7	7/26/2006
	A75-T36	$-0.75f'_{ci}$	$7.0\sqrt{f'_{ci}}$	3960	7	7/27/2006

Table 6-6: Range of parameters for the non-standard girders in database

Parameter	Scaled Beams	Full-Scale Beams
Length (ft.)	15	40
f'_{ci} (psi)	3,465 to 4,320	3,960 to 5,500
Comp. Stress at Release (x f'_{ci})	0.75 to 0.91	0.55 to 0.75
Coarse Aggregate Type	1 – Round river gravel 1 – Crushed limestone	1 – Round river gravel
Age at Release (hrs.)	10 to 15	7 to 14

6.3   INITIAL CAMBER MEASUREMENTS

Two different techniques were used to measure the initial camber of the girders in the database. For the 209 full-scale girders, the initial camber was evaluated with a measuring tape onsite at the precast pretensioned beam fabrication plant. For the 14 scaled girders, the initial camber was recorded with a linear potentiometer at the midspan of the beam (Castro et al., 2004). Both of these operations are described in this section.

6.3.1   Full-scale specimens

The initial camber data of the full-scale girders in the database was obtained from the three following precast pretensioned beam fabrication plants:

- Heldenfels Enterprises, Inc. San Marcos, TX plant
- Texas Concrete, Inc. Victoria, TX plant
- Heldenfels Enterprises, Inc. Corpus Christi, TX plant

For all of the full-scale specimens, the initial camber was determined with a measuring tape relative to the bottom surface of the formwork. The method of obtaining the camber data from each of these plants is discussed herein.

At the Heldenfels Enterprises, Inc. (HEI) San Marcos plant, the majority of the camber data was obtained from detailed records of their quality control department. As part of the Precast/Prestressed Concrete Institute (PCI) Plant Certification Program, HEI was required to measure the initial camber of the girders produced at their facility. These camber data were stored with the shop drawings, strand stressing reports, mixture design, and a summary worksheet for that particular line of prestressed concrete beams. With the permission of HEI, detailed reports consisting of this information were obtained for 177 pretensioned members. To document the prestress transfer operation and initial camber measurement technique, the author worked with the quality control department at HEI. During this collaborative work, the initial camber of 12 beams was measured personally by the author. The prestress transfer operation is discussed below.

A counter-weight was placed over each hold-down location while the strand restraining the hold-down mechanism was flame-cut. Then, the remaining prestressing force was transferred to the beams by hydraulic rams positioned at the live-end of the prestressing bed. The steel bulkhead supporting the chucks of the prestressing strands was slowly released towards the beams by the hydraulic rams. This "multi-strand release" operation ensured the slow and symmetric transfer of the prestressing force. After the force was transferred, the strands were cut at the ends of each beam; and the counter-weight and formwork were removed. At this time, the

initial camber was measured at the midspan of each girder. The measurement was taken approximately ten-minutes after the full prestressing force was transferred. A typical camber measurement is illustrated in Figure 6-4. Due to the chamfer along the bottom edge of the beam, the camber was measured from the top of the chamfer edge to the top edge of the steel formwork. The initial camber was 1 ¾–inches for this particular specimen.
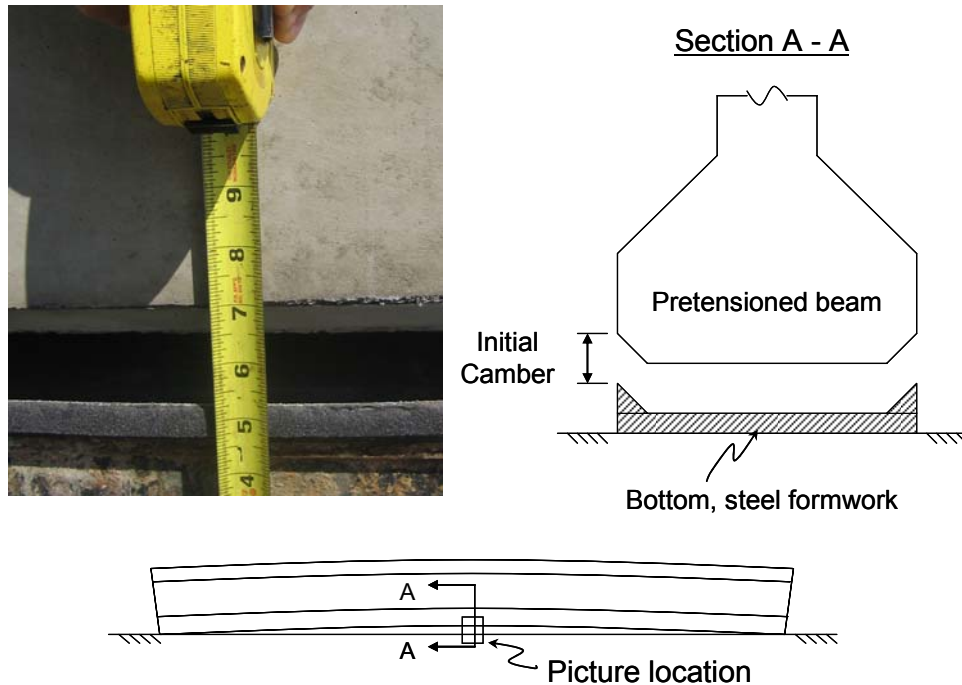
Figure 6-4: Picture of onsite camber measurement

At the Texas Concrete Inc. (TCI) Victoria plant, no records of previous fabricated beams were available. The camber data of the 20 pretensioned specimens from this plant were obtained personally by the author. The prestress transfer operation was slightly different at this fabrication yard. First, the steel formwork was removed before the concrete counter-weights were placed at the hold-down locations. Then, the vertical force at the hold-down location was transferred to the beam by loosening a nut on a threaded rod that restrained the depressed strands. Before the remaining prestressing force was released, each end of the beam was lifted so that a 1/8-inch thick bearing pad could be placed between the formwork and the beam. This pad removed any restraint due to friction between the bottom of the beam and the steel formwork. Finally, a "multi-strand release" operation similar to that of the HEI San Marcos plant was performed. The unstressed strands at the ends of each beam were flame-cut, and the initial camber was measured at midspan. The measurement was taken approximately ten-minutes after the prestressing force was fully transferred. The compressed thickness of the bearing pads was subtracted from the initial camber measurement. A line of Type-IV girders after prestress transfer is illustrated in Figure 6-5.

Figure 6-5: Line of Type-IV girders after release at TCC Victoria plant

The HEI Corpus Christi, TX plant also produced some pretensioned beams used in the initial camber database. As part of the live-load portion of the current research project, twelve TxDOT Type-A beams were fabricated at this facility. The details of their fabrication were discussed in Section 3.3.2. Each beam was fabricated individually on the small prestressing bed illustrated in Figure 6-6. The strand restraining the hold-down mechanism was cut first by an oxy-acetylene torch. The strands at the end of the member were then flame-cut one wire at a time and in a symmetric pattern. After the prestressing force was transferred to the beam, the initial camber of each of these specimens was measured by a quality control inspector of HEI. A measuring tape was used at midspan as at the other precast pretensioned beam fabrication yards.

Figure 6-6: Small bed at HEI Corpus Christi plant used to cast Type-A beams (photograph courtesy of Chris Leonard)

137

6.3.2 Scaled specimens

In TxDOT Project 4086, the initial camber of each beam was measured with a single linear potentiometer at midspan supported by a steel tube running the length of each beam. The tube was supported at each end of the beam with threaded rods that were cast in the specimen. This configuration enabled the beam to shift longitudinally at release without disrupting the initial camber measurement. The setup for the initial camber measurements of the scaled beams is illustrated in Figure 6-7 and 6-8. The linear potentiometer is shown in Figure 6-9.
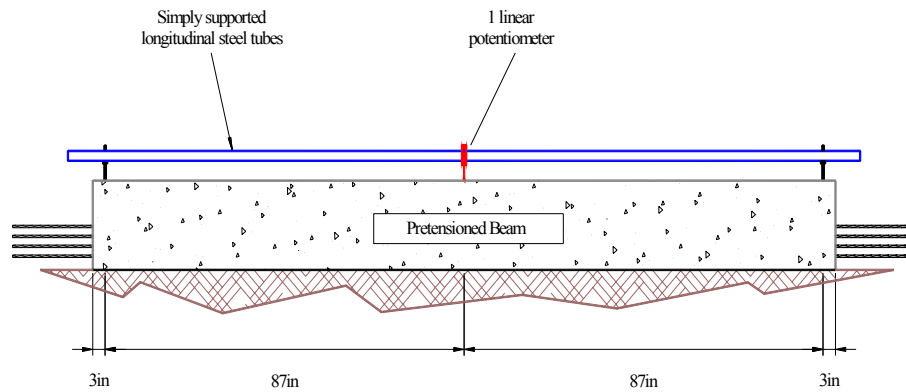
Figure 6-7: Setup for initial camber measurement (Castro et al., 2003)

Figure 6-8: Picture of initial camber setup (photograph courtesy of Alfredo Castro)
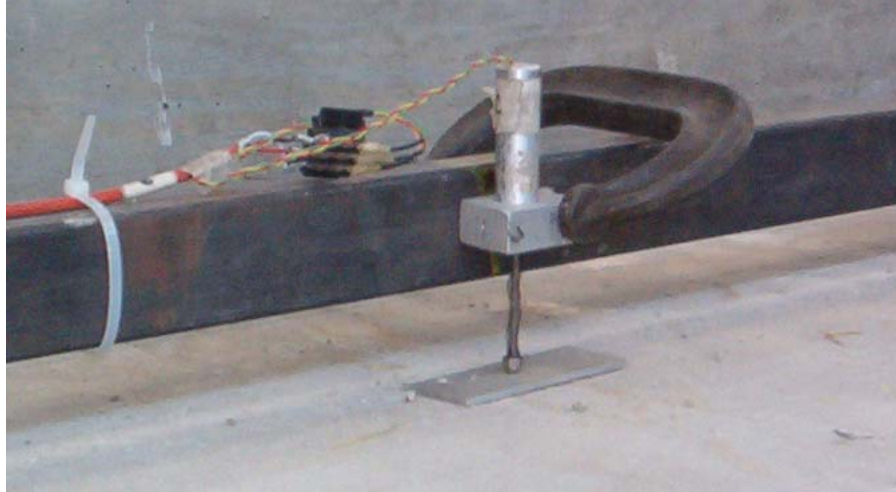
Figure 6-9: Close-up of linear potentiometer at midspan (photograph courtesy of Alfredo Castro)

Immediately prior to prestress transfer, the side formwork for each small-scale beam was removed. The wet burlap on the top surface of the specimen was also removed so that the linear potentiometer could be installed as shown in Figure 6-9. During the strand cutting operation, the potentiometer recorded data continuously. The camber measurement corresponding to the time when all of the prestressing strands were fully flame-cut was used as the initial camber measurement. In general, the flame-cutting operation took five-minutes (Castro et al., 2004).

6.4   INITIAL CAMBER ESTIMATES

In this section, the simple deflection equations used to estimate the initial camber and two empirical relationships used to approximate the concrete modulus of elasticity are presented.

6.4.1   Equations for Initial Camber

In the current research project, initial camber was calculated with simple linear-elastic expressions relating curvatures along the member to the deflection at the midspan of the beam. The downward deflection due to dead load was subtracted from the upward deflection due to the eccentric prestressing force. The net upward deflection was the initial camber. The downward deflection due to dead load was calculated as illustrated in Figure 6-10 and with Equation 6-1. For straight prestressing strands, the upward deflection due to the prestressing force was calculated as illustrated in Figure 6-11 and with Equation 6-2. For two-point depressed prestressing strands, the upward deflection was calculated as illustrated in Figure 6-12 and with Equation 6-3.

139
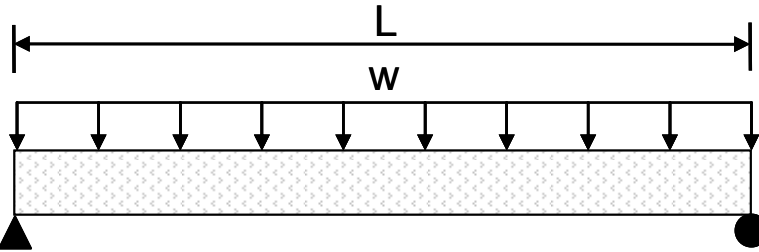
Figure 6-10: Downward deflection due to member dead load

$$\Delta_{dl} = \frac{5wL^4}{384E_cI_g} \downarrow \qquad (6\text{-}1)$$

where,
w = weight of the member per in (k/in.)
L = length of the member (in.)
E_c = modulus of elasticity of concrete (ksi)
I_g = moment of inertia of the section (in.[4])
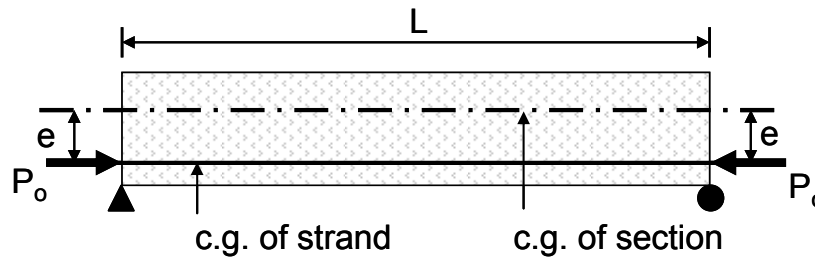
Figure 6-11: Upward deflection due to straight, eccentric prestressing strands (PCI, 2004)

$$\Delta_{p\_s} = \frac{P_o e L^2}{8E_cI_g} \uparrow \qquad (6\text{-}2)$$

where,
P_o = prestressing force after elastic shortening loss (kip)
e = eccentricity of the prestressing force (in.)
L = length of the member (in.)
E_c = modulus of elasticity of concrete (ksi)
I_g = moment of inertia of the gross section (in.[4])
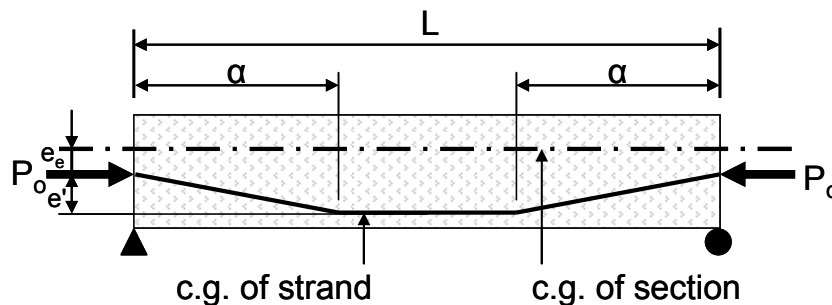
Figure 6-12: Upward deflection due to two-point depressed prestressing strands (PCI, 2004)

$$\Delta_{p\_d} = \frac{P_o e_e L^2}{8 E_c I_g} + \frac{P_o e'}{E_c I_g}\left(\frac{L^2}{8} - \frac{\alpha^2}{6}\right)\uparrow$$ (6-3)

where, P_o = prestressing force after elastic shortening loss (kip)
e_e = end eccentricity of the prestressing force (in.)
L = length of the member (in.)
E_c = modulus of elasticity of concrete (ksi)
I_g = moment of inertia of the gross section (in.[4])
e' = difference between end eccentricity and center eccentricity (in)
α = distance from end of member to hold-down location (in.)

Using simple, linear elastic methods to estimate initial camber are justified due to the level of accuracy of those estimates. Also, by and large, the conventional beams are subjected to stress levels well within the linear-elastic range for concrete. As seen in Equations 6-1 to 6-3, there are several variables that affect the initial camber prediction. Examining the variability of each of these parameters exposes the uncertainty of the initial camber estimate. For instance, at precast beam production plants, the prestressing force is verified with pressure readings in the hydraulic rams and with elongation of the prestressing strands. This redundancy ensures that the actual prestressing force is well within ±5-percent of the targeted force. In addition, the geometric variables, namely the moment of inertia, the eccentricity of the prestressing strands, and the length of the member, are very well controlled in the repetitive environment of a precast yard. Similarly, the weight of the member is generally well known due to its dependence on the controlled geometry and the unit weight of the concrete and the steel in the section. The last variable, the concrete modulus of elasticity, E_c, is associated with the most scatter. From the research studies by Cetin and Carrasquillo (1998), Myers and Carrasquillo (1998), and Mokhtarzadeh and French (2000), it is evident that the elastic modulus varies greatly depending on a wide range of variables of its own. As such, improving the accuracy of the concrete modulus of elasticity estimations will greatly improve the accuracy of the initial camber estimate. This task was emphasized in the current study.

6.4.2 Equations for the Concrete Modulus of Elasticity

There are several empirical relationships for the concrete modulus of elasticity available in the literature. The most widely-used expression was derived for normal-strength concrete in 1960 by Pauw (1960) and was adopted by the ACI 318 Building Code and the AASHTO Standard and LRFD Bridge Design Specifications. It is included as Equation 6-4 and is referred to as the ACI-318 equation in this chapter.

$$E_c = w_c^{1.5} \cdot 33 \cdot \sqrt{f'_c}\, psi$$ (6-4)

where, w_c = unit weight of concrete (pcf)
f'_c = compressive strength of the concrete (psi)

Over the last few decades, a lot of research on the modulus of elasticity of concrete has been performed. In a technical report by Myers and Carrasquillo (1998), they state that

empirical relationships for the elastic modulus of normal-strength concrete was easier than for higher-strength concrete because in the case of the former, the cement paste was always the weakest link. In the case of high-strength concrete, the elastic modulus is more dependent on the stiffness of the aggregates. This conclusion was echoed in research studies reviewed in Section 2.3 by Cetin and Carrasquillo (1998) and Mokhtarzadeh and French (2000).

In 1996, Irvani presented a solution to account for the dependence of the concrete modulus on the coarse aggregate type. The use of an aggregate coefficient to modify the empirical relationship for the concrete modulus was recommended (Irvani, 1996). Coefficients for a general category of coarse aggregate, such as limestone, dolomite, or granite, were developed from data in the literature. The shortcoming of this approach was that two aggregates within one of these groups but from different regions can differ greatly in terms of their physical and chemical properties (Myers and Carrasquillo, 1998).

In 2003, in the NCHRP Report 496, Tadros et al. recommended an empirical relationship for the modulus of elasticity of concrete that included a K_1 factor (Tadros et al., 2003). This factor accounts for differences in local materials as compared to the materials for which the empirical relationship was originally derived. The recommended expression is included as Equation 6-5 and is referred to as the NCHRP equation in this report.

$$E_c = 33,000 K_1 K_2 \left(0.140 + \frac{f'_c}{1000} \right)^{1.5} \sqrt{f'_c} \ ksi \qquad (6-5)$$

where, K_1 = factor accounting for variability of local materials
                               K_2 = factor accounting for average, upper-, or lower-bound value
                               f'_c = compressive strength of the concrete (ksi)

Equation 6-5 also included a K_2 factor that accounted for the application of the modulus of elasticity estimate. K_2 varied based on whether an average, upper-, or lower-bound estimate for the modulus of elasticity was required. For the purposes of the current research project, a K_2 factor of 1.0 was used because the accuracy of the camber predictions was desired.

These two equations for the concrete modulus of elasticity (6-5 and 6-6) were used in the current research project in the estimation of the initial camber of pretensioned beams. Equation 6-4 was included to illustrate the accuracy of current camber prediction for beams fabricated in the state of Texas. Equation 6-5 was included so that local material variability, particularly in regards to the coarse aggregate, could be incorporated into the initial camber estimates with the purpose of improving the accuracy of those estimates.

For Equation 6-5, a K_1 factor for each coarse aggregate present in the initial camber database was determined. In the NCHRP Report 496, K_1 factors were developed from the results of material testing. However, for the coarse aggregates present in the initial camber database, data from material testing was not obtained. In addition, one objective of this portion of the current study was not to correlate data from material testing with empirical equations but rather to correlate measured initial camber with estimated camber. For these reasons, a different method for developing the K_1 factors was used. For each coarse aggregate, a K_1 factor was selected such that the initial camber estimate using the NCHRP modulus of elasticity equation best agreed with the measured initial camber. Essentially, the K_1 factor was used as an

142

"adjustment" factor. Each of the K_1 factors determined in the current study is presented with the predicted camber of the beams with the corresponding coarse aggregate.

6.5   COMPARISON OF MEASURED AND PREDICTED INITIAL CAMBER

Initial camber measurements were obtained from 223 pretensioned girders. These measurements were compared to initial camber predicted with simple expressions and one of two modulus of elasticity equations. The current state of initial camber prediction for beams fabricated in Texas was evaluated with the results of the comparisons for the conventional, full-scale girders. The effect of increasing the allowable compressive stress at release on the initial camber of the member was evaluated with the results of the comparisons for the non-standard, overstressed girders. Both of these objectives are discussed in this section.

6.5.1   Camber Data of Conventional Girders

In this section, the measured initial camber data of the 197 conventional girders described in Section 6.2.1 was compared to estimated values. In these estimates, the simple equations for camber presented in Section 6.4.1 were used with either the ACI-318 or the NCHRP equation for the concrete modulus of elasticity. For the purposes of comparing the measured and predicted camber, the girders were grouped by the coarse aggregate used in their mixture design. For each coarse aggregate, a K_1 factor was determined from the analysis of the camber data to be used in the NCHRP equation for the concrete modulus of elasticity.

6.5.1.1   Round, River Rock from TXI-Owens Pit

A round, river gravel from the TXI-Owens pit was used in several AASHTO Type-IV and TxDOT Type-C girders compiled in the initial camber database. In Figure 6-13, the measured initial camber of 46 AASHTO Type-IV girders is presented with the corresponding predicted camber in which the ACI-318 equation for the modulus of elasticity was used. In Figure 6-14, the measured camber of the same 46 Type-IV girders is presented with predicted camber in which the NCHRP equation for the modulus of elasticity was used. In the NCHRP equation, a K_1 factor equal to 1.35 was selected from the camber data for girders with this particular river gravel.
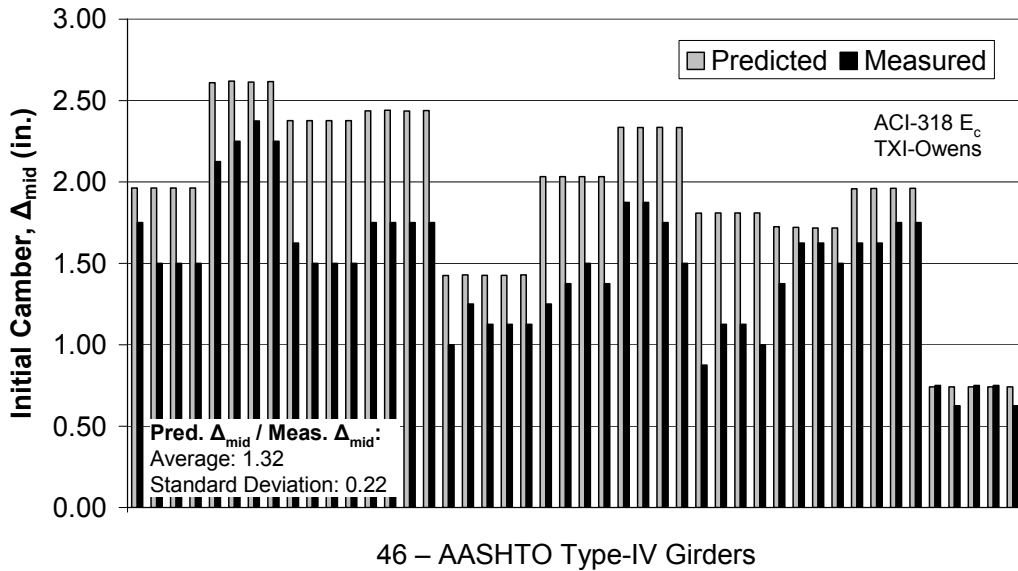
Figure 6-13: Measured and predicted (ACI-318 E_c) initial camber for Type IVs with TXI-Owens aggregate
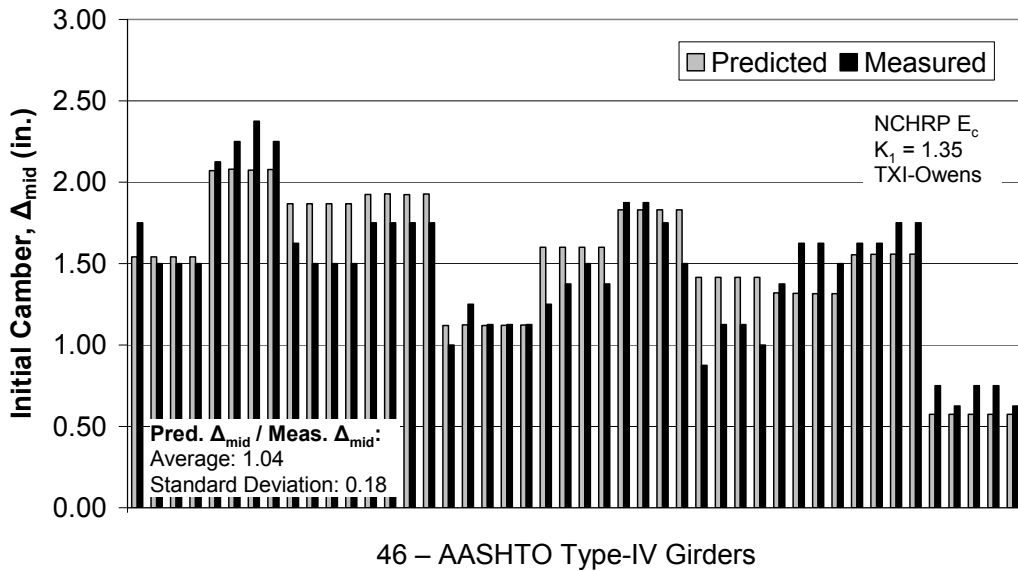
Figure 6-14: Measured and predicted (NCHRP E_c) initial camber for Type-IV with TXI-Owens aggregate

In Figure 6-13, the accuracy of conventional camber predictions was illustrated. The initial camber was consistently overestimated by simple camber equations and the conventional ACI-318 modulus of elasticity expression. In Figure 6-14, the camber estimates were greatly improved with the inclusion of a K_1 factor equal to 1.35 in the NCHRP modulus of elasticity equation.

The positive effect of using this K_1 factor was evident from comparing the predicted camber to the measured camber of 18 TxDOT Type-C girders as well. In Figure 6-15, the ACI-318 modulus of elasticity equation was used in the camber predictions of these Type-C girders. In Figure 6-16, the NCHRP equation was used in the initial camber predictions.
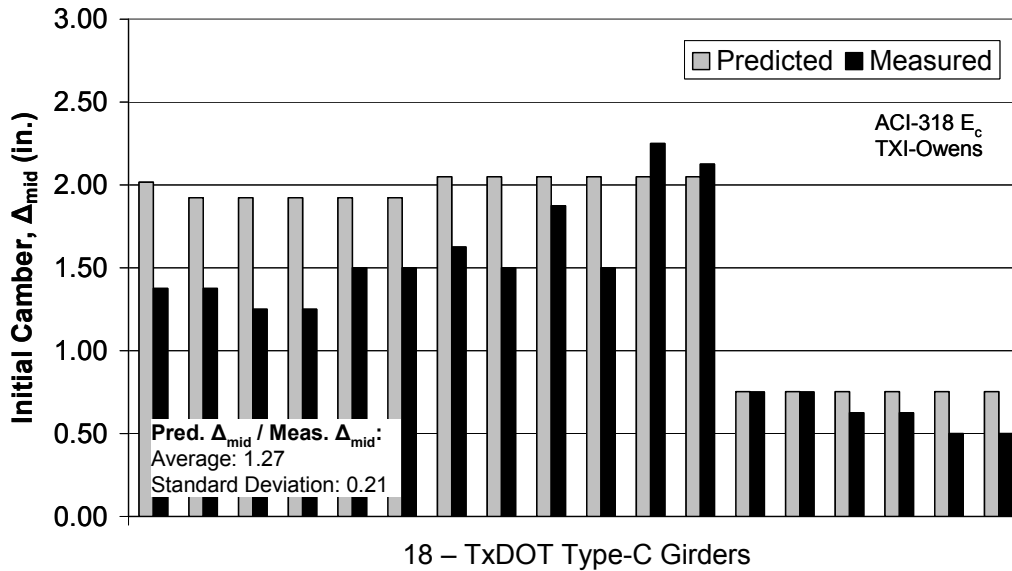
Figure 6-15: Measured and predicted (ACI-318 E_c) initial camber for Type-Cs with TXI-Owens aggregate
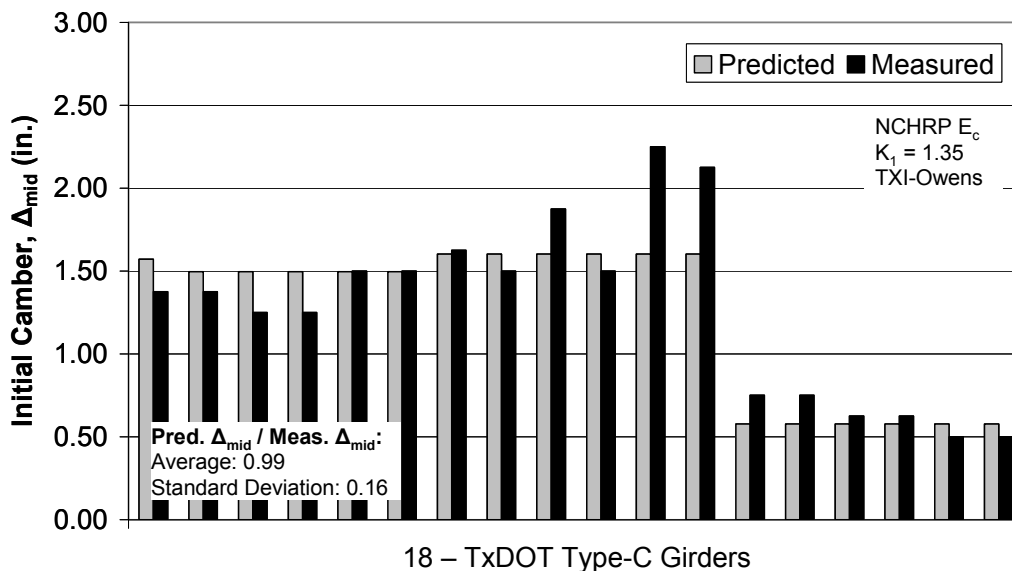
Figure 6-16: Measured and predicted (NCHRP E_c) initial camber for Type-Cs with TXI-Owens aggregate

145

In general, the initial camber data of the Type-IV and the Type-C girders with this round, river gravel supported the increase of the concrete modulus of elasticity with a K_1 factor of 1.35. In a few cases, the camber measurements deviated from the average condition. Due to the variability of the parameters that affect initial camber, this deviation was expected.

6.5.1.2 *Crushed Limestone from Hansen Ogden Quarry*

The concrete mixture designs of several AASHTO Type-IV and TxDOT Type-C girders in the initial camber database used a crushed limestone from the Hansen Ogden quarry as the coarse aggregate. As before, the measured initial camber was compared to the predicted initial camber for both beam types. For 42 Type-IV girders, this comparison is illustrated in Figure 6-17 where the ACI-318 modulus of elasticity equation was used in the camber estimates. For the estimates in which the NCHRP equation was used, the measured-to-predicted camber comparison is provided in Figure 6-18. In addition, the measured initial camber of 47 Type-C girders was compared to predicted camber in Figure 6-19 and 6-20. The ACI-318 modulus of elasticity equation was used in the camber estimates shown in Figure 6-19. The NCHRP modulus of elasticity equation was used in the camber estimates shown in Figure 6-20. A K_1 factor equal to 1.55 was selected for the girders with this crushed limestone from the analysis of these camber plots.
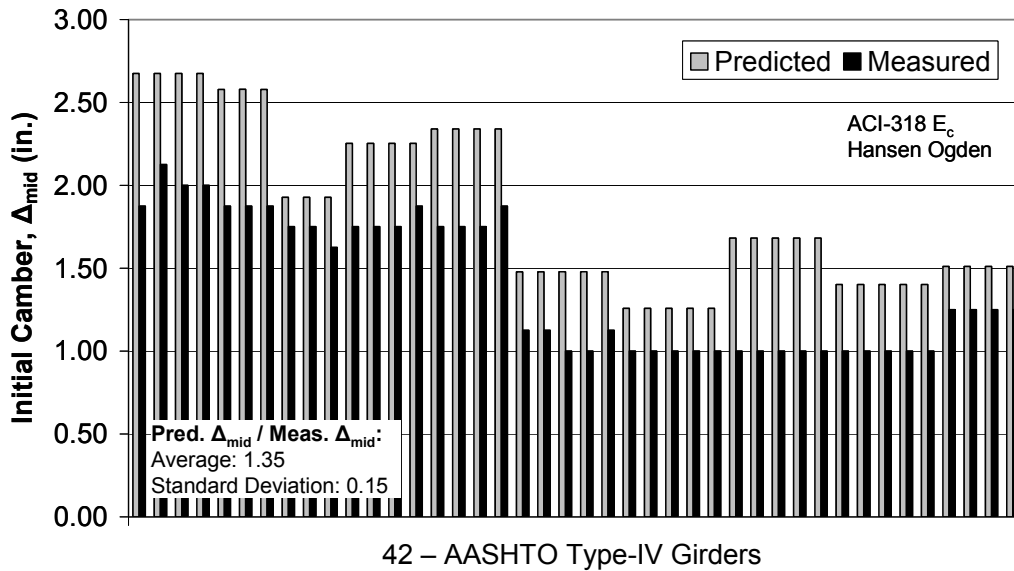
Figure 6-17: Measured and predicted (ACI-318 E_c) initial camber for Type-IVs with Hansen Ogden aggregate

146
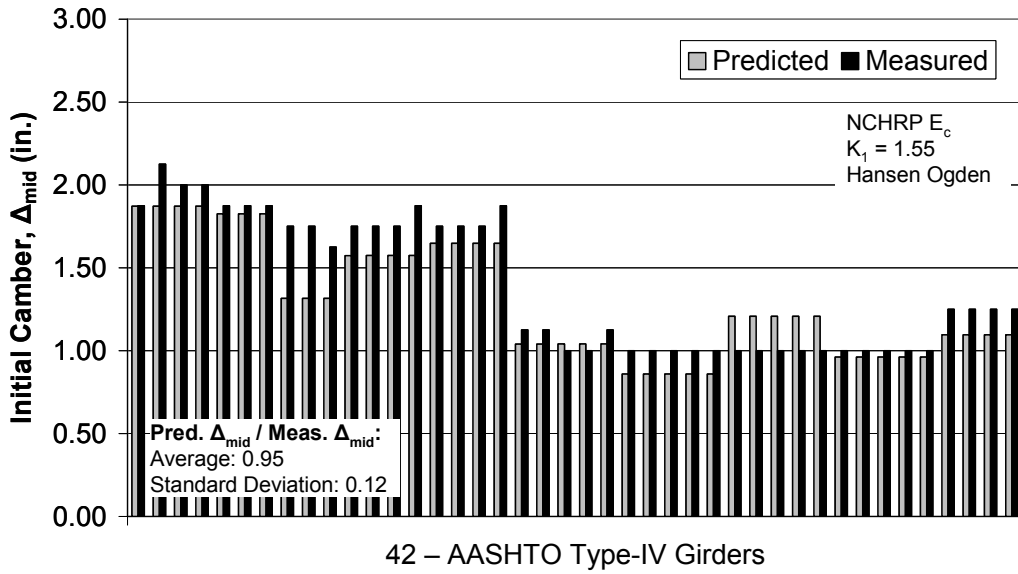
Figure 6-18: Measured and predicted (NCHRP E_c) initial camber for Type-IVs with Hansen Ogden aggregate
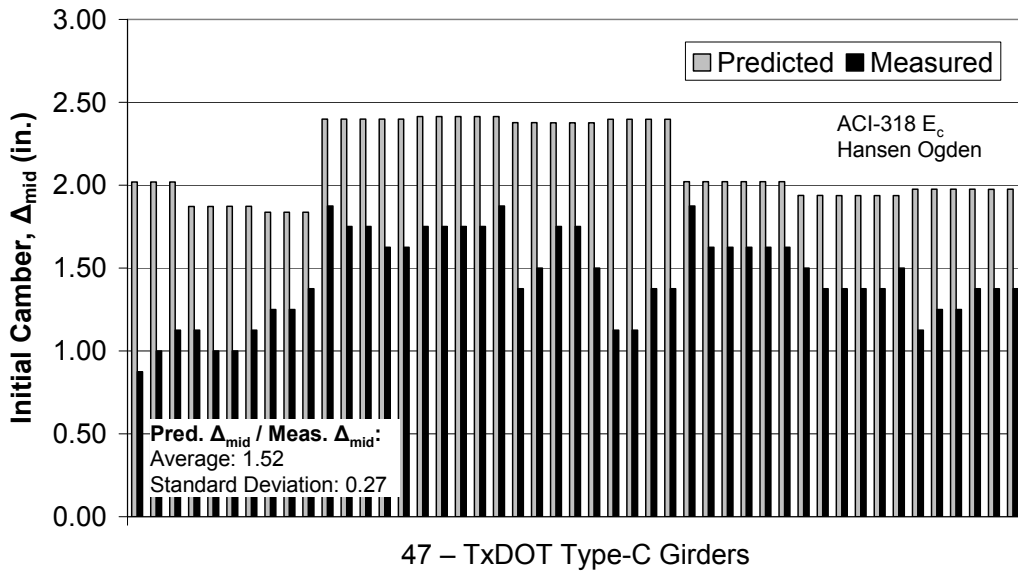
Figure 6-19: Measured and predicted (ACI-318 E_c) initial camber for Type-Cs with Hansen Ogden aggregate
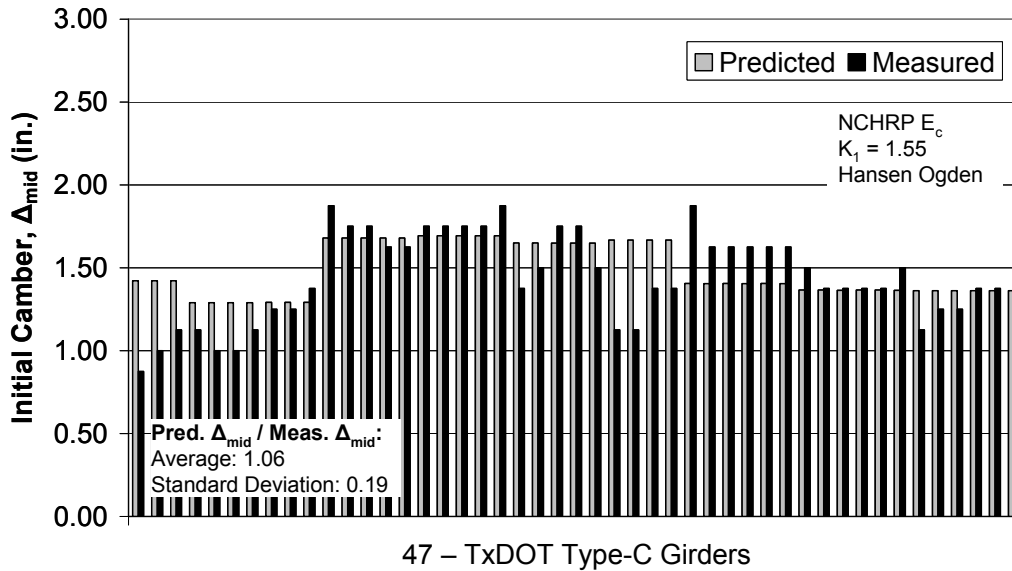
Figure 6-20: Measured and predicted (NCHRP E_c) initial camber for Type-Cs with Hansen Ogden aggregate

For the girders with the crushed limestone from the Hansen Ogden quarry as the coarse aggregate, the modulus of elasticity was increased by the K_1 factor. As such, the initial camber estimates were significantly improved. It is interesting to note that a higher K_1 factor was determined for a crushed limestone than for a round, river gravel. In a research study by Mokhtarzadeh and French (2000) (Section 2.3.3), the modulus of elasticity of concrete with crushed limestone was less than that with round, river gravel. Also, in Texas, crushed limestone and river gravel are commonly referred to as "soft rock" and "hard rock," respectively. However, the difference between the two K_1 factors determined from the camber data was only 15-percent (1.55/1.35). Considering the variability in aggregate properties across the state and in modulus of elasticity data in general, this distinction was justifiable.

6.5.1.3 *Crushed River Gravel from Yarrington Road*

In addition, a crushed, river gravel from the Yarrington Road pit was used as the coarse aggregate for 24 AASHTO Type-IV girders in the initial camber database. These beams were fabricated in July 2003. In Figure 6-21, the measured initial camber is presented with the corresponding estimated camber utilizing the ACI-318 modulus of elasticity expression. A K_1 factor was not developed for this coarse aggregate.
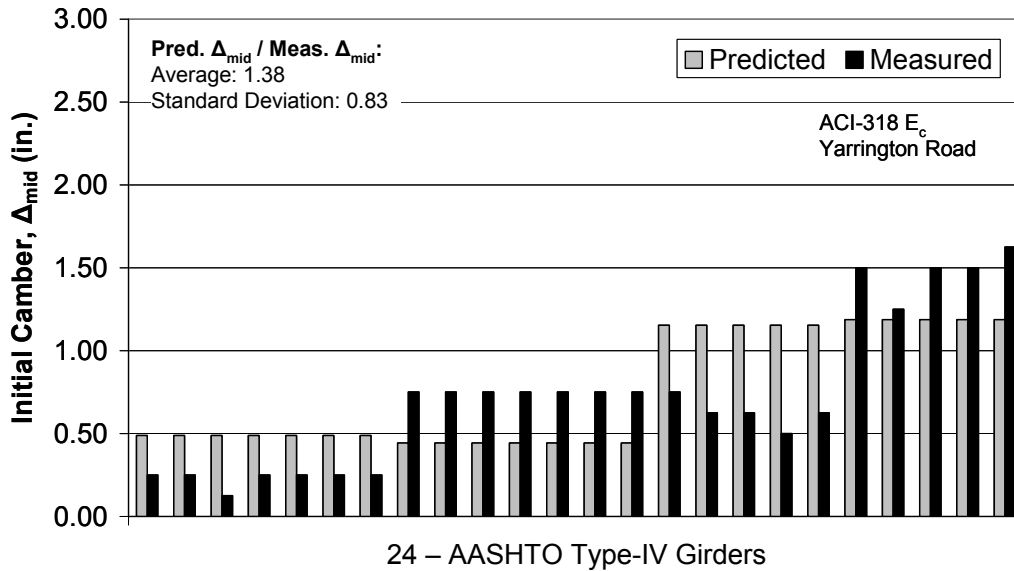
Figure 6-21: Measured and predicted (ACI-318 E_c) initial camber for Type-IVs with Yarrington Road aggregate

As seen in Figure 6-21, the camber was not consistently overestimated or underestimated when the ACI-318 modulus of elasticity equation was used. While only a relatively small sample size was available, this level of inconsistency was not present in any grouping of camber data from a single coarse aggregate in the initial camber database. In a personal conversation with Jason Tucker of the Texas Department of Transportation, a reason for the inconsistent camber of girders with the Yarrington Road aggregate was provided. In January 2003, magnesium sulfate and sodium sulfate soundness tests on the aggregate revealed abnormally high concentrations of both compounds. The concentrations exceeded those permitted by the TxDOT Standard Specifications and were significantly higher than in previous years (Tucker, 2006). The use of this coarse aggregate in bridge girders was suspended pending the results of future material testing.

6.5.1.4   *Round River Gravel from Fordyce Murphy pit*

A round, river gravel from the Fordyce Murphy pit was used in the concrete mixture designs of 20 AASHTO Type-IV girders included in the initial camber database. In Figure 6-22, the measured initial camber of these girders is compared to the predicted camber in which the ACI-318 modulus of elasticity expression was used. In Figure 6-23, the same measured camber is compared to the predicted camber in which the NCHRP modulus of elasticity expression was utilized. For this coarse aggregate, a K_1 factor of 1.65 was determined from the analysis of the data.

149
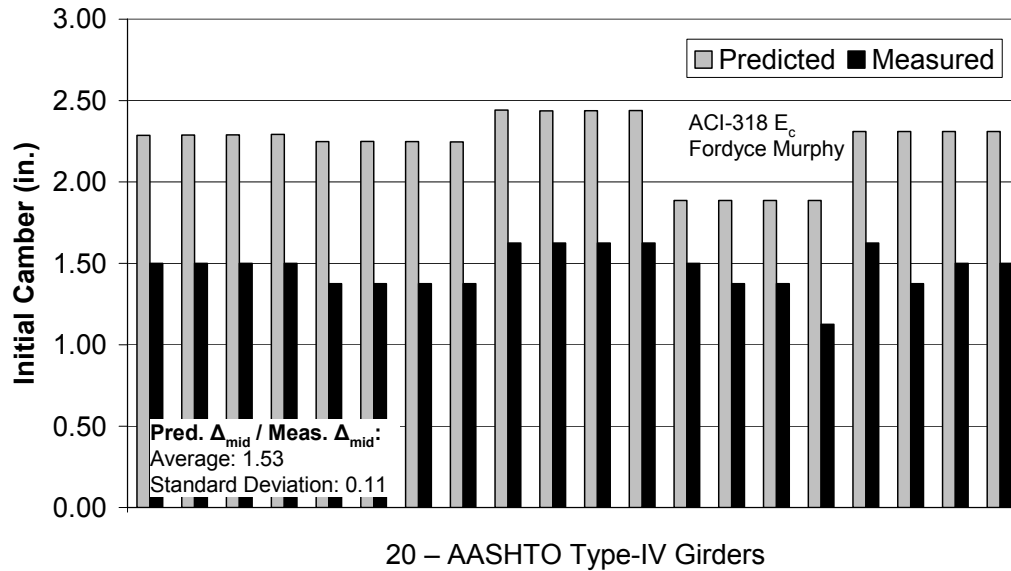
Figure 6-22: Measured and predicted (ACI-318 E_c) initial camber for Type-IVs with Fordyce Murphy aggregate
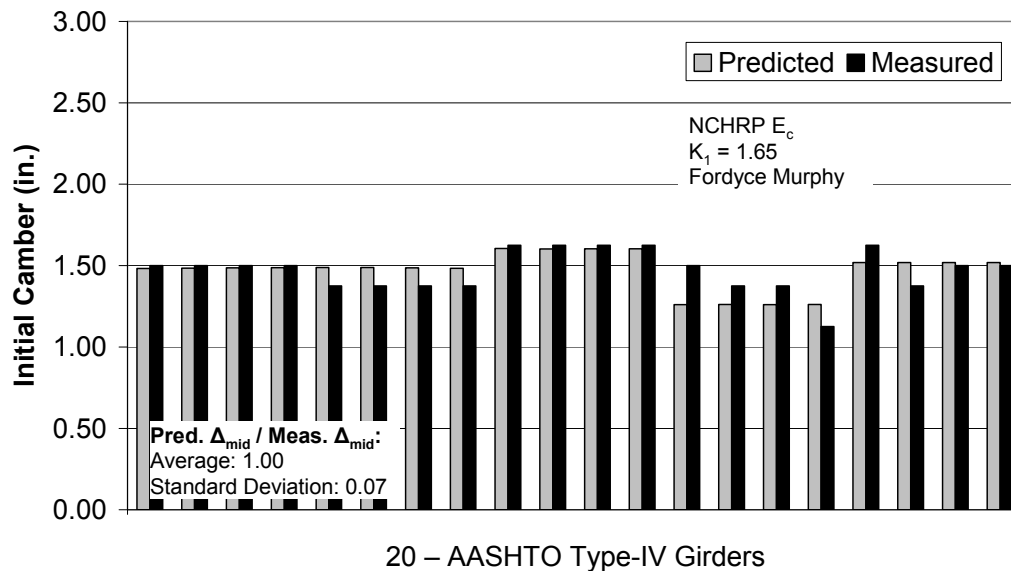
Figure 6-23: Measured and predicted (NCHRP E_c) initial camber for Type-IVs with Fordyce Murphy aggregate

After comparing Figure 6-22 to Figure 6-23, it is evident that the initial camber data supported a K_1 factor of 1.65. It should be emphasized that this K_1 factor was determined with data from only 20 Type-IV girders.

6.5.1.5 Analysis of the Results

From the visual inspection of the measured and predicted camber plots, several observations were made. The initial camber of the 197 conventional girders in the database was substantially overestimated using simple equations for camber and the ACI-318 modulus of elasticity expression. In fact, for girders with the Fordyce Murphy round, river gravel, the camber was overestimated by approximately 65-percent. Even though the scope of the current camber study was limited, it was evident from the beams in the database that the state of current camber prediction is inadequate.

In the current study, a simple solution utilizing the recommendations of the NCHRP Report 496 was presented. While a lot of variables affect the accuracy of initial camber estimates, some are more important than others. Improving the modulus of elasticity empirical expression was emphasized in this project. Based on the coarse aggregate in the concrete mixture design, the modulus of elasticity was altered by a K_1 factor. Each factor was calculated by comparing the measured initial camber to the predicted camber utilizing the NCHRP modulus of elasticity expression. By design, the measured initial camber was closely matched by the initial camber estimates through the use of the selected K_1 factors. To gauge the scatter of the camber estimates, the standard deviation of the ratio of the predicted camber to the measured camber was calculated. The standard deviation equation is presented as Equation 6-6. A summary of the K_1 factors developed with the data in this study and the standard deviation of the estimates using those factors are listed in Table 6-7.

$$\sigma_i = \sqrt{\frac{\sum_1^n \left(X_i - \overline{X}_i\right)^2}{n-1}}$$ (6-6)

where, i = corresponds to the NCHRP E_c or the ACI-318 E_c expression
n = sample size
$\overline{X}$ = mean of the X_i values in the sample

$X_i = \dfrac{\Delta_{predicted\_i}}{\Delta_{measured}}$

$\Delta_{measured}$ = measured camber (in.)
$\Delta_{predicted\_i}$ = predicted camber using NCHRP or ACI-318 E_c (in.)

Table 6-7: Results of camber data analysis

Aggregate Information			# of Beams		NCHRP E_c		ACI-318 E_c	
Supplier	Type	K_1	IV	C	Avg. X_n	σ_n	Avg. X_a	σ_a
TXI-Owens	Round, river gravel	1.35	46	18	1.02	0.17	1.31	0.22
Hansen-Ogden	Crushed limestone	1.55	42	47	1.01	0.17	1.44	0.23
Fordyce Murphy	Round, river gravel	1.65	20	0	1.00	0.07	1.53	0.11

As seen in Table 6-7, accurate initial camber estimates were obtained with the selection of the K_1 factors and the use of the NCHRP equation for the concrete modulus of elasticity. For

the girders with coarse aggregates from the TXI-Owens pit and the Hansen Ogden quarry, the standard deviation of the predicted to measured camber was 17-percent. This level of accuracy indicated the amount of variability consistent with initial camber. For the girders with the Fordyce Murphy coarse aggregate, the standard deviation was 7-percent. However, only 20-girders with this coarse aggregate are included in the database. It is likely that the standard deviation would increase with the inclusion of additional beams with the Fordyce Murphy round, river gravel. On the other hand, the predicted to measured initial camber was significantly greater than 1.0 when the conventional ACI-318 modulus of elasticity equation was used in the camber estimates. It is evident from the compiled data that local material variability must be included to accurately estimate initial camber. It should be noted that the average X_n values for the initial camber estimates in which the ACI-318 modulus equation was used did not match the recommended K_1 factors due to slight variations between the NCHRP and ACI-318 equations for the modulus of elasticity.

In the current study, the feasibility of using the K_1 factor in the NCHRP modulus of elasticity expression for a particular coarse aggregate was emphasized. Consistent estimates for initial camber were provided for two beam types, albeit similar, and a fairly wide range of lengths, compressive strengths at release, and ages at release. To date, the initial camber database is far from comprehensive even for the coarse aggregates that are represented. The developed K_1 factors were determined from the available data and should be confirmed with camber measurements of additional pretensioned beams. In addition, there are numerous other parameters that should be included in the database, particularly other coarse aggregates widely-used in Texas.

The coarse aggregates investigated within the current camber study contributed to concrete modulus of elasticity values ranging from 35 to 65-percent higher than the national average. While Texas is known for stiff aggregates, the investigation of other production facilities across the state will undoubtedly reveal a wider range of the modulus of elasticity of concrete. For instance, the growth of the modulus of elasticity of concrete at two precast plants was evaluated in a previous portion of the TxDOT Research Project 5197. One of the plants was the TCC Victoria facility discussed in this chapter. The other plant was Bexar Concrete Works in San Antonio, TX. The results of the modulus of elasticity tests on 4x8-inch concrete cylinders according to ASTM C469-02 are shown in Figure 6-24.

152
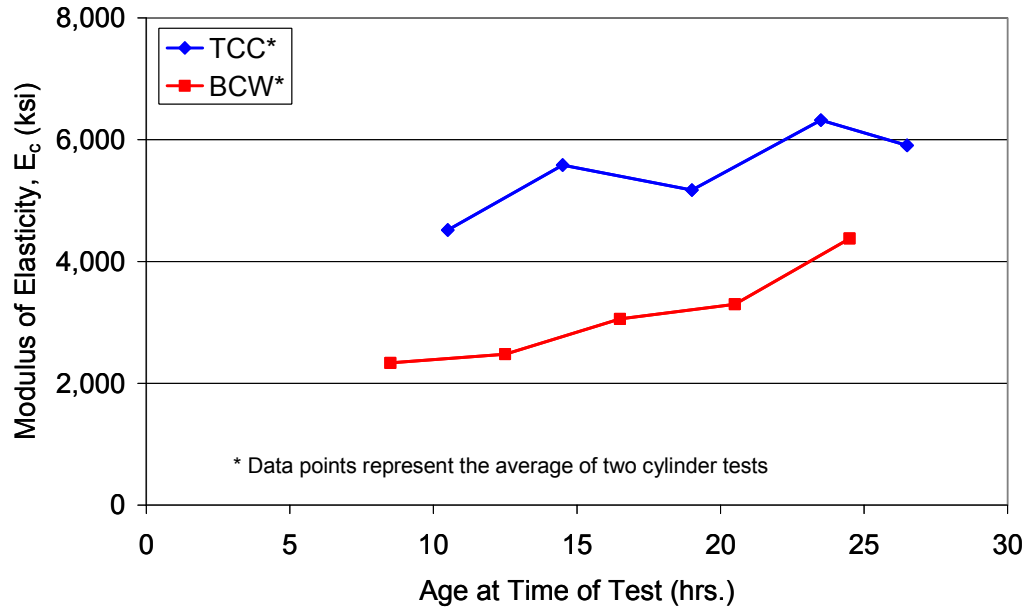
Figure 6-24: Modulus of elasticity test data from two precast plants

In Figure 6-24, the large difference in the elastic modulus of concrete at two Texas precast facilities was illustrated. At typical prestress release times, the elastic modulus of the two different mixes differed by up to a factor of 2. While the stiffness of these two concrete mixture designs represented extremes cases, they illustrated the variability of concrete mechanical properties in the state of Texas. Furthermore, these results supported the development of and the need for K_1 factors for typical coarse aggregates used in Texas.

6.5.2 Camber Data of Non-standard Girders

In this section, the initial camber data of the non-standard beams described in Section 6.2.2 was evaluated. The non-standard beams consisted of 12 TxDOT Type-A girders and 14 small-scale rectangular, tee, and inverted-tee specimens. For each beam type, the measured initial camber was compared to the predicted camber as with the conventional girders. The main objective of this section was to evaluate the influence of increasing the compressive stress at prestress transfer on the initial camber of the pretensioned member. As such, the camber data was plotted versus the maximum compressive stress subjected to each member at prestress release. In a previous research study by Castro et al. (2004), the initial and long-term camber of the 14 scaled specimens was monitored. In general, the camber growth of the overstressed beams was emphasized by Castro et al. (2004). Only the initial camber of these girders was evaluated herein.

6.5.2.1 TxDOT Type-A Girders

The initial camber of 12 TxDOT Type-A girders was measured at the HEI Corpus Christi precast pretensioned beam fabrication plant. The same coarse aggregate was used in all of the specimens, a round, river gravel from the Wrights Reralitos pit. In Figure 6-25, the measured initial camber is compared to the camber predicted utilizing the ACI-318 modulus of elasticity

153

expression. In Figure 6-26, the camber predicted utilizing the NCHRP modulus of elasticity expression was presented with the measured data. A K_1 factor equal to 1.1 was used in the NCHRP equation for this coarse aggregate.
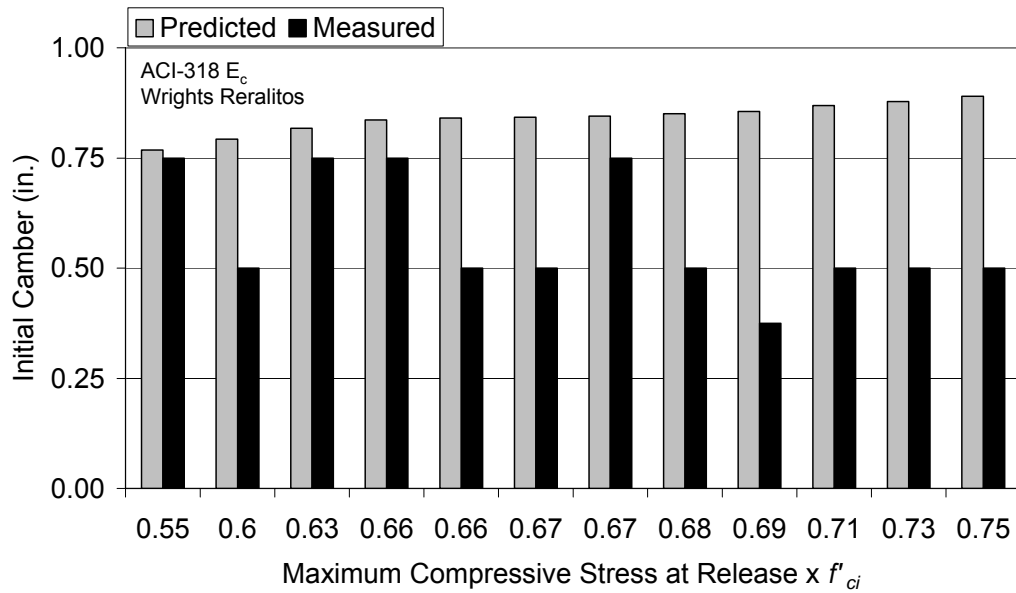
Figure 6-25: Measured and predicted (ACI-318 E_c) initial camber for Type-A girders
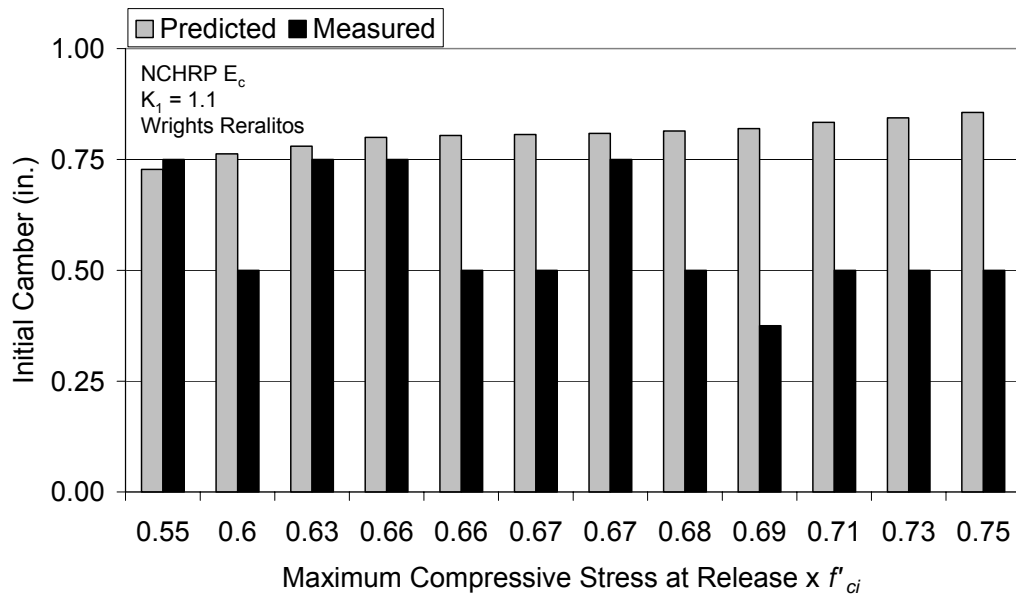
Figure 6-26: Measured and predicted (NCHRP E_c) initial camber for Type-A girders

In Figure 6-25 and 6-27, the variability of the measured initial camber was shown. This variability and the limited number of beams with the Wrights Reralitos aggregate prevented the development of a K_1 factor from the camber data. As discussed in Section 5.2.2.2, measured

modulus of elasticity data was used to determine the value of K_1 for this aggregate. While a factor of 1.1 agreed with four of the specimens, it did not agree with the other eight. This data set illustrated the difficult nature of initial camber prediction, particularly when sample sizes are small.

In regards to the compressive stress at release, the data did not support any trend. The ability to estimate the camber, or lack thereof, was independent of the compressive release stress. In addition, the measured camber did not increase with higher levels of compressive stress at release. It is important to note that the same prestressing force was applied to all twelve members; the compressive stress at release was increased by decreasing the strength at release. Therefore, the fact that the camber did not increase with increasing release stress suggested that the modulus of elasticity did not vary according to the empirical relationship with f'_{ci}.

6.5.2.2 Project 4086 Scaled Beams

Lastly, the measured initial camber of the scaled beams was compared to estimated values. As before, two different modulus of elasticity equations were used in the camber predictions. The camber estimates in which the ACI-318 E_c expression was used are presented with the measured initial camber in Figure 6-27. The same measured values are compared to those predicted with the help of the NCHRP E_c expression in Figure 6-28. Since three concrete mixture designs and two coarse aggregates were used in the fabrication of these girders, different K_1 factors were developed. For concrete mixture design 1 and concrete mixture design 3, K_1 equaled 1.0. For concrete mixture design 2, a K_1 of 0.8 was justified because the coarse aggregate was a crushed limestone.
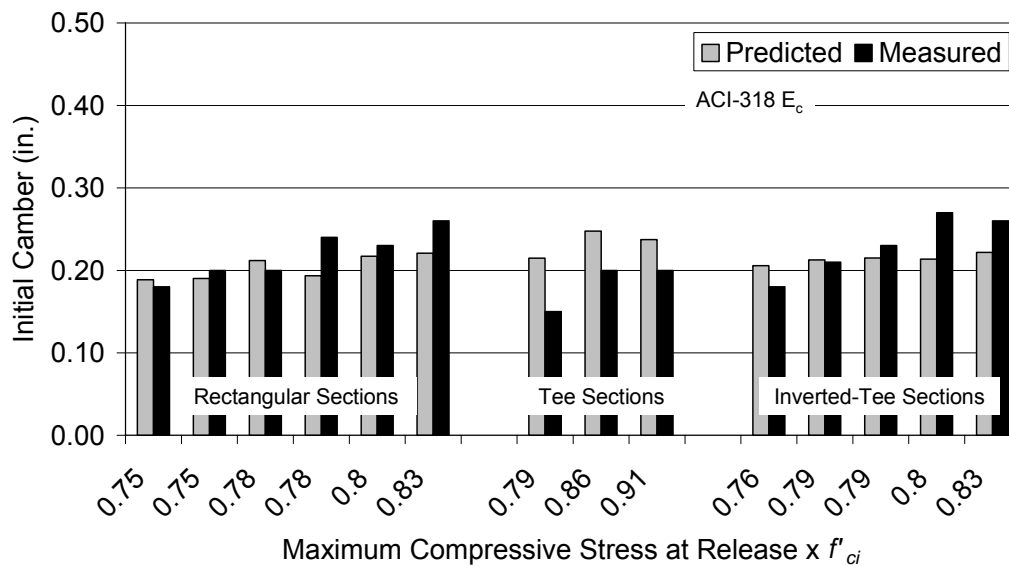
Figure 6-27: Measured and predicted (ACI-318 E_c) initial camber for scaled Project 4086 girders
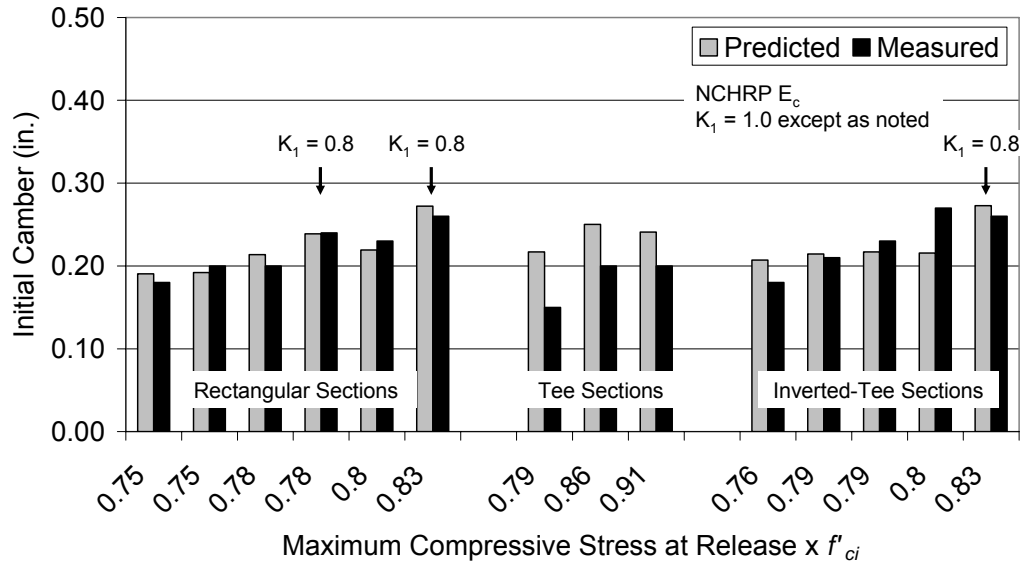
Figure 6-28: Measured and predicted (NCHRP E_c) initial camber for scaled Project 4086 girders

From the comparison of Figure 6-27 to Figure 6-28, the magnitude of each K_1 factor, particularly K_1 equal to 0.8 for mixture 2, was justified. Since a small number of beams were cast with each coarse aggregate, camber data was not sufficient to develop the factors. Rather, material data as presented in Section 5.2.2.2 was the basis of each K_1 factor. In addition, in Section 5.3.1.2, each factor was confirmed when measured elastic shortening losses compared favorably to those estimated with these K_1 factors taken into account. There was little merit in associating these K_1 factors to the coarse aggregate used in the mixture design due to the small sample size of the beams with each aggregate and since the concrete for these specimens was mixed in the laboratory.

In Figure 6-27 and 6-28, the measured initial camber of the rectangular and inverted-tee specimens was fairly well estimated. However, for the three tee-specimens, the initial camber was consistently underestimated. The reason for this inaccuracy is not clear due to the limited variables covered with the three specimens. Since mixture 1 and mixture 3 were represented with these specimens and no similar inconsistencies were detected with the other beam types that used the same mixture designs, the inaccuracy did not appear to be related to the concrete mixture design.

In regards to the impact of the compressive stress at transfer on the initial camber of the beams, a couple of observations can be made. In general, within each beam type, the measured initial camber increased with the increase in release stress. This finding is expected for cases in which additional prestressing force is added to a given section. Similarly, if the same prestressing force exists in two members but one was released sooner, the beam that is released early is expected to have a lower concrete modulus and therefore, a higher camber. However, as in the case of the Type-A beams, this latter scenario may not always be true. Another observation from Figure 6-27 and 6-28 was in regards to the accuracy of the initial camber estimate as the release stress increased. From the data available, a noticeable effect of increasing the stress at release on the accuracy of the camber estimates was not detected.

156

In short, the camber of the overstressed girders in the database was predicted with similar and acceptable variability as that of the conventional, full-scale girders.

6.6   SUMMARY

The results of the initial camber evaluation of 223 pretensioned girders are summarized in Figure 6-29 and 11-30. In Figure 6-29, the measured camber is compared to estimated camber in which the ACI 318 modulus of elasticity equation was used. In Figure 6-30, the measured camber is compared to estimated camber in which the NCHRP modulus of elasticity equation with the developed K_1 factors was used.
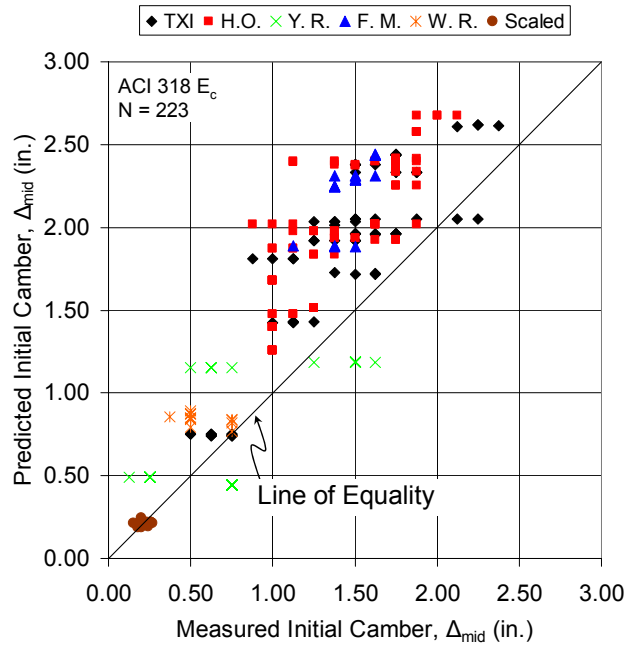
Figure 6-29: Accuracy of initial camber estimates using ACI E_c equation
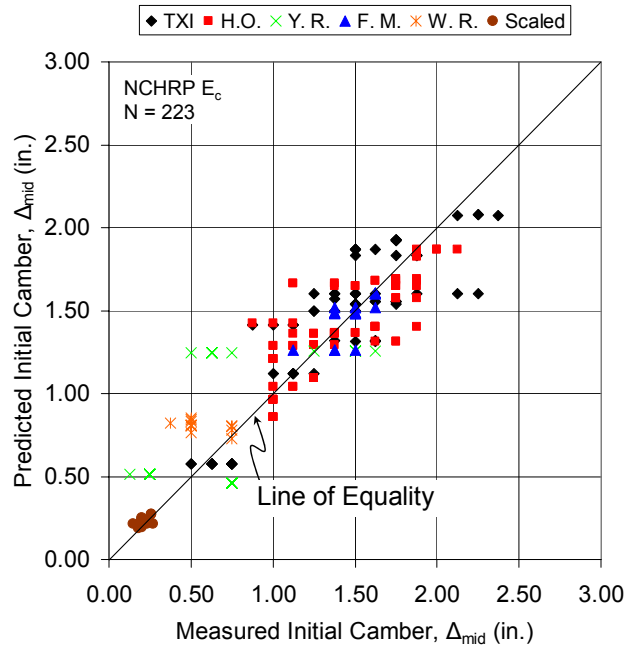
Figure 6-30: Accuracy of initial camber estimates using NCHRP E_c equation

From the comparison of the two plots, the benefit of accounting for local material variability in the form of the specific coarse aggregate was evident, particularly for the 197 conventional, full-scale pretensioned girders. For these specimens, the value of K_1 in the NCHRP modulus of elasticity equation was altered depending upon the coarse aggregate present in the beam. The K_1 factor was determined by comparing the initial camber to the predicted camber of all the beams cast with that particular coarse aggregate. With the use of the developed K_1 factors, the initial camber of the conventional beams was estimated within ±17-percent (Figure 6-30). It should be noted that these beams covered a range of compressive release strengths, ages at release, and lengths. Additional work should be performed to develop K_1 factors for other coarse aggregates and to test these factors with other section types prevalent in Texas.

In addition, the other objectives of the camber study were to evaluate the effect of increasing the release stress of a pretensioned beam on (i) the magnitude of the initial camber and (ii) the ability to accurately estimate it. For the 26 overstressed beams represented in Figure 6-29 and 6-30, the accuracy of the initial camber estimates was comparable to that of the conventional girders. As such, increasing the compressive stress at release did not affect the accuracy of the initial camber prediction. However, if the compressive stress at release is increased for a given section, a higher initial camber is to be expected in most cases.

158

CHAPTER 7
Summary, Conclusions, and Recommendations

7.1 SUMMARY OF THE RESEARCH PROGRAM

The portion of Project 0-5197 discussed in this report was conducted at the Ferguson Structural Engineering Laboratory at the University of Texas at Austin to investigate the structural feasibility of increasing the allowable compressive stress at release (currently $0.60f'_{ci}$) for prestressed concrete girders. For this purpose, (i) the live-load performance and (ii) the initial camber of pretensioned beams subjected to compressive stresses in excess of the current allowable compressive stress limit were evaluated.

In the live-load performance evaluation part of the current study, 36 static-load tests and 4 fatigue tests were conducted. In the static-load tests, the cracking loads of 36 pretensioned beams were experimentally evaluated. Twenty-four specimens were scaled rectangular, tee, and inverted-tee beams subjected to maximum compressive stresses at release ranging from $0.46f'_{ci}$ to $0.91f'_{ci}$. Twelve specimens were full-scale TxDOT Type-A girders subjected to maximum compressive stresses at release ranging from $0.55f'_{ci}$ to $0.75f'_{ci}$. For all of the beams, the measured cracking load was compared to three cracking loads predicted using typical design calculations ($P/A \pm Mc/I$) and three procedures for estimating prestress losses. These prestress loss calculation procedures included the PCI Design Handbook Loss of Prestress Estimate (PCI, 2004), the NCHRP Report 496 Detailed Prestress Loss Method (Tadros et al., 2003), and the AASHTO LRFD Refined Loss of Prestress Estimate (AASHTO, Interim 2005). One effect of increasing the allowable compressive stress at release of $0.60f'_{ci}$ on the live-load performance of a pretensioned girder was evaluated with the ability to conservatively estimate the cracking load of the member as the compressive stress at release increased. In the fatigue-load tests, the cyclic-load performance of four scaled beams was monitored to investigate potential fatigue concerns related to the increase of $0.60f'_{ci}$. Two of the specimens tested under fatigue loads were subjected to conventional stresses at release ($\sim0.50f'_{ci}$); two were subjected to elevated stresses at release ($\sim0.80f'_{ci}$). The results of the static-load and the fatigue-load tests were presented and analyzed in this report.

In the initial camber evaluation part of the current study, a database of initial camber information from 223 pretensioned beams was compiled. For all of the beams, the measured initial camber was compared to predicted initial camber. Twenty-six beams in the database were subjected to a range of compressive stresses at release exceeding the allowable limit. The impact of increasing $0.60f'_{ci}$ on the initial camber of a pretensioned girder was evaluated with the analysis of the camber data from these 26 beams. The remaining 197 beams were conventional, full-scale AASHTO Type-IV and TxDOT Type-C girders fabricated in the state of Texas. The current state of camber prediction, i.e. accuracy and scatter in estimating camber, for beams fabricated in Texas was evaluated with the analysis of the camber data from these 197 girders. In this context, recommendations for improving the accuracy of the initial camber prediction by accounting for the mechanical properties of the specific coarse aggregate were presented. Also, the accuracy of the initial camber estimates for the conventional beams provided the baseline for

which that of the overstressed beams were compared. The initial camber database and the analysis of the compiled data are provided in this report.

7.2   CONCLUSIONS AND RECOMMENDATIONS

The impact of increasing the allowable compressive stress at release of $0.60f'_{ci}$ on the live-load performance and the initial camber of pretensioned girders was evaluated in the current study. The conclusions and recommendations of the current study in regards to these two aspects of prestressed concrete beam behavior are discussed herein. Unless otherwise noted, the following conclusions are based on the research conducted within the experimental study:

7.2.1   Live-Load Performance Evaluation

1). Thirty-six static-load beam tests were conducted and analyzed in the current study. For the beams subjected to compressive stresses at release in excess of approximately $0.65f'_{ci}$, premature cracking in flexure was identified. Two potential explanations for this premature cracking are related to the nonlinear deformation of the highly-stressed member at prestress transfer. First, the nonlinear deformation as a result of microcracking, or internal damage, reduced the tensile capacity of the bottom-fiber concrete as shown in studies by Delibes Liniers (1987) and Gettu et al. (1996). Second, in regards to the cracking load estimate, the nonlinear deformation at prestress transfer is not conservatively estimated by the typical, linear-elastic calculations used in design (P/A ± Mc/I).

2). For the thirty-six pretensioned beams tested in the current study, increasing the allowable compressive stress at release to $0.65f'_{ci}$ is justified. In general, the test specimens subjected to compressive stresses up to approximately $0.65f'_{ci}$ performed comparably to those subjected to compressive stresses at release within the allowable limit ($< 0.60f'_{ci}$). It should be emphasized that the test specimens in the current study included twenty-four scaled beam types and one full-scale beam type fabricated at a single precast beam fabrication plant.

3). The fatigue tests of four scaled beams were performed to evaluate the performance of the bottom-fibers of the sections due to the repeated opening and closing of the flexural cracks. From the test results of these four specimens (two conventional and two highly-stressed), no appreciable difference in performance between the conventional and highly-stressed beams was detected.

4). From the findings of the live-load performance evaluation of TxDOT Project 5197, the status of the allowable compressive stress at release as a serviceability limit was confirmed. This limit ensures the satisfactory condition of the precompressed tensile zone of the prestressed concrete beam. It limits internal microcracking in the bottom fibers of the member and guarantees the application of typical design calculations used to estimate the cracking load.

7.2.2   Initial Camber Evaluation

1). If the compressive stress at release is increased for a given section, a higher initial camber is to be expected in most cases.

2). Increasing the compressive stress at release did not negatively affect the ability to estimate initial camber. The initial camber of pretensioned beams subjected to release stresses within and in excess of the allowable limit was predicted with similar accuracy.

3). To improve initial camber estimates of conventional, pretensioned beams, local material variability in the form of the specific coarse aggregate should be accounted for. In the current project, the equation for the modulus of elasticity of concrete recommended by the NCHRP Report 496 (Tadros et al., 2003) was utilized for this purpose. The modulus of elasticity was adjusted by a K_1 factor (local materials correction factor) present in the equation.

4). With the use of a K_1 factor determined for each coarse aggregate, the initial camber of the conventional, full-scale beams in the database was estimated within ±17-percent accuracy. For these beams, the compressive strengths at release ranged from 4,800- to 8,400-psi, the ages at release ranged from 11- to 71-hours, and the lengths ranged from 60- to 120-feet.

7.3 RECOMMENDATIONS FOR FUTURE WORK

1). In regards to the impact of the allowable compressive stress at release on the live-load performance of pretensioned beams, future testing should be performed. Additional section types and concrete mixture designs with different coarse aggregates prevalent in Texas that might be more critical than those considered in the current study should be investigated prior to the adoption of the $0.65f'_{ci}$ limit in design codes. In addition, the effects of potential adverse conditions at the ends of pretensioned members due to high levels of compressive stress at release and associated internal microcracking such as a reduction in shear capacity, transfer length, or development length should be addressed.

2). In regards to the initial camber study, future work should also be performed. The current investigation of the initial camber of conventional, full-scale girders can be considered as a feasibility study towards improving initial camber predictions. Additional beam types, coarse aggregates, and other variables of Texas pretensioned beams should be included into the initial camber database.

161

APPENDIX A

Additional Information for Scaled TxDOT Project 4086 Beams

Appendix A includes the following for the TxDOT Project 4086 scaled pretensioned beams:
- Shop Drawings
- Section / Material properties
- Stress Calculations at Prestress Release
- Prestress Losses / Cracking Load Calculations
    - PCI Handbook, NCHRP 496, and AASHTO LRFD 2005
- Components of Total Prestress Losses
    - Concrete Shrinkage and Steel Relaxation

Shop Drawings
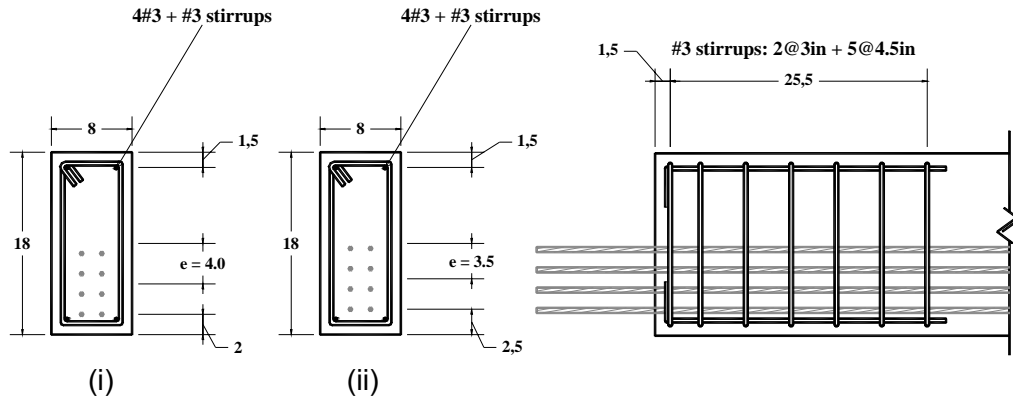
Figure A-1: Rectangular beams (Castro et al., 2004)

(i):   R3-78-3-T3, R3-83-4-T12, R3-80-5-T4
(ii):   R3-75-3-T9, R3-78-4-T11, R3-75-5-T10
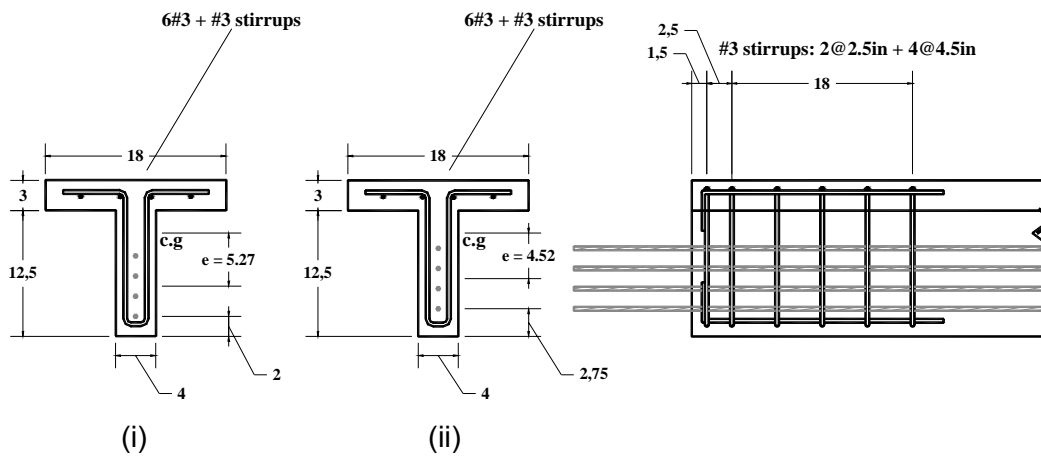
Figure A-2: Tee beams (Castro et al., 2004)

(i):   T2-79-3-T16, T2-91-5-T14
(ii):   T2-86-3-T15

164
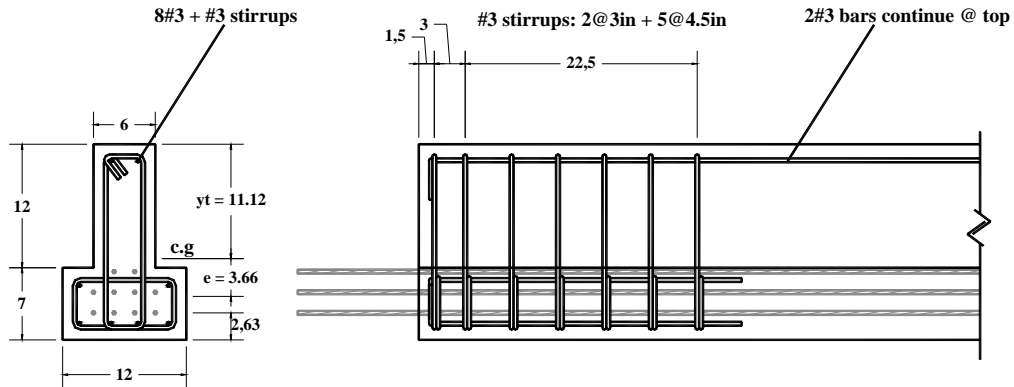
Figure A-3: Inverted tee beams with top nonprestressed reinforcement

(Castro et al., 2004)

IT3-79-3-T21, IT3-83-4-T24, and IT3-79-5-T23
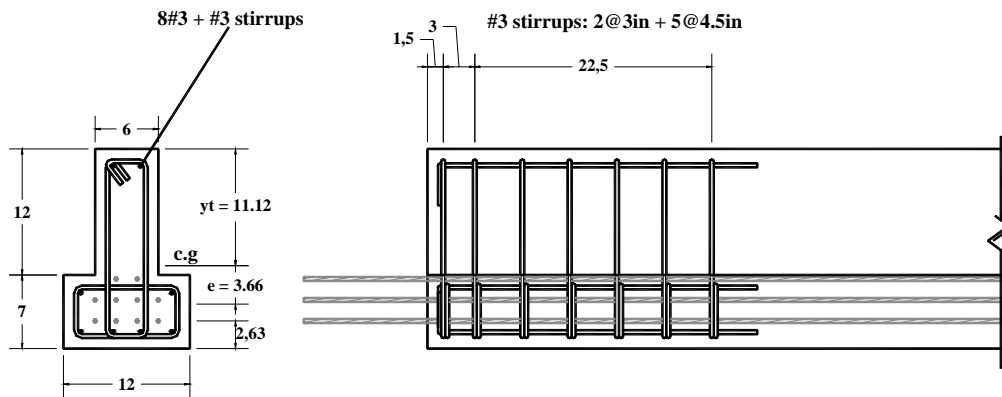
Figure A-4: Inverted tee beams without top nonprestressed reinforcement

(Castro et al., 2004)

IT2-76-3-T22 and IT2-80-5-T13

Section / Material Properties

Table A-1: Section and material properties for scaled Project 4086 beams

Mixture Design	Test Specimen Designation	Section Properties					Prestressed / Non-Prestressed Steel Properties						Concrete Properties		
		A_g (in.^{2})	I_g (in.^{4})	h (in.)	y_b (in.)	y_t (in.)	A_{ps} (in.^{2})	e (in.)	E_{ps} (ksi)	f_{pi} (ksi)	f_{po} (ksi)	A_s (in.^{2})	f'_{ci} (psi)	f'_c (psi)	w_c (pcf)
1	R1-52-1-T8	108	2916	18	9	9	0.92	3.25	29000	181	168	0	5735	9660	150
	R1-52-1-T7	108	2916	18	9	9	0.92	3.25	29000	182	169	0	5735	9660	150
	R1-50-1-T1	108	2916	18	9	9	0.92	3.25	29000	181	168	0	6025	9660	150
	R1-49-1-T2	108	2916	18	9	9	0.92	3.25	29000	178	166	0	6025	9660	150
	R1-46-1-T5	108	2916	18	9	9	0.92	3.25	29000	177	164	0	6275	9660	150
	R1-48-1-T6	108	2916	18	9	9	0.92	3.25	29000	180	168	0	6275	9660	150
	T1-68-2-T17	106	2280	15.5	10.3	5.17	0.46	5.53	29000	191	180	0	4220	10015	150
	T1-62-2-T18	113	2470	15.5	10.1	5.36	0.46	6.09	29000	185	168	0	4220	10015	150
	IT1-68-2-T20	153	4350	18.3	7.69	10.56	1.22	3.19	29000	191	174	0	3815	10015	150
	IT1-73-2-T19	152	4320	18.3	7.57	10.68	1.22	3.82	29000	192	171	0	3815	10015	150
	R3-75-3-T9	144	3888	18	9	9	1.22	3.5	29000	181	165	0	4065	10050	154
	R3-78-3-T3	144	3888	18	9	9	1.22	4	29000	178	159	0	4065	10050	154
	T2-79-3-T16	104	2251	15.5	10.27	5.23	0.61	4.52	29000	182	168	0	3950	10050	154
	T2-86-3-T15	104	2251	15.5	10.27	5.23	0.61	5.27	29000	181	165	0	3950	10050	154
	IT3-79-3-T21	156	4706	19	7.88	11.12	1.53	3.66	29000	189	168	0.22	4065	10050	154
	IT2-76-3-T22	156	4706	19	7.88	11.12	1.53	3.66	29000	188	170	0	4320	10050	154
2	R3-78-4-T11	144	3888	18	9	9	1.22	3.5	29000	180	161	0	3800	10000	155
	R3-83-4-T12	144	3888	18	9	9	1.22	4	29000	180	159	0	3800	10000	155
	IT3-83-4-T24	156	4706	19	7.88	11.12	1.53	3.66	29000	191	164	0.22	3800	10000	155
3	R3-75-5-T10	144	3888	18	9	9	1.22	3.48	29000	182	165	0	4045	7390	150
	R3-80-5-T4	144	3888	18	9	9	1.22	3.97	29000	182	164	0	4045	7390	150
	T2-91-5-T14	104	2251	15.5	10.27	5.23	0.61	4.6	29000	186	168	0	3465	7390	150
	IT3-79-5-T23	156	4706	19	7.88	11.12	1.53	3.69	29000	189	167	0.22	4045	7390	150
	IT2-80-5-T13	156	4706	19	7.88	11.12	1.53	3.67	29000	189	167	0	4045	7390	150

Stress Calculations at Prestress Release

Material Properties		
Concrete	f'_{ci} (psi)	4045
	E_{ci} (ksi)[1]	N/A
Steel	E_{ps} (ksi)	29000
	f_{pi} (ksi)[1]	N/A
	f_{po} (ksi)[2]	165
	A_{ps_1} (in^2/N)	0.153
	N_{total}	8

Section Properties	
A_g (in^2)	144
I_g (in^4)	3888
y_b (in)	9
y_t (in)	9
e_{cl} (in)	3.48
e_{end} (in)	3.48
w_u (k/ft)	0.15
L (ft)	15

Name	R3-75-5-T10
Set	5
Test	10

STRESS CALCULATIONS AT RELEASE								
Section	x (ft)	x/L	P_o/A (ksi)	e (in)	$P_o e y_b/I$ (ksi)	$P_o e y_t/I$ (ksi)	M_g (in-k)	$M_g y_b/I$ (ksi)	$M_g y_t/I$ (ksi)
ends	0.0	0.00	1.40	3.48	1.62	1.62	0.00	0.00	0.00
transfer	2.1	0.14	1.40	3.48	1.62	1.62	24.22	0.06	0.06
critical	5.1	0.34	1.40	3.48	1.62	1.62	45.37	0.11	0.11
midspan	7.5	0.50	1.40	3.48	1.62	1.62	50.63	0.12	0.12

SUMMARY				
Section	Bottom Stress		Top Stress	
	(ksi)	% of f'_{ci}	(ksi)	*$\sqrt{f'_{ci}}$
ends	-3.03	-74.8	0.22	3.5
transfer	-2.97	-73.4	0.17	2.6
critical	-2.92	-72.2	0.12	1.9
midspan	-2.91	-71.9	0.11	1.7

$$f_{bot} = \frac{P_o}{A} + \frac{P_o e y_b}{I} - \frac{M_g y_b}{I}$$

$$f_{top} = \frac{P_o}{A} - \frac{P_o e y_t}{I} + \frac{M_g y_t}{I}$$

[1]E_c & f_{pi} were not needed because p/s force after transfer was known

[2]Inferred from strains measured with gauges afixed to prestressing strands

Figure A-5: Sample stress calculations at prestress transfer for scaled beam   R3-75-5-T10

Table A-2: Summary of compressive stresses at release at various sections for the scaled beams

Mix Type	Cast Date	Test Specimen Designation	Compressive Stress at Release (x f'_{ci})		
			At Ends[1]	At Location of Transfer[2]	At Critical Section[3]
Mix # 1	6/26/2002	R1-52-1-T8	0.52	0.51	0.50
		R1-52-1-T7	0.52	0.51	0.50
		R1-50-1-T1	0.5	0.48	0.48
		R1-49-1-T2	0.49	0.48	0.47
		R1-46-1-T5	0.46	0.45	0.45
		R1-48-1-T6	0.48	0.47	0.46
	8/13/2002	T1-68-2-T17	0.68	0.65	0.64
		T1-62-2-T18	0.62	0.60	0.58
		IT1-68-2-T20	0.68	0.67	0.66
		IT1-73-2-T19	0.73	0.72	0.71
	9/24/2002	R3-75-3-T9	0.75	0.73	0.72
		R3-78-3-T3	0.78	0.76	0.75
		T2-79-3-T16	0.79	0.77	0.75
		T2-86-3-T15	0.86	0.84	0.82
		IT3-79-3-T21	0.79	0.78	0.77
		IT2-76-3-T22	0.76	0.74	0.74
Mix # 2	12/5/2002	R3-78-4-T11	0.78	0.76	0.75
		R3-83-4-T12	0.83	0.81	0.80
		IT3-83-4-T24	0.83	0.82	0.81
Mix # 3	3/4/2003	R3-75-5-T10	0.75	0.73	0.72
		R3-80-5-T4	0.8	0.79	0.77
		T2-91-5-T14	0.91	0.89	0.87
		IT3-79-5-T23	0.79	0.79	0.78
		IT2-80-5-T13	0.8	0.78	0.77

[1]Calculated stress used in the test specimen designation

[2]Calculated stress 25-inches from end of the member

[3]Calculated stress used in live-load analysis of scaled beams (plotted on x-axis)

Loss of Prestress / Cracking Load Calculations

PCI - Prestress Losses / Cracking Load Calculations

SET	5	BEAM	1		TEST	10

NAME R3-75-5-T10

Material Properties		
Concrete	f'_{ci} (psi)	4045
	E_{ci} (ksi)	3856
	f'_c (psi)	7390
	E_c (ksi)	5212
	w_c (pcf)	150
	M_g (in-k)	47.3
Steel	E_{ps} (ksi)	29000
	A_{ps} (in^2)	1.224
	f_{pi} (ksi)	182

Section Properties	
A_g (in^2)	144
I_g (in^4)	3888
e_p (in)	3.48
c_b (in)	9
L (ft)	14.5

TL = ES + CR + SH + RE

Elastic Shortening Losses

ES = $K_{es}*(E_{ps}/E_{ci})*f_{cir}$

$$f_{cir} := K_{cir} \cdot \left(\frac{P_i}{A_g} + \frac{P_i \cdot e^2}{I_g} \right) - \frac{M_g \cdot e}{I_g}$$

K_{es}	1
K_{cir}	0.9
f_{cir} (ksi)	1.97
ES (ksi)	**14.85**

Creep Losses

CR = $K_{cr}*(E_{ps}/E_c)*(f_{cir}-f_{cds})$

$$f_{cds} := \frac{M_{sd} \cdot e}{I_g}$$

M_{sd} = zero b/c no additional sustained load

K_{cr}	2
f_{cds} (ksi)	0
CR (ksi)	**21.97**

Shrinkage Losses

SH = (8.2 x 10-6)*$K_{sh}*E_{ps}*(1-0.06*(V/S))*(100-R.H.)$

$$\frac{\text{Volume}}{\text{Surface Area}} \qquad \frac{(8 \cdot 18 \cdot 15 \cdot 12)}{(52 \cdot 15 \cdot 12) + (18 \cdot 8 \cdot 2)} = 2.687$$

K_{sh}	1
R.H.	70
V/S	2.687
SH (ksi)	**5.98**

Relaxation Losses

RE = [$K_{re}-J*(SH+CR+ES)]*C$

Table 4.7.3.1

PCI Handbook Table 4.7.3.2

K_{re} (ksi)	5
J	0.04
C	0.63
RE (ksi)	**2.07**

Total Losses

TL = ES + CR + SH + RE	TL (ksi)	44.88

Figure A-6: Prestress losses / cracking load calculations according to PCI procedure for R3-75-5-T10, page 1 of 2

SECTIONAL ANALYSIS AT CRACKING LOAD

| $\dfrac{P_{eff}}{A_g}$ | $\dfrac{P_{eff} \cdot e_p \cdot c_b}{I_g}$ | $\dfrac{M_g \cdot c_b}{I_g}$ | $\dfrac{M_{cr} \cdot c_b}{I_g}$ | f_r |
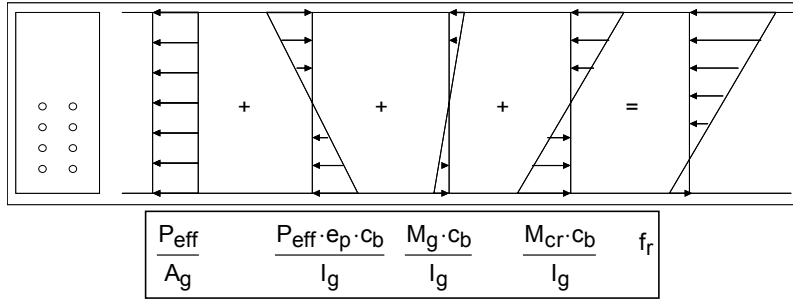
Effective Prestressing Force		
$f_{p\_eff} = f_{pi} - TL$	f_{pi} (ksi)	182
$P_{eff} = f_{p\_eff} * A_{ps}$	TL	44.88
	f_{p_eff}	137.12
	P_{eff}	**167.8**

Predicted Cracking Moment		
$f_r := 7.5 \cdot \sqrt{f'_c}$	f_r (ksi)	0.645
$M_{cr} := \left(\dfrac{I_g}{c_b}\right) \cdot \left(\dfrac{P_{eff}}{A_g} + \dfrac{P_{eff} \cdot e_p \cdot c_b}{I_g} - \dfrac{M_g \cdot c_b}{I_g} + f_r\right)$	M_{cr} (in-k)	**1319**

Predicted Cracking Load		
Loaded at third points: $P_{cr} = M_{cr} * (6/L)$	P_{cr} (kips)	**45.5**

Figure A-7: Prestress losses / cracking load calculations according to PCI procedure for R3-75-5-T10, page 2 of 2

NCHRP Report 496 - Prestress Losses / Cracking Load Calculations

SET	**5**	BEAM	**1**	TEST	**10**

DATE of CAST	3/4/2003	t_i (days)	1
DATE of RELEASE	3/5/2003	t_t (days)	881
DATE of STATIC TEST	8/2/2005		

INPUT

NAME **R3-75-5-T10**

INFO	SECTION PROPERTIES					
	Term	At Release			At Static Test	
Section Type: R3		Gross	Net	Trans.	Gross	Trans.
	A (in^2)	144	142.8	152.6	144	149.8
	y_b (in)	9	9.03	8.80	9	8.87
	I (in^4)	3888	3873	3986	3888	3955
	A_s (in^2)	0	0	0	0	0
	A_{ps} (in^2)	1.224	0	0	1.224	0
	e (in)	3.48	3.51	3.28	3.48	3.35
	y_p (in)	5.52	5.52	5.52	5.52	5.52
	E_c (ksi)	3628	3628	3628	5076	5076
	E_{ps} (ksi)	29000	29000	29000	29000	29000
	n	7.99	7.99	7.99	5.71	5.71

INFO	MATERIAL PROPERTIES			
	CONCRETE		STEEL	
	f'_{ci} (ksi)	4.045	f_{pi} (ksi)	182
	f'_{c_28} (ksi)	7.39	A_{ps} (in^2)	1.224
	f_{r_28} (ksi)	0.645	f_{py} (ksi)	243
$E_c := 33000 \cdot K_1 \cdot K_2 \cdot \left(0.140 + \dfrac{f'_c}{1000}\right)^{1.5} \sqrt{f'_c}$	E_{ci} (ksi)	3628	f_{pu} (ksi)	270
	K_1	1.0		
	K_2	1		
	E_{c_28} (ksi)	5076	ADDITIONAL	
	w (pcf)	150	L (ft)	14.5
	M_g (in-k)	47.3	H (%)	70
			V (in^3)	25920
			S (in^2)	9648
			V/S (in)	2.69

LOSS CALCULATIONS

ELASTIC SHORTENING		
Equations	Stress Loss - ES	
	Item	Quantity
$f_{cgp} := P_i \cdot \left(\dfrac{1}{A_{ti}} + \dfrac{e_{pti}^2}{I_{ti}}\right) - \dfrac{M_g \cdot e_{pti}}{I_{ti}}$	f_{cgp} (ksi)	2.02
$\Delta f_{pES} := n_i \cdot f_{cgp}$	Δf_{pES} (ksi)	16.18

PRESTRESSING FORCE		
INITIAL	f_{pi} (ksi)	182
AFTER ES	f_{po} (ksi)	165.8

Figure A-8: Prestress losses / cracking load calculations according to NCHRP procedure for R3-75-5-T10, page 1 of 3

SHRINKAGE

Equations	Shrinkage strain		Equations	Stress Loss - Shrinkage	
	Item	Quantity		Item	Quantity

Equations (left):

$$\varepsilon_{sh} := 0.00048 \cdot \gamma_{sh} \cdot K_1 \cdot K_2$$

$$\gamma_{sh} := k_{td} \cdot k_s \cdot k_{hs} \cdot k_f$$

$$k_{td} := \frac{t}{61 - 4 \cdot f_{ci} + t}$$

$$k_s := \frac{1064 - 94 \cdot \frac{V}{S}}{735}$$

$$k_{hs} := 2.00 - 0.0142 \cdot H$$

$$k_f := \frac{5}{1 + f_{ci}}$$

Shrinkage strain:

Item	Quantity
ε_{sh}	0.000499
K_1	1
K_2	1

Factors

Item	Quantity
γ_{sh}	1.04
k_{td}	0.95
k_s	1.10
k_{hs}	1.00
k_f	0.99

Equations (right):

$$K_{it} := \frac{1}{1 + n_i \cdot \rho_n \cdot \alpha_n \cdot (1 + \chi \cdot \psi_{ult})}$$

$$n_i := \frac{E_{ps}}{E_{ci}}$$

$$\rho_n := \frac{A_{ps}}{A_n}$$

$$\alpha_n := \left(1 + \frac{e_p^2 \cdot A_n}{I_n}\right)$$

$$\Delta f_{pSR} := \varepsilon_{sh} \cdot E_p \cdot K_{it}$$

Stress Loss - Shrinkage:

Item	Quantity
K_{it}	0.80
n_i	7.99
ρ_n	0.0086
α_n	1.45
X	0.7
Δf_{pSR} (ksi)	11.6

CREEP

Equations (left):

$$\psi(t, t_i) := 1.90 \cdot \gamma_{cr} \cdot K_1 \cdot K_2$$

$$\gamma_{cr} := k_{td} \cdot k_{la} \cdot k_s \cdot k_{hc} \cdot k_f$$

$$k_{td} := \frac{t}{61 - 4 \cdot f_{ci} + t}$$

$$k_{la} := t_i^{-0.118}$$

$$k_s := \frac{1064 - 94 \cdot \frac{V}{S}}{735}$$

$$k_{hc} := 1.56 - 0.008 \cdot H$$

$$k_f := \frac{5}{1 + f_{ci}}$$

Creep strain:

Item	Quantity
ψ_t	1.98
ψ_{ult}	2.08
K_1	1
K_2	1

Equations (mid):

$$\Delta f_{pCR} := n_i \cdot f_{cgp} \cdot \psi_t \cdot K_{it}$$

Stress Loss - Creep:

Item	Quantity
Δf_{pCR} (ksi)	25.7

Factors at test, t		Factors at ultimate	
Item	Quantity	Item	Quantity
γ_{cr}	1.04	γ_{cr}	1.09
k_{td}	0.95	k_{td}	1.00
k_{la}	1.00	k_{la}	1.00
k_s	1.10	k_s	1.10
k_{hc}	1.00	k_{hc}	1.00
k_f	0.99	k_f	0.99

RELAXATION

Equations:

$$\phi_i := 1 - \frac{3 \cdot (\Delta f_{pSR} + \Delta f_{pCR})}{f_{po}}$$

$$L_i := \frac{f_{po}}{45} \cdot \left(\frac{f_{po}}{f_{py}} - 0.55\right) \cdot \log\left(\frac{24 t + 1}{24 \cdot t_i + 1}\right)$$

$$\Delta f_{pR} := \phi_i \cdot L_i \cdot K_{it}$$

Stress Loss - Relax:

Item	Quantity
φ_i	0.32
L_i	1.43
Δf_{pR} (ksi)	0.37

TOTAL LOSSES

ES	Δf_{pES} (ksi)	16.2
Shrinkage	Δf_{pSR} (ksi)	11.6
Creep	Δf_{pCR} (ksi)	25.7
Relaxation	Δf_{pR} (ksi)	0.4
TOTAL	Δf_{pT} (ksi)	53.9
TOTAL-ES	$\Delta f_{pT\text{-}ES}$ (ksi)	37.7

Figure A-9: Prestress losses / cracking load calculations according to NCHRP procedure for R3-75-5-T10, page 2 of 3

CRACKING LOAD

CRACKING LOAD PREDICTION			
Equations	Bottom Fiber Stress		Notes
	Item	Quantity	
After Transfer	f_{cbi} (ksi)	2.97	Accounts for ES automatically
$f_{cbi} := \dfrac{P_i}{A_{ti}} + \dfrac{P_i \cdot e_{pti} \cdot y_{bti}}{I_{ti}} - \dfrac{M_g \cdot y_{bti}}{I_{ti}}$			
Long term losses, no ES	Δf_{cb} (ksi)	-0.70	
	f_{cbt} (ksi)	2.27	Bottom fiber stress after losses before load application
Predicted Cracking Load	Cracking Prediction		
	Item	Quantity	
$M_{cr} := \dfrac{I_{tt}}{y_{btt}} \cdot \left(f_{cbt} + f_{r\_28} \right)$	M_{cr} (in-kip)	1301	
$P_{cr} := \left(\dfrac{M_{cr}}{12} \right) \left(\dfrac{6}{L} \right)$	P_{cr} (kip)	44.9	Loaded at third points

Figure A-10: Prestress losses / cracking load calculations according to NCHRP procedure for R3-75-5-T10, page 3 of 3

AASHTO LRFD Interim 2005 - Prestress Losses / Cracking Load Calculations

SET	5	BEAM	1	TEST	10

DATE of CAST	3/4/2003	t_i (days)	1
DATE of RELEASE	3/5/2003	t_t (days)	881
DATE of STATIC TEST	8/2/2005		

INPUT

NAME: R3-75-5-T10

INFO	SECTION PROPERTIES					
Section Type: R3	Term	At Release			At Static Test	
		Gross	Net	Transformed	Gross	Transformed
	A (in^2)	144			144	
	y_b (in)	9			9	
	I (in^4)	3888			3888	
	A_s (in^2)	0			0	
	A_{ps} (in^2)	1.224			1.224	
	e (in)	3.48			3.48	
	y_p (in)	5.52			5.52	
	E_c (ksi)	3856			5212	
	E_{ps} (ksi)	29000			29000	
	n	7.52			5.56	

INFO	MATERIAL PROPERTIES			
	CONCRETE		STEEL	
	f'_{ci} (ksi)	4.045	f_{pi} (ksi)	182
$f_r := 7.5 \sqrt{f'_{c\_28}}$ f'c in psi	f'_{c_28} (ksi)	7.39	A_{ps} (in^2)	1.224
	f_{r_28} (ksi)	0.645	f_{py} (ksi)	243
	E_{ci} (ksi)	3856	f_{pu} (ksi)	270
$E_c := 33000 \cdot K_1 \cdot w_c^{1.5} \cdot \sqrt{f'_c}$	K_1	1.0		
			ADDITIONAL	
	E_{c_28} (ksi)	5212	L (ft)	14.5
	w (pcf)	150	H (%)	70
	M_g (in-k)	47.3	V (in^3)	25920
			S (in^2)	9648
			V/S (in)	2.69

LOSS CALCULATIONS

ELASTIC SHORTENING		
Equations	Stress Loss - ES	
$f_{cgp} := 0.9 P_i \left(\dfrac{1}{A_g} + \dfrac{e_p^2}{I_g} \right) - \dfrac{M_g \cdot e_p}{I_g}$	Item	Quantity
	f_{cgp} (ksi)	1.97
$\Delta f_{pES} := \dfrac{E_p}{E_{ci}} \cdot f_{cgp}$	Δf_{pES} (ksi)	14.85

PRESTRESSING FORCE		
INITIAL	f_{pi} (ksi)	182
AFTER ES	f_{pt} (ksi)	167.1

Figure A-11: Prestress losses / cracking load calculations according to AASHTO procedure for R3-75-5-T10, page 1 of 3

174

SHRINKAGE

Equations	Shrinkage strain		Equations	Stress Loss - Shrinkage	
$\varepsilon_{sh} := k_{vs} \cdot k_{hs} \cdot k_f \cdot k_{td} \cdot 0.00048$	Item	Quantity		Item	Quantity
	ε_{sh}	0.000498	$K_{it} := \dfrac{1}{1 + \dfrac{E_p}{E_{ci}} \dfrac{A_{ps}}{A_g} \left(1 + \dfrac{A_g \cdot e_{pg}^2}{I_g}\right)\left(1 + 0.7 \cdot \psi_{ult}(t_f, t_i)\right)}$	K_{it}	0.82
$k_{vs} := 1.45 - 0.13 \cdot \dfrac{V}{S}$					
$k_{hs} := 2.00 - 0.0142 \cdot H$	**Factors**		$\Delta f_{pSR} := \varepsilon_{sh} \cdot E_p \cdot K_{it}$		
	Item	Quantity			
$k_f := \dfrac{5}{1 + f'_{ci}}$	k_{vs}	1.10		Δf_{pSR} (ksi)	11.8
	k_{hs}	1.00			
$k_{td} := \dfrac{t}{61 - 4 \cdot f'_{ci} + t}$	k_f	0.99			
	k_{td}	0.95			

CREEP

Equations	Creep strain		Equations	Stress Loss - Creep	
$\psi(t, t_i) := 1.90 \cdot k_{vs} \cdot k_{hc} \cdot k_f \cdot k_{td} \cdot t_i^{-.118}$	Item	Quantity	$\Delta f_{pCR} := \dfrac{E_p}{E_{ci}} \cdot f_{cgp} \cdot \psi_t \cdot K_{it}$	Item	Quantity
	ψ_t	1.97			
	ψ_{ult}	2.07		Δf_{pCR} (ksi)	23.9
$k_{vs} := 1.45 - 0.13 \cdot \dfrac{V}{S}$					
$k_{hc} := 1.56 - 0.008 \cdot H$					

	Factors at test, t		Factors at ultimate	
$k_f := \dfrac{5}{1 + f'_{ci}}$	Item	Quantity	Item	Quantity
	k_{vs}	1.10	k_{vs}	1.10
$k_{td} := \dfrac{t}{61 - 4 \cdot f'_{ci} + t}$	k_{hc}	1.00	k_{hc}	1.00
	k_f	0.99	k_f	0.99
	k_{td}	0.95	k_{td}	1.00

RELAXATION

Equations	Stress Loss - Relax	
$\Delta f_{pR} := \dfrac{f_{pt}}{K_L}\left(\dfrac{f_{pt}}{f_{py}} - 0.55\right)$	Item	Quantity
	K_L	30.00
	Δf_{pR} (ksi)	0.77

TOTAL LOSSES

ES	Δf_{pES} (ksi)	14.9
Shrinkage	Δf_{pSR} (ksi)	11.8
Creep	Δf_{pCR} (ksi)	23.9
Relaxation	Δf_{pR} (ksi)	0.8
TOTAL	Δf_{pT} (ksi)	51.3

Figure A-12: Prestress losses / cracking load calculations according to AASHTO procedure for R3-75-5-T10, page 2 of 3

CRACKING LOAD

CRACKING LOAD PREDICTION			
Equations			Notes
$f_{eff} := f_i - \Delta f_{pT}$	Item	Quantity	
	f_{eff} (ksi)	130.7	
	P_{eff} (kips)	160.03	
Predicted Cracking Load	Cracking Prediction		
	Item	Quantity	
$M_{cr} := \left(\dfrac{I_g}{c_b}\right)\left(\dfrac{P_{eff}}{A_g} + \dfrac{P_{eff} \cdot e_p \cdot c_b}{I_g} - \dfrac{M_g \cdot c_b}{I_g} + f_r\right)$	M_{cr} (in-kip)	1268	Effective P/S force and gross section properties were used
$P_{cr} := \left(\dfrac{M_{cr}}{12}\right)\cdot\left(\dfrac{6}{L}\right)$	P_{cr} (kip)	43.7	Loaded at third points

Figure A-13: Prestress losses / cracking load calculations according to AASHTO procedure for R3-75-5-T10, page 3 of 3

Components of Total Prestress Losses

Table A-3: Estimated prestress losses due to concrete shrinkage of scaled beams

Mix Design	Project 5197 Designation	Shrinkage Losses (ksi)		
		PCI	NCHRP	AASHTO
Mix # 1	R1-52-1-T8	6.2	10.0	10.0
	R1-52-1-T7	6.2	10.0	10.0
	R1-50-1-T1	6.2	9.5	9.6
	R1-49-1-T2	6.2	9.6	9.6
	R1-46-1-T5	6.2	9.3	9.4
	R1-48-1-T6	6.2	9.3	9.4
	T1-68-2-T17	6.5	13.2	13.3
	T1-62-2-T18	6.5	13.0	13.1
	IT1-68-2-T20	6.1	12.8	12.9
	IT1-73-2-T19	6.1	12.5	12.6
	R3-75-3-T9	6.0	11.7	11.9
	R3-78-3-T3	6.0	11.4	11.6
	T2-79-3-T16	6.5	13.5	13.8
	T2-86-3-T15	6.5	13.0	13.3
	IT3-79-3-T21	6.1	11.7	11.9
	IT2-76-3-T22	6.1	11.3	11.5
Mix # 2	R3-78-4-T11	6.0	11.5	11.8
	R3-83-4-T12	6.0	11.2	11.6
	IT3-83-4-T24	6.1	11.4	11.8
Mix # 3	R3-75-5-T10	6.0	11.6	11.8
	R3-80-5-T4	6.0	11.4	11.5
	T2-91-5-T14	6.5	14.3	14.6
	IT3-79-5-T23	6.1	11.6	11.8
	IT2-80-5-T13	6.1	11.6	11.7
Average		6.2	11.5	11.7

Table A-4: Estimated prestress losses due to strand relaxation of scaled beams

Mix Design	Project 5197 Designation	Relaxation Losses (ksi)		
		PCI	NCHRP	AASHTO
Mix # 1	R1-52-1-T8	2.2	0.7	0.8
	R1-52-1-T7	2.2	0.7	0.8
	R1-50-1-T1	2.2	0.7	0.8
	R1-49-1-T2	2.0	0.7	0.8
	R1-46-1-T5	2.0	0.7	0.7
	R1-48-1-T6	2.1	0.8	0.8
	T1-68-2-T17	2.8	0.6	1.1
	T1-62-2-T18	2.4	0.5	0.9
	IT1-68-2-T20	2.9	0.5	1.0
	IT1-73-2-T19	2.7	0.4	1.0
	R3-75-3-T9	2.1	0.4	0.8
	R3-78-3-T3	1.9	0.3	0.6
	T2-79-3-T16	2.2	0.3	0.8
	T2-86-3-T15	2.0	0.2	0.7
	IT3-79-3-T21	2.4	0.3	0.9
	IT2-76-3-T22	2.4	0.4	0.9
Mix # 2	R3-78-4-T11	2.1	0.2	0.6
	R3-83-4-T12	2.0	0.1	0.6
	IT3-83-4-T24	2.5	0.1	0.8
Mix # 3	R3-75-5-T10	2.1	0.4	0.8
	R3-80-5-T4	2.0	0.3	0.7
	T2-91-5-T14	2.3	0.2	0.9
	IT3-79-5-T23	2.2	0.3	0.9
	IT2-80-5-T13	2.2	0.3	0.9
Average		2.3	0.4	0.8

APPENDIX B

Additional Information for Full-Scale TxDOT Type-A Beams

Appendix B includes the following for the full-scale TxDOT Type-A pretensioned beams:
- Shop Drawings
- Section / Material properties
- Stress Calculations at Prestress Release
- Prestress Losses / Cracking Load Calculations
    - PCI Handbook, NCHRP 496, and AASHTO LRFD 2005
- Components of Total Prestress Losses
    - Elastic shortening, concrete creep and shrinkage, and steel relaxation

Shop Drawings

Figure B-1: Sample shop drawing for A67 Type-A beam

Section / Material Properties

Table B-1: Section and material properties for full-scale TxDOT Type-A beams

Mixture Design	Test Specimen Designation	Section Properties					Prestressed / Non-Prestressed Steel Properties						Concrete Properties		
		A_g (in.^{2})	I_g (in.^{4})	h (in.)	y_b (in.)	y_t (in.)	A_{ps} (in.^{2})	e_{cl} (in.)	e_{end} (in.)	E_{ps} (ksi)	f_{pi} (ksi)	A_s (in.^{2})	f'_{ci} (psi)	f'_c (psi)	w_c (pcf)
5	A55-T25	275.4	22658	28	12.61	15.39	2.142	8.61	6.32	29000	202.5	0.61	5500	8320	150
4	A60-T26	275.4	22658	28	12.61	15.39	2.142	8.61	6.32	29000	202.5	0.61	5010	7789	150
5	A63-T27	275.4	22658	28	12.61	15.39	2.142	8.61	6.32	29000	202.5	0.61	4790	8453	150
	A66-T28	275.4	22658	28	12.61	15.39	2.142	8.61	6.32	29000	202.5	0.61	4550	9581	150
	A67-T29	275.4	22658	28	12.61	15.39	2.142	8.61	6.32	29000	202.5	0.61	4450	7073	150
	A66-T30	275.4	22658	28	12.61	15.39	2.142	8.61	6.32	29000	202.5	0.61	4500	8121	150
	A69-T31	275.4	22658	28	12.61	15.39	2.142	8.61	6.32	29000	202.5	0.61	4330	7670	150
	A68-T32	275.4	22658	28	12.61	15.39	2.142	8.61	6.32	29000	202.5	0.61	4390	7776	150
	A67-T33	275.4	22658	28	12.61	15.39	2.142	8.61	6.32	29000	202.5	0.61	4480	8360	150
	A73-T34	275.4	22658	28	12.61	15.39	2.142	8.61	6.32	29000	202.5	0.61	4080	9103	150
	A71-T35	275.4	22658	28	12.61	15.39	2.142	8.61	6.32	29000	202.5	0.61	4180	9236	150
	A75-T36	275.4	22658	28	12.61	15.39	2.142	8.61	6.32	29000	202.5	0.61	3960	8824	150

Stress Calculations at Prestress Release

Material Properties		
Concrete	f'_{ci} (psi)	4505
	E_{ci} (ksi)[1]	4232
	K_1	1.1
	K_2	1.0
Steel	E_{ps} (ksi)	29000
	f_{pi} (ksi)	202.5
	A_{ps_1} (in²/N)	0.153
	N_{total}	14

Section Properties	
A_g (in²)	275.4
I_g (in⁴)	22658
y_b (in)	12.61
y_t (in)	15.39
e_{cl} (in)	8.61
e_{end} (in)	6.32
w_u (k/ft)	0.287
L (ft)	40

Name	A66-30
Test	30

Elastic Shortening[2]	
f_{cgp} (ksi)	2.43
ES (ksi)	16.7
f_{po} (ksi)	185.8
P_o (kips)	398.0

Strand Pattern	c. l.	end
	6 at 2	6 at 2
	4 at 4	4 at 4
	2 at 6	2 at 14
	2 at 8	2 at 16

STRESS CALCULATIONS AT RELEASE								
Section	x (ft)	x/L	P_o/A (ksi)	e (in)	$P_o e y_b$/I (ksi)	$P_o e y_t$/I (ksi)	M_g (in-k)	$M_g y_b$/I (ksi)	$M_g y_t$/I (ksi)
ends	0.0	0.00	1.45	6.32	1.40	1.71	0.00	0.00	0.00
transfer	2.1	0.05	1.45	6.64	1.47	1.80	136.03	0.08	0.09
	5.0	0.13	1.45	7.09	1.57	1.92	301.35	0.17	0.20
	10.0	0.25	1.45	7.85	1.74	2.12	516.60	0.29	0.35
holddown	15.0	0.38	1.45	8.61	1.91	2.33	645.75	0.36	0.44
critical	17.5	0.44	1.45	8.61	1.91	2.33	678.04	0.38	0.46
midspan	20.0	0.50	1.45	8.61	1.91	2.33	688.80	0.38	0.47

SUMMARY					
Section	Bottom Stress		Top Stress		LRFD CHECK
	(ksi)	% of f'_{ci}	(ksi)	*√f'_{ci}	
ends	-2.85	-63.2	0.26	3.9	OK
transfer	-2.84	-63.1	0.26	3.8	OK
	-2.85	-63.2	0.27	4.0	OK
	-2.90	-64.3	0.33	4.9	OK
holddown	-2.99	-66.4	0.44	6.6	OK
critical	-2.98	-66.0	0.42	6.3	OK
midspan	-2.97	-65.9	0.41	6.2	OK

$$f_{bot} = \frac{P_o}{A} + \frac{P_o e y_b}{I} - \frac{M_g y_b}{I}$$

$$f_{top} = \frac{P_o}{A} - \frac{P_o e y_t}{I} + \frac{M_g y_t}{I}$$

[1] NCHRP 496 / AASHTO LRFD Equation:

$$E_c = 33000 K_1 K_2 \left(0.140 + \frac{f'_c}{1000} \right)^{1.5} \sqrt{f'_c}$$

[2] AASHTO LRFD Procedure

Figure B-2: Sample stress calculations at prestress transfer for Type-A beam A66-T30

Loss of Prestress / Cracking Load Calculations
NCHRP Report 496 - Prestress Losses / Cracking Load Calculations
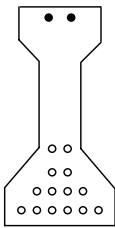
NAME   A66-T30   TEST   30 FS-6

DATE of CAST	7/19/2006 t_i (days) 1
DATE of RELEASE	7/20/2006 t_t (days) 27
DATE of STATIC TEST	8/16/2006

INPUT

INFO		SECTION PROPERTIES					
	Term	At Release			At Static Test		
		Gross	Net	Trans.	Gross	Net	Trans.
Section Type: Type A	A (in^2)	275.4	276.8	291.5	275.4	275.7	286.2
	y_b (in)	12.61	12.85	12.40	12.61	12.79	12.47
	I (in^4)	22658	23094	24218	22658	22901	23704
	A_s (in^2)	0.612	0	0	0.612	0	0
	y_s (in)	26	26	26	26	26	26
	A_{ps} (in^2)	2.142	0	0	2.142	0	0
	e_{cl} (in)	8.61	8.85	8.40	8.61	8.79	8.47
	y_p (in)	4	4	4	4	4	4
	E_c (ksi)	4230	4230	4230	5897	5897	5897
@ midspan	E_{ps} (ksi)	29000	29000	29000	29000	29000	29000
	n	6.86	6.86	6.86	4.92	4.92	4.92

INFO	MATERIAL PROPERTIES		
	CONCRETE		STEEL
	f'_{ci} (ksi) 4.5		f_{pi} (ksi) 202.5
	f'_{c_28} (ksi) 8.12		A_{ps} (in^2) 2.142
			f_{py} (ksi) 243
$f_r := 7.5 \cdot \sqrt{f'_{c\_28}}$ f'_c in psi	f_{r_28} (ksi) 0.676		f_{pu} (ksi) 270
	E_{ci} (ksi) 4230		
$E_c := 33000 \cdot K_1 \cdot K_2 \cdot \left(0.140 + \dfrac{f'_c}{1000}\right)^{1.5} \cdot \sqrt{f'_c}$	K_1 1.1		
	K_2 1		ADDITIONAL
	E_{c_28} (ksi) 5897		L (ft) 39.33
	w (pcf) 150		H (%) 70
	M_g (in-k) 665.7		V (in^3) 132192
			S (in^2) 44052
			V/S (in) 3.00

LOSS CALCULATIONS

ELASTIC SHORTENING	
Equations	Stress Loss - ES

ELASTIC SHORTENING		PRESTRESSING FORCE		
Equations	Stress Loss - ES	INITIAL	f_{pi} (ksi)	202.5
	Item Quantity	AFTER ES	f_{po} (ksi)	185.2

$f_{cgp} := P_i \left(\dfrac{1}{A_{ti}} + \dfrac{e_{pti}^2}{I_{ti}} \right) - \dfrac{M_g \cdot e_{pti}}{I_{ti}}$

f_{cgp} (ksi)   2.52

$\Delta f_{pES} := n_i \cdot f_{cgp}$

Δf_{pES} (ksi)   17.29

Figure B-3: Prestress losses / cracking load calculations according to NCHRP procedure for A66-T30, page 1 of 3

SHRINKAGE

Equations	Shrinkage strain		Equations	Stress Loss - Shrinkage	

Equations:

$$\varepsilon_{sh} := 0.00048 \cdot \gamma_{sh} \cdot K_1 \cdot K_2$$

$$\gamma_{sh} := k_{td} \cdot k_s \cdot k_{hs} \cdot k_f$$

$$k_{td} := \frac{t}{61 - 4 \cdot f_{ci} + t}$$

$$k_s := \frac{1064 - 94 \cdot \frac{V}{S}}{735}$$

$$k_{hs} := 2.00 - 0.0142 \cdot H$$

$$k_f := \frac{5}{1 + f_{ci}}$$

Shrinkage strain:

Item	Quantity
ε_{sh}	0.000179
K_1	1
K_2	1

Factors:

Item	Quantity
γ_{sh}	0.37
k_{td}	0.39
k_s	1.06
k_{hs}	1.00
k_f	0.91

Equations:

$$K_{it} := \frac{1}{1 + n_i \cdot \rho_n \cdot \alpha_n \cdot (1 + \chi \cdot \psi_{ult})}$$

$$n_i := \frac{E_{ps}}{E_{ci}}$$

$$\rho_n := \frac{A_{ps}}{A_n}$$

$$\alpha_n := \left(1 + \frac{e_p^2 \cdot A_n}{I_n}\right)$$

$$\Delta f_{pSR} := \varepsilon_{sh} \cdot E_p \cdot K_{it}$$

Stress Loss - Shrinkage:

Item	Quantity
K_{it}	0.81
n_i	6.86
ρ_n	0.0077
α_n	1.94
X	0.7
Δf_{pSR} (ksi)	4.2

CREEP

Equations:

$$\psi(t, t_i) := 1.90 \cdot \gamma_{cr} \cdot K_1 \cdot K_2$$

$$\gamma_{cr} := k_{td} \cdot k_{la} \cdot k_s \cdot k_{hc} \cdot k_f$$

$$k_{td} := \frac{t}{61 - 4 \cdot f_{ci} + t}$$

$$k_{la} := t_i^{-0.118}$$

$$k_s := \frac{1064 - 94 \cdot \frac{V}{S}}{735}$$

$$k_{hc} := 1.56 - 0.008 \cdot H$$

$$k_f := \frac{5}{1 + f_{ci}}$$

Creep strain:

Item	Quantity
ψ_t	0.71
ψ_{ult}	1.84
K_1	1
K_2	1

Equations:

$$\Delta f_{pCR} := n_i \cdot f_{cgp} \cdot \psi_t \cdot K_{it}$$

Stress Loss - Creep:

Item	Quantity
Δf_{pCR} (ksi)	9.9

Factors at test, t		Factors at ultimate	
Item	Quantity	Item	Quantity
γ_{cr}	0.37	γ_{cr}	0.97
k_{td}	0.39	k_{td}	1.00
k_{la}	1.00	k_{la}	1.00
k_s	1.06	k_s	1.06
k_{hc}	1.00	k_{hc}	1.00
k_f	0.91	k_f	0.91

RELAXATION

Equations:

$$\phi_i := 1 - \frac{3 \cdot (\Delta f_{pSR} + \Delta f_{pCR})}{f_{po}}$$

$$L_i := \frac{f_{po}}{45} \cdot \left(\frac{f_{po}}{f_{py}} - 0.55\right) \cdot \log\left(\frac{24t_t + 1}{24 \cdot t_i + 1}\right)$$

$$\Delta f_{pR} := \phi_i \cdot L_i \cdot K_{it}$$

Stress Loss - Relax:

Item	Quantity
ϕ_i	0.77
L_i	1.24
Δf_{pR} (ksi)	0.77

TOTAL LOSSES

	Item	Quantity
ES	Δf_{pES} (ksi)	17.3
Shrinkage	Δf_{pSR} (ksi)	4.2
Creep	Δf_{pCR} (ksi)	9.9
Relaxation	Δf_{pR} (ksi)	0.8
TOTAL	Δf_{pT} (ksi)	32.2
TOTAL-ES	$\Delta f_{pT\text{-}ES}$ (ksi)	14.9

Figure B-4: Prestress losses / cracking load calculations according to NCHRP procedure for A66-T30, page 2 of 3

CRACKING LOAD

CRACKING LOAD PREDICTION			
Equations	Bottom Fiber Stress		Notes
After Transfer	Item	Quantity	
$f_{cbi} := \dfrac{P_i}{A_{ti}} + \dfrac{P_i \cdot e_{pti} \cdot y_{bti}}{I_{ti}} - \dfrac{M_g \cdot y_{bti}}{I_{ti}}$	f_{cbi} (ksi)	3.01	Accounts for ES automatically
Long term losses, no ES	Δf_{cb} (ksi)	-0.27	
	f_{cbt} (ksi)	2.74	Bottom fiber stress after losses before load application
Predicted Cracking Load	Cracking Prediction		
	Item	Quantity	
$M_{cr} := \dfrac{I_{tt}}{y_{btt}} \cdot \left(f_{cbt} + f_{r\_28} \right)$	M_{cr} (in-kip)	6496	
	P_{cr} (kip)	63.1	Loaded at third points
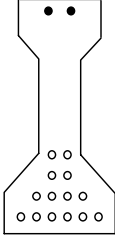
Figure B-5: Prestress losses / cracking load calculations according to NCHRP procedure for A66-T30, page 3 of 3

AASHTO LRFD Interim 2005 - Prestress Losses / Cracking Load Calculations

Name	A66-T30		TEST	30 FS-6

DATE of CAST	7/19/2006	t_i (days)		1
DATE of RELEASE	7/20/2006	t_t (days)		27
DATE of STATIC TEST	8/16/2006			

INPUT

INFO	SECTION PROPERTIES				
Section Type: Type A	Term	At Release			At Static Test	

Term	Gross	Net	Trans.	Gross	Trans.
A (in^2)	275.4			275.4	
y_b (in)	12.61			12.61	
I (in^4)	22658			22658	
A_s (in^2)	0.612			0.612	
y_s (in)	26			26	
A_{ps} (in^2)	2.142			2.142	
e_{cl} (in)	8.61			8.61	
y_p (in)	4			4	
E_c (ksi)	4474			6010	
E_{ps} (ksi)	29000			29000	
n	6.48			4.83	

@ midspan

INFO	MATERIAL PROPERTIES		
	CONCRETE		STEEL

CONCRETE		STEEL	
f'_{ci} (ksi)	4.5	f_{pi} (ksi)	202.5
f'_{c_28} (ksi)	8.12	A_{ps} (in^2)	2.142
		f_{py} (ksi)	243
f_{r_28} (ksi)	0.676	f_{pu} (ksi)	270
E_{ci} (ksi)	4474		
K_1	1.1	ADDITIONAL	
E_{c_28} (ksi)	6010	L (ft)	39.33
w (pcf)	150	H (%)	70
M_{g_test} (in-k)	665.7	V (in^3)	132192
		S (in^2)	44052
		V/S (in)	3.00

$$f_r := 7.5 \cdot \sqrt{f'_{c\_28}} \qquad f'_c \text{ in psi}$$

$$E_c := 33000 \cdot K_1 \cdot w_c^{1.5} \cdot \sqrt{f'_c}$$

LOSS CALCULATIONS

ELASTIC SHORTENING		
Equations	Stress Loss - ES	

Equations	Item	Quantity
$f_{cgp} := 0.9 P_i \cdot \left(\dfrac{1}{A_g} + \dfrac{e_p^2}{I_g} \right) - \dfrac{M_g \cdot e_p}{I_g}$	f_{cgp} (ksi)	2.44
$\Delta f_{pES} := \dfrac{E_p}{E_{ci}} \cdot f_{cgp}$	Δf_{pES} (ksi)	15.83

PRESTRESSING FORCE		
INITIAL	f_{pi} (ksi)	202.5
AFTER ES	f_{pt} (ksi)	186.7

Figure B-6: Prestress losses / cracking load calculations according to AASHTO procedure for A66-T30, page 1 of 3

SHRINKAGE

Equations	Shrinkage strain		Equations	Stress Loss - Shrinkage	
$\varepsilon_{sh} := k_{vs} \cdot k_{hs} \cdot k_f \cdot k_{td} \cdot 0.00048$	Item	Quantity		Item	Quantity
	ε_{sh}	0.000178	$K_{it} := \dfrac{1}{1 + \dfrac{E_p}{E_{ci}} \dfrac{A_{ps}}{A_g} \left(1 + \dfrac{A_g \cdot e_{pg}^2}{I_g}\right) \cdot \left(1 + 0.7 \cdot \psi_{ult}(t_t, t_i)\right)}$	K_{it}	0.82
$k_{vs} := 1.45 - 0.13 \cdot \dfrac{V}{S}$					
$k_{hs} := 2.00 - 0.0142 \cdot H$			$\Delta f_{pSR} := \varepsilon_{sh} \cdot E_p \cdot K_{it}$		
	Factors				
$k_f := \dfrac{5}{1 + f'_{ci}}$	Item	Quantity			
	k_{vs}	1.06		Δf_{pSR} (ksi)	4.2
$k_{td} := \dfrac{t}{61 - 4 \cdot f'_{ci} + t}$	k_{hs}	1.00			
	k_f	0.91			
	k_{td}	0.39			

CREEP

Equations	Creep strain		Equations	Stress Loss - Creep	
$\psi(t, t_i) := 1.90 \cdot k_{vs} \cdot k_{hc} \cdot k_f \cdot k_{td} \cdot t_i^{-.118}$	Item	Quantity	$\Delta f_{pCR} := \dfrac{E_p}{E_{ci}} \cdot f_{cgp} \cdot \psi_t \cdot K_{it}$	Item	Quantity
	ψ_t	0.71			
	ψ_{ult}	1.83		Δf_{pCR} (ksi)	9.2
$k_{vs} := 1.45 - 0.13 \cdot \dfrac{V}{S}$					
$k_{hc} := 1.56 - 0.008 \cdot H$					

	Factors at test, t		Factors at ultimate	
$k_f := \dfrac{5}{1 + f'_{ci}}$	Item	Quantity	Item	Quantity
	k_{vs}	1.06	k_{vs}	1.06
	k_{hc}	1.00	k_{hc}	1.00
$k_{td} := \dfrac{t}{61 - 4 \cdot f'_{ci} + t}$	k_f	0.91	k_f	0.91
	k_{td}	0.39	k_{td}	1.00

RELAXATION

Equations	Stress Loss - Relax	
$\Delta f_{pR} := \dfrac{f_{pt}}{K_L} \cdot \left(\dfrac{f_{pt}}{f_{py}} - 0.55\right)$	Item	Quantity
	K_L	30.00
	Δf_{pR} (ksi)	1.36

TOTAL LOSSES

	Item	Quantity
ES	Δf_{pES} (ksi)	15.8
Shrinkage	Δf_{pSR} (ksi)	4.2
Creep	Δf_{pCR} (ksi)	9.2
Relaxation	Δf_{pR} (ksi)	1.4
TOTAL	Δf_{pT} (ksi)	30.6

Figure B-7: Prestress losses / cracking load calculations according to AASHTO procedure for A66-T30, page 2 of 3

CRACKING LOAD

CRACKING LOAD PREDICTION			
Equations			Notes
	Item	Quantity	
$f_{eff} := f_i - \Delta f_{pT}$	f_{eff} (ksi)	171.9	
	P_{eff} (kips)	368.21	
Predicted Cracking Load	Cracking Prediction		
	Item	Quantity	
$M_{cr} := \left(\dfrac{I_g}{c_b}\right)\cdot\left(\dfrac{P_{eff}}{A_g} + \dfrac{P_{eff}\cdot e_p\cdot c_b}{I_g} - \dfrac{M_g\cdot c_b}{I_g} + f_r\right)$	M_{cr} (in-kip)	6121	Effective P/S force and gross section properties were used
$P_{cr} := \dfrac{2\cdot M_{cr}}{\left(\dfrac{L}{2} - \dfrac{5}{2}\right)}$	P_{cr} (kip)	59.4	Loaded with 5' constant moment region

Figure B-8: Prestress losses / cracking load calculations according to AASHTO procedure for A66-T30, page 3 of 3

Components of Total Prestress Losses

Table B-2: Components of total prestress losses for full-scale Type-A beams using NCHRP procedure

Mixture Design	Test Specimen Designation	Components of Total Prestress Losses using NCHRP Procedure (ksi)				
		Elastic Shortening	Concrete Shrinkage	Concrete Creep	Steel Relaxation	Total Loss
5	A55-T25	15.6	3.9	8.3	0.9	28.7
4	A60-T26	16.4	4.1	9.3	0.8	30.6
5	A63-T27	16.8	4.1	9.4	0.8	31.1
	A66-T28	17.2	4.2	9.8	0.8	32.0
	A67-T29	17.4	4.2	10.0	0.8	32.4
	A66-T30	17.3	4.2	9.9	0.8	32.2
	A69-T31	17.6	4.3	10.3	0.8	32.9
	A68-T32	17.5	4.2	10.1	0.8	32.6
	A67-T33	17.3	4.3	10.2	0.8	32.6
	A73-T34	18.1	4.5	11.0	0.7	34.4
	A71-T35	17.9	4.3	10.6	0.7	33.6
	A75-T36	18.4	4.4	11.1	0.7	34.6
Average		17.3	4.2	10.0	0.8	32.3

Table B-3: Components of total prestress losses for full-scale Type-A beams using AASHTO procedure

Mixture Design	Test Specimen Designation	Components of Total Prestress Losses using AASHTO Procedure (ksi)				
		Elastic Shortening	Concrete Shrinkage	Concrete Creep	Steel Relaxation	Total Loss
5	A55-T25	14.3	3.9	7.7	1.4	27.3
4	A60-T26	15.0	4.2	8.5	1.4	29.1
5	A63-T27	15.3	4.1	8.7	1.4	29.5
	A66-T28	15.8	4.2	9.1	1.4	30.4
	A67-T29	15.9	4.3	9.3	1.4	30.8
	A66-T30	15.8	4.2	9.2	1.4	30.6
	A69-T31	16.1	4.3	9.5	1.3	31.3
	A68-T32	16.0	4.3	9.4	1.4	31.1
	A67-T33	15.9	4.3	9.4	1.4	31.0
	A73-T34	16.6	4.5	10.2	1.3	32.7
	A71-T35	16.4	4.4	9.8	1.3	31.9
	A75-T36	16.9	4.5	10.3	1.3	32.9
Average		15.8	4.3	9.3	1.4	30.7

APPENDIX C
Initial Camber Database

Appendix C includes the following in regards to the initial camber study within TxDOT Project 5197:

- Sample Calculations
- Initial Camber Database
    - HEI, San Marcos, TX plant
    - TCC, Victoria, TX plant
    - Overstressed Beam Data

Sample Initial Camber Calculation

Name	2990-D1-G37
Beam Type	IV
Coarse Aggregate	Hansen Ogden

Material Properties		
Concrete	f'_{ci} (psi)	6457
	wc (psf)	148
	NCHRP E_c (ksi)	7285
	K_1	1.55
	K_2	1.0
	ACI 318 E_c (ksi)	4779
Steel	E_{ps} (ksi)	28000
	f_{pi} (ksi)	203
	# straight	48
	# depressed	12
	A_{ps} (in^2)[1]	9.18

Section Properties	
A_g (in^2)	788.4
I_g (in^4)	260403
y_b (in)	24.75
y_t (in)	29.25
w_u (k/ft)	0.821
L (ft)	119.65
α (ft)	53.8
M_g (in-kips)	17630
e_{cl} (in)	18.48
e_{end} (in)	10.48

Modulus of Elasticity Equation	Predicted E. S. Losses	
	ES_loss (ksi)[2]	f_{po} (ksi)
Using NCHRP E_c	12.5	190
Using ACI 318 E_c	18.2	184

Modulus of Elasticity Equation	Predicted Initial Camber			Measure Initial	Predicted / Measured
	Δ_{dl} (in)	Δ_{p_d} (in)	Δ_{mid} (in)		
Using NCHRP E_c	2.00	3.87	1.87	1.88	1.00
Using ACI 318 E_c	3.04	5.72	2.67	1.88	1.42

$$\Delta_{dl} = \frac{5wL^4}{384 E_c I_g} \downarrow$$

Downward deflection due to dead load

$$\Delta_{p-s} = \frac{P_o e L^2}{8 E_c I_g} \uparrow$$

Upward deflection if beam has straight strands

$$\Delta_{p-d} = \frac{P_o e_e L^2}{8 E_c I_g} + \frac{P_o e'}{E_c I_g}\left(\frac{L^2}{8} - \frac{\alpha^2}{6}\right) \uparrow$$

Upward deflection if beam has depressed strands

[1]1/2-inch diameter, 270-ksi strand
[2]Equation C5.9.5.2.3a-1 in AASHTO LRFD Interim 2006

Figure C-1: Sample initial camber calculation for Type IV beam in database

Initial Camber Database

Table C-1: Legend for Initial Camber Database

Abbreviation	Description
T.O.	TXI Owens, round, river gravel
H. O.	Hansen Ogden, crushed limestone
Y. R.	Yarrington Road, crushed river gravel
F. M.	Fordyce Murphy, round, river gravel
W. R.	Wrights Reralitos, round, river gravel
R. R.	river rock
C. L.	crushed limestone
B. R.	Boral Rockdale Fly Ash
R.	Rockdale Fly Ash
C.	Class C Fly Ash
N/A	Not Applicable
U. O.	Unknown Origin

Table C-2: HEI Camber Data, Type IV Beams, Coarse Aggregate = TXI Owens, 46 Beams

Section Type	Beam ID	Cast Date	Length, L (ft)	f'_{ci} (psi)	Rel. Time (hrs)	w_c (pcf)	Coarse Agg.	Fly Ash	NCHRP E_c (ksi)	K_1	K_2	ACI 318 E_c (ksi)	# of Straight Strands	# of Dep. Strands	E_{ps} (ksi)	α (ft)	e_{cl} (in.)	e_{end} (in.)	f_i (ksi)	Using NCHRP E_c (in)	Using ACI 318 E_c (in)	Meas. Δ_{mid} (in.)
Type IV 3097	3097-C1-66	6/22/2006	99.72	5940	12	148.3	T. O.	B. R.	6053	1.35	1.0	4593	38	8	28000	44.9	19.88	12.23	202.5	1.54	1.96	1.75
	3097-C2-68	6/22/2006	99.72	5940	12	148.3	T. O.	B. R.	6053	1.35	1.0	4593	38	8	28000	44.9	19.88	12.23	202.5	1.54	1.96	1.50
	3097-C3-67	6/22/2006	99.72	5940	12	148.3	T. O.	B. R.	6053	1.35	1.0	4593	38	8	28000	44.9	19.88	12.23	202.5	1.54	1.96	1.50
	3097-C4-67	6/22/2006	99.72	5940	12	148.3	T. O.	B. R.	6053	1.35	1.0	4593	38	8	28000	44.9	19.88	12.23	202.5	1.54	1.96	1.50
Type IV 3061	3061-D1-192	4/4/2006	112.63	6758	14	149.5	T. O.	B. R.	6511	1.35	1.0	4959	48	14	28000	50.3	18.23	9.65	202.5	2.07	2.61	2.13
	3061-D2-195	4/4/2006	114.31	6758	14	149.5	T. O.	B. R.	6511	1.35	1.0	4959	48	14	28000	51.2	18.23	9.65	202.5	2.08	2.62	2.25
	3061-D3-193	4/4/2006	113.19	6758	14	149.5	T. O.	B. R.	6511	1.35	1.0	4959	48	14	28000	50.6	18.23	9.65	202.5	2.07	2.61	2.38
	3061-D4-194	4/4/2006	113.75	6758	14	149.5	T. O.	B. R.	6511	1.35	1.0	4959	48	14	28000	50.9	18.23	9.65	202.5	2.08	2.62	2.25
Type IV 3061	3061-D1-1v	7/17/2006	107.56	6470	37	148.3	T. O.	B. R.	6352	1.35	1.0	4794	44	12	28750	48.3	18.89	10.32	202.5	1.87	2.38	1.63
	3061-D2-2v	7/17/2006	107.56	6470	37	148.3	T. O.	B. R.	6352	1.35	1.0	4794	44	12	28750	48.3	18.89	10.32	202.5	1.87	2.38	1.50
	3061-D3-2v	7/17/2006	107.56	6470	37	148.3	T. O.	B. R.	6352	1.35	1.0	4794	44	12	28750	48.3	18.89	10.32	202.5	1.87	2.38	1.50
	3061-D4-2v	7/17/2006	107.56	6470	37	148.3	T. O.	B. R.	6352	1.35	1.0	4794	44	12	28750	48.3	18.89	10.32	202.5	1.87	2.38	1.50
Type IV 3061	3061-C1v	7/17/2006	106.10	6010	34	148.3	T. O.	B. R.	6093	1.35	1.0	4620	44	12	28750	47.6	18.89	10.32	202.5	1.93	2.44	1.75
	3061-C2v	7/17/2006	106.43	6010	34	148.3	T. O.	B. R.	6093	1.35	1.0	4620	44	12	28750	47.7	18.89	10.32	202.5	1.93	2.44	1.75
	3061-C3v	7/17/2006	105.94	6010	34	148.3	T. O.	B. R.	6093	1.35	1.0	4620	44	12	28750	47.5	18.89	10.32	202.5	1.92	2.44	1.75
	3061-C4v	7/17/2006	106.27	6010	34	148.3	T. O.	B. R.	6093	1.35	1.0	4620	44	12	28750	47.6	18.89	10.32	202.5	1.93	2.44	1.75
Type IV 3061	3061-D1-38	5/11/2006	90.51	5390	11	148.3	T. O.	B. R.	5734	1.35	1.0	4375	30	6	28000	40.3	20.75	13.08	202.5	1.12	1.43	1.00
	3061-D2-42	5/11/2006	91.05	5390	11	148.3	T. O.	B. R.	5734	1.35	1.0	4375	30	6	28000	40.5	20.75	13.08	202.5	1.12	1.43	1.25
	3061-D3-39	5/11/2006	90.65	5390	11	148.3	T. O.	B. R.	5734	1.35	1.0	4375	30	6	28000	40.3	20.75	13.08	202.5	1.12	1.43	1.13
	3061-D4-40	5/11/2006	90.75	5390	11	148.3	T. O.	B. R.	5734	1.35	1.0	4375	30	6	28000	40.4	20.75	13.08	202.5	1.12	1.43	1.13
	3061-D5-41	5/11/2006	90.91	5390	11	148.3	T. O.	B. R.	5734	1.35	1.0	4375	30	6	28000	40.5	20.75	13.08	202.5	1.12	1.43	1.13
Type IV 3061	3061-C1-58	5/8/2006	110.27	6160	14	148.3	T. O.	B. R.	6178	1.35	1.0	4678	38	10	28000	49.1	19.67	10.92	202.5	1.60	2.03	1.25
	3061-C2-57	5/8/2006	110.27	6160	14	148.3	T. O.	B. R.	6178	1.35	1.0	4678	38	10	28000	49.1	19.67	10.92	202.5	1.60	2.03	1.38
	3061-C3-56	5/8/2006	110.27	6160	14	148.3	T. O.	B. R.	6178	1.35	1.0	4678	38	10	28000	49.1	19.67	10.92	202.5	1.60	2.03	1.50
	3061-C4-56	5/8/2006	110.25	6160	14	148.3	T. O.	B. R.	6178	1.35	1.0	4678	38	10	28000	49.1	19.67	10.92	202.5	1.60	2.03	1.38
Type IV 3061	3061-D1-8	5/15/2006	105.28	6470	13	148.3	T. O.	B. R.	6352	1.35	1.0	4794	44	10	28000	47.1	19.12	11.34	202.5	1.83	2.33	1.88
	3061-D2-9	5/15/2006	105.27	6470	13	148.3	T. O.	B. R.	6352	1.35	1.0	4794	44	10	28000	47.1	19.12	11.34	202.5	1.83	2.33	1.88
	3061-D3-10	5/15/2006	105.28	6470	13	148.3	T. O.	B. R.	6352	1.35	1.0	4794	44	10	28000	47.1	19.12	11.34	202.5	1.83	2.33	1.75
	3061-D4-11	5/15/2006	105.27	6470	13	148.3	T. O.	B. R.	6352	1.35	1.0	4794	44	10	28000	47.1	19.12	11.34	202.5	1.83	2.33	1.50
Type IV 3113	3113-C1-M1	5/9/2006	99.69	6140	12	148.2	T. O.	B. R.	6167	1.35	1.0	4663	36	8	28000	44.8	20.02	12.02	202.5	1.41	1.81	0.88
	3113-C2-M2	5/9/2006	99.72	6140	12	148.2	T. O.	B. R.	6167	1.35	1.0	4663	36	8	28000	44.9	20.02	12.02	202.5	1.41	1.81	1.13
	3113-C3-M4	5/9/2006	99.71	6140	12	148.2	T. O.	B. R.	6167	1.35	1.0	4663	36	8	28000	44.9	20.02	12.02	202.5	1.41	1.81	1.13
	3113-C4-M5	5/9/2006	99.72	6140	12	148.2	T. O.	B. R.	6167	1.35	1.0	4663	36	8	28000	44.9	20.02	12.02	202.5	1.41	1.81	1.00
Type IV 3113	3113-C1-M8	5/12/2006	100.43	8400	71	148.4	T. O.	B. R.	7381	1.35	1.0	5470	38	10	28000	45.1	19.67	10.92	202.5	1.32	1.73	1.38
	3113-C2-M9	5/12/2006	99.98	8400	71	148.4	T. O.	B. R.	7381	1.35	1.0	5470	38	10	28000	44.9	19.67	10.92	202.5	1.32	1.72	1.63
	3113-C3-M11	5/12/2006	99.72	8400	71	148.4	T. O.	B. R.	7381	1.35	1.0	5470	38	10	28000	44.9	19.67	10.92	202.5	1.31	1.72	1.63
	3113-C4-M12	5/12/2006	99.70	8400	71	148.4	T. O.	B. R.	7381	1.35	1.0	5470	38	10	28000	44.9	19.67	10.92	202.5	1.31	1.72	1.50
Type IV 3113	3113-C1-M7	5/15/2006	99.20	5060	12	148.4	T. O.	B. R.	5537	1.35	1.0	4244	36	8	28000	44.6	20.02	12.02	202.5	1.55	1.96	1.63
	3113-C2-M6	5/15/2006	99.63	5060	12	148.4	T. O.	B. R.	5537	1.35	1.0	4244	36	8	28000	44.8	20.02	12.02	202.5	1.56	1.96	1.63
	3113-C3-M1	5/15/2006	99.75	5060	12	148.4	T. O.	B. R.	5537	1.35	1.0	4244	36	8	28000	44.9	20.02	12.02	202.5	1.56	1.96	1.75
	3113-C4-M3	5/15/2006	99.75	5060	12	148.4	T. O.	B. R.	5537	1.35	1.0	4244	36	8	28000	44.9	20.02	12.02	202.5	1.56	1.96	1.75
Type IV 3105	3105-C1-R3	7/12/2006	74.66	5920	17	148.3	T. O.	B. R.	6042	1.35	1.0	4585	20	4	28750	32.3	21.75	17.08	202.5	0.57	0.74	0.75
	3105-C2-R6	7/12/2006	74.66	5920	17	148.3	T. O.	B. R.	6042	1.35	1.0	4585	20	4	28750	32.3	21.75	17.08	202.5	0.57	0.74	0.63
	3105-C3-R2b	7/12/2006	74.66	5920	17	148.3	T. O.	B. R.	6042	1.35	1.0	4585	20	4	28750	32.3	21.75	17.08	202.5	0.57	0.74	0.75
	3105-C4-R2b	7/12/2006	74.66	5920	17	148.3	T. O.	B. R.	6042	1.35	1.0	4585	20	4	28750	32.3	21.75	17.08	202.5	0.57	0.74	0.75
	3105-C5-R2b	7/12/2006	74.66	5920	17	148.3	T. O.	B. R.	6042	1.35	1.0	4585	20	4	28750	32.3	21.75	17.08	202.5	0.57	0.74	0.63

Table C-3: HEI Camber Data, Type C Beams, Coarse Aggregate = TXI Owens, 18 Beams

Section Type	Beam ID	Cast Date	Length, L (ft)	f'$_{ci}$ (psi)	Rel. Time (hrs)	w$_c$ (pcf)	Coarse Agg.	Fly Ash	NCHRP E$_c$ (ksi)	K$_1$	K$_2$	ACI 318 E$_c$ (ksi)	# of Straight Strands	# of Dep. Strands	E$_{ps}$ (ksi)	α (ft)	e$_{cl}$ (in.)	e$_{end}$ (in.)	f$_i$ (ksi)	Using NCHRP E$_c$ (in)	Using ACI 318 E$_c$ (in)	Meas. Δ$_{mid}$ (in.)
Type C 3091	3091-B1-W18	6/19/2006	84.67	7590	18	149.2	T. O.	B. R.	6959	1.35	1.0	5239	28	8	28750	37.3	12.42	7.53	202.5	1.57	2.02	1.38
	3091-B2-W14a	6/19/2006	79.67	7590	18	149.2	T. O.	B. R.	6959	1.35	1.0	5239	28	8	28750	34.8	12.42	7.53	202.5	1.50	1.92	1.38
	3091-B3-W13	6/19/2006	79.67	7590	18	149.2	T. O.	B. R.	6959	1.35	1.0	5239	28	8	28750	34.8	12.42	7.53	202.5	1.50	1.92	1.25
	3091-B4-W12a	6/19/2006	79.67	7590	18	149.2	T. O.	B. R.	6959	1.35	1.0	5239	28	8	28750	34.8	12.42	7.53	202.5	1.50	1.92	1.25
	3091-B5-W12a	6/19/2006	79.67	7590	18	149.2	T. O.	B. R.	6959	1.35	1.0	5239	28	8	28750	34.8	12.42	7.53	202.5	1.50	1.92	1.50
	3091-B6-W12a	6/19/2006	79.67	7590	18	149.2	T. O.	B. R.	6959	1.35	1.0	5239	28	8	28750	34.8	12.42	7.53	202.5	1.50	1.92	1.50
Type C 3091	3091-B1-W13	6/21/2006	79.67	6640	17	148.4	T. O.	B. R.	6446	1.35	1.0	4863	28	8	28750	34.8	12.42	7.53	202.5	1.60	2.05	1.63
	3091-B2-W14b	6/21/2006	79.67	6640	17	148.4	T. O.	B. R.	6446	1.35	1.0	4863	28	8	28750	34.8	12.42	7.53	202.5	1.60	2.05	1.50
	3091-B3-W12	6/21/2006	79.67	6640	17	148.4	T. O.	B. R.	6446	1.35	1.0	4863	28	8	28750	34.8	12.42	7.53	202.5	1.60	2.05	1.88
	3091-B4-W12b	6/21/2006	79.67	6640	17	148.4	T. O.	B. R.	6446	1.35	1.0	4863	28	8	28750	34.8	12.42	7.53	202.5	1.60	2.05	1.50
	3091-B5-W12b	6/21/2006	79.67	6640	17	148.4	T. O.	B. R.	6446	1.35	1.0	4863	28	8	28750	34.8	12.42	7.53	202.5	1.60	2.05	2.25
	3091-B6-W12b	6/21/2006	79.67	6640	17	148.4	T. O.	B. R.	6446	1.35	1.0	4863	28	8	28750	34.8	12.42	7.53	202.5	1.60	2.05	2.13
Type C 3100	3100-A1-M6	6/3/2006	59.68	6920	43	148.3	T. O.	B. R.	6600	1.35	1.0	4958	14	4	28750	24.8	14.18	11.07	202.5	0.58	0.75	0.75
	3100-A2-M6	6/3/2006	59.68	6920	43	148.3	T. O.	B. R.	6600	1.35	1.0	4958	14	4	28750	24.8	14.18	11.07	202.5	0.58	0.75	0.75
	3100-A3-M4	6/3/2006	59.69	6920	43	148.3	T. O.	B. R.	6600	1.35	1.0	4958	14	4	28750	24.8	14.18	11.07	202.5	0.58	0.75	0.63
	3100-A4-M3	6/3/2006	59.68	6920	43	148.3	T. O.	B. R.	6600	1.35	1.0	4958	14	4	28750	24.8	14.18	11.07	202.5	0.58	0.75	0.63
	3100-A5-M5	6/3/2006	59.69	6920	43	148.3	T. O.	B. R.	6600	1.35	1.0	4958	14	4	28750	24.8	14.18	11.07	202.5	0.58	0.75	0.50
	3100-A6-M5	6/3/2006	59.70	6920	43	148.3	T. O.	B. R.	6600	1.35	1.0	4958	14	4	28750	24.9	14.18	11.07	202.5	0.58	0.75	0.50

Table C-4: HEI Camber Data, Type IV Beams, Coarse Aggregate = Hansen Ogden, 42 Beams

	Beam Properties			Concrete Properties									Strand Properties							Predicted Δ_mid		Meas. Δ_mid
Section Type	Beam ID	Cast Date	Length, L (ft)	f'_{ci} (psi)	Rel. Time (hrs)	w_c (pcf)	Coarse Agg.	Fly Ash	NCHRP E_c (ksi)	K_1	K_2	ACI 318 E_c (ksi)	# of Straight Strands	# of Dep. Strands	E_{ps} (ksi)	α (ft)	e_{cl} (in.)	e_{end} (in.)	f_i (ksi)	Using NCHRP E_c (in)	Using ACI 318 E_c (in)	(in.)
Type IV 2990	2990-D1-G37	3/9/2006	119.65	6457	16	148.1	H. O.	U. O.	7285	1.55	1.0	4780	48	12	28000	53.8	18.48	10.48	202.5	1.87	2.67	1.88
	2990-D2-G35	3/9/2006	119.66	6457	16	148.1	H. O.	U. O.	7285	1.55	1.0	4780	48	12	28000	53.8	18.48	10.48	202.5	1.87	2.67	2.13
	2990-D3-G28	3/9/2006	119.65	6457	16	148.1	H. O.	U. O.	7285	1.55	1.0	4780	48	12	28000	53.8	18.48	10.48	202.5	1.87	2.67	2.00
	2990-D4-G28	3/9/2006	119.65	6457	16	148.1	H. O.	U. O.	7285	1.55	1.0	4780	48	12	28000	53.8	18.48	10.48	202.5	1.87	2.67	2.00
Type IV 2990	2990-C1-G34	3/8/2006	119.72	6789	14	150.0	H. O.	N/A	7495	1.55	1.0	4997	48	12	28000	53.9	18.48	10.48	202.5	1.83	2.58	1.88
	2990-C2-G38	3/8/2006	119.70	6789	14	150.0	H. O.	N/A	7495	1.55	1.0	4997	48	12	28000	53.9	18.48	10.48	202.5	1.83	2.58	1.88
	2990-C3-G38	3/8/2006	119.72	6789	14	150.0	H. O.	N/A	7495	1.55	1.0	4997	48	12	28000	53.9	18.48	10.48	202.5	1.83	2.58	1.88
Type IV 2993	2993-D1-S482	8/19/2005	107.58	7911	65	148.7	H. O.	U. O.	8184	1.55	1.0	5322	40	10	28000	48.3	19.47	11.07	202.5	1.32	1.93	1.75
	2993-D2-S483	8/19/2005	107.63	7911	65	148.7	H. O.	U. O.	8184	1.55	1.0	5322	40	10	28000	48.3	19.47	11.07	202.5	1.32	1.93	1.75
	2993-D3-S484	8/19/2005	107.72	7911	65	148.7	H. O.	U. O.	8184	1.55	1.0	5322	40	10	28000	48.4	19.47	11.07	202.5	1.32	1.93	1.63
Type IV 2993	2993-D1-S507	8/17/2005	111.88	7212	16	150.0	H. O.	N/A	7759	1.55	1.0	5146	44	10	28000	49.9	19.12	11.34	202.5	1.57	2.25	1.75
	2993-D2-S508	8/17/2005	111.95	7212	16	150.0	H. O.	N/A	7759	1.55	1.0	5146	44	10	28000	50.0	19.12	11.34	202.5	1.57	2.25	1.75
	2993-D3-S509	8/17/2005	112.02	7212	16	150.0	H. O.	N/A	7759	1.55	1.0	5146	44	10	28000	50.0	19.12	11.34	202.5	1.57	2.25	1.75
	2993-D4-S510	8/17/2005	112.05	7212	16	150.0	H. O.	N/A	7759	1.55	1.0	5146	44	10	28000	50.0	19.12	11.34	202.5	1.57	2.25	1.88
Type IV 2993	2993-C1-S511	8/17/2005	112.12	6603	12	150.0	H. O.	N/A	7378	1.55	1.0	4924	44	10	28000	50.1	19.12	11.34	202.5	1.65	2.34	1.75
	2933-C2-S512	8/17/2005	112.19	6603	12	150.0	H. O.	N/A	7378	1.55	1.0	4924	44	10	28000	50.1	19.12	11.34	202.5	1.65	2.34	1.75
	2933-C3-S513	8/17/2005	112.25	6603	12	150.0	H. O.	N/A	7378	1.55	1.0	4924	44	10	28000	50.1	19.12	11.34	202.5	1.65	2.34	1.75
	2933-C4-S514	8/17/2005	112.38	6603	12	150.0	H. O.	N/A	7378	1.55	1.0	4924	44	10	28000	50.2	19.12	11.34	202.5	1.65	2.34	1.88
Type IV 3012	3012-C1-K134a	2/17/2005	96.39	5548	21	149.9	H. O.	N/A	6690	1.55	1.0	4511	30	8	28000	43.2	20.54	11.70	202.5	1.04	1.48	1.13
	3012-C2-K134a	2/17/2005	96.40	5548	21	149.9	H. O.	N/A	6690	1.55	1.0	4511	30	8	28000	43.2	20.54	11.70	202.5	1.04	1.48	1.13
	3012-C3-K135	2/17/2005	96.52	5548	21	149.9	H. O.	N/A	6690	1.55	1.0	4511	30	8	28000	43.3	20.54	11.70	202.5	1.04	1.48	1.00
	3012-C4-K136	2/17/2005	96.60	5548	21	149.9	H. O.	N/A	6690	1.55	1.0	4511	30	8	28000	43.3	20.54	11.70	202.5	1.04	1.48	1.00
	3012-C5-K137	2/17/2005	96.70	5548	21	149.9	H. O.	N/A	6690	1.55	1.0	4511	30	8	28000	43.4	20.54	11.70	202.5	1.04	1.48	1.13
Type IV 3012	3012-C1-K134b	2/18/2005	96.42	8003	65	149.9	H. O.	N/A	8239	1.55	1.0	5418	30	8	28000	43.2	20.54	11.70	202.5	0.86	1.26	1.00
	3012-C2-K134b	2/18/2005	96.45	8003	65	149.9	H. O.	N/A	8239	1.55	1.0	5418	30	8	28000	43.2	20.54	11.70	202.5	0.86	1.26	1.00
	3012-C3-K134	2/18/2005	96.46	8003	65	149.9	H. O.	N/A	8239	1.55	1.0	5418	30	8	28000	43.2	20.54	11.70	202.5	0.86	1.26	1.00
	3012-C4-K134	2/18/2005	96.44	8003	65	149.9	H. O.	N/A	8239	1.55	1.0	5418	30	8	28000	43.2	20.54	11.70	202.5	0.86	1.26	1.00
	3012-C5-K134	2/18/2005	96.41	8003	65	149.9	H. O.	N/A	8239	1.55	1.0	5418	30	8	28000	43.2	20.54	11.70	202.5	0.86	1.26	1.00
Type IV 3015	3015-C1-J1a	4/12/2004	99.67	4885	14	150.9	H. O.	N/A	6235	1.55	1.0	4277	32	8	28000	44.3	20.35	11.55	202.5	1.21	1.68	1.00
	3015-C2-J2a	4/12/2004	99.71	4885	14	150.9	H. O.	N/A	6235	1.55	1.0	4277	32	8	28000	44.4	20.35	11.55	202.5	1.21	1.68	1.00
	3015-C3-J2a	4/12/2004	99.67	4885	14	150.9	H. O.	N/A	6235	1.55	1.0	4277	32	8	28000	44.3	20.35	11.55	202.5	1.21	1.68	1.00
	3015-C4-J2a	4/12/2004	99.69	4885	14	150.9	H. O.	N/A	6235	1.55	1.0	4277	32	8	28000	44.3	20.35	11.55	202.5	1.21	1.68	1.00
	3015-C5-J3a	4/12/2004	99.70	4885	14	150.9	H. O.	N/A	6235	1.55	1.0	4277	32	8	28000	44.4	20.35	11.55	202.5	1.21	1.68	1.00
Type IV 3015	3015-C1-J1b	4/9/2004	99.71	7616	62	149.7	H. O.	B. R.	8006	1.55	1.0	5277	32	8	28000	44.4	20.35	11.55	202.5	0.96	1.40	1.00
	3015-C2-J2b	4/9/2004	99.72	7616	62	149.7	H. O.	B. R.	8006	1.55	1.0	5277	32	8	28000	44.4	20.35	11.55	202.5	0.96	1.40	1.00
	3015-C3-J2b	4/9/2004	99.71	7616	62	149.7	H. O.	B. R.	8006	1.55	1.0	5277	32	8	28000	44.4	20.35	11.55	202.5	0.96	1.40	1.00
	3015-C4-J2b	4/9/2004	99.70	7616	62	149.7	H. O.	B. R.	8006	1.55	1.0	5277	32	8	28000	44.4	20.35	11.55	202.5	0.96	1.40	1.00
	3015-C5-J3b	4/9/2004	99.69	7616	62	149.7	H. O.	B. R.	8006	1.55	1.0	5277	32	8	28000	44.3	20.35	11.55	202.5	0.96	1.40	1.00
Type IV 3015	3015-C1-J1c	4/8/2004	99.75	5928	14	153.7	H. O.	N/A	6942	1.55	1.0	4841	32	8	28000	44.4	20.35	11.55	202.5	1.10	1.51	1.25
	3015-C2-J2c	4/8/2004	99.75	5928	14	153.7	H. O.	N/A	6942	1.55	1.0	4841	32	8	28000	44.4	20.35	11.55	202.5	1.10	1.51	1.25
	3015-C3-J2c	4/8/2004	99.75	5928	14	153.7	H. O.	N/A	6942	1.55	1.0	4841	32	8	28000	44.4	20.35	11.55	202.5	1.10	1.51	1.25
	3015-C4-J2c	4/8/2004	99.75	5928	14	153.7	H. O.	N/A	6942	1.55	1.0	4841	32	8	28000	44.4	20.35	11.55	202.5	1.10	1.51	1.25

Table C-5: HEI Camber Data, Type C Beams, Coarse Aggregate = Hansen Ogden, 47 Beams

Section Type	Beam ID	Cast Date	Length, L (ft)	f'$_{ci}$ (psi)	Rel. Time (hrs)	w$_c$ (pcf)	Coarse Agg.	Fly Ash	NCHRP E$_c$ (ksi)	K$_1$	K$_2$	ACI 318 E$_c$ (ksi)	# of Straight Strands	# of Dep. Strands	E$_{ps}$ (ksi)	α (ft)	e$_{cl}$ (in.)	e$_{end}$ (in.)	f$_i$ (ksi)	Using NCHRP E$_c$ (in)	Using ACI 318 E$_c$ (in)	Meas. Δ$_{mid}$ (in.)
Type C 3043	3043-B1-K24	3/13/2006	89.67	5819	23	148.8	H. O.	N/A	6871	1.55	1.0	4567	26	8	28750	39.8	12.61	6.03	202.5	1.42	2.02	0.88
	3043-B2-K24	3/13/2006	89.68	5819	23	148.8	H. O.	N/A	6871	1.55	1.0	4567	26	8	28750	39.8	12.61	6.03	202.5	1.42	2.02	1.00
	3043-B3-K24a	3/13/2006	89.66	5819	23	148.8	H. O.	N/A	6871	1.55	1.0	4567	26	8	28750	39.8	12.61	6.03	202.5	1.42	2.02	1.13
Type C 3043	3043-B1-K25	3/9/2006	89.65	7063	19	148.1	H. O.	N/A	7666	1.55	1.0	4999	26	8	28750	39.8	12.61	6.03	202.5	1.29	1.87	1.13
	3043-B2-K23	3/9/2006	89.62	7063	19	148.1	H. O.	N/A	7666	1.55	1.0	4999	26	8	28750	39.8	12.61	6.03	202.5	1.29	1.87	1.00
	3043-B3-K24b	3/9/2006	89.67	7063	19	148.1	H. O.	N/A	7666	1.55	1.0	4999	26	8	28750	39.8	12.61	6.03	202.5	1.29	1.87	1.00
	3043-B4-K24	3/9/2006	89.66	7063	19	148.1	H. O.	N/A	7666	1.55	1.0	4999	26	8	28750	39.8	12.61	6.03	202.5	1.29	1.87	1.13
Type C 3043	3043-A1-K24	3/8/2006	89.70	7045	19	150.5	H. O.	N/A	7655	1.55	1.0	5114	26	8	28750	39.9	12.61	6.03	202.5	1.29	1.84	1.25
	3043-A2-K24	3/8/2006	89.66	7045	19	150.5	H. O.	N/A	7655	1.55	1.0	5114	26	8	28750	39.9	12.61	6.03	202.5	1.29	1.84	1.25
	3043-A3-K24	3/8/2006	89.70	7045	19	150.5	H. O.	N/A	7655	1.55	1.0	5114	26	8	28750	39.9	12.61	6.03	202.5	1.29	1.84	1.38
Type C 3062	3062-B1-W2	5/24/2005	86.01	7102	18	150.1	H. O.	N/A	7691	1.55	1.0	5114	32	10	28000	38.0	11.76	6.99	202.5	1.68	2.40	1.88
	3062-B2-W2	5/24/2005	86.01	7102	18	150.1	H. O.	N/A	7691	1.55	1.0	5114	32	10	28000	38.0	11.76	6.99	202.5	1.68	2.40	1.75
	3062-B3-W5a	5/24/2005	86.02	7102	18	150.1	H. O.	N/A	7691	1.55	1.0	5114	32	10	28000	38.0	11.76	6.99	202.5	1.68	2.40	1.75
	3062-B4-W3	5/24/2005	86.01	7102	18	150.1	H. O.	N/A	7691	1.55	1.0	5114	32	10	28000	38.0	11.76	6.99	202.5	1.68	2.40	1.63
	3062-B5-W4	5/24/2005	86.02	7102	18	150.1	H. O.	N/A	7691	1.55	1.0	5114	32	10	28000	38.0	11.76	6.99	202.5	1.68	2.40	1.63
Type C 3062	3062-B1-W5	5/23/2005	86.02	6992	18	150.1	H. O.	N/A	7622	1.55	1.0	5074	32	10	28000	38.0	11.76	6.99	202.5	1.69	2.41	1.75
	3062-B2-W5a	5/23/2005	86.02	6992	18	150.1	H. O.	N/A	7622	1.55	1.0	5074	32	10	28000	38.0	11.76	6.99	202.5	1.69	2.41	1.75
	3062-B3-W5b	5/23/2005	86.02	6992	18	150.1	H. O.	N/A	7622	1.55	1.0	5074	32	10	28000	38.0	11.76	6.99	202.5	1.69	2.41	1.75
	3062-B4-W5	5/23/2005	86.02	6992	18	150.1	H. O.	N/A	7622	1.55	1.0	5074	32	10	28000	38.0	11.76	6.99	202.5	1.69	2.41	1.75
	3062-B5-W5	5/23/2005	86.02	6992	18	150.1	H. O.	N/A	7622	1.55	1.0	5074	32	10	28000	38.0	11.76	6.99	202.5	1.69	2.41	1.88
Type C 3062	3062-B1-W5	5/20/2005	86.06	7359	18	149.4	H. O.	N/A	7849	1.55	1.0	5170	32	10	28000	38.0	11.76	6.99	202.5	1.65	2.38	1.38
	3062-B2-W5b	5/20/2005	86.04	7359	18	149.4	H. O.	N/A	7849	1.55	1.0	5170	32	10	28000	38.0	11.76	6.99	202.5	1.65	2.38	1.50
	3062-B3-W5c	5/20/2005	86.00	7359	18	149.4	H. O.	N/A	7849	1.55	1.0	5170	32	10	28000	38.0	11.76	6.99	202.5	1.65	2.38	1.75
	3062-B4-W6	5/20/2005	86.00	7359	18	149.4	H. O.	N/A	7849	1.55	1.0	5170	32	10	28000	38.0	11.76	6.99	202.5	1.65	2.38	1.75
	3062-B5-W6	5/20/2005	86.00	7359	18	149.4	H. O.	N/A	7849	1.55	1.0	5170	32	10	28000	38.0	11.76	6.99	202.5	1.65	2.38	1.50
Type C 3062	3062-B1-W2	5/18/2005	85.98	7205	18	149.4	H. O.	N/A	7754	1.55	1.0	5115	32	10	28000	38.0	11.76	6.99	202.5	1.67	2.40	1.13
	3062-B2-W2	5/18/2005	86.00	7205	18	149.4	H. O.	N/A	7754	1.55	1.0	5115	32	10	28000	38.0	11.76	6.99	202.5	1.67	2.40	1.13
	3062-B3-W2	5/18/2005	85.98	7205	18	149.4	H. O.	N/A	7754	1.55	1.0	5115	32	10	28000	38.0	11.76	6.99	202.5	1.67	2.40	1.38
	3062-B4-W3	5/18/2005	86.00	7205	18	149.4	H. O.	N/A	7754	1.55	1.0	5115	32	10	28000	38.0	11.76	6.99	202.5	1.67	2.40	1.38
Type C 3040	3040-B1-H6	5/10/2005	79.68	6772	18	149.5	H. O.	N/A	7485	1.55	1.0	4964	28	8	28000	34.8	12.42	7.53	202.5	1.40	2.02	1.88
	3040-B2-H6	5/10/2005	79.67	6772	18	149.5	H. O.	N/A	7485	1.55	1.0	4964	28	8	28000	34.8	12.42	7.53	202.5	1.40	2.02	1.63
	3040-B3-H6	5/10/2005	79.68	6772	18	149.5	H. O.	N/A	7485	1.55	1.0	4964	28	8	28000	34.8	12.42	7.53	202.5	1.40	2.02	1.63
	3040-B4-H6	5/10/2005	79.66	6772	18	149.5	H. O.	N/A	7485	1.55	1.0	4964	28	8	28000	34.8	12.42	7.53	202.5	1.40	2.02	1.63
	3040-B5-H6	5/10/2005	79.68	6772	18	149.5	H. O.	N/A	7485	1.55	1.0	4964	28	8	28000	34.8	12.42	7.53	202.5	1.40	2.02	1.63
	3040-B6-H6	5/10/2005	79.65	6772	18	149.5	H. O.	N/A	7485	1.55	1.0	4964	28	8	28000	34.8	12.42	7.53	202.5	1.40	2.02	1.63
Type C 3040	3040-A1-H6	1/5/2005	79.69	7162	20	151.6	H. O.	N/A	7728	1.55	1.0	5213	28	8	28000	34.8	12.42	7.53	202.5	1.36	1.94	1.50
	3040-A2-H7	1/5/2005	79.69	7162	20	151.6	H. O.	N/A	7728	1.55	1.0	5213	28	8	28000	34.8	12.42	7.53	202.5	1.36	1.94	1.38
	3040-A3-H2	1/5/2005	79.65	7162	20	151.6	H. O.	N/A	7728	1.55	1.0	5213	28	8	28000	34.8	12.42	7.53	202.5	1.36	1.94	1.38
	3040-A4-H2	1/5/2005	79.67	7162	20	151.6	H. O.	N/A	7728	1.55	1.0	5213	28	8	28000	34.8	12.42	7.53	202.5	1.36	1.94	1.38
	3040-A5-H2	1/5/2005	79.68	7162	20	151.6	H. O.	N/A	7728	1.55	1.0	5213	28	8	28000	34.8	12.42	7.53	202.5	1.36	1.94	1.38
	3040-A6-H4	1/5/2005	79.64	7162	20	151.6	H. O.	N/A	7728	1.55	1.0	5213	28	8	28000	34.8	12.42	7.53	202.5	1.36	1.94	1.50
Type C 3040	3040-A1-H11	12/29/2004	79.69	7193	17	149.2	H. O.	N/A	7747	1.55	1.0	5099	28	8	28000	34.8	12.42	7.53	202.5	1.36	1.98	1.13
	3040-A2-H6	12/29/2004	79.66	7193	17	149.2	H. O.	N/A	7747	1.55	1.0	5099	28	8	28000	34.8	12.42	7.53	202.5	1.36	1.97	1.25
	3040-A3-H6	12/29/2004	79.67	7193	17	149.2	H. O.	N/A	7747	1.55	1.0	5099	28	8	28000	34.8	12.42	7.53	202.5	1.36	1.98	1.25
	3040-A4-H6	12/29/2004	79.68	7193	17	149.2	H. O.	N/A	7747	1.55	1.0	5099	28	8	28000	34.8	12.42	7.53	202.5	1.36	1.98	1.38
	3040-A5-H7	12/29/2004	79.65	7193	17	149.2	H. O.	N/A	7747	1.55	1.0	5099	28	8	28000	34.8	12.42	7.53	202.5	1.36	1.97	1.38
	3040-A6-H9	12/29/2004	79.66	7193	17	149.2	H. O.	N/A	7747	1.55	1.0	5099	28	8	28000	34.8	12.42	7.53	202.5	1.36	1.97	1.38

Table C-6: HEI Camber Data, Type IV Beams, Coarse Aggregate = Yarrington Road, 24 Beams

Section Type	Beam ID	Cast Date	Length, L (ft)	f'$_{ci}$ (psi)	Rel. Time (hrs)	w$_c$ (pcf)	Coarse Agg.	Fly Ash	NCHRP E$_c$ (ksi)	K$_1$	K$_2$	ACI 318 E$_c$ (ksi)	# of Straight Strands	# of Dep. Strands	E$_{ps}$ (ksi)	α (ft)	e$_{cl}$ (in.)	e$_{end}$ (in.)	f$_i$ (ksi)	Using NCHRP E$_c$ (in)	Using ACI 318 E$_c$ (in)	Meas. Δ$_{mid}$ (in.)
Type IV 2983	2983-D1-M3	7/14/2003	69.68	5270	<24	151.0	Y. R.	B. R.	4195	1.00	1.0	4443	14	4	28600	29.8	22.08	18.97	202.5	0.51	0.49	0.25
	2983-D2-M1	7/14/2003	69.73	5270	<24	151.0	Y. R.	B. R.	4195	1.00	1.0	4443	14	4	28600	29.9	22.08	18.97	202.5	0.52	0.49	0.25
	2983-D3-M2a	7/14/2003	69.72	5270	<24	151.0	Y. R.	B. R.	4195	1.00	1.0	4443	14	4	28600	29.9	22.08	18.97	202.5	0.52	0.49	0.13
	2983-D4-M2a	7/14/2003	69.70	5270	<24	151.0	Y. R.	B. R.	4195	1.00	1.0	4443	14	4	28600	29.9	22.08	18.97	202.5	0.52	0.49	0.25
	2983-D5-M2a	7/14/2003	69.68	5270	<24	151.0	Y. R.	B. R.	4195	1.00	1.0	4443	14	4	28600	29.8	22.08	18.97	202.5	0.51	0.49	0.25
	2983-D6-M2a	7/14/2003	69.68	5270	<24	151.0	Y. R.	B. R.	4195	1.00	1.0	4443	14	4	28600	29.8	22.08	18.97	202.5	0.51	0.49	0.25
	2983-D7-M2a	7/14/2003	69.66	5270	<24	151.0	Y. R.	B. R.	4195	1.00	1.0	4443	14	4	28600	29.8	22.08	18.97	202.5	0.51	0.49	0.25
Type IV 2983	2983-D1-M1	7/9/2003	69.66	6500	<24	151.0	Y. R.	B. R.	4718	1.00	1.0	4935	14	4	28600	29.8	22.08	18.97	202.5	0.46	0.44	0.75
	2983-D2-M3	7/9/2003	69.67	6500	<24	151.0	Y. R.	B. R.	4718	1.00	1.0	4935	14	4	28600	29.8	22.08	18.97	202.5	0.46	0.44	0.75
	2983-D3-M2b	7/9/2003	69.64	6500	<24	151.0	Y. R.	B. R.	4718	1.00	1.0	4935	14	4	28600	29.8	22.08	18.97	202.5	0.46	0.44	0.75
	2983-D4-M2b	7/9/2003	69.71	6500	<24	151.0	Y. R.	B. R.	4718	1.00	1.0	4935	14	4	28600	29.9	22.08	18.97	202.5	0.46	0.44	0.75
	2983-D5-M2b	7/9/2003	69.68	6500	<24	151.0	Y. R.	B. R.	4718	1.00	1.0	4935	14	4	28600	29.8	22.08	18.97	202.5	0.46	0.44	0.75
	2983-D6-M2b	7/9/2003	69.69	6500	<24	151.0	Y. R.	B. R.	4718	1.00	1.0	4935	14	4	28600	29.8	22.08	18.97	202.5	0.46	0.44	0.75
	2983-D7-M2b	7/9/2003	69.64	6500	<24	151.0	Y. R.	B. R.	4718	1.00	1.0	4935	14	4	28600	29.8	22.08	18.97	202.5	0.46	0.44	0.75
Type IV 2983	2983-B1-M6	7/30/2003	91.70	4820	13	153.7	Y. R.	N/A	3993	1.00	1.0	4364	24	6	28600	39.8	21.15	15.55	202.5	1.25	1.15	0.75
	2983-B2-M6	7/30/2003	91.67	4820	13	153.7	Y. R.	N/A	3993	1.00	1.0	4364	24	6	28600	39.8	21.15	15.55	202.5	1.25	1.15	0.63
	2983-B3-M5a	7/30/2003	91.68	4820	13	153.7	Y. R.	N/A	3993	1.00	1.0	4364	24	6	28600	39.8	21.15	15.55	202.5	1.25	1.15	0.63
	2983-B4-M5a	7/30/2003	91.66	4820	13	153.7	Y. R.	N/A	3993	1.00	1.0	4364	24	6	28600	39.8	21.15	15.55	202.5	1.25	1.15	0.50
	2983-B5-M5a	7/30/2003	91.67	4820	13	153.7	Y. R.	N/A	3993	1.00	1.0	4364	24	6	28600	39.8	21.15	15.55	202.5	1.25	1.15	0.63
Type IV 2983	2983-B1-M4	7/21/2003	91.76	4771	<24	151.0	Y. R.	B. R.	3970	1.00	1.0	4228	24	6	28600	39.9	21.15	15.55	202.5	1.25	1.19	1.50
	2983-B2-M4	7/21/2003	91.72	4771	<24	151.0	Y. R.	B. R.	3970	1.00	1.0	4228	24	6	28600	39.9	21.15	15.55	202.5	1.25	1.19	1.25
	2983-B3-M5b	7/21/2003	91.72	4771	<24	151.0	Y. R.	B. R.	3970	1.00	1.0	4228	24	6	28600	39.9	21.15	15.55	202.5	1.25	1.19	1.50
	2983-B4-M5b	7/21/2003	91.72	4771	<24	151.0	Y. R.	B. R.	3970	1.00	1.0	4228	24	6	28600	39.9	21.15	15.55	202.5	1.25	1.19	1.50
	2983-B5-M5b	7/21/2003	91.70	4771	<24	151.0	Y. R.	B. R.	3970	1.00	1.0	4228	24	6	28600	39.9	21.15	15.55	202.5	1.25	1.19	1.63

Table C-7: TCC Camber Data, Type IV Beams, Coarse Aggregate = Fordyce Murphy, 20 Beams

Beam Properties				Concrete Properties									Strand Properties							Predicted Δ$_{mid}$		Meas. Δ$_{mid}$
Section Type	Beam ID	Cast Date	Length, L (ft)	f'$_{ci}$ (psi)	Rel. Time (hrs)	w$_c$ (pcf)	Coarse Agg.	Fly Ash	NCHRP E$_c$ (ksi)	K$_1$	K$_2$	ACI 318 E$_c$ (ksi)	# of Straight Strands	# of Dep. Strands	E$_{ps}$ (ksi)	α (ft)	e$_{cl}$ (in.)	e$_{end}$ (in.)	f$_i$ (ksi)	Using NCHRP E$_c$ (in)	Using ACI 318 E$_c$ (in)	(in.)
Type IV 158	158-7G1	8/1/2006	108.80	7060	22	147.7	F. M.	R	8159	1.65	1.0	4976	44	10	28500	48.9	19.12	11.34	202.5	1.48	2.29	1.50
	158-7G2	8/1/2006	109.09	7060	22	147.7	F. M.	R	8159	1.65	1.0	4976	44	10	28500	49.0	19.12	11.34	202.5	1.48	2.29	1.50
	158-7G3	8/1/2006	109.38	7060	22	147.7	F. M.	R	8159	1.65	1.0	4976	44	10	28500	49.2	19.12	11.34	202.5	1.49	2.29	1.50
	158-7G4	8/1/2006	109.67	7060	22	147.7	F. M.	R	8159	1.65	1.0	4976	44	10	28500	49.3	19.12	11.34	202.5	1.49	2.29	1.50
Type IV 303	303-A11	8/1/2006	111.30	5600	15	147.7	F. M.	R	7159	1.65	1.0	4431	40	10	28500	50.2	19.47	11.07	202.5	1.49	2.25	1.38
	303-A12	8/1/2006	110.49	5600	15	147.7	F. M.	R	7159	1.65	1.0	4431	40	10	28500	49.7	19.47	11.07	202.5	1.49	2.25	1.38
	303-A13	8/1/2006	108.88	5600	15	147.7	F. M.	R	7159	1.65	1.0	4431	40	10	28500	48.9	19.47	11.07	202.5	1.49	2.25	1.38
	303-A14	8/1/2006	108.07	5600	15	147.7	F. M.	R	7159	1.65	1.0	4431	40	10	28500	48.5	19.47	11.07	202.5	1.48	2.25	1.38
Type IV 158	158-6F1	8/1/2006	109.96	6080	16	147.7	F. M.	R	7496	1.65	1.0	4617	44	10	28500	49.5	19.12	11.34	202.5	1.61	2.44	1.63
	158-6F2	8/1/2006	109.24	6080	16	147.7	F. M.	R	7496	1.65	1.0	4617	44	10	28500	49.1	19.12	11.34	202.5	1.60	2.44	1.63
	158-6F3	8/1/2006	109.39	6080	16	147.7	F. M.	R	7496	1.65	1.0	4617	44	10	28500	49.2	19.12	11.34	202.5	1.60	2.44	1.63
	158-6F4	8/1/2006	109.55	6080	16	147.7	F. M.	R	7496	1.65	1.0	4617	44	10	28500	49.3	19.12	11.34	202.5	1.60	2.44	1.63
Type IV 158	158-3C1-ST87	8/2/2006	106.48	6410	22	150.8	F. M.	N/A	7723	1.65	1.0	4892	38	8	28500	47.7	19.76	12.24	202.5	1.26	1.89	1.50
	158-3C2-ST78	8/2/2006	107.27	6410	22	150.8	F. M.	N/A	7723	1.65	1.0	4892	38	8	28500	48.1	19.76	12.24	202.5	1.26	1.89	1.38
	158-3C3-ST77	8/2/2006	106.46	6410	22	150.8	F. M.	N/A	7723	1.65	1.0	4892	38	8	28500	47.7	19.76	12.24	202.5	1.26	1.89	1.38
	158-3C4-ST68	8/2/2006	107.24	6410	22	150.8	F. M.	N/A	7723	1.65	1.0	4892	38	8	28500	48.1	19.76	12.24	202.5	1.26	1.89	1.13
Type IV 169	169-8H1-DC71	8/2/2006	108.27	6000	20	147.7	F. M.	R	7441	1.65	1.0	4587	42	10	28500	48.6	19.27	11.20	202.5	1.52	2.31	1.63
	169-8H2-DC72	8/2/2006	108.27	6000	20	147.7	F. M.	R	7441	1.65	1.0	4587	42	10	28500	48.6	19.27	11.20	202.5	1.52	2.31	1.38
	169-8H3-DC73	8/2/2006	108.27	6000	20	147.7	F. M.	R	7441	1.65	1.0	4587	42	10	28500	48.6	19.27	11.20	202.5	1.52	2.31	1.50
	169-8H4-DC64	8/2/2006	108.27	6000	20	147.7	F. M.	R	7441	1.65	1.0	4587	42	10	28500	48.6	19.27	11.20	202.5	1.52	2.31	1.50

Table C-8: Project 5197 Camber Data, Type A Beams, Coarse Aggregate = Wrights Reralitos, 12 Beams

Beam Properties				Concrete Properties									Strand Properties							Predicted Δ_mid		Meas. Δ_mid
Section Type	Beam ID	Cast Date	Length, L (ft)	f'_{ci} (psi)	Rel. Time (hrs)	w_c (pcf)	Coarse Agg.	Fly Ash	NCHRP E_c (ksi)	K_1	K_2	ACI 318 E_c (ksi)	# of Straight Strands	# of Dep. Strands	E_{ps} (ksi)	α (ft)	e_{cl} (in.)	e_{end} (in.)	f_i (ksi)	Using NCHRP E_c (in)	Using ACI 318 E_c (in)	(in.)
Type A 5197	A55-T25	7/13/2006	40.00	5500	11	149.0	W.R.	N/A	4725	1.1	1.0	4449	10	4	29000	15.0	8.61	6.32	202.5	0.73	0.77	0.75
Type A 5197	A60-T26	7/12/2006	40.00	5010	6	150.2	W.R.	N/A	4487	1.1	1.0	4298	10	4	29000	15.0	8.61	6.32	202.5	0.76	0.79	0.50
Type A 5197	A63-T27	7/14/2006	40.00	4790	11	149.0	W.R.	N/A	4377	1.1	1.0	4152	10	4	29000	15.0	8.61	6.32	202.5	0.78	0.82	0.75
Type A 5197	A66-T28	7/17/2006	40.00	4550	7	149.0	W.R.	N/A	4255	1.1	1.0	4047	10	4	29000	15.0	8.61	6.32	202.5	0.80	0.84	0.75
Type A 5197	A67-T29	7/18/2006	40.00	4450	14	149.0	W.R.	N/A	4204	1.1	1.0	4002	10	4	29000	15.0	8.61	6.32	202.5	0.81	0.85	0.50
Type A 5197	A66-T30	7/19/2006	40.00	4500	9	149.0	W.R.	N/A	4230	1.1	1.0	4025	10	4	29000	15.0	8.61	6.32	202.5	0.80	0.84	0.50
Type A 5197	A69-T31	7/20/2006	40.00	4330	8	149.0	W.R.	N/A	4142	1.1	1.0	3948	10	4	29000	15.0	8.61	6.32	202.5	0.82	0.86	0.38
Type A 5197	A68-T32	7/21/2006	40.00	4390	9	149.0	W.R.	N/A	4173	1.1	1.0	3975	10	4	29000	15.0	8.61	6.32	202.5	0.81	0.85	0.50
Type A 5197	A67-T33	7/24/2006	40.00	4480	7	149.0	W.R.	N/A	4219	1.1	1.0	4016	10	4	29000	15.0	8.61	6.32	202.5	0.81	0.84	0.75
Type A 5197	A73-T34	7/25/2006	40.00	4080	10	149.0	W.R.	N/A	4010	1.1	1.0	3832	10	4	29000	15.0	8.61	6.32	202.5	0.84	0.88	0.50
Type A 5197	A71-T35	7/26/2006	40.00	4180	7	149.0	W.R.	N/A	4063	1.1	1.0	3879	10	4	29000	15.0	8.61	6.32	202.5	0.83	0.87	0.50
Type A 5197	A75-T36	7/27/2006	40.00	3960	7	149.0	W.R.	N/A	3946	1.1	1.0	3775	10	4	29000	15.0	8.61	6.32	202.5	0.86	0.89	0.50

Table C-9: Project 4086 Camber Data, Scaled Beams, Coarse Aggregate = Varied, 14 Beams

Beam Properties				Concrete Properties									Strand Properties							Predicted Δ_mid		Meas. Δ_mid
Section Type	Beam ID	Cast Date	Length, L (ft)	f'_{ci} (psi)	Rel. Time (hrs)	w_c (pcf)	Coarse Agg.	Fly Ash	NCHRP E_c (ksi)	K_1	K_2	ACI 318 E_c (ksi)	# of Straight Strands	# of Dep. Strands	E_{ps} (ksi)	α (ft)	e_{cl} (in.)	e_{end} (in.)	f_i (ksi)	Using NCHRP E_c (in)	Using ACI 318 E_c (in)	(in.)
R3-78-3	3	9/24/2002	15.00	4065	10	145.0	R.R.	N/A	3638	1.0	1.0	3674	8	0	29000	7.5	4.00	4.00	178.0	0.21	0.21	0.20
R3-80-5	4	3/4/2003	15.00	4045	15	145.0	C.L.	C	3628	1.0	1.0	3665	8	0	29000	7.5	4.00	4.00	182.0	0.22	0.22	0.23
R3-75-3	9	9/24/2002	15.00	4065	10	145.0	R.R.	N/A	3638	1.0	1.0	3674	8	0	29000	7.5	3.50	3.50	181.0	0.19	0.19	0.18
R3-75-5	10	3/4/2003	15.00	4045	15	145.0	C.L.	C	3628	1.0	1.0	3665	8	0	29000	7.5	3.50	3.50	182.0	0.19	0.19	0.20
R3-78-4	11	12/5/2002	15.00	3800	14	145.0	C.L.	N/A	2806	0.8	1.0	3552	8	0	29000	7.5	3.50	3.50	180.0	0.24	0.19	0.24
R3-83-4	12	12/5/2002	15.00	3800	14	145.0	C.L.	N/A	2806	0.8	1.0	3552	8	0	29000	7.5	4.00	4.00	180.0	0.27	0.22	0.26
T2-91-5	14	3/4/2003	15.00	3465	15	145.0	C.L.	C	3338	1.0	1.0	3392	4	0	29000	2.5	4.60	4.60	186.0	0.24	0.24	0.20
T2-86-3	15	9/24/2002	15.00	3950	10	145.0	R.R.	N/A	3582	1.0	1.0	3621	4	0	29000	2.5	5.27	5.27	181.0	0.25	0.25	0.20
T2-79-3	16	9/24/2002	15.00	3950	10	145.0	R.R.	N/A	3582	1.0	1.0	3621	4	0	29000	2.5	4.52	4.52	182.0	0.22	0.21	0.15
IT2-80-5	13	3/4/2003	15.00	4045	15	145.0	C.L.	C	3628	1.0	1.0	3665	10	0	29000	2.5	3.67	3.67	189.0	0.22	0.21	0.27
IT3-79-3	21	9/24/2002	15.00	4065	10	145.0	R.R.	N/A	3638	1.0	1.0	3674	10	0	29000	2.5	3.66	3.66	189.0	0.21	0.21	0.21
IT3-76-3	22	9/24/2002	15.00	4320	10	145.0	R.R.	N/A	3761	1.0	1.0	3787	10	0	29000	2.5	3.66	3.66	188.0	0.21	0.21	0.18
IT3-79-5	23	3/4/2003	15.00	4045	15	145.0	C.L.	C	3628	1.0	1.0	3665	10	0	29000	2.5	3.69	3.69	189.0	0.22	0.21	0.23
IT3-83-4	24	12/5/2002	15.00	3800	14	145.0	C.L.	N/A	2806	0.8	1.0	3552	10	0	29000	2.5	3.66	3.66	191.0	0.27	0.22	0.26

BIBLIOGRAPHY

1. AASHTO, *Standard Specifications for Highway Bridges*, 8th Edition, American Association of State Highway and Transportation Officials, Washington, D.C., 1961

2. AASHTO, *LRFD Bridge Design Specifications*, 3rd Edition, American Association of State Highway and Transportation Officials, Washington, D.C., 2004.

3. AASHTO, *LRFD Bridge Design Specifications*, Interim 2005 Edition, American Association of State Highway and Transportation Officials, Washington, D.C., 2005.

4. ACI Committee 318, *Building Code Requirements for Reinforced Concrete (ACI 318-63)*, American Concrete Institute, Detroit, MI, 1963.

5. ACI Committee 318, *Building Code Requirements for Reinforced Concrete (ACI 318-05)*, American Concrete Institute, Farmington Hills, MI, 2005.

6. ACI-ASCE Joint Committee 323, "Tentative Recommendations for Prestressed Concrete," *Journal of the American Concrete Institute–Proceedings*, Vol. 54, January 1958, pp. 545-578.

7. ACI-ASCE Joint Committee 323, "Tentative Recommendations for Prestressed Concrete – Committee Closure," *Journal of the American Concrete Institute–Proceedings*, Vol. 54, Part 2, December 1958, pp. 1291-1299.

8. ACI Committee 209, *Prediction of Creep, Shrinkage, and Temperature Effects in Concrete Structures (ACI 209R-92)*, American Concrete Institute, Farmington Hills, MI, 1992.

9. Aswad, A., "PCI Standard Design Practice," *Journal of the Precast / Prestressed Concrete Institute*, Vol. 42, March-April 1997, p. 47.

10. Carrasquillo, R.L., Nilson, A.H., and Slate, F.O., "Properties of High Strength Concrete Subject to Short-Term Loads," *Journal of the American Concrete Institute–Proceedings*, Vol. 78, No. 3, May-June 1981, pp. 171-178.

11. Castro, A., Kreger, M. E., Bayrak, O., Breen, J. E., and Wood, S. L., "Allowable Design Release Stresses for Pretensioned Concrete Beams," Research Report 0-4086-2, Center for Transportation Research, The University of Texas at Austin, August 2004, 142 pp.

12. Cetin, A. and Carrasquillo, R. L., "High Performance Concrete: Influence of Coarse Aggregates on Mechanical Properties," *ACI Materials Journal*, Vol. 95, No. 3, May-June 1998, pp. 252-261.

13. Collins, M. P. and Mitchell, D., *Prestressed Concrete Structures*, Response Publications, Toronto and Montreal, Canada, 1997.

14. D'Arcy, T. J., "Good Performance – The Engineer's Quest," *Journal of the Precast / Prestressed Concrete Institute*, Vol. 50, July-August 2005, p. 15.

15. Davis, R. E., and Davis, H. E., "Flow of Concrete under the Actions of Sustained Loads," *Journal of the American Concrete Institute–Proceedings*, Vol. 27, pp. 837-901.

16. Delibes Liniers, A., "Microcracking of concrete under compression and its influence on tensile strength," *Materials and Structures*, Vol. 20, No. 116, pp. 111-116.

17. Erickson, E.L., "The Bureau of Public Roads 'Criteria for Prestressed Concrete Bridges,'" *Proceedings World Conference on Prestressed Concrete*, San Francisco, CA, July 1957, pp. A9-1-A9-8.

18. Gettu, R., Aguado, A., and Oliveira, O. F., "Damage in High-Strength Concrete Due to Monotonic and Cyclic Compression–A Study Based on Splitting Tensile Strength," *ACI Materials Journal*, Vol. 93, No. 6, November-December 1996, pp. 519-523.

19. Hale, W. M. and Russell, B. W., "Effect of Allowable Compressive Stress at Release on Prestress Losses and on the Performance of Precast, Prestressed Concrete Girders," *Journal of the Precast / Prestressed Concrete Institute*, Vol. 51, No. 2, March-April 2006, pp. 14-25.

20. Hawkins, N.M., *Impact of Research on Prestressed Concrete Specimens*, ACI SP-72-7, American Concrete Institute, Detroit, MI, 1981, pp. 163-176.

21. Hennessey, S. A. and Tadros, M. K., "Significance of Transformed Section Properties in Analysis for Required Prestressing," Open Forum Problems and Solutions, *Journal of the Precast / Prestressed Concrete Institute*, Vol. 47, No. 6, November-December 2002, pp. 104-107.

22. Hognestad, E., Hanson, N. W., and McHenry, D., "Concrete stress distribution in ultimate strength design," *Journal of the American Concrete Institute–Proceedings*, Vol. 52, 1955, pp. 455-480.

23. Hsu, T.T.C., Slate, F.O., Sturman, G.M., and Winter, G., "Microcracking of Plain Concrete and the Shape of the Stress-Strain Curve," *Journal of the American Concrete Institute–Proceedings*, Vol. 60, No. 2, February 1963, pp. 209-223.

24. Huang, T., "Estimating Stress for a Prestressed Concrete Member," *Journal of the Prestressed Concrete Institute*, Vol. 17, No. 1, January-February 1972, pp. 29-34.

25. Huo, X., and Tadros, M., "Allowable Compressive Strength of Concrete at Prestress Release," Open Forum Problems and Solutions, *Journal of the Precast / Prestressed Concrete Institute*, Vol. 42, No. 1, January-February 1997, pp. 95-99.

26. Irvani, S., "Mechanical Properties of High-Performance Concrete," *ACI Materials Journal*, Vol. 93, No. 5, September-October 1996, pp. 416-426.

27. Karsan, I. D. and Jirsa, J. O., "Behavior of Concrete Under Varying Strain Gradients," *Journal of the Structural Division, ASCE*, Vol. 96, No. ST8, August 1970, pp. 1675-1696.

28. Kerekes, F. and Reid, H. B., "Fifty Years of Development in Building Code Requirements for Reinforced Concrete," *Journal of the American Concrete Institute–Proceedings*, Vol. 50, No. 6, February, 1954, pp. 441-470.

29. Khan A., Cook W., and Mitchell, D., "Early Age Compressive Stress-Strain Properties of Low-, Medium, and High-Strength Concretes," *ACI Materials Journal*, Vol. 92, No. 6, November-December 1995, pp. 617-624.

30. Kreger, M. E., and Bayrak, O., "Project 0-4086: Allowable Design Release Stresses for Pretensioned Concrete Beams," Project Summary Report 0-4086-S, Center for Transportation Research, The University of Texas at Austin, July 2005, 4 pp.

31. Lin, T. Y., "Tentative Recommendations for Prestressed Concrete," *Journal of the American Concrete Institute–Proceedings*, Vol. 54, Part 2, September 1958, pp. 1232-1233.

32. Lin, T. Y. and Burns, N., *Design of Prestressed Concrete Structures*, Second Edition, John Wiley & Sons, Inc., New York, 1963.

33. MacGregor, J. G., *Reinforced Concrete Mechanics and Design*, Third Edition, Prentice Hall, New Jersey, 1997.

34. Mokhtarzadeh, A. and French, C., "Mechanical Properties of High-Strength Concrete with Consideration for Precast Applications," *ACI Materials Journal*, Vol. 97, No. 2, March-April 2000, pp. 136-147.

35. Myers, J. J. and Carrasquillo, R. L., "Production and Quality Control of High Performance Concrete in Texas Bridge Structures," Research Report 580/589-1, Center for Transportation Research, The University of Texas at Austin, December 1998, 563 pp.

36. Neville, A. M., "Role of Cement in the Creep of Mortar," *Journal of the American Concrete Institute–Proceedings*, Vol. 55, No. 9, March 1959, pp. 963-984.

37. Ngab, A. S., Nilson, A. H., and Slate, F. O., "Shrinkage and Creep of High Strength Concrete," *Journal of the American Concrete Institute–Proceedings*, Vol. 78, No. 4, July-August 1981, pp. 255-261

38. Ngab, A. S., Slate, F. O., and Nilson, A. H., "Microcracking and Time-Dependent Strains in High Strength Concrete," *Journal of the American Concrete Institute–Proceedings*, Vol. 78, No. 4, July-August 1981, pp. 262-268.

39. Nilson, A. H., *Design of Prestressed Concrete*, Second Edition, John Wiley & Sons, Inc., 1987.

40. Noppakunwijai P., Tadros, M.K., Ma, Z., and Mast, R.F., "Strength Design of Pretensioned Flexural Concrete Members at Prestress Transfer," *Journal of the Precast / Prestressed Concrete Institute*, Vol. 46, No. 1, January-February 2001, pp. 34-52.

41. Noppakunwijai P., Tadros, M.K., Ma, Z., and Mast, R.F., "Authors Closure," Readers Comments, *Journal of the Precast / Prestressed Concrete Institute*, Vol., 47, No. 1, January-February 2002, pp. 107-109.

42. Pang, J. P., "Allowable compressive stresses for prestressed concrete," MS Thesis, The University of Oklahoma, May 1997, 178 pp.

43. Pauw, A., "Static Modulus of Elasticity of Concrete as Affected by Density," *Journal of the American Concrete Institute–Proceedings*, Vol. 32, No. 6, November-December 1960.

44. PCI Technical Activities Council and PCI Committee on Building Code, "PCI Standard Design Practice," *Journal of the Precast / Prestressed Concrete Institute*, Vol. 41, No. 4, July-August 1996, pp. 31-43.

45. PCI Technical Activities Council and PCI Committee on Building Code, "PCI Standard Design Practice," *Journal of the Precast / Prestressed Concrete Institute*, Vol. 42, No. 4, March-April 1997, pp. 43-51.

46. PCI Technical Activities Council and PCI Committee on Building Code, "PCI Standard Design Practice," *Journal of the Precast / Prestressed Concrete Institute*, Vol. 48, No. 1, January-February 2003.

47. PCI, *PCI Design Handbook*, Sixth Edition, Precast/Prestressed Concrete Institute, Chicago, IL, 2004.

48. Reese, G. A., "Fatigue Strength of Prestressed Concrete Girders," MS Thesis, The University of Texas as Austin, August 1983, 138 pp.

49. Richart, F.E., Brandtzaeg, A., and Brown, R.L., "The Failure of Plain and Spirally Reinforced Concrete in Compression," Bulletin No. 190, University of Illinois Engineering Experiment Station, Urbana, Ill., April 1929, pp. 1-74.

50. Rogers, S., "Allowable Design Release Stresses for Pretensioned Concrete Beams– Preliminary Results, MS Thesis, The University of Texas at Austin, 2002.

51. Russell, B. W. and Pang, J. P., "Investigation of Allowable Compressive Stresses for High Strength, Prestressed Concrete," *Proceedings of the PCI/FHWA Intl. Symposium on High Performance Concrete*, New Orleans, LA, October 1997, pp. 554-565.

52. Seguirant, S. J., Letters to the Editor, *Journal of the Precast / Prestressed Concrete Institute*, Vol. 50, No. 5, September-October 2005, p. 125-126.

53. Seguirant, S. J., Readers Comments, *Journal of the Precast / Prestressed Concrete Institute*, Vol., 47, No. 1, January-February 2002, pp. 106-107.

54. Shah, S.P. and Winter, G., "Inelastic Behavior and Fracture of Concrete," *Journal of the American Concrete Institute–Proceedings*, Vol. 63, No. 9, September 1966, pp. 925-930.

55. Smadi, M. M., Slate, F. O., and Nilson, A. H., "High-, Medium-, and Low-Strength Concretes Subject to Sustained Overloads–Strains, Strengths, and Failure Mechanisms," *ACI Materials Journal*, Vol. 82, No. 5, September-October 1985, pp. 657-664.

56. Smadi, M. M., Slate, F. O., and Nilson, A. H., "Shrinkage and Creep of High-, Medium-, and Low-Strength Concretes, Including Overloads," *ACI Materials Journal*, Vol. 84, No. 3, May-June 1987, pp. 224-234.

57. Tadros, M. K., Al-Omaishi, N., Seguirant, S. J., and Gallt, J. G., "Prestress Losses in Pretensioned High-Strength Concrete Bridge Girders," NCHRP Report 496, Transportation Research Board, Washington, D. C., 2003.

58. Tadros, M. K., Letters to the Editor, *Journal of the Precast / Prestressed Concrete Institute*, Vol. 50, No. 5, September-October 2005, p. 125.

59. Tadros, M. K., Letters to the Editor, *Journal of the Precast / Prestressed Concrete Institute*, Vol. 50, No. 5, September-October 2005, p. 125.

60. Thorenfeldt, E., Tomaszewicz, A., and Jensen, J. J., "Mechanical Properties of High-Strength Concrete and Application in Design," *Proceedings of the Symposium*

"Utilization of High Strength Concrete," Stavanger, Norway, June 1987, Tapir, Trondheim, pp. 149-159.

61. Tucker, J., Personal Correspondence, November 2006.

62. Texas Department of Transportation, www.dot.state.tx.us, Bridge Division Standard Drawings, 2005.

63. Zia, P., Preston, H. K., Scott, N. L., and Workman, E. B., "Estimating Prestress Loss," *Concrete International Design and Construction*, Vol. 1, No. 6, June 1979, pp. 32-38.